PhD THESIS

Uptake, Metabolism, and Cellular Activities of Native and Chlorinated Sphingolipids in Neurons

submitted by

Mag. rer. nat. Christoph Nußhold

to obtain the academic degree of

Doctor of Philosophy (Ph.D.)

at the

Medical University of Graz

Institute of Molecular Biology and Biochemistry

under Supervision of Ao.Prof. Dr. Wolfgang Sattler

2011

Declaration

I hereby declare that this thesis is my own original work and that I have fully acknowledged by name all of those individuals and organisations that have contributed to the research for this thesis. Due acknowledgement has been made in the text to all other material used. Throughout this thesis and in all related publications I followed the guidelines of “Good Scientific Practice”.

Date,

Signature

TABLE OF CONTENTS

ACKNOWLEDGEMENTS

First of all, I would like to particularly appreciate my supervisor and mentor Prof. Wolfgang Sattler for giving me the opportunity to do my thesis in his group and for the excellent guidance, help, and the continuous support during the last four years.

Very special thanks go to all members of our lab for their kind help and support: Thank you Helga, Matthias, Doris, Andreas, Eva, Gerald, Sabine Waltl, Sabine Damm, Ingrid, and Andrea! Furthermore I want to thank Ernst Malle for critical reading this thesis as well as the members of his group for their support.

I am grateful to my thesis committee members, Prof. Akos Heinemann and Prof. Wolfgang Graier for scientific support.

I am thankful to all the collaborators, including A. Hammer, M. Kollroser, G. Rechberger, H. Hackl, Z. Trajanosky, R. Malli, A. Hrzenjak, A. Hermetter, and H. Köfeler, who contributed with excellent methods and outstanding knowledge to this project.

I am grateful to thank all my friends for all the “Friday Night Sessions” with very amusing, long-lasting, and relaxing scientific and non-scientific discussions.

Last, but not least I would like to thank my family and my girlfriend Gudrun for the emotional support all through my studies.

ABBREVIATIONS

2-ClHDA	2-chlorohexadecanal
2D-DIGE	two-dimensional difference gel electrophoresis
3-chloro-Tyr	3-chlorotyrosine
AC	acid ceramidase
ACH	*S*-α-chlorohydrin
ACN	acetonitrile
AD	Alzheimer's disease
AIF	apoptosis inducing factor
ApoA-1	apolipoprotein A-1
ApoB-100	apolipoprotein B-100
aSMase	acidic sphingomyelinase
ASMKO	acidic sphingomyelinase knock-out
Aβ	amyloid-beta
BBB	blood-brain-barrier
BE	back-exchange
BMP	bismonoacylglycerophosphate
BODIPY FL C_{12}-SM	N-(4,4-difluoro-5,7-dimethyl-4-bora-3a,4a-diaza-*s*-indacine-3-dodecanoyl)sphingosyl phosphocholine
BODIPY-Cer	N-(4,4-difluoro-5,7-dimethyl-4-bora-3a,4a-diaza-*s*-indacene-3-pentanoyl)sphingosine
BODIPY-SM	N-(4,4-difluoro-5,7-dimethyl-4-bora-3a,4a-diaza-*s*-indacine-3-pentanoyl)sphingosyl phosphocholine
CARD	caspase recruitment domain
Cer	ceramide
Cer1P	ceramide-1-phosphate
CerS	ceramide synthase
CERT	ceramide transfer protein
CHEL	chelerythrine chloride
Chol	cholesterol

CNS	central nervous system
CP	chlorpromazine
CRF	corticotrophin-releasing factor
CVD	cardiovascular disease
Cy	cyanine
DAG	diacylglycerol
dbcAMP	2'-O-dibutyryladenosine 3',5' cyclic monophosphate
DED	death effector domains
DES	dihydroceramide desaturase
DF-BSA	fatty acid-free bovine serum albumine
DHB	dihydroxybenzoic acid
DHCer	dihydroceramide
DISC	death inducing signaling complex
EAE	experimental autoimmune enzephalomyelitis
EI	electron impact
EndoG	endonuclease G
ER	endoplasmic reticulum
ESI	electrospray ionization
FA	fatty acid
FADD	Fas-associated death domain
FasL	Fas ligand
FCCP	carbonyl cyanide 4-(trifluoromethoxy)phenylhydrazone
FCS	fetal calf serum
FFA	free fatty acid
FI	fluorescence intensity
GalCer	galactosylceramide
GAPDH	glyceraldehyde-3-phosphate dehydrogenase
GC-MS	gas chromatography mass spectrometry
GE	genistein
GlcCer	glucosylceramide
GO	Gene Ontology
GSH	glutathione

GSL	glycosphingolipid
GSSG	oxidized glutathione
H_2DCFDA	2',7'-dichlorofluorescin diacetate
HBSS	Hank's buffered salt solution
HD	Huntington's disease
HDL	high-density lipoprotein
HexCer	monohexosylceramide
HFB	heptafluorobutyrate
HNE	hydroxynonenal
HOBr	hypobromous acid
HOCl	hypochlorous acid
HOCl-HDL	hypochlorite-modified high-density lipoprotein
HOCl-LDL	hypochlorite-modified low-density lipoprotein
HOSCN	hypothiocyanous acid
HOX	hypohalous acid
HPLC	high performance liquid chromatography
HRP	horse radish peroxidase
HS	horse serum
IAP	inhibitor of apoptosis proteins
IEF	isoelectric focusing
IL	interleukin
IPA	Ingenuity Pathway Analysis
JC-1	5,5',6,6'-tetrachloro-1,1',3,3'-tetraethyl-benzamidazolocarbocyanin iodide
LacCer	lactosylceramide
LCB	long chain base
LC-FT-MS	Fourier-transform ion cyclotron resonance mass spectrometry
LDH	lactate dehydrogenase
LDL	low-density lipoprotein
LPA	lysophosphatidic acid
LPS	lipopolysaccharide
LSM	laser scanning microscopy

LysoPL	lysophospholipid
MALDI-TOF	matrix-assisted laser desorption ionization time of flight
MPO	myeloperoxidase
MPTP	1-methyl-4-phenyl-1,2,3,6-tetrahydropyridine
MS	multiple sclerosis
MTT	3-(4,5-dimethyl-2-thiazolyl)-2,5-diphenyl-2H-tetrazolium bromide
MβCD	methyl-β-cyclodextrin
NBD-SM	N-[12-[(7-nitro-2-1,3-benzoxadiazol-4-yl)amino]dodecanoyl]-sphingosine-1-phosphocholine
NGF	nerve growth factor
NHS	N-hydroxysuccinamide
NICI	negative ion chemical ionization
NPD	Niemann-Pick disease
nSMase	neutral sphingomyelinase
NY	nystatin
PAGE	polyacrylamide gel electrophoresis
PAPC	1-palmitoyl-2-arachidonoyl-*sn*-glycer-3-phosphocholine
PARP	poly (ADP-ribose) polymerase
PC	phosphatidylcholine
PCD	programmed cell death
PD	Parkinson's disease
PE	phosphatidylethanolamine
PFB	pentafluorobenzyl
PI	phosphatidylinositol
Pi	propidium iodide
PICI	positive ion chemical ionization
PKA	protein kinase A
PKB	protein kinase B
PKC	protein kinase C
PL	phospholipid
PLPC	1-palmitoyl-2-linoleoyl-*sn*-glycer-3-phosphocholine

PM	plasma membrane
PMA	phorbol myristate acetate
POPC	1-palmitoyl-2-oleoyl-*sn*-glycer-3-phosphocholine
PRDX	peroxiredoxin
PS	phosphatidylserine
PTP	permeability transition pore
PYRENE-SM	10-(1-pyrene)decanoyl-sphingosyl-1-phosphocholine
ROS	reactive oxygen species
RT	room temperature
S1P	sphingosine-1-phosphate
SAPC	1-stearoyl-2-arachidonoyl-*sn*-glycero-3-phosphocholine
SL	sphingolipid
SLPC	1-stearoyl-2-linoleoyl-*sn*-glycero-3-phosphocholine
SM	sphingomyelin
SMase	sphingomyelinase
SMS	sphingomyelin synthase
SOPC	1-stearoyl-2-oleoyl-*sn*-glycero-3-phosphocholine
Sph	sphingosine
SphK	sphingosine kinase
SPPase	sphingosine-1-phosphate phosphatase
SPT	serine palmitoyltransferase
sSMase	secreted sphingomyelinase
TBS	Tris-buffered saline
TFA	trifluoroacetic acid
TGN	*trans*-Golgi network
TLR	toll-like receptor
TMS	trimethylsilyl
TNFR	tumor necrosis factor receptor
TNFα	tumor necrosis factor alpha
TRADD	TNF-receptor associated death domain

ABSTRACT

Normal brain function depends on a delicately balanced set of remarkably diverse lipids. Consequently, short- and long term alterations in brain lipid composition during neuroinflammatory conditions associated with oxidative stress are casually involved in central nervous system (CNS) disorders (e. g. Alzheimer's disease, Parkinson's disease, multiple sclerosis, stroke, or traumatic brain injury). Within the different cerebral lipid subclasses sphingolipids take a central role in the CNS and in particular neuronal function. Consequently dysfunctional brain sphingolipid homeostasis is associated with the development of neurodegenerative diseases. Besides mitochondria, Aβ peptides, redox-active iron, and the NADPH-oxidase complex, recent studies point towards myeloperoxidase (MPO) as a source of reactive oxygen/radical species. After activation of phagocytes, MPO uses chloride ions and hydrogen peroxide generated from superoxide anion radicals to form hypochlorous acid (HOCl). This potent oxidant targets unsaturated lipids to form a battery of chlorinated lipotoxic compounds. Of note, due to the presence of an unsaturated said chain and amide group sphingomyelin (SM) could be subject to modification by MPO-derived HOCl. Therefore this study aimed at investigating SM uptake and metabolism in a neuronal cell line (CATH.a) as well as the impact of SM and HOCl-modified SM (HOCl-SM) on mitochondrial function, cell viability, and proteome alterations of PC12 neurons.

I*n vitro* experiments performed during the present study demonstrate that fluorescently-labeled (BODIPY and PYRENE derivatives) SM and ceramide (Cer) analogues are efficiently internalized by caveolae-mediated endocytosis and metabolized by differentiated and undifferentiated CATH.a cells. SMase-mediated BODIPY-SM hydrolysis is a process starting already at the plasma membrane. SM-derived BODIPY-Cer diffuses into intracellular compartments and accumulates in the Golgi apparatus and the endoplasmic reticulum. In contrast, the majority of BODIPY-SM remains at the extracellular leaflet of the plasma membrane. Intracellular Cer is partially used as SMSase substrate to re-synthesize SM. Another part of the intracellular Cer pool is metabolized to an as yet unidentified polar sphingolipid species that is secreted by the cells.

Using rat pheochromacytoma (PC12) cells I could demonstrate that HOCl-modified SM, generated by HOCl-treatment or enzymatically *via* the MPO/H_2O_2/Cl^- system induces formation of reactive oxygen species in contrast to unmodified SM. Furtherore, HOCl-SM provokes mitochondrial dysfunction, decreases PC12 cell viability, induces the apoptotic machinery, and leads to pronounced proteomic alterations.

In summary, the present study indicates that oxidation/chlorination of SM by MPO-derived HOCl might play a central role in neuronal cell death in CNS-related diseases. These findings may be valuable in understanding the role of MPO-derived oxidants on dysregulated sphingolipid homeostasis as observed in chronic neurodegenerative diseases.

ZUSAMMENFASSUNG

Die intakte Funktion des Gehirns ist von der Balance der im Gehirn vorkommenden Lipide abhängig. Deswegen sind lang- oder kurzfristige Veränderungen in der Lipidzusammensetzung, ausgelöst durch Entzündungen und/oder oxidativen Stress, welche bei Patienten mit akuten oder chronischen neurologischen Erkrankungen (z. B. Alzheimer, Parkinson, Multiple Sklerose bzw. Insult oder traumatischen Hirnverletzungen) auftreten, häufig mit Störungen des Zentralnevensystems (ZNS) verbunden. Unter diesen zerebralen Lipiden kommt der Klasse der Sphingolipide eine besondere Bedeutung zu. Sphingolipide sind essentiell für die Gewährleistung neuronaler Funktionen. Daher ist es nicht überraschend, dass Störungen im Sphingolipid Metabolismus, die eine Veränderung des zellulären Sphingolipid-Musters zur Folge haben, bei der Entstehung und dem Verlauf von neurodegenerativen Erkrankungen eine zentrale Rolle spielen. Unter vielen Systemen die bei der Bildung von reaktiven Spezies bedeutsam sind, nimmt das Enzym Myeloperoxidase (MPO) von Phagozyten eine Sonderstellung ein. Das Enzym kann aus Wasserstoffperoxid in Gegenwart von Cl^- Ionen hypochlorige Säure (HOCl) generieren. Dieses starke Oxidationsmittel kann mit ungesättigten Lipiden interagieren, diese oxidieren und dabei chlorierte, lipotoxische Verbindungen bilden. Das Phospholipid Sphingomyelin (SM) aus der Klasse der Sphingolipide besitzt eine ungesättigte Seitenkette sowie eine Amid-Bindung und ist somit ein potentielles Target für HOCl. Ziel dieser Studie war es, die Aufnahme und Metabolisierung von SM in einer neuronalen Zelllinie (CATH.a) zu untersuchen. Weiters sollte geprüft werden, ob SM oder durch HOCl oxidiertes SM (HOCl-SM) cytotoxische Eigenschaften aufweisen. Dabei sollte nach Inkubation mit HOCl-SM nicht nur die Viabilität von PC12 Zellen, sondern auch deren mitochondriale Funktionalität sowie Änderungen im Proteom dieser Zellen untersucht werden.

In *in vitro* Experimenten konnte dabei gezeigt werden, dass differenzierte sowie undifferenzierte CATH.a Zellen effizient fluoreszierende SM- und Ceramid (Cer) Analoga über Caveolae-vermittelte Endozytose aufnehmen und diese rasch verstoffwechseln. Dabei wird das grün-fluoreszierende BODIPY-SM bereits an der Plasma Membran durch Sphingomyelinasen hydrolisiert. Das dabei entstandene BODIPY-Cer kann über Diffusion ins Zellinnere gelangen, wobei es sich im Golgi Apparat sowie im Endoplasmatischen Reticulum anhäuft, wohingegen BODIPY-SM vermehrt an der extrazellulären Seite der Plasma

Membran zu finden ist. Endozytiertes Cer dient einerseits zur Synthese von SM, andererseits zur Synthese einer bis jetzt unbekannten, polaren Sphingolipid Spezies, welche umgehend von den Zellen sekretiert wird.

Weiters konnte ich in dieser Arbeit zeigen, dass hypochlorit-modifiziertes SM, im Gegensatz zu SM, die Bildung reaktiver Sauerstoff-Spezies in PC12 Zellen bewirkt. Dabei konnte bewiesen werden, dass dieses modifizierte Lipid negative Auswirkungen auf die Viabilität und mitochondriale Funktion der Zellen aufweist und Apoptose sowie Änderungen im Proteom initiieren kann.

Zusammenfassend lässt sich sagen, dass die Generierung von HOCl-SM durch das Enzym MPO eine entscheidende Rolle bei Erkrankungen des ZNS spielen könnte. Um bei der Entstehung und dem Verlauf von akuten sowie neurodegenerativen Erkrankungen entgegenwirken zu können, bedarf es deshalb einer genauen Untersuchung der zytotoxischen Wirkunsweise von HOCl-SM.

I. INTRODUCTION

1. SPHINGOLIPID METABOLISM

Normal brain function depends on a delicately balanced set of remarkably diverse lipids. Consequently, short- and long term alterations in brain lipid composition during neuroinflammatory conditions associated with oxidative stress are casually involved in central nervous system (CNS) disorders (e. g. Alzheimer's disease (AD), Parkinson's disease (PD), multiple sclerosis (MS)) or traumatic brain injury. Within the different cerebral lipid subclasses sphingolipids (SL) take a central role in CNS and in particular neuronal function. Dysfunctional brain lipid biochemistry that deregulates levels of SL is associated with the development of neurodegenerative diseases (Haughey et al., 2010). The highly divergent group of SL covers sphingosines (Sph), ceramides (Cer), sphingomyelins (SM), and various phosphorylated and glycosylated derivates. In contrast to many other membrane lipids, SL do not contain glycerol as the backbone to which fatty acids (FA) are attached. Instead a FA acyl residue is linked to a long-chain base *via* an amide bound. In addition the enormous variety of head-group modifications makes this lipid class unique compared to other membrane lipids playing important roles in barrier function and endocytic- and signaling processes.

1.1. Sphingolipid Biosynthesis

1.1.1. De novo synthesis

Due to their high abundance in the CNS, SL are often considered as "brain lipids". Their synthesis which follows the secretory pathway is performed by a variety of membrane-embedded enzymes. The first step in SL synthesis is the head-to-head condensation of L-serine and palmitoyl-CoA to form 3-ketosphinganines catalyzed by the enzyme serine palmitoyltransferase (SPT) (Hanada, 2003; Merrill, 2002) (***Figure 1***). In

mammals two gene products are necessary (SPT1 and SPT2) for its activity (Dickson et al., 2000; Gable et al., 2000). Another SPT2-like gene was discovered recently and was also proposed to be involved in SPT activity (Hornemann et al., 2006).

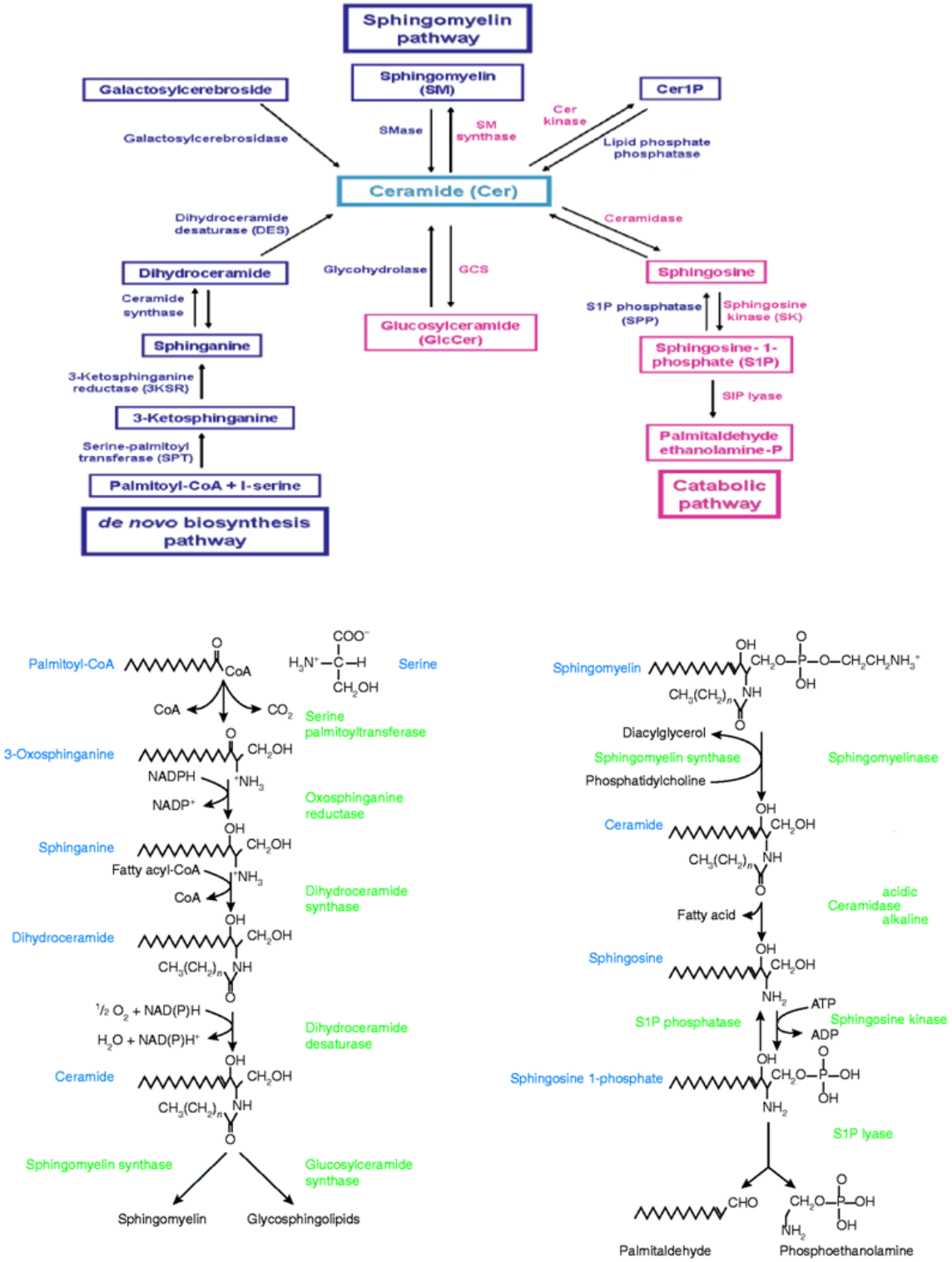

Figure 1: SL metabolism in eukaryotic cells (Mimeault et al., 2008; Pyne and Pyne, 2000)

This irreversible condensation reaction yealding 3-ketosphinganine takes place at the cytosolic surface of the endoplasmic reticulum (ER) and represents the rate limiting step in *de novo* SL biosynthesis (Dickson et al., 2006; Hannun and Obeid, 2008). SPT is responsible for controlling the amount and molecular species of generated Sph bases. Point mutations in SPT2 are associated with hereditary sensory and autonomic neuropathy type I (Chen et al., 2010). Previously it was demonstrated that SPT can also use L-alanine as substrate yielding to the formation of 1-deoxy-sphinganine (Zitomer et al., 2009). Also in respect to the activated FA SPT is able to accept acyl-CoAs other than palmitoyl-CoA, although with a significant lower selectivity. Beside activated palmitic acid (C16) the enzyme can also accept and utilize pentadecanoyl- and heptadecanoyl-CoAs (C15 and C17) and with even lower selectivity also stearoyl-CoA (C18), and as the only exception for an unsaturated acyl-CoA species, palmitelaidic-CoA (C16:1 with a *trans*-double bond) (Chen et al., 2010; Hanada et al., 2000; Williams et al., 1984).

3-Ketosphinganine is then converted to D-*erythro*-sphinganine by 3-ketosphinganine reductase (FVT1) (Mandon et al., 1992). This reduction step is followed by N-acylation *via* a family of ceramide synthases (CerS) yielding dihydroceramides (DHCer) (Pewzner-Jung et al., 2006). So far six different mammalian CerS have been identified, all of them showing differences in substrate specificity and in tissue expression (Lahiri and Futerman, 2005; Laviad et al., 2008; Mizutani et al., 2005) (***Figure 2***). Out of them, CerS1 is mainly found in brain and skeletal muscle, whereas other CerS are predominantly expressed in kidney/liver (CerS2), testes (CerS3), heart/liver/skin/leucocytes (CerS4), lung and epithelia (CerS5), and in the intestine (CerS6) (Laviad et al., 2008; Riebeling et al., 2003; Stiban et al., 2010). In respect to their preferred fatty acyl-CoAs CerS1 shows specificity for C18 and C18:1, CerS2 for C20, C22, C24, C24:1, and C26, CerS3 for C26 and higher, CerS4 for C18 and C20, CerS5 for C14, C16, C18, and C18:1, and CerS6 for C14, C16, and C18 (Lahiri and Futerman, 2005; Stiban et al., 2010; Venkataraman et al., 2002).

All CerS can utilize either sphinganine from the biosynthetic pathway or Sph from SL recycling as long chain base (LCB) substrates (Stiban et al., 2010). Therefore, Cer can be synthesized in a *de novo* pathway or *via* the *salvage pathway* using Sph as substrate (van Echten-Deckert and Herget, 2006). The proof that Sph is not a *de novo* intermediate was first demonstrated in neuroblastoma cells (Rother et al., 1992). The reacetylation of Sph to

form Cer is often observed in neurons, astrocytes, and neuroblastoma cells (Riboni et al., 1999; Riboni et al., 2000).

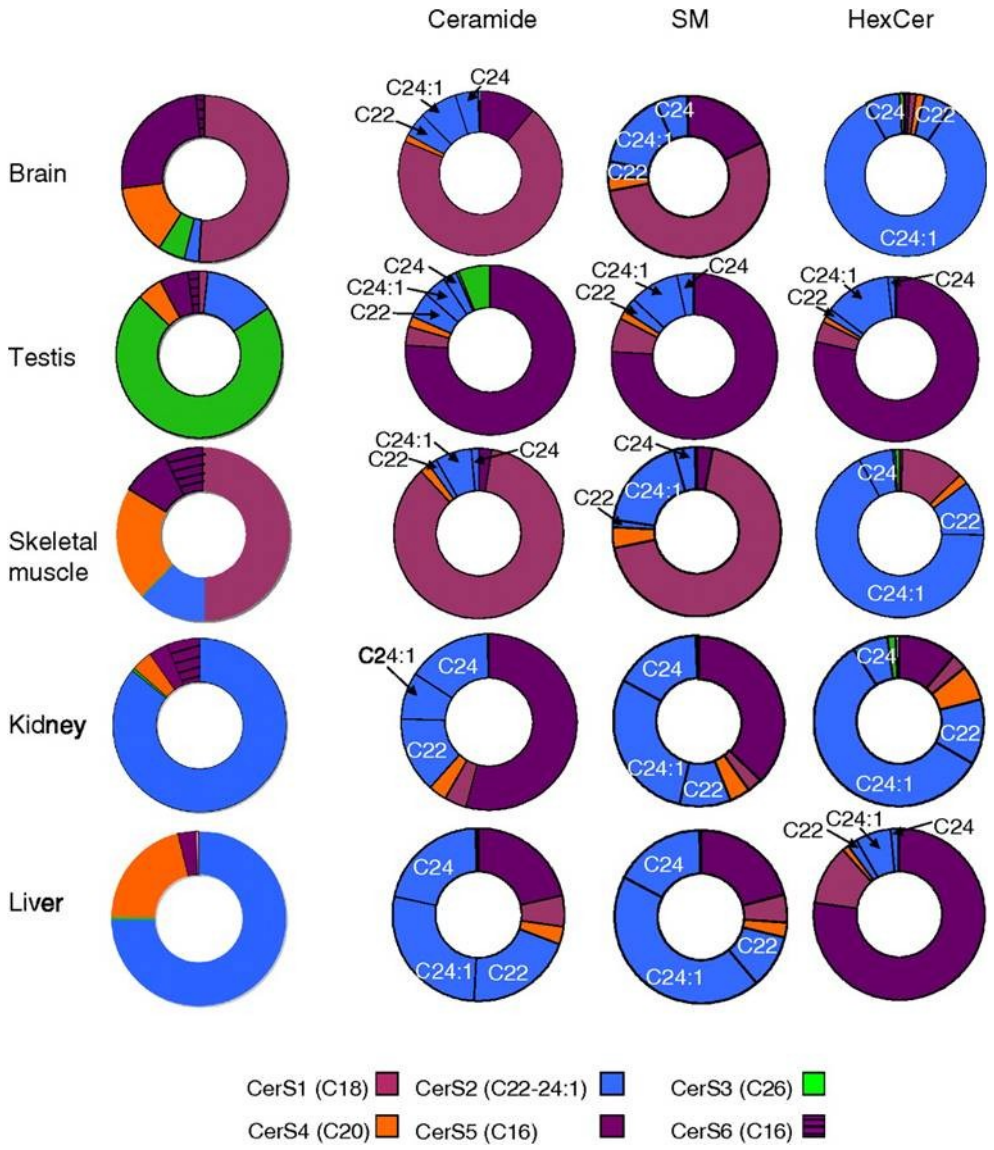

Figure 2: mRNA expression of CerS and distribution of respective SM, Cer, and monohexosylceramides (HexCer) species in specific mouse tissues (taken from Laviad et al., 2008)

Once synthesized, DHCer can be converted to Cer *via* insertion of a 4,5-*trans*-double bond into the backbone of the LCB (sphinganine backbone) catalyzed by the enzymes dihydroceramide desaturases 1 and 2 (DES1 and DES2) (Michel et al., 1997). In mammals DES1 exhibits only desaturase activity whereas DES2 can also perform 4 hydroxylation catalyzing the formation of phytoceramides (Omae et al., 2004).

1.1.2. The salvage pathway

Cer represent the branching point in SL metabolism and its most important functions as a central lipid second messenger molecule will be discussed below. In the ER Cer can be hydrolyzed *via* ceramidase – also present in lysosomes and other membranes – generating LCB Sph (Linke et al., 2001b; Tani et al., 2005). This reaction is reversible and Sph can be further utilized to generate Cer or can undergo phosphorylation *via* Sph kinases (SphK1 and SphK2) yielding the potent lipid second messenger sphingosine-1-phosphate (S1P) (Maceyka et al., 2009; Maceyka et al., 2005). In this reaction SphK1 is responsible for generation of S1P and concomitantly for inhibition of *de novo* Cer synthesis whereas SphK2 presumably acts in concert with S1P phosphatase (SPPase) to convert S1P back to Sph (Maceyka et al., 2005). S1P is a potent lipid mediator regulating cell signaling regulating growth, survival, differentiation, angiogenesis, and motility (Anliker and Chun, 2004; Saba and Hla, 2004; Spiegel and Milstien, 2003). Therefore, cellular S1P levels are tightly controlled by synthesis, dephosphorylation *via* SPPases, and degradation *via* irreversible cleavage mediated by ER localized S1P lyase leading to generation of the respective alkyl aldehyde (mostly hexadecenal) and phosphoethanolamine.

Cer can be further transported to the Golgi apparatus where synthesis of the more complex SL is accomplished. To reach the Golgi, Cer which exhibits very low solubility in an aqueous environment can be either transported *via* vesicular- or non-vesicular transport mechanisms the latter involving the ceramide transfer protein (CERT) (Funato and Riezman, 2001; Hanada et al., 2003). In the vesicular transport mechanism Cer is transported in a coatomer protein- and tubulin-dependent way (Palmer et al., 2005; Watson and Stephens, 2005) and presumably represents the major pathway for Cer transport to the *cis*-Golgi for glycosphingolipid synthesis.

In CERT-dependent transport the protein that contains at least four functional domains is responsible for (i) recognizing of donor and acceptor membranes (ER and Golgi) as well as for (ii) substrate binding during direct transfer of Cer to the Golgi (Gault et al., 2010). Thereby, CERT shows differences in substrate specificity according to FA residue and the LCB backbone. CERT displays preferences for acyl chains of <C22 and exhibits lower specificity for phyto- and DHCer (Kudo et al., 2008; Kumagai et al., 2007).

1.1.3. Synthesis of complex SL in the catabolic pathway

Once transported to the Golgi apparatus, Cer can be converted to complex SL. The simplest species out of them are represented by ceramide-1-phosphate (Cer1P) generated *via* cermide kinase (Van Overloop et al., 2006), ceramide phosphoethanolamine generated *via* a SM synthase 1- (SMS1) related enzyme (Vacaru et al., 2009), 1-o-acyl ceramides (Shayman and Abe, 2000), and SM. The latter lipid which is generated *via* phopshocholine transfer mediated by SMS1 or SMS2 (Huitema et al., 2004) is a central topic of this thesis and, therefore, SM functions as well as synthesis and degradation of the lipid will be discussed in more detail below.

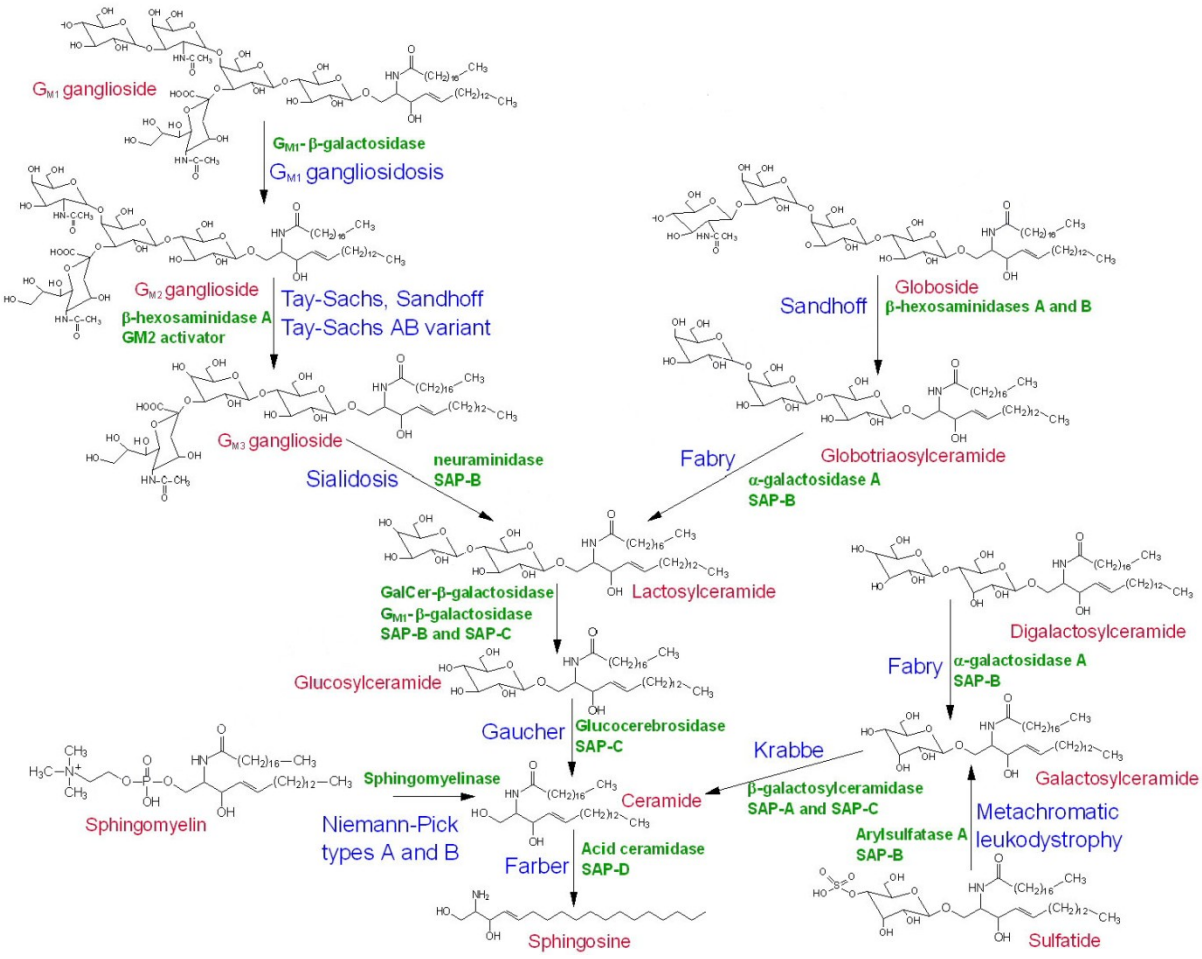

Figure 3: Overview of complex SL structures, enzymes involved in interconversion (green text), and associated diseases (blue text)
(taken from http://themedicalbiochemistrypage.org/images/sphingolipid-degradation.jpg; copyright 2008 Michael W. King, PhD)

In addition, mammalian cells are able to synthesize complex SL (***Figure 3*** and ***4***). The three major enzymes involved in complex SL synthesis are SMS, ceramide galactosyltransferase, and glucosylceramidesynthase. Catalyzing head-group modification of Cer the two latter enzymes are responsible for conversion of galactosylceramide (GalCer) and glucosylceramide (GlcCer), respectively, two monohexosylceramides that represent the starting point for glycosphingolipid (GSL) synthesis. GalCer which is synthesized in the lumen of the ER and its metabolite sulfatide are mainly generated in Schwann cells, oligodendrocytes, testis, kidney, and intestine. Moreover these complex SL are found to be highly enriched in the myelin sheath (up to 30%) of neuronal cells (Baumann and Pham-Dinh, 2001). Mice lacking GlcCer were previously shown to harbor defects in the myelin sheath (unstable myelin leading to demyelination) accompanied with severe motor coordination deficits (Coetzee et al., 1996). These mice contained GlcCer in their myelin sheath which is normally not a component of this cell organelle. These defects in myelination may be due to a lack of sulfatide production *via* sulfotransferases.

GlcCer represents the abundant GSL in most cells and is usually synthesized in the *cis*-Golgi apart from neuronal tissue in which GlcCer is generated in the ER (van Echten and Sandhoff, 1989) (***Fig. 4***). GlcCer are essential SL for the development of mammals (Yamashita et al., 1999). Defects in GlcCer synthesis results in lethality at embryonic day 6.5 - 7.5 in mice. Although the major amount of GlcCer is transported to the plasma membrane (PM) right after synthesis it also represents the precursor for most complex GSL that are synthesized *via* step-wise addition of carbohydrate molecules to GlcCer which mainly occurs in the Golgi apparatus. These complex SL play an essential role in cell-cell recognition during embryonic development (Yamashita et al., 1999). Defects in GSL synthesis prevents normal skin development and provokes dissipation of neuronal function and brain maturation (Jennemann et al., 2007; Jennemann et al., 2005).

After initial glycosylation the GlcCer series branches into the ganglio-, lacto-, neolacto-, globo-, and isogloboseries. Out of these series gangliosides are particularly abundant in the CNS, especially in neurons. These complex SL were shown to be crucial during differentiation of embryonic and mesenchymal stem cells into neuronal cells (Kwak et al., 2006) and in maintenance of axon-myelin stability and function by binding to the myelin-associated glycoprotein (Quarles, 2007). Interestingly, gangliosides of neurons

contain longer sphingoid bases (C20 instead of the usually found C18) which appear upon differentiation of neuronal cells and accumulate with rising age (Sonnino and Chigorno, 2000). All the glycosylation steps leading to formation of complex SL species derived from GlcCer are thought to occur at the luminal site of the Golgi apparatus suggesting a so far unknown "flipping mechanism" for GlcCer from the cytosolic site to the luminal site of the Golgi (Lannert et al., 1994; van Meer and Hoetzl, 2010).

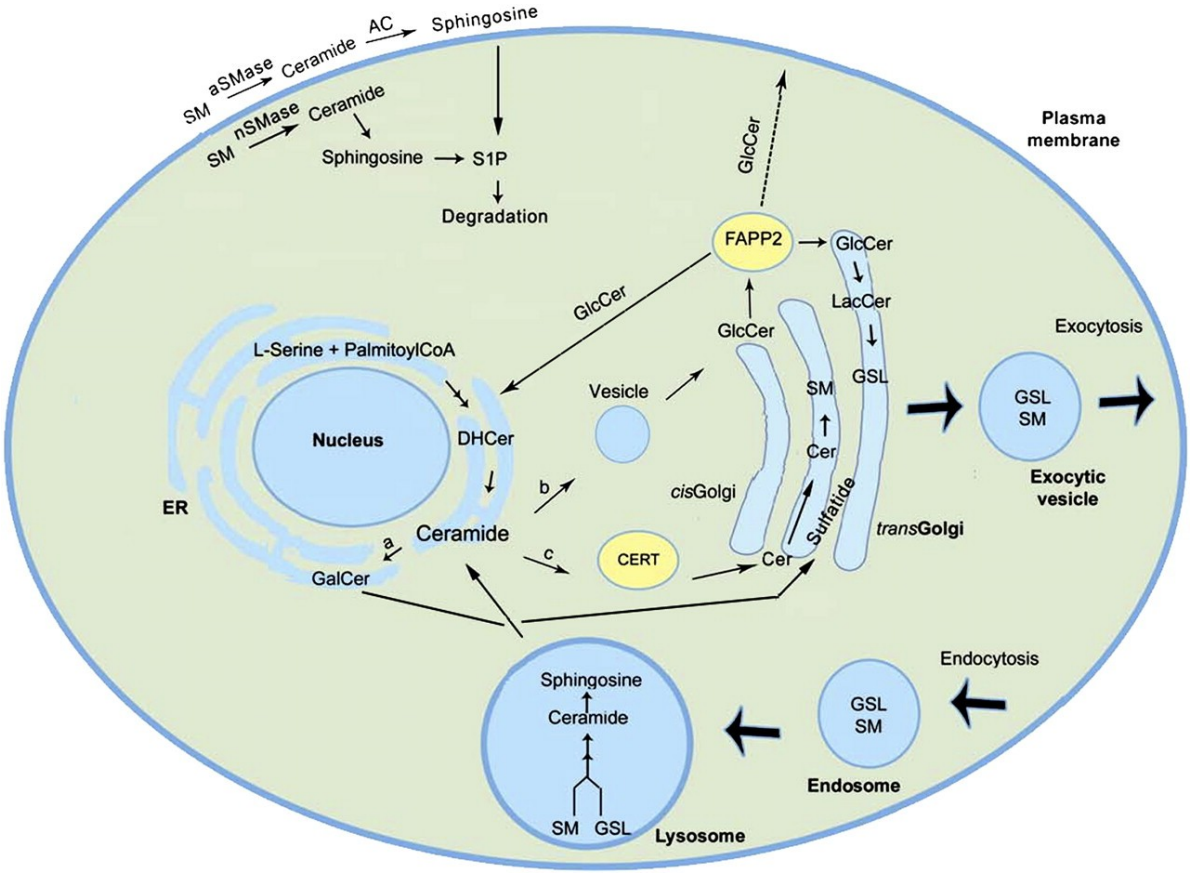

Figure 4: Site of SL synthesis and illustration of their cellular trafficking (taken from Xu et al., 2010)
aSMase, acidic sphingomyelinase; *nSMase*, neutral sphingomyelinase; *AC*, acid ceramidase; *LacCer*, lactosylceramide

Once synthesized GSL are transported to the PM *via* a vesicular transport mechanism where they fulfill their diverse functions. Therefore, these SL are present at the outer-leaflet of the PM while GlcCer is present in both, the extracellular- and intracellular leaflet of the PM (van Echten-Deckert and Herget, 2006).

As mentioned above most reactions in SL synthesis are reversible. Apart from that SL homeostasis is maintained by SL turnover und degradation. In most cases, SL turnover is

mediated by endocytosis of the respective SL from the PM, followed by sorting in early endosomes (***Fig. 4***). From there a part of SL is then recycled to the PM a process which is very often accompanied by remodeling of respective SL species (Steinman et al., 1983; Tettamanti et al., 2003). However, the rest of the SL is transported to the lysosomes leading to degradation *via* specific acid hydrolases (Kolter and Sandhoff, 2006). GSL are catabolized *via* step-wise hydrolysis of the terminal monosaccharides and SM is hydrolyzed to form Cer *via* activation of sphingomyelinases (SMase) which will be discussed below in more detail. Degradation of Cer into less complex SL and the involved enzymes were already discussed above. Defects in these degradation processes are accompanied by the development of lysosomal lipid storage diseases which are schematically summarized in ***Fig. 3***.

1.2. Sphingomyelin

Among all other SL species SM displays a unique character for being the only SL resembling phospholipid (PL)-like properties. Besides amounts of ceramide phosphoethanolamine SM is the only mammalian PL that is not derived from glycerol. SM consists of a Sph base, a FA residue, and a phosphocholine headgroup. As mentioned above, the synthesis of SM occurs mainly in the *trans*-Golgi network (TGN) and, to a lesser extent, at the PM both *via* phosphocholine transfer from phosphatidylcholine (PC) or SM to Cer, mediated in mammalian cells by either by SMS1 or SMS2 (Huitema et al., 2004). Recent observations suggest the existence of a third member in SMS family known as SMS-related protein (Tafesse et al., 2006). SMS1 is located exclusively to the Golgi apparatus, whereas SMS2 is localized at the Golgi and the PM (Huitema et al., 2004; Tafesse et al., 2007). SMS harbor six transmembrane-spanning domains and orientation of their catalytic domain is at the luminal site of the Golgi or faces the extracellular space, respectively. Thereby, SMS1 is the major SMS in eukaryotic cells and is responsible for synthesis of at least 60-80% of total SM (Tafesse et al., 2007). SMS2 only accounts in between 20-40% of total SM synthesis but its primary localization to the PM enables cells to control their SM pool directly at the PM. Therefore, SMS2 may play a crucial role in the maintenance of cellular growth (e. g. pro- and anti-apoptotic stimuli of SM-derived lipids) and signaling processes by regulating the

PM-SM pool in response to extracellular stimuli. SMS1 and SMS2 are able to recognize short-chain synthetic SM analogues (NBD-C_6-SM) as well as naturally occurring SM (C16 - C26) as substrates (Huitema et al., 2004).

Once synthesized, the majority of SM is transported to the PM *via* a vesicular transport mechanism. Like other complex SL, SM is mainly found at the extracellular leaflet (80 - 85% of PM-associated SM; (Whatmore and Allan, 1994)) of the PM due to the fact that SM travels in the luminal site of Golgi-derived vesicles and is not able to flip between the two membrane leaflets (van Meer et al., 2008). Among SL, SM is the most abundant one and can make up to 10% of total mammalian cellular lipids (van Echten-Deckert and Herget, 2006). SM is ubiquitously expressed in tissues and cells but highly abundant in the nervous system, especially in neurons and myelinating oligodendrocytes (Piccinini et al., 2010). SM is an essential lipid in eukaryotic cells; yeast cells cannot survive in culture in the absence of SM due to CERT mutations or defects in *de novo* SL synthesis (Tafesse et al., 2007). As mentioned above the major portion of SM is localized to the PM (up to 23% of total PL) but a minor SM portion was also found in the Golgi (up to 12% of total PL), the ER (up to 4% of total PL), mitochondria (up to 2% of total PL), and lysosomes (up to 22% of total PL) (Koval and Pagano, 1991; van Meer and Holthuis, 2000). In adult mouse brain the SM content is approx. 1 nmol/mg fresh tissue (Scandroglio et al., 2008). In the gray matter SM(d18:1/18:0) predominates whereas in the white matter SM(d18:1/24:1) is the main SM species (Staellberg-Stenhagen and Svennerholm, 1965).

In the PM SM fulfils diverse functions: (i) SM accumulates in the extracellular leaflet and creates a rigid barrier to the environment due to its high packaging density and affinity for cholesterol (Chol). (ii) Together with Chol and other complex SL, SM forms highly specialized membrane microdomains termed lipid rafts. These SM enriched membrane sections serve as specialized platforms for endocytic and signaling events. (iii) SM can be converted to important lipid second-messenger molecules such as Sph, S1P, or Cer *via* activation of SMases as a consequence of biological stimuli. (iv) By influencing the Cer- (pro-apoptotic) and diacylglycerol (DAG) pool (mitogenic) in an opposite way (both lipid mediators are generated during SM synthesis), SM can directly impact on life span and cell proliferation.

In contrast to other PL, SM and other complex SL usually contain longer, saturated (or *trans*-unsaturated) FA acyl chains. Thus, on the one hand, SM and complex SL are able to deeply interdigitate between the leaflets of the PM and on the other hand to form longer, narrower cylinders than PC with comparable chain length (Niemela et al., 2006; van Meer et al., 2008). This phenomenon provides a very tight packing of these lipids adopting the solid 'gel' or s_0 phase which is different from the 'liquid-disordered' or l_d phase (found in membrane domains that contain mostly PC). Tight packaging of SL is a consequence of a direct interaction of SL which is favored by the ability of SL molecules to undergo intermolecular hydrogen bounding (Simons and Vaz, 2004). Hydrogen bonding is also assumed to provoke the preferred interaction of SL with Chol in membranes. However, so far it is not completely clear if this intermolecular interactions or shielding of the non-polar Chol by the SL headgroup is responsible for the preferred SL-Chol packaging (Ikonen, 2008). Nevertheless, fluidity of SL rich domains is increased by sterols thus generating 'liquid-ordered' or l_o domains, thicker membrane domains which coexist with thinner l_d phases (Veatch and Keller, 2005). These l_o domains are called lipid rafts and resemble non-ionic detergent resistant membrane domains (Brown and Rose, 1992) that differ in their lipid and protein composition as well as in their stability from the remaining membrane surface (Pike, 2009). Lipid rafts can determine the lipid environment of membrane associated- or transmembrane proteins localized within the raft by influencing protein-protein interaction. Therefore, these dynamic, liquid-ordered domains display important structures within the cell having essential roles in endocytosis, signal transduction (Becher and McIlhinney, 2005; Manes and Viola, 2006), apoptosis, polarization (Manes et al., 1999), adhesion, migration, cytoskeletal tethering (Viola and Gupta, 2007), synaptic transmission, and maintenance of the blood-brain-barrier (BBB) during leukocyte transmigration (Dodelet-Devillers et al., 2009).

1.2.1. SM processing

In addition to its role as PM lipid and its unique function in generating special membrane domains, the PM-SM pool is of significant importance in signaling processes based on SL-derived lipid second-messengers. *Via* activation of different kinds of SMases in

response to a variety of biological stimuli, SM can be converted to Cer which is the most important lipid second-messenger molecule leading to cell apoptosis, growth arrest, and differentiation. Accordingly, SM hydrolysis can directly affect the SL rheostat where levels of anti-apoptotic S1P and pro-apoptotic Cer regulate cell responses to various stimuli (Breslow and Weissman, 2010). In mammalian cells Cer can be generated either by *de novo* synthesis (i. e. by reacetylation of Sph in the salvage pathway which is also mediated by CerS) or *via* breakdown of SM mediated by SMases. Intracellular Cer levels can also increase by decreasing Cer clearance through inhibition of SMS, glycosylceramide synthase, or ceramidases (Ogretmen and Hannun, 2004). Pathways of Cer generation are highly distinct from each other and Cer synthesis is tightly controlled by different subcellular location of enzymes involved in Cer synthesis or different tissue expression as it is the case for CerS. The latter enzymes are not only characterized by tissue specific expression patterns but also exhibit distinct substrate specificity according to the FA acyl chain as already mentioned above. In contrast, SMases show differences mainly in their subcellular distribution but also display difference in expression levels in different mammalian tissues. In general, SMases can be classified according to their pH optimum into acidic, neutral, and alkaline SMases and are sub-characterized according to their co-factor dependence on divalent cations (Goni and Alonso, 2002; Marchesini and Hannun, 2004). So far four putative SMases have been cloned (SMPD1 – 4): out of these four acid SMase (aSMase; SMPD1) and Mg^{2+}-dependent neutral SMase (nSMase; SMPD3) were shown to be the most important SMases involved in Cer generation due to biological stimuli and are, therefore, best characterized.

The 72 kDa glycoprotein aSMase that shows optimal activity at pH 4.5 – 5, was first described in 1963 (Gatt, 1963). The gene encoding aSMase was cloned in 1992 (Schuchman et al., 1992). Originally, aSMase has been assumed to be localized exclusively in the lysosomes. Recent observations however, report the existence of a secreted form of SMPD1, designated as secreted SMase (sSMase) (Schissel et al., 1996). sSMase arises from differential protein trafficking of a common SMPD1 precursor protein. Although the exact mechanism behind this difference in intracellular trafficking of the SMPD1 precursor is not fully understood yet, aSMase and sSMase show differences according to their *N*-glycosylation pattern (Hurwitz et al., 1994; Schissel et al., 1998b), proteolytic processing (Schissel et al., 1998b), and on their dependence on Zn^{2+}. Whereas aSMase acquires Zn^{2+}

during its maturation and, therefore, its activity is not dependent on addition of further Zn^{2+}, sSMase is sequestered from cellular Zn^{2+} pools and thus requires Zn^{2+} in *in vitro* assays (Schissel et al., 1998b).

sSMase was already shown to be implicated in apoptosis. I. e. elevated levels of sSMase were found in patients undergoing radiation treatment (Sathishkumar et al., 2005), in sepsis (Claus et al., 2005), and in LPS-treated mice (Wong et al., 2000). Recently, sSMase was considered to play a crucial role in early stages of atherosclerosis. The enzyme was shown to hydrolyze SM in aggregated low-density lipoprotein (LDL). The resulting Cer enriched LDL is susceptible to aggregation and, therefore, atherogenic (Schissel et al., 1998a). Moreover sSMase was suggested to be involved in insulin resistance (Gorska et al., 2003), heart failure (Doehner et al., 2007), platelet function (Romiti et al., 2000), and infection/inflammation, respectively (McCollister et al., 2007).

Similar to sSMase, aSMase was also found to translocate to the PM in response to physiological stimuli. aSMase can then hydrolyze SM that is present at the extracellular leaflet of the PM. These stimuli contain UV radiation (Charruyer et al., 2005), cisplatin (Zeidan et al., 2008), phorbol esters (Charruyer et al., 2005; Zeidan and Hannun, 2007), Fas ligand (FasL)/CD95 (Rotolo et al., 2005), and cell wounding (Tam et al., 2010). Thereby, Cer generation promotes apoptosis, cytoskeletal reorganization, activation of pro-apoptotic proteins, and PM repair *via* endocytic mechanisms. Also tumor necrosis factor alpha (TNFα) receptor (TNFR) (Schutze et al., 1992), interleukin-1 (IL-1) (Mathias et al., 1993), irradiation (Paris et al., 2001), and reactive oxygen radicals (Gulbins et al., 1996) were shown to stimulate aSMase within a few seconds.

However, deficiency in aSMase results in severe diseases. Recessive mutations in the *SMPD1* gene are accompanied by the onset of the genetic disorders Niemann-Pick disease Type A or B (NPD-A or NPD-B). NPD-A causes progressive neurodegeneration that leads to death at age 2-3 years (Schuchman, 2010). In contrast, NPD-B patients mostly do not exhibit any neurological abnormalities but may suffer from hepatosplenomegaly, pulmonary insufficiency, and cardiovascular disease (McGovern and Schuchman, 1993). Differences in disease pattern may be caused by different amounts of residual aSMase (Graber et al., 1994). In addition, decreased aSMase activity was also found in patients suffering from Niemann-Pick Type C (NPD-C), which results from mutations in either gene *NPC1* or *NPC2* and is characterized by defects in cholesterol trafficking in endo-lysosomal

vesicles accompanied by accumulation of unesterified cholesterol in these compartments. The low levels of aSMase activity in NPD-C are obviously caused by a post-translational mechanism (Reagan et al., 2000).

In cultured neurons of aSMase knock-out (ASMKO) mice an aberrant distribution of GPI-anchored proteins, important signaling proteins that are preferentially localized to lipid rafts, was identified due to an increased SM content of the PM. Reducing SM levels ameliorated this effect (Galvan et al., 2008). In addition microglia of ASMKO mice were identified with a decrease in IL-1β secretion and microparticle shedding following activation of the ATP receptor P2X7 (Bianco et al., 2009). Additionally synaptic membranes of ASMKO mice showed enhanced levels of SM and Sph which was accompanied with enhanced interaction of docking molecules Munc18 and Syntaxin1 (Camoletto et al., 2009).

Several lipid species such as bismonoacylglycerophosphate (BMP), lysophosphatidic acid (LPA), and phosphatidylinositol (PI) were shown to increase activity of aSMase (Linke et al., 2001a), whereas other lipids (e. g. phoshatidylinositol-3,5-bisphosphate, phosphatidylinositol-3,4,5-trisphosphate) markedly reduce its activity (Testai et al., 2004). Other activity inhibitors of aSMase activity include SM-antimetabolites such as the thiourea SM derivate AD2765 (Darroch et al., 2005) or phenyl SM derivates (Yokomatsu et al., 2003), biological compounds such as scyphostatin (Nara et al., 1999) and its derivates or α-mangostin (Nakagawa et al., 2007), and synthetic agents such as SR33557 (Jaffrezou et al., 1991) and the lysosomotropic inhibitors desipramine, imipramine, and NB6 (Claus et al., 2009; Delgado et al., 2007; Kornhuber et al., 2008; Loidl et al., 2003).

In contrast, nSMase2 (designated as nSMase in this thesis) is an SM hydrolyzing enzyme that exhibits optimal activity at pH 7.4 and requires millimolar concentrations of Mg^{2+} or Mn^{2+}. The 71 kDa membrane bound protein is ubiquitously expressed in mammalian tissue. It was first isolated from mammalian brain a tissue where nSMase exhibits its highest activity. The enzyme consists of a C-terminal catalytic domain and two hydrophobic domains located in the N-terminal region (Hofmann et al., 2000). The definitive subcellular localization of nSMase is still a matter of debate. Several studies identified nSMase to be associated with the Golgi apparatus; these reports have been confirmed using specific Golgi trackers in PC12 and SH-SY5Y neuroblastoma cells (Hofmann et al., 2000). Other studies performed in various cancer cell lines report that overexpressed

nSMase localizes to the PM (Kim et al., 2008; Rutkute et al., 2007). Recent observations suggested that nSMase can translocate from the Golgi to the PM in response to confluence, H_2O_2, and TNFα (Clarke et al., 2007; Levy et al., 2006). From these data one may conclude that nSMase exhibits its hydrolytic properties mainly at the PM. Interestingly, the catalytic domain of nSMase is facing the cytosol, although SM is more or less exclusively localized to the extracellular leaflet of the PM (see above). Since it was shown that nSMase is activated by phosphatidylserine (PS) which is localized to the cytosolic leaflet of the PM (Marchesini et al., 2003) and after demonstrating that a SM pool exists at the inner PM leaflet (Linardic and Hannun, 1994), localization of nSMase is out of debate. Other studies suggest that at the PM nSMase is preferentially localized within lipid rafts. Indeed the enzyme was shown to be activated in these PM compartments in neuronal cell lines after treatment with staurosporine, daunorubicin, and other chemotherapeutic agents (Kilkus et al., 2003). These observations highlight the importance of SM/Chol-rich membrane domains to speciffically regulate enzyme activity.

Similar to aSMase, nSMase is also implicated in apoptosis following treatment with a variety of biological stimuli. Besides the chemicals mentioned above, the enzyme is activated by FasL/CD95 and TNFR1 which both are directed to lipid raft membrane fractions following activation (Milhas et al., 2010). In addition nSMase was shown to be activated by oxidized LDL which is present in atherosclerotic lesions (Chatterjee, 1999). This suggests a potential role of the enzyme in disease progression. Additionally nSMase is activated by CD40 (Segui et al., 1999), by negatively charged lipids including PS, cardiolipin, phosphtidylglycerol, but also by arachidonic acid (Hofmann et al., 2000; Marchesini et al., 2003), IL-1 (Singh et al., 1998), during hypoxia (Yoshimura et al., 1999), by nitric oxide (NO) (Kondo et al., 2002), vitamin D3 (Okazaki et al., 1989), and amyloid-beta (Aβ) (Jana and Pahan, 2004). Cer generated *via* these pathways may act in the executioner phase of the apoptotic cascade as was demonstrated for CD95 engagement (Tepper et al., 2000). Recent studies point towards an upstream-caspase-3 involvement of the lipid second-messenger (Neumeyer et al., 2006) possibly acting upstream of mitochondria (Luberto et al., 2002) but downstream of initiator caspases upon TNFR or CD95 activation (Cuvillier et al., 1998; Dbaibo et al., 1997). Other reports predict a caspase-3-dependent regulation of nSMase (Kondo et al., 2002). Most of these studies have been performed in neuronal cell lines due to high activity of nSMase in these cells.

Novel nSMase inhibitors include natural compounds such as the structural analogues scyphostatin which displays a 50-times lower IC_{50} (1 µM) for nSMase than for aSMase (49 µM), scyphostatin derivates, manumycin A (Arenz et al., 2001), and glutathione (GSH), synthetic inhibitors (e. g. the family of sphingolactones (Wascholowski and Giannis, 2006), aminoguanidine derivates such as C11AG (Amtmann and Zoller, 2005), or GW4869 (Luberto et al., 2002)), as well as by a variety of other SM analogues (for review see (Delgado et al., 2007).

1.2.2. Cer as second messenger

Cer resembles a unique lipid second-messenger molecule. As mentioned above Cer plays a crucial role in apoptosis, cell growth, cell cycle arrest, differentiation, senescence, insulin-resistance, inflammation, atherosclerosis, and neurodegenerative disorders. Cer is generated *via* SM hydrolysis, breakdown of complex SL species, *de novo* synthesis, or *via* the SL salvage pathway.

Cer synthesis correlates with protein levels of the Bcl-2 family, the expression of Bcl-x_S, caspase-9 splice-variants (Chalfant et al., 2002), and the cellular Bax/Bcl-2 content (Sawada et al., 2000). Mitochondrial generation of Cer was shown to contribute to Bax-dependent apoptotic events (Birbes et al., 2005) and the formation of mitochondrial permeability transition pores (PTP) (Kashkar et al., 2005; Pastorino et al., 1999).

In respect to Bcl-2 it was reported that Cer can indirectly influence the phosphorylation status of the anti-apoptotic protein. To ensure its activity, Bcl-2 must become phosphorylated at serine 70 by PKCα which can be inhibited by Cer (Ruvolo et al., 1999). Increased synthesis of Cer results in activation of PP2A which provides an alternative pathway of apoptosis induction. On the one hand PP2A dephosphorylates Bcl-2 thereby inactivating it (Lin et al., 2006) and on the other hand stimulates activation of Bax and release of mitochondrial cytochrome *c* (Xin and Deng, 2006) (***Figure 5***).

Beside the protein family Bcl-2, an involvement of mitochondria in Cer-mediated cell death became more and more evident over the last years. Cer was shown to contribute to mitochondrial PTP formation, accelerate permeabilization of the inner mitochondrial membrane, to interfere with complex III of the mitochondrial respiratory chain, thus

inhibiting oxidative phosphorylation, and to enhance the permeability of the outer mitochondrial membrane, which is accompanied with release of proteins localized in the intermembrane space such as cytochrome *c* (Gudz et al., 1997; Novgorodov et al., 2005; Siskind et al., 2002). In addition Cer can maintain cytochrome *c* in an oxidized state which directly affects the mitochondrial membrane potential ($\Delta\psi_m$), Ca^{2+} release from mitochondria, and the organelle's oxygen consumption (Ghafourifar et al., 1999). However, most studies suggest that Cer can exert its apoptotic effects only when present at mitochondria (Birbes et al., 2001).

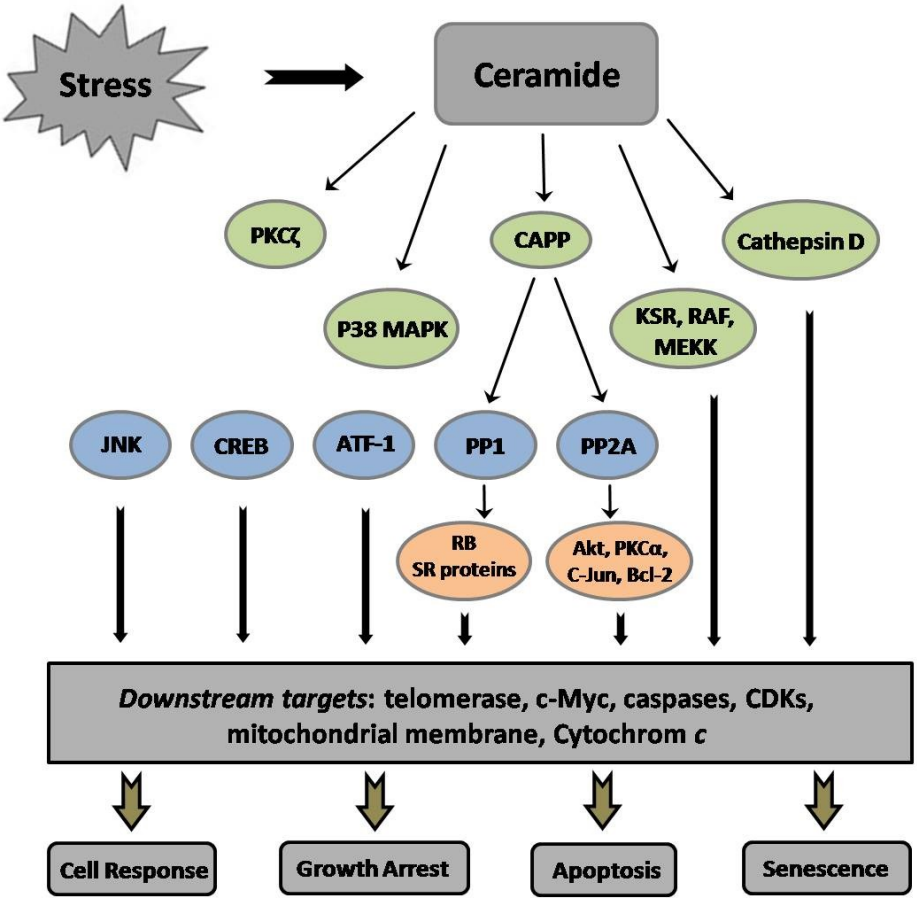

Figure 5: Ceramide signaling pathways
(modified from http://www.fmhs.uaeu.ac.ae/images/Biochemistry/Profile17May2010_5.jpg)

Cer also plays a crucial role in protease-dependent apoptosis. As already mentioned, Cer is acting downstream of initiator caspases but upstream of executioner caspases. In addition, Cer generated *via* aSMase was shown to activate the non-caspase protease cathepsin D (Heinrich et al., 1999) which also represents a cell death protease.

Recent studies revealed that the FA acyl chain length is a major determinant of the biological effects of Cer. Whereas C24 Cer, generated *via* nSMase activation, was shown to induce senescence in confluent MCF-7 cells (Marchesini et al., 2004), C16 Cer leads to apoptosis in a caspase-independent manner after B-cell receptor cross linking (Kroesen et al., 2003).

2. MYELOPEROXIDASE AS A CONTRIBUTOR TO OXIDATIVE STRESS IN THE CNS

Oxidative stress is closely linked to disease progression in neurodegenerative disorders. Due to its high oxygen consumption and a variety of susceptible macromolecules (e. g. unsaturated lipids, proteins, and DNA) the mammalian brain is highly susceptible towards oxidative damage (Halliwell, 2006). Chronic inflammation accompanied by reactive oxygen species (ROS) formation was shown to be an excellent marker for progression of neurodegenerative diseases (Lin and Beal, 2006). Beside mitochondria, Aβ peptides, redox-active iron, and the NADPH-oxidase complex, recent studies point towards myeloperoxidase (MPO) as a source of reactive oxygen/radical species (Yap et al., 2007). Therefore, MPO displays a disease-amplifying enzyme in neurodegenerative processes that also contributes to tissue injury in acute CNS-related diseases such as brain stroke or traumatic brain injury. After activation of phagocytes, MPO uses chloride ions and hydrogen peroxide (H_2O_2) generated from superoxide anion radicals (O_2^-) to form hypochlorous acid (HOCl). This potent oxidant targets unsaturated lipids to form a battery of chlorinated lipotoxic compounds. Of note, due to the presence of an unsaturated said chain and amide group SM could be subject to modification by MPO-derived HOCl. This reaction might be of particular importance in MS where MPO was localized to demyelinating areas (Chen et al., 2008).

2.1. Synthesis and processing

MPO was originally isolated from canine pus and purulent fluid from patients that suffered from tuberculous empyema (Agner, 1941). Due to its intense green color the

enzyme was first named verdoperoxidase (Agner, 1941). Later observations referred verdoperoxidase to be expressed only in myeloid cells which resulted in renaming of the enzyme to MPO (Yamada and Kurahashi, 1984). As evident from the name, the iron-containing enzyme MPO belongs to the peroxidase family. Like other peroxidases such as thyroid peroxidase, lactoperoxidase, and eosinophil peroxidase MPO uses H_2O_2 as substrate, although all these enzymes were identified to harbor a different source of this reactive oxidant (Hansson et al., 2006).

During differentiation of granulocytes in the bone marrow, only promyelocytes and promyelomonocytes are able to actively synthesize MPO (Gullberg et al., 1999). Differentiation into tissue macrophages is generally accompanied by termination of MPO synthesis (Klebanoff, 2005). However, under certain circumstances MPO expression can be retained in certain types of tissue macrophages. In neutrophilic polymorphonuclear leucocytes (neutrophils) MPO can make up to 5% of the dry weight of the cells (Schultz and Kaminker, 1962). Thereby, MPO is stored in the azurophilic granules of these cells which are heterogeneous regarding to their density and morphology (Bainton et al., 1971; Kinkade et al., 1983). As mentioned above, monocytes also contain MPO-positive granules, however they are fewer in number than in neutrophils (Nichols and Bainton, 1973).

MPO is encoded by a single gene on the long arm of chromosome 17 (Johnson et al., 1987). The synthesis of the MPO glycoprotein starts in the ER resulting in a primary 80 kDa translation product termed preproMPO (***Figure 6***). preproMPO is converted to the 90 kDa apoproMPO by undergoing N-linked glycosylation, cleavage of the signal peptide, and limited deglycosylation. At this stage, apoproMPO associates with the ER-located chaperones calreticulin, calnexin, and ERp57 and is thereby subject of further enzymatic processing. After heme incorporation the enzyme becomes enzymatically active proMPO. At this level, proMPO exits the ER to reach the Golgi and later on late endosomes and granules which are the sites for final processing of MPO. These processes include the proteolytic removal of the propetide, a hexapeptide between the heavy and the light subunits, and a C-terminal serine residue which is followed by cleavage of the two subunits and concomitant dimerization to gain mature MPO. The two monomers are linked *via* a single disulphide bridge and the dimer with a molecular weight of 146 kDa is stored in granules. Part of proMPO is glycosylated with complex carbohydrates in the TGN and,

therefore, escapes granule targeting and becomes constitutively secreted in the extracellular environment as a 90 kDa proMPO monomer (Hansson et al., 2006).

Klebanoff (Klebanoff, 2005) indicated an important role of MPO in killing of ingested microorganism which is based on the release of MPO from azurophilic granules into phagosomes during degranulation in the neutrophil oxidative burst. In this process, highly positive charged MPO (isoelectric point > 10) strongly binds to negatively charged surfaces and, therefore, coats ingested microbes.

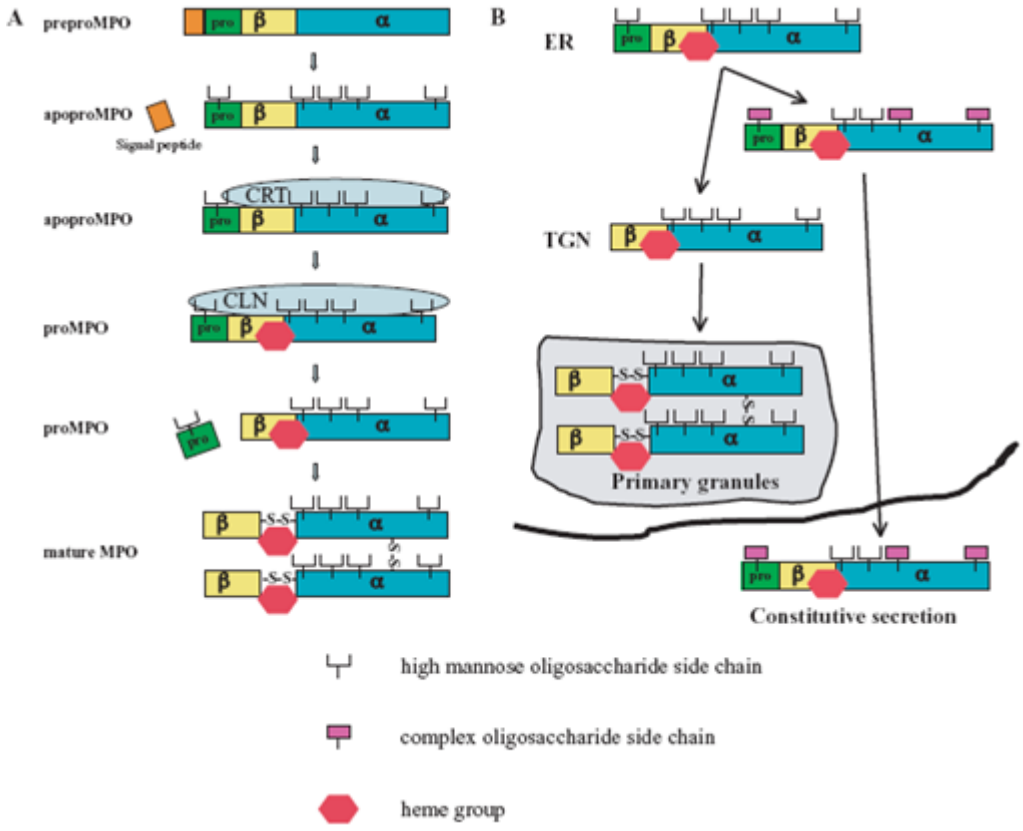

Figure 6: MPO biosynthesis, processing, and trafficking (taken from Hansson et al., 2006)
A: Biosynthesis of mature MPO starting from the preproMPO translation product
B: Processing of MPO in the ER, TGN, and primary granules and its intracellular trafficking. The majority of MPO is stored intracellularly but part of proMPO acquiring complex carbohydrate side chains is constitutively secreted.

In addition, MPO can be released as enzymatically active proMPO (mentioned above), by leakage before complete closure of the developing phagosome, by cell lysis, or in situations that involve phagocytosis of microorganism too large to be ingested, and thereby also contributes to bacterial death (Klebanoff, 2005).

After phagocytosis of microorganism the first stages of the oxidative burst are characterized by activation of the NADPH oxidase (Rossi and Zatti, 1964) and concomitant generation of O_2^- and other ROS. O_2^- can act as an electron acceptor and is, therefore, converted to H_2O_2. Upon releasing MPO from granules into the phagolysosome or the extracellular space, H_2O_2 can be efficiently converted to reactive hypohalous acids (HOX) in the presence of the respective halides (Klebanoff, 1967; Klebanoff, 1968; Klebanoff et al., 1966) according to the chemical formula:

$$\mathbf{H_2O_2 + X^- + H^+ \longrightarrow HOX + H_2O}$$

Under *in vivo* conditions, chloride (Cl^-) concentrations are higher as compared to other halides such as bromide (Br^-), iodide (I^-), or the pseudohalide thiocyanate (SCN^-). Therefore, Cl^- is the most abundant substrate for MPO resulting in the generation of the potent antimicrobial oxidant HOCl that is in equilibrium with its anion hypochlorite (OCl^-) at pH 7.53 (Malle et al., 2007). Beside its halogenation activity, MPO also exhibits peroxidase activity. Halogenation as well as peroxidation reactions start by reduction of H_2O_2 to water leading to the formation of compound I (Arnhold and Flemmig, 2010; Malle et al., 2007) (***Figure 7***). Because of harboring two more oxidizing equivalents than native MPO, compound I is a strong oxidant that can initiate one- or two-electron oxidation reactions. In the halogenations cycle compound I is able to abstract two electrons from halides leading to formation of the corresponding HOX and recycling of compound I to the native enzyme (***Fig. 7***, reaction 2), whereas the peroxidation cycle is characterized by two consecutive one-electron steps *via* the formation of compound II, a protonated oxoiron(IV) species (Malle et al., 2007) (***Fig.7***, reaction 3 and 4). Substrates that are oxidized in the peroxidation cycle by compound I and II include amino acids such as Tyr and Trp, sulfhydryls, nitrite (NO_2^-), xenobiotics, and H_2O_2 (Arnhold and Flemmig, 2010; Furtmuller et al., 2003) and the corresponding products also exhibit antimicrobial properties. Because HOX and MPO-derived peroxidation products resemble highly reactive compounds they are able, depending on the environment, to initiate secondary reactions, thus leading to amplification of the toxic capacity.

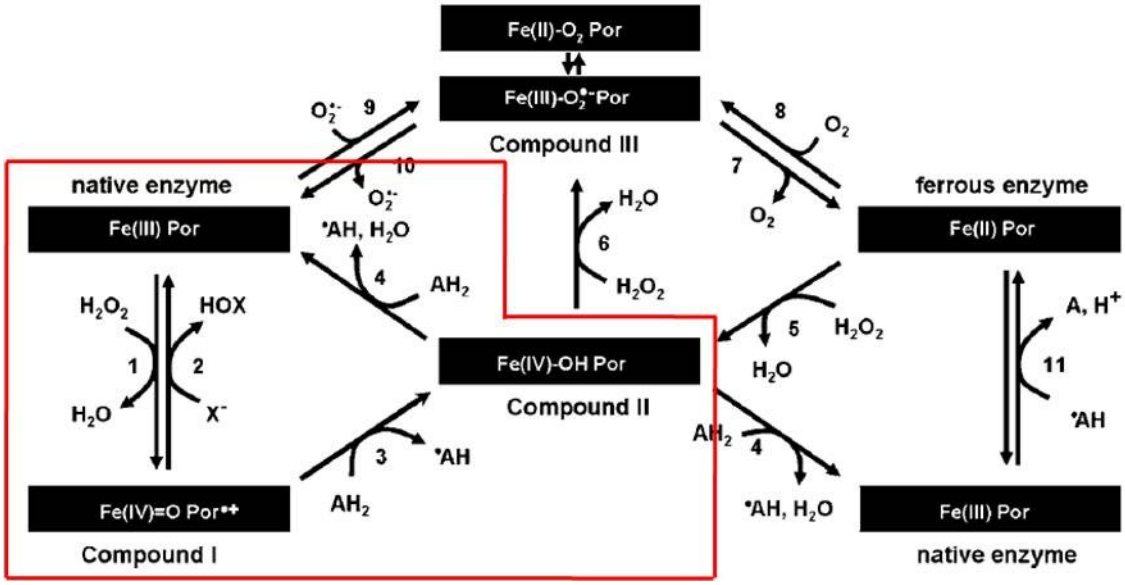

Figure 7: The MPO oxidation cycle (taken from Malle et al., 2007)
The halogenation- and peroxidation cycle is shown in the red polygon.

HOCl was previously shown to interfere with a variety of macromolecules such as lipids, (lipo)proteins, and DNA. Oxidative targeting of these cellular compounds includes mechanisms such as chlorination, nitration, and oxidative cross-linking (Malle et al., 2006). The formation of MPO-derived oxidants is beneficial in immune defense but chronic activation of MPO in activated phagocytes exhibits numerous adverse effects.

2.2. Myeloperoxidase – when a friend becomes a foe

MPO plays a crucial role in host defense because many primary and secondary MPO products act as antimicrobial substances. These substances are toxic to bacteria, fungi, viruses, worms, and protozoa (Klebanoff, 2005). A long time ago it was found that peroxidase inhibitors such as azide, cyanide (CN^-), and sulfonamides decrease the microbicidal activity of activated neutrophils but exhibited little effects on MPO-deficient neutrophils (Koch, 1974; Lehrer, 1971). So-called neutroplasts (neutrophils that hardly contain granules and, therefore, MPO) are able to phagocytose *Staphylococcus aureus* but fail in bacterial killing during the oxidative burst as long as the microorganism is coated with MPO (Odell and Segal, 1988). The role of MPO in bacterial killing can be considered to be more powerful than expected because long-term absence of MPO as it is evident in

neutroplasts stimulates their overall microbicidal activity which was not detected in short-term events when neutrophils were treated with MPO inhibitors (Klebanoff, 2005). Furthermore, $MPO^{-/-}$ mice display enhanced susceptibility to the development of pulmonary infections in response to *Candida albicans*, *C. tropicalis*, *Trichosporon asahii*, or *Pseudomonas aeruginosa* infections (Aratani et al., 2000). In addition $MPO^{-/-}$ mice were shown to be more susceptible to intra-abdominal infection and sepsis following cecal ligation and puncture than their wild-type littermates (Gaut et al., 2001). Recently, in a similar study it was demonstrated that high levels of *C. albicans* provoked the involvement of MPO and oxidants liberated during the oxidative burst in antimicrobial activity whereas at a lower fungal load ROS generated by activation of the NADPH oxidase was identified to be sufficient to control infection (Aratani et al., 2002). Considering that MPO levels in murine neutrophils are approx. 10% of that of human neutrophils it is very likely that MPO is a potential key-player in human host-defense. Further, the $MPO/H_2O_2/Cl^-$ system exhibits toxicity towards HIV-1 which clearly depends on the generation of H_2O_2 (Klebanoff and Kazazi, 1995). MPO also contributes to detoxification of certain microbial toxins such as diphtheria and tetanus toxin (Agner, 1950).

However, beside all these beneficial aspects, excessive generation of MPO products is often accompanied by tissue injury. In particular in settings of chronic inflammation that are characterized by sustained MPO activation primary and secondary MPO-derived oxidants can cause cell and tissue injury. The highly positive charged MPO protein is able to bind negatively charged surfaces (e. g. membranes, proteins). The level of MPO-derived ROS mediated damage is strongly determined by the presence of scavengers. In serum, proteins such as albumin readily react with primary MPO-derived oxidants which results in prevention of oxidative damage to more sensitive targets. Thereby, highly reactive primary MPO products such as HOX, halogens, or peroxidation products act mostly at the site of MPO location, whereas secondary MPO products of lower reactivity (e. g. chloramines, chloramides, chlorohydrins) as well as MPO substrates such as H_2O_2 can penetrate and exert their toxic effects at longer distances.

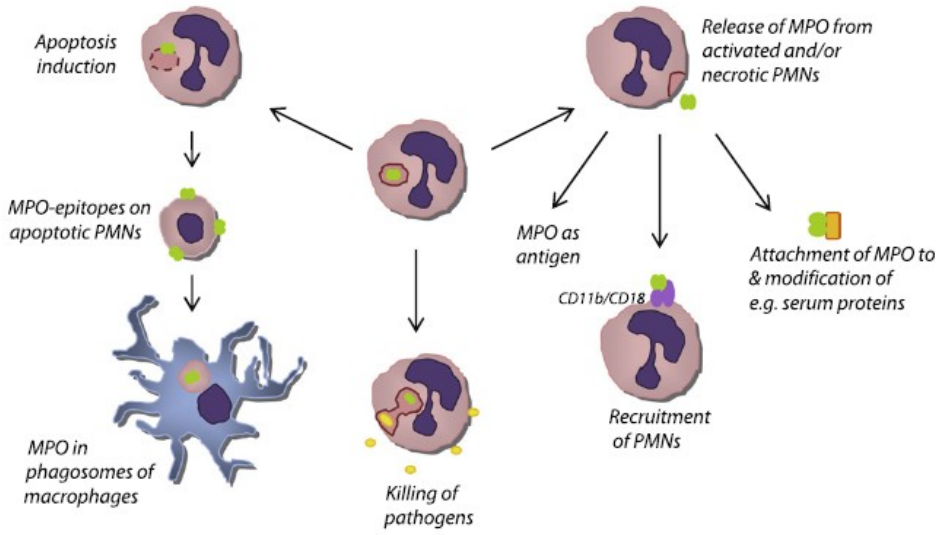

Figure 8: (Patho)physiological roles of MPO at inflammatory sites (taken from Arnhold and Flemmig, 2010)

It is well established that activation of MPO is closely linked to the development of cardiovascular diseases (CVD). MPO was indicated to play a crucial role in disease progression of atherosclerosis, a driving force for CVD. Enzymatically active MPO was isolated from human atherosclerotic arteries (Daugherty et al., 1994) and the HOCl-derived DNA marker 5-chlorouracil was detected in atherosclerotic tissue (Takeshita et al., 2006). Moreover, 3-chlorotyrosine (3-chloro-Tyr) a specific biomarker for MPO-induced oxidation was found to be enriched in atherosclerotic lesions and also in lesion-derived lipoproteins (e. g. LDL and high-density lipoprotein (HDL)) (Hazen and Heinecke, 1997; Zheng et al., 2004). In this respect, oxidative modification of lipoproteins by MPO-derived products is implicated in development of atherosclerosis. Using a monoclonal antibody against HOCl-modified proteins/epitopes (Malle et al., 1995) it was demonstrated that the major apolipoprotein of LDL, apolipoprotein B-100 (apoB-100) resembles a target for oxidative modification *via* the MPO/H_2O_2/Cl^- system of activated phagocytes in lesion material (Hazell et al., 1996). The higher the HOCl:LDL molar ratio the lower was the capacity of LDL to bind to the LDL-receptor. However, HOCl-modified LDL (HOCl-LDL) is recognized by several scavenger receptors on macrophages resulting in uncontrolled lipid uptake and foam cell formation as a further consequence (Malle et al., 2006; Marsche et al., 2003). Recently, protein carbamylation was identified to enable LDL to bind to macrophage-scavenger receptor class A, thus rendering the lipoprotein atherogenic (Wang et al., 2007). In addition, MPO also contributes to oxidative modification of antiatherogenic HDL which

mediates cholesterol efflux from macrophages *via* adenosine 5'-triphosphate-binding cassette transporter A1 (ABCA-1). HDL isolated from atherosclerotic plaques as well as circulating HDL from patients that suffer from coronary artery disease exhibited elevated nitro- and chloro-Tyr content in their apolipoprotein moiety in particular in apoA-1 (Pennathur et al., 2004; Zheng et al., 2004). Thereby, chlorination of Tyr-192 of apoA-1 impairs ABCA-1 binding and, hence, cholesterol efflux (Shao et al., 2005) which also contributes to the maintenance and/or progression of the inflammatory process.

Beside its role in generation of oxidatively modified lipoproteins MPO also contributes to endothelial dysfunction which is a major complication in CVD (Targonski et al., 2003). Furthermore, MPO can locally oxidize NO which acts as regulator of endothelial function (van der Veen et al., 2009).

2.3. The role of MPO in CNS-related diseases

Breckwoldt and colleagues (Breckwoldt et al., 2008) used an enzyme activatable magnetic resonance imaging agent to follow *in vivo* kinetics of MPO activation in a murine stroke model. Using this MPO sensor the authors identified infiltrating neutrophils and microglia/macrophages as sources of cerebral MPO (Breckwoldt et al., 2008). Another study showed that hyperbaric oxygen treatment of rats following middle cerebral artery occlusion decreased MPO activity (Miljkovic-Lolic et al., 2003). This finding was closely associated with smaller infarcts and better neurologic outcome which rather correlated with MPO activity than with infarct volume.

The adverse effects of MPO in diseases (e. g. chronic inflammation) are well documented. As mentioned above, MPO also contributes to tissue injury in neurodegenerative disorders. The enzyme was shown to be upregulated in human PD postmortem brain tissue as well as in the ventral midbrain in a mouse model of PD (Choi et al., 2005). In this model loss of ventral midbrain dopaminergic neurons was modeled by treatment with the neurotoxin 1-methyl-4-phenyl-1,2,3,6-tetrahydropyridine (MPTP) (Choi et al., 2005). Concomitant to increased MPO expression valid MPO biomarkers such as HOCl-modified proteins and 3-chloro-Tyr were also identified in MPTP-treated mice.

Findings that $MPO^{-/-}$ mice were more resistant to the neurotoxin underscore the central role of MPO during disease progression (Choi et al., 2005).

MPO also affects the progression of other neurodegenerative diseases that are characterized by neuronal loss. For instance, elevated levels of MPO were found in caudate nucleus tissue after autopsy from patients that suffer from HD when compared to the control cohort (Choi et al., 2005).

In postmortem sections of AD patients it was demonstrated that microglia that are localized within Aβ plaques contain MPO (Green et al., 2004; Reynolds et al., 1999). These results were strengthened by *in vitro* studies where treatment of rodents with aggregated Aβ increased MPO mRNA expression in microglia. Also inheritance of the ApoE4 allele, the major risk factor that is associated with the formation of Aβ plaques was shown to correlate with increased MPO deposition in Aβ deposits (Reynolds et al., 1999). Recent observations favor the theory that MPO is not exclusively expressed in microglial cells but also in several primary neuronal cultures and neuronal cell lines. The fact that neurons exhibit increased MPO expression in AD brains indicates an involvement of MPO-derived oxidative stress in AD progression (Green et al., 2004). The human MPO -463G allele that is linked to increased MPO expression was found to be associated with a higher risk for AD (Leininger-Muller et al., 2003; Zappia et al., 2004). Previously, expression of this allele was identified in astrocytes of transgenic mice overexpressing human MPO which were crossed to an AD mouse model. In contrast, neither the MPO -463A allele nor mouse MPO was expressed in these cells (Maki et al., 2009). MPO deposition in amyloid plaques was accompanied by increased levels of 4-hydroxynonenal (4-HNE) and PL-specific oxidation products. Behavioral testing revealed significantly greater memory deficits for the MPO overexpressing AD mouse model (Maki et al., 2009).

In MS MPO was detected in macrophages/microglia at lesion sites (Gray et al., 2008b; Nagra et al., 1997). Using a paramagnetic MPO sensor the expression of MPO in areas of inflammation and demyelination as well as the correlation of MPO activity with disease severity was confirmed in experimental autoimmune enzephalomyelitis (EAE), a mouse model for MS (Chen et al., 2008). Recently, cortical demyelination as a matter of elevated MPO activity was also demonstrated in paraffin-embedded postmortem tissue of MS patients (Gray et al., 2008a). In human pattern III lesions and rodent brain lesions caused by focal injection of bacterial lipopolysaccharide (LPS) into the spinal white matter

MPO expression was detected in both, predemyelinating and actively demyelinating areas (Marik et al., 2007). These authors (Marik et al., 2007) concluded that focal activation of microglia leads to generation of reactive species causing mitochondrial dysfunction and hypoxia-like degeneration of surrounding neurons. As a consequence inflammatory processes are augmented due to concomitant severe tissue injury and oligodendrocyte apoptosis and demyelination. Under these conditions, MPO activation occurs in close vicinity to axons and, therefore, myelin associated proteins and/or lipids are likely targets for oxidative damage caused by the MPO/H_2O_2/Cl^- system.

2.4. Secondary MPO metabolites

As already mentioned MPO and MPO-derived oxidants can oxidatively modify a variety of macromolecules including proteins, lipids, nucleic acids, vitamins, antioxidants, and others. An overview of primary and secondary MPO metabolites is shown in ***Figure 9***.

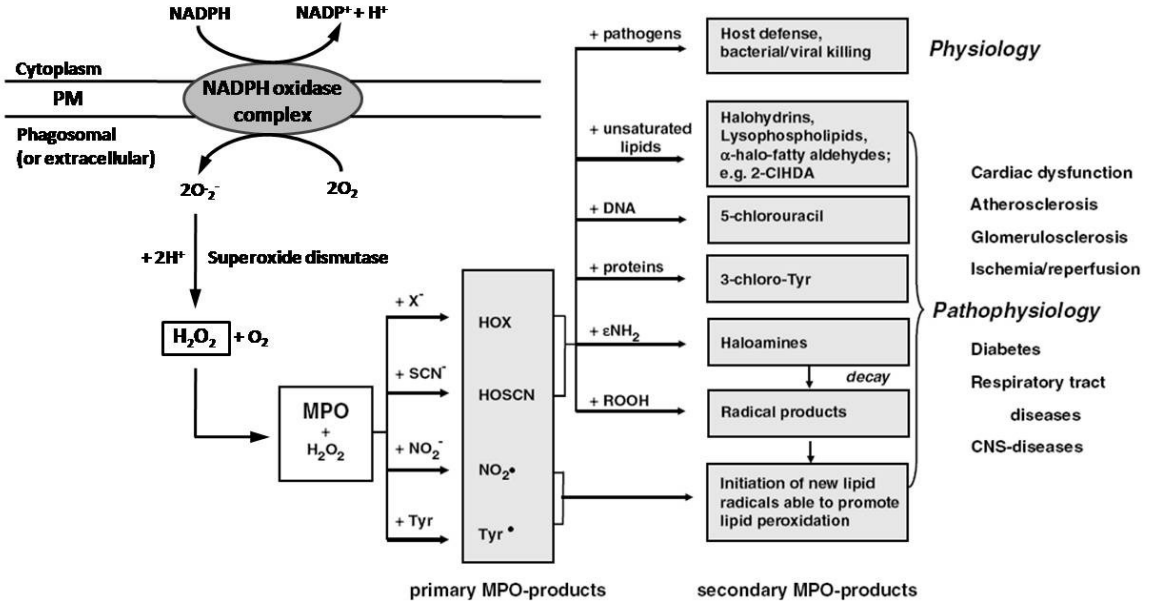

Figure 9: The NADPH oxidase – MPO system and primary and secondary MPO products of (patho)physiological significance (modified from Malle et al., 2007)

MPO can oxidize halides and pseudohalides (predominantly Cl^-, Br^-, and SCN^-) that bind to the heme-iron or are in close vicinity (Malle et al., 2006) using H_2O_2 generated *via*

NADPH-oxidase activation in the initial phase of the oxidative burst of activated phagocytes (***Fig. 9***). Considering the different selectivity of MPO towards these anions ($SCN^- > Br^- > Cl^-$) that occur at physiological plasma concentrations of 100-140 mM (Cl^-), 20-100 µM (Br^-), and 20-120 µM (SCN^-) approx. 45% of H_2O_2 consumed by MPO accounts for HOCl formation whereas 5% and 50% are used to generate HOBr and HOSCN, respectively (Pattison and Davies, 2006; van Dalen et al., 1997). However, absolute concentrations of these HOX strongly depend on the tissue environment and HOCl and HOSCN can be considered to be only ones with high biological significance. In scope of this thesis I will mainly focus on the reaction of HOCl with macromolecules. All these reactions are strongly pH dependent because the reactivity of the anions is considered to be much lower compared to the acid (pK_a HOCl = 7.59) (Pattison and Davies, 2006). Therefore, a lower pH as present in inflammatory lesions sites favors halogenations of substrates.

2.4.1. Proteins

In a physiological environment the substrates for HOCl-mediated oxidation/chlorination are lipids and proteins (e. g. > 95% of HOCl reacts with apoB-100 during HOCl-mediated LDL oxidation; (Pattison et al., 2003)). A number of studies investigated the reactions of HOCl with peptides as well as with selected amino acids (Fu et al., 2002; Pattison and Davies, 2001; Winterbourn, 1985). In one study Pattison and Davies (Pattison and Davies, 2001) determined second-order rate constants for the reaction of HOCl with all reactive sites within a protein. The sulfur-containing amino acids Met and Cys react most rapidly with HOCl (k_2 = 3.8 x 10^7 and 3.2 x 10^7 L mol^{-1} sec^{-1}, respectively) leading to formation of Met sulfoxide in case of Met and disulfides and cysteic acid in case of Cys (Hawkins et al., 2003). Also amine groups-containing amino acids such as His and Lys as well as the α-amino groups of free amino acids are highly sensitive to HOCl-mediated oxidation (k_2(His/α-amino groups) = 1.0 x 10^5 L mol^{-1} sec^{-1}, k_2(Lys) = 5 x 10^3 L mol^{-1} sec^{-1}) (Pattison and Davies, 2001). Products of these reactions are unstable, reactive chloramines that can induce secondary reactions leading to tissue damage (Pattison and Davies, 2005). A more complex but also fast reaction is HOCl-mediated modification of Trp whereas oxidation of other amino acids occurs with much slower second-order reaction rates. Oxidation of Tyr

leads to formation of 3-chloro-Tyr, 3,5-di-chloro-Tyr and, to a lesser degree, to generation of *o-o'* dityrosine (Pattison and Davies, 2006). In contrast to other potential biomarkers of HOCl-mediated protein oxidation such (e. g. chloramines), 3-chloro-Tyr and 3,5-di-chloro-Tyr are the only stable products after protein modification and especially 3-chloro-Tyr is widely used to detect MPO activation *in vivo* (Domigan et al., 1995). Other potential stable oxidation markers such as Met sulfoxide and cysteic acids can be generated also by several other oxidants. Tyr can be directly oxidized by MPO using H_2O_2 to form Tyr radicals which can induce dityrosine formation (Jacob et al., 1996), generation of Tyr peroxides (Winterbourn et al., 1997), or initiation of lipid peroxidation (Malle et al., 2007). Although rather slow, this reaction leads to protein backbone modification, crosslinks, and formation of chloramides (from Asn and Gln residues) with similar chemical properties as observed for chloramines (Prutz et al., 2000). The kinetics of this reaction strongly depends on the environment of the amide group. Negatively-charged groups in vicinity of the amide group provoke a decrease in reaction rate whereas amide groups of cyclic molecules react more rapidly with HOCl. Therefore, second-order reaction rates vary from 10^{-3} to 25 L mol^{-1} sec^{-1} (Pattison and Davies, 2001). Taken together the susceptibility of protein amino acids towards HOCl modification decreases as follows: Met > Cys >> cystine ~ His ~ α-amino group > Trp > Lys >> Tyr ~ Arg > backbone amide ~ Gln ~ Asn (Pattison and Davies, 2001). Therefore, HOCl at low concentrations is predicted to target sulfur containing amino acids whereas higher HOCl concentrations promote formation of reactive chloramines when Met and Cys side-chains within the protein are fully oxidized (Pattison and Davies, 2001; Pattison et al., 2009).

Oxidative modifications can result in the generation of dysfunctional proteins. For instance, oxidation of Met and nitration and bromination of Tyr residues of serum albumin after MPO binding enables the complex to bind the endothelium followed by transcytosis (Tiruppathi et al., 2004; Willard et al., 2003). Ceruloplasmin was shown to exacerbate inactivation and clearance of extracellular MPO, whereas oxidation of critical Met residues of α_1-antitrypsin by MPO leads to loss of neutrophil elastase inactivation (Arnhold and Flemmig, 2010). The contribution of MPO in oxidation of apoB-100 of LDL and apoA-1 of HDL leading to foam cell formation or defective cholesterol efflux from macrophages was discussed above. In addition secondary MPO products generated during protein oxidation such as chloramines can fuel further oxidative damage. These rather long-living reactive

halogenated nitrogen species that can diffuse in and between cells preferentially target, similar to HOCl, thiol groups of proteins leading to enzyme inactivation, modulation of apoptotic pathways, and/or cell death (Arnhold and Flemmig, 2010; Pattison and Davies, 2006). Chloramines can induce various other secondary reactions like e. g. auto-hydrolysis to aldehydes that can form Schiff bases with proteins and lipids (Pattison and Davies, 2006). Chloramines can transform to centered radicals that can initiate lipid peroxidation (Malle et al., 2007; Spickett, 2007).

2.4.2. Antioxidants

Various compounds are able to scavenge MPO-derived oxidants. The most powerful antioxidants are thiol containing molecules. The major cellular antioxidant, reduced GSH, reacts with HOCl with comparable second-order kinetics as Cys (Peskin and Winterbourn, 2001). This leads to generation of the oxidized disulphide form of glutathione (GSSG) and of glutathione sulfonamide (Winterbourn and Brennan, 1997). Also GSSG itself and taurine, (present at high concentrations in neutrophils (20 mM)) are efficient HOCl scavengers (Pattison and Davies, 2006). In addition, amine containing compounds such as histamine (100 mM in mast cells) and carnosine (up to 20 mM in human skeletal and cardiac muscle) readily react with HOCl to form chloramines (Pattison and Davies, 2006). Though, halogenation of these compounds is associated with adverse side effects due to the toxicity of released products. Furthermore, water-soluble substances such as ascorbate (Vitamin C) and, to a lesser degree, urate represent favourable antioxidants with high second-order rate constants towards HOCl modification (Pattison and Davies, 2006). In contrast, lipid-soluble compounds such as α-tocopherol, ubiquinole-10, or β-carotene were identified to react with HOCl although they exhibit lower second-order kinetics (10^3 to 10^4 L mol^{-1} sec^{-1}) and are present in lower concentrations. Therefore, these compounds play minor roles in HOCl scavenging (Pattison and Davies, 2006).

2.4.3. Lipid targets

Beside proteins, lipids resemble potential targets for HOCl modification especially in an environment which is rich in unsaturated lipids (e. g. the brain). PL, free FA (FFA), and Chol were shown to be readily oxidized by HOCl, added as a reagent or generated enzymatically *via* the MPO/H_2O_2/Cl^- system (Albert et al., 2001; Arnhold et al., 2001; Carr et al., 1996; Winterbourn et al., 1992). Thereby, reactions of HOCl with unsaturated lipids can lead to the formation of chlorohydrins or PL modified at the headgroup (Spickett, 2007).

HOCl specifically targets the double bond in the second ring of Chol to form α- and β-chlorohydrins as well as other chlorinated products which were identified *in vitro* after HOCl treatment of Chol as well as in LDL and cell membranes after HOCl incubation (Spickett, 2007) (***Figure 10***). These chlorinated sterols include 6-β-chloro-cholestane-(3β,5α)-diol, 5-α-chloro-cholestane-(3β,6β)-diol (Carr et al., 1996), and 6-α-chloro-cholestane-(3β,5β)-diol (Carr et al., 1997b). The formation of a dichlorinated Chol molecule (5,6-dichloro-cholestane-3β-ol) is rather because of generation of molecular chlorine (Cl_2) under acidic conditions than a HOCl-dependent modification (Hazen et al., 1996). α- and β-chlorohydrins can decompose to form their respective epoxides (cholesterol 5α,6α-epoxide and cholesterol 5β,6β-epoxide, respectively) (Vissers et al., 1998). Moreover, HOCl was identified to play a crucial role in formation of secosterols found *in vitro* and *in vivo* (Tomono et al., 2011). Thereby, HOCl can induce formation of singlet oxygen in the presence of H_2O_2 which can react with Chol to yield 5α-hydroperoxy cholesterol. Hock-cleavage of this intermediate leads to generation of 3β-hydroxy-5-oxo-5,6-secocholestan-6-al (secosterol-A), 3β-hydroxy-5β-hydroxy-B-norcholestane-6β-carboxaldehyde (secosterol-B), and the corresponding autoxidation- and dehydration products 3β-hydroxy-5-oxo-secocholestan-6-oic acid, 3β-hydroxy-5β-hydroxy-B-norcholestane-6-oic acid, and 3β-hydroxy-B-norcholest-5-ene (***Fig. 10***).

In case of PL, HOCl can attack unsaturated double bonds in FA acyl side chains or PL head-groups. As an exception, plasmalogens, an ether PL class that is particular sensitive towards HOCl modification harbors a vinyl ether bond in the *sn*-1 position that is rapidly oxidized by HOCl (***Fig. 10***).

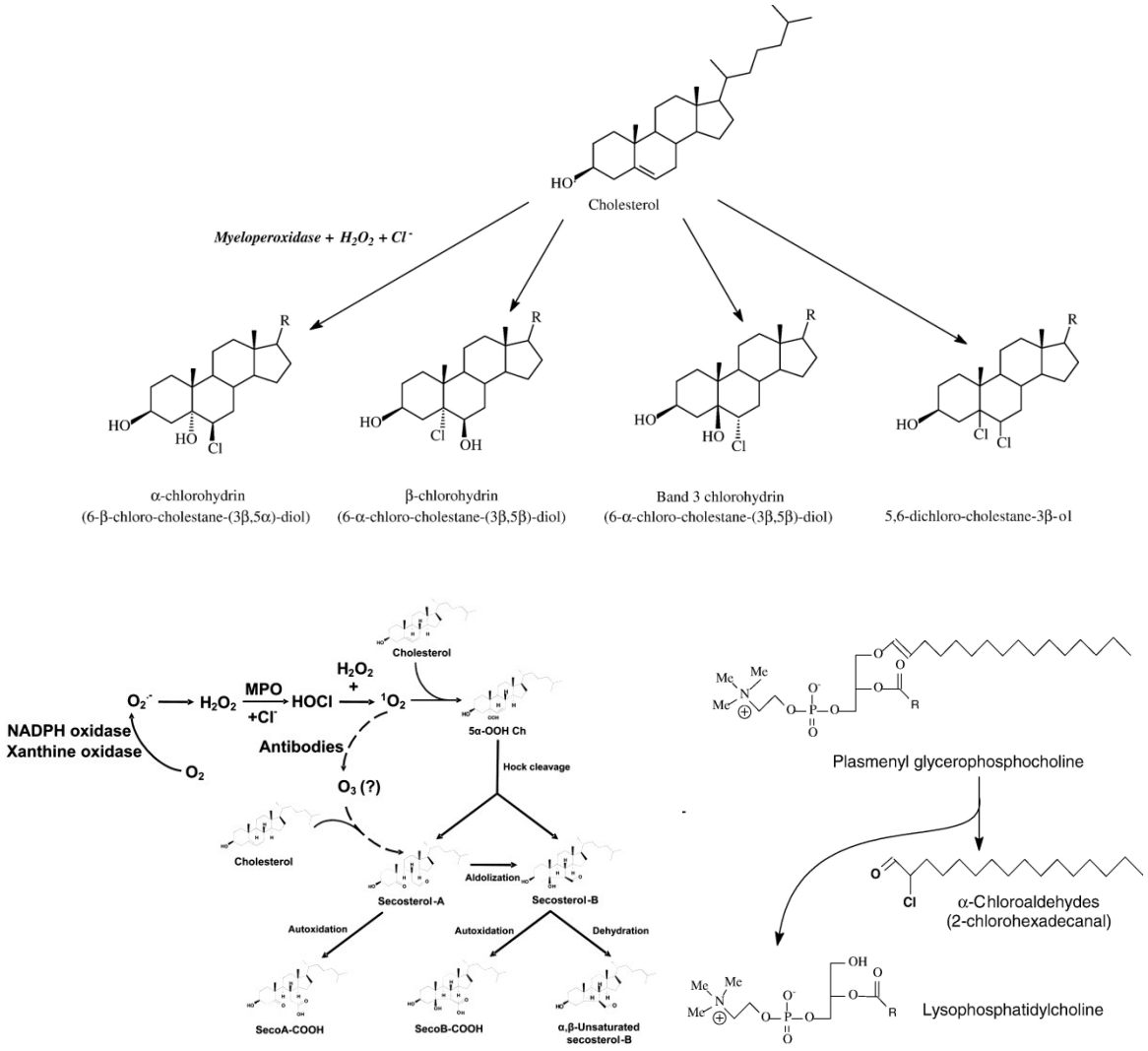

Figure 10: Reaction of HOCl with Chol and plasmalogens (taken from Spickett, 2007 and Tomono et al., 2011)
HOCl attacks Chol double bonds and vinyl ether linkages of plasmalogens leading to formation of chlorohydrins and α-chloro-fatty aldehydes and remnant lysophospholipids, respectively. HOCl-dependent formation of singlet oxygen leads to generation of secosterols.

HOCl-targeting of this susceptible vinyl ether bond yields α-chloro-fatty aldehydes (predominantly 2-chlorohexadecanal (2-ClHDA) and 2-chlorooctadecanal) and the remnant lysophospholipids (LysoPL) (Albert et al., 2001). Plasmalogens mainly consist of phosphatidylethanolamine (PE) and PC species of which PE plasmalogens are highly abundant in the brain; however, PC plasmalogen species are enriched in the heart (Nagan and Zoeller, 2001). PC plasmalogens exhibit a second-order reaction rate towards HOCl of 55 ± 7 L mol^{-1} sec^{-1} which is slightly higher compared to that of ester PC (~ 5 L mol^{-1} sec^{-1} for 1-palmitoyl-2-oleoyl-*sn*-glycer-3-phosphocholine (POPC)) (Skaff et al., 2008). α-Chloro-fatty

aldehydes have been detected in human atherosclerotic lesions and infracted myocardium as well as in mouse brain after systemic administration of LPS and are favourable *in vivo* lipid biomarkers for MPO-derived HOCl modification (Thukkani et al., 2005; Thukkani et al., 2003; Ullen et al., 2010). 2-ClHDA has been identified a potent chemoattractant *in vitro* that recruits circulating neutrophils to areas of inflammation (Thukkani et al., 2002). Moreover, this halogenated aldehyde promotes endothelial dysfunction, adversely effects the performance of Langendorff-perfused rat hearts, attenuates the expression and activity of endothelial nitric oxide synthase, and forms Schiff bases with primary amines of PE and lysine (Marsche et al., 2004; Thukkani et al., 2005; Wildsmith et al., 2006).

Regarding PL, HOCl-targeting primarily depends on the PL species. In case of PE and PS HOCl preliminary reacts with the PL headgroup thus yielding formation of chloramines (***Figure 11 A***). PE chloramines decompose *via* formation of dichloramines into nitrogen-centered radicals that can induce lipid peroxidation, whereas PS chloramines break down into phosphatidylglycoaldehydes or into phosphatidylnitriles *via* dichloramine and chlorimine formation (Flemmig et al., 2009; Kawai et al., 2006). All these reactive lipid species are able to induce further damage to the surrounding tissue. In contrast to PE and PS the choline headgroup from PC is relatively inert towards HOCl modification (Pattison et al., 2003).

Whereas PE and PS headgroups exhibit high second-order rate constants to HOCl (~ 10^4 L mol^{-1} sec^{-1}), the reaction mechanism of HOCl with unsaturated double bonds in FA acyl chains is rather low (5 - 50 L mol^{-1} sec^{-1}) (Arnhold et al., 1995; Pattison et al., 2003). Nevertheless, addition of HOCl to double bonds in aliphatic side chains lead to formation of chlorohydrins, chlorohydroxy derivates (2 isomers are possible) of the original PL (***Fig. 11 B***). In course of this reaction, Cl^+ electrophilically attacks the π-system of the double bond to form a carbenium ion which is followed by the electrophilic attack of water-derived OH^- at the C^+ (Spickett, 2007). Recent studies demonstrated the formation of an unsaturated monochlorinated chlorohydrin adduct (Spalteholz et al., 2004). This derivate which exhibits a decrease in mass of 17 Da results from the removal of H^+ during OH^- attack on the carbenium intermediate (Spalteholz et al., 2004). Under alkaline conditions, the resulting chlorohydrins can be converted to the respective epoxides (Spickett, 2007).

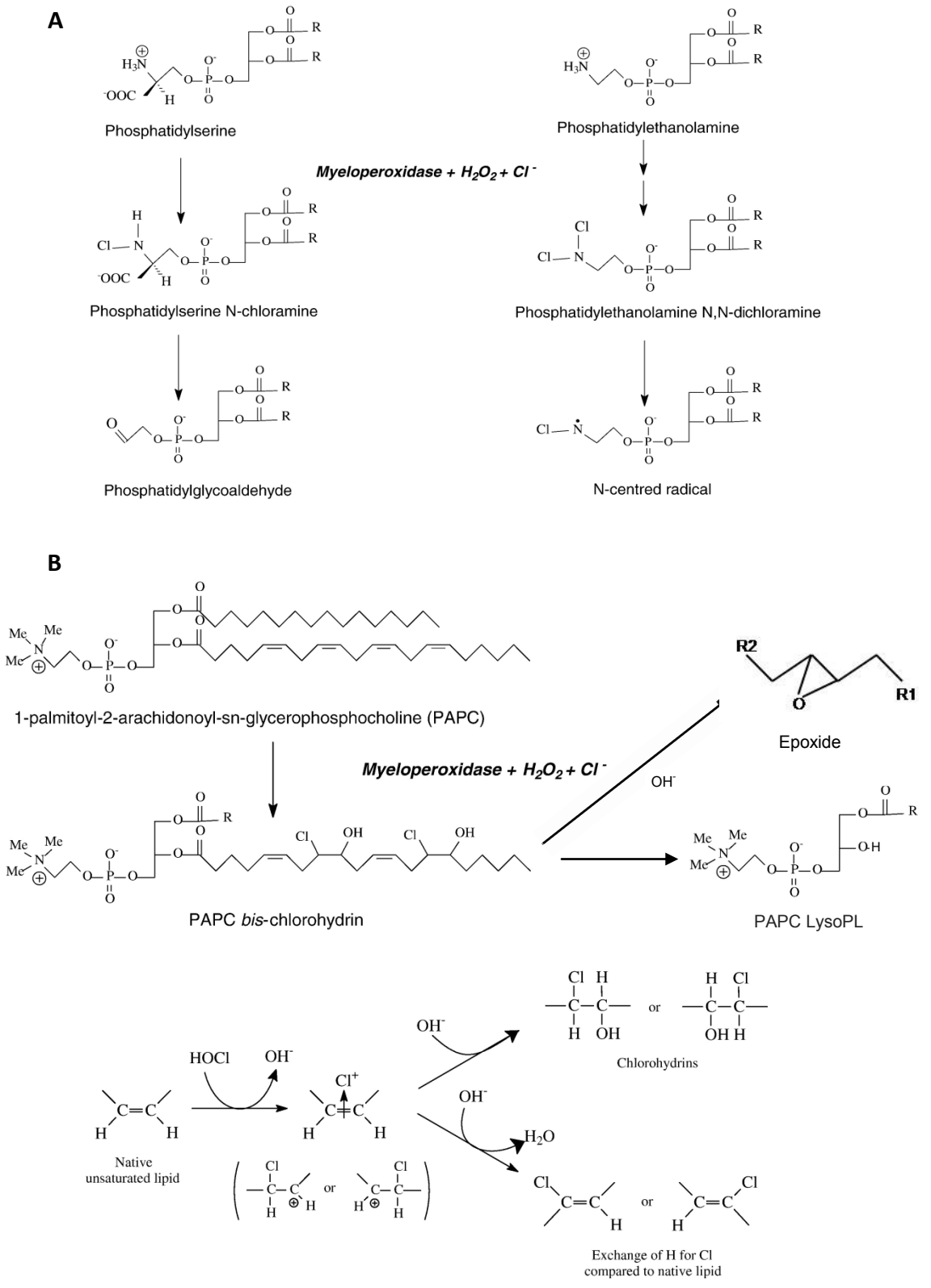

Figure 11: Reaction of HOCl with PL (modified from Spickett, 2007)

A: PS- and PE-derived lipid spezies after HOCl-mediated headgroup modifiction

B: Reaction of HOCl with double bonds of unsaturated PL leading to chlorohydrin, LysoPL, and epoxide formation. The lower panel shows reactions steps in chlorohydrin formation.

The stability of PL chlorohydrins dramatically depends on the degree of unsaturation of the FA acyl residue and/or the intramolecular positions of the double-bonds. Whereas chlorohydrins of POPC are very stable, an increasing number of double bonds leads to chlorohydrin decomposition into the chlorinated FA and the remnant LysoPL (Arnhold et al., 2002). Treatment of 1-palmitoyl-2-linoleoyl-*sn*-glycer-3-phosphocholine (PLPC) resulted in formation of almost equal amounts of the *bis*-chlorohydrin and the remaining LysoPL when lipids were treated with a 5-fold molar excess of HOCl (Arnhold et al., 2002). The ratio of generated monochlorohydrin or *bis*-chlorohydrin strongly depends on the molar HOCl:lipid ratio in which higher amounts of the oxidant favor *bis*-chlorohydrin formation (Spickett, 2007). However, incubation of 1-palmitoyl-2-arachidonoyl-*sn*-glycer-3-phosphocholine (PAPC) liposomes with a 5-fold molar excess of HOCl mainly provoked generation of PAPC-derived LysoPL and concomitant depletion of the respective monochloro-, *bis*-, *tris*-, and *tetrakis*-chlorohydrin species which were only slightly above detection limit (Arnhold et al., 2002). The likely reason for hydrolysis of PL chlorohydrins is probably a weakening of the susceptible ester bond by introduction of electron-attracting substitutes upon chlorohydrin formation (Arnhold et al., 2002). This time- and concentration-dependent effect (longer incubation times and increasing concentrations of HOCl lead to LysoPL generation) is stronger, the nearer the Cl^+ and OH^- group is located to the ester bond and presumably accumulates with increasing numbers of intramolecular double-bonds. Another possibility is that introduction of the bulky groups disorders the PL's structure in the lipid layer thus rendering the molecule more susceptible towards hydrolyzing species (Arnhold et al., 2002).

Up to now the biological significance of FFA and PL chlorohydrins is poorly understood. Although chlorohydrins of FFA and FA acyl residues that contain only one double-bond are considered to be relatively stable molecules they have not been detected *in vivo* so far. However, FFA and Chol chlorohydrins generated by treatment of erythrocyte membranes were shown to cause hydrolysis of human red blood cells *in vitro* which is due to cell membrane damage caused by these halogenated lipids (Carr et al., 1997a). In addition FFA chlorohydrins displayed necrotic cytotoxicity to endothelial cells, an effect which was even more pronounced when cells were incubated in the presence of bromohydrins (Vissers et al., 2001).

Previous studies exhibited that a variety of PL chlorohydrins caused ATP depletion and decreased viability in human myeloid cells (Dever et al., 2003). Furthermore, activation of caspase-3 in these cells was detected in response to PL chlorohydrin treatment (Dever et al., 2006). Incubation of artery segments from ApoE$^{-/-}$ and C57Bl/6 wild-type mice with 1-stearoyl-2-oleoyl-*sn*-glycero-3-phosphocholine (SOPC) chlorohydrin resulted in increased splenocyte-arterial adhesion *via* upregulation of P-selectin (Dever et al., 2006; Dever et al., 2008). Preincubation of artery segments with anti-P-selectin or anti-ICAM-1 antibodies prevented enhanced leukocyte adhesion. Moreover, it was found that incubation with the chlorohydrin significantly induced ROS generation in phorbol myristate acetate (PMA)-stimulated ApoE$^{-/-}$ leukocytes derived from spleen (Dever et al., 2008). In a more recent study it was shown that SOPC, 1-stearoyl-2-linoleoyl-*sn*-glycero-3-phosphocholine (SLPC), and 1-stearoyl-2-arachidonoyl-*sn*-glycero-3-phosphocholine (SAPC) chlorohydrins were more rapidly incorporated into erythrocyte membranes compared to the respective unmodified lipids which was accompanied by cell aggregation, changes in cell morphology, transformation into echinocytes, and erythrocyte hemolysis (Robaszkiewicz et al., 2010). Presumably, FFA and PL chlorohydrins exacerbate their toxic potential to biomembranes by introducing more amphiphilic groups into the hydrophobic environment of these lipid double-layers leading to membrane disorganization and rupture. These studies suggest that halohydrins generated by MPO-derived oxidants are highly cytotoxic lipid mediators formed under inflammatory conditions. As mentioned before, chlorohydrin formation of polyunsaturated FA acyl residues is accompanied with LysoPL generation. These LysoPL as well as plasmalogen-derived LysoPL may also adversely affect membrane dynamics leading to cell lysis (Malle et al., 2007). The latter LysoPL were abundantly present in human atherosclerotic lesions and led to a significant upregulation of P-selectin in coronary arteries (Thukkani et al., 2003). Interestingly, lysophosphatidylcholine chlorohydrin formation as a product of secondary oxidations at the *sn*-2 position can follow HOCl-mediated LysoPL generation of plasmalogens as already observed in human coronary artery endothelial cells (Messner et al., 2006).

Some chlorinated lipids were previously reported to have beneficial properties. For instance, chlorinated prostaglandins displayed increased reactivity with nucleophiles, and exhibited antiinflammatory and antitumour activity (Spickett, 2007). In addition, oxidatively-modified PL and oxysterols are able to prevent Toll-like receptor-mediated

signaling in response to bacterial pathogen-associated molecular pattern such as LPS, thus enhancing antiinflammatory conditions (Erridge and Spickett, 2007).

2.5. Analysis of HOCl-modified lipids

Whereas previously thin-layer chromatography has been mainly used for identification of chlorinated lipids, mass spectrometry became more and more important in analysis during the last years. Chol chlorohydrins have been mainly identified by gas chromatography mass spectrometry (GC-MS) as trimethylsilyl (TMS) ethers or heptafluorobutyrate (HFB) derivates using positive and negative ionization (Carr et al., 1996; Heinecke et al., 1994) or by matrix-assisted laser desorption ionization time of flight (MALDI-TOF) (Schiller et al., 2001). Plasmalogen-derived chlorinated aldehydes have been detected *via* GC-MS as pentafluorobenzyl (PFB) oximes or esters thereby applying mainly negative ion chemical ionization (NICI) and selected single-ion monitoring (Thukkani et al., 2002; Ullen et al., 2010). Chlorohydrin formation of FFA was followed using GC-MS and electron impact (EI)-MS after suitable derivatization to TMS ethers and esters or to methyl esters (Winterbourn et al., 1992). Also ELISA-based techniques using an monoclonal antichlorohydrin antibody were applied to identify fatty acyl chlorohydrins (Carr et al., 1997a).

PL chlorohydrins were originally treated with phospholipase A_2 and the generated FFA chlorohydrins were measured as described above. More recently, electrospray ionization (ESI)- and particularly MALDI-TOF-MS became the most important methods for PL- and Chol chlorohydrin analysis as well as for the respective LysoPL. Both techniques do not require analyte-derivatization prior analysis and yield identification of the intact lipid as well as of fragmentation products due to the soft ionization which further prevents formation of artefacts such as conversion of Chol chlorohydrins to epoxides.

ESI-MS which can be coupled to high performance liquid chromatography (HPLC) for prior separation was used to detect chlorohydrin formation of Chol and PL in a complex lipid matrix (erythrocyte membranes or LDL after HOCl treatment; stressed cells) as well as purified samples (PL liposomes) (Dever et al., 2003; Hazen et al., 1996; Messner et al.,

2006). Thereby, measurements were mainly performed in the positive ion chemical ionization (PICI) mode.

MALDI-TOF-MS (***Figure 12***) is particularly suitable to analyze chlorohydrins derived from SM, PC, and Chol by measuring in the PICI mode. Therefore, lipid samples are diluted in organic solvents (mainly methanol) and mixed with a matrix which in most cases is dihydroxybenzoic acid (DHB) resulting in a molar lipid:matrix ratio of approx. 1:100 – 1:10,000. This mixture is then spotted onto a target plate for subsequent measurement after drying. Matrix molecules enhance desorption of the analyte from the target plate. Usually, spectra are recorded in the reflector mode using delayed extraction to increase resolution. PE and PS and their respective chlorinated species are mainly measured in the negative ion mode (Flemmig et al., 2009; Richter et al., 2008). Taken together, MALDI-TOF-MS provides a very rapid, sensible, and sensitive method for detection of chlorinated PL and sterols and LysoPL in pure samples as well as in complex biological lipid matrices (Panasenko et al., 2007; Schiller et al., 2001; Schober et al., 2009).

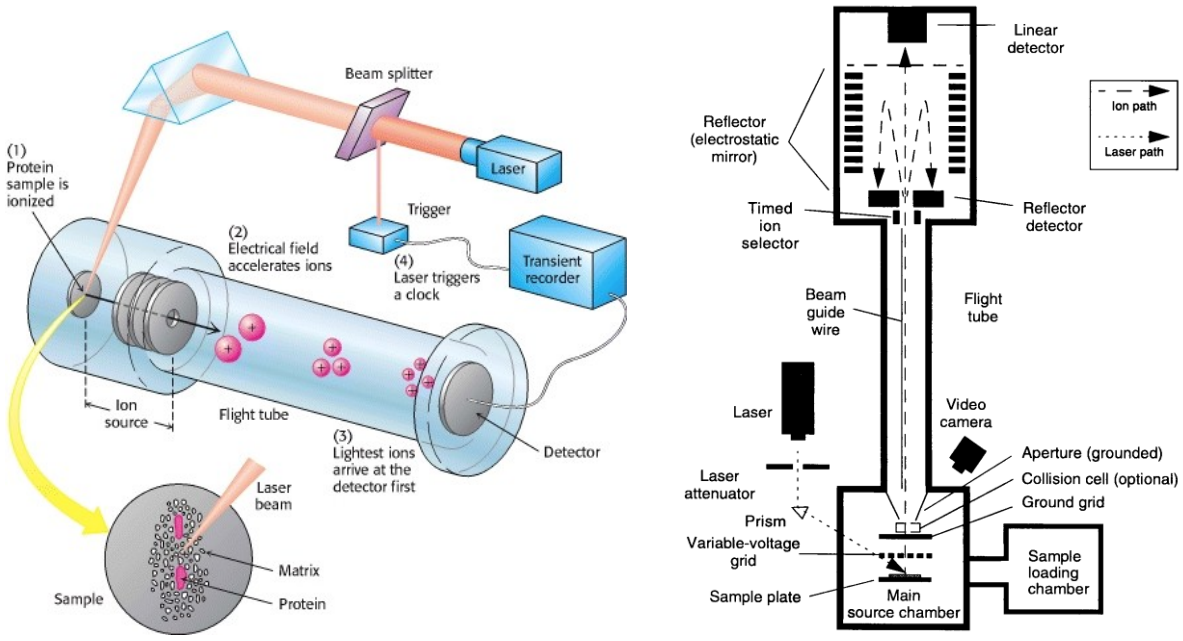

Figure 12: Assembly of a typical (left side) ***and a Voyager*** (right side) ***MALDI-TOF system*** (taken from Berg et al., 2005 and www.chem.cmu.edu/cma/toffig.gif)

3. APOPTOSIS – WHEN CELLS DECIDE TO COMMIT SUICIDE

It is becoming increasingly clear that bioactive lipids that are generated by enzymatic or non-enzymatic pathways can function as potent inducers of apoptosis and necrosis in brain cells. Native or (MPO)-modified members of the SL family generated under neuroinflammatory conditions are of particular importance in this pathological setting as they are able to activate either the extrinsic or intrinsic pathway of the apoptotic machinery.

3.1. Programmed- versus accidental cell death

In contrast to necrotic cell death apoptosis is an energy-dependent process that is characterized by activation of a set of cysteine proteases called caspases, cell shrinkage, cytoplasmic condensation, DNA fragmentation, pyknosis (a result of chromatin condensation), DNA and concomitant nuclear fragmentation, membrane blebbing, and formation of apoptotic bodies (Rastogi et al., 2009). Unlike necrosis which resembles a energy-independent, toxic cell death that is associated with cell swelling, condensation and/or swelling and rupture of mitochondria, ER distension, formation of cytoplasmic vacuoles, ruptured lysosomes, and disintegration and disruption of the PM, apoptosis is referred to happen in single cells or small cell clusters without effecting the surrounding tissue (Majno and Joris, 1995; Trump et al., 1997). Apoptotic bodies are enclosed by an intact PM and rapidly cleared by phagocytosis, mediated by macrophages, parenchymal cells, or neoplastic cells (Elmore, 2007), thus preventing inflammatory reactions. During necrosis, inflammation is mediated by the release of cytoplasm and cellular constituents into the surrounding tissue and concomitant recruitment of inflammatory cells. Despite these differences there are also several common pathways in apoptosis and necrosis, sometimes termed the “apoptosis-necrosis continuum” (Zeiss, 2003). Furthermore, there are certain types of necrotic-like cell deaths that display adjusted forms of necrosis which require gene activation and protein synthesis and are, therefore, also part of the programmed cell death (PCD) family (Proskuryakov et al., 2003). These processes that

harbor typical apoptotic and necrotic events are often referred the terms “aponecrosis” or “necroptosis” (Formigli et al., 2000; Galluzzi and Kroemer, 2008).

Apoptosis can be induced by a variety of stimuli such as oxidative stress, UV radiation, ionizing radiation, high temperature, bioactive lipids, hypoxia, viral infections, replication/recombination errors, or cytotoxic anticancer drugs (Batista et al., 2009; Nagata, 1997; Norbury and Zhivotovsky, 2004). In addition, apoptotic cell death can occur by the withdrawal of apoptosis-inhibitory factors (e. g. hormones, cytokines, growth factors). Although certain steps vary between different forms of PCD and also in the apoptotic cascade itself, apoptosis is always characterized by cleavage and concomitant activation of caspase-3 followed by DNA-fragmentation, degradation of certain proteins, protein cross-linking, generation of apoptotic bodies, and their phagocytosis (Elmore, 2007). Up to now, three different pathways of apoptosis are described: (i) the extrinsic pathway which involves activation of death receptors, (ii) the intrinsic pathway in which mitochondria play a crucial role in eliciting apoptosis, and (iii) the perforin/granzyme pathway. As mentioned above the three pathways cover the same terminal reaction steps upon caspase-3 activation and the two most important apoptotic pathways, the intrinsic and extrinsic one, are linked and may influence each other (Igney and Krammer, 2002).

3.2. The extrinsic pathway of apoptosis

The extrinsic or death receptor pathway of apoptosis can be initiated by a variety of stimuli and prototypically proceeds *via* death receptors signaling. So far identified death receptors which localize to the PM belong to the TNFR gene superfamily (Locksley et al., 2001) and perform signaling from the cell surface to the interior of the cell after ligand binding. The best-characterized ligand-receptor couples include TNFα/TNFR1 (p55), FasL/Fas (CD95), Apo3L/DR3 (Apo3), Apo2L/DR4 (TRAIL-R1), and Apo2L/DR5 (TRAIL-R2) (Elmore, 2007; Yan and Shi, 2005).

The extrinsic pathway of apoptosis involves ligand binding of the respective death receptors which is accompanied with clustering and activation of the receptors. As a consequence, adaptor molecules are recruited that bind to death receptors *via* receptor-

associated death domains (Ashkenazi and Dixit, 1998). For the two best-characterized couples these adaptor molecules are called Fas-associated death domain (FADD) and TNF-receptor-associated death domain (TRADD) (Elmore, 2007). Subsequent to TNFR1 activation TRADD recruits FADD and RIP (Wajant, 2002). Together with two caspase-8 zymogens death receptors and FADD lead to formation of the death inducing signalling complex (DISC) which is ensured by binding of procaspase-8 to FADD *via* death effector domains which are present on both, procaspase-8 and FADD (Boldin et al., 1996). This in turn stimulates the autocatalytic cleavage of procaspase-8 which then mediates activation of executioner caspases.

In some cases the mitochondrial protein Bid is also activated *via* cleavage by caspase-8, thus making a branch to the intrinsic pathway of apoptosis (Luo et al., 1998). ***Figure 13*** shows a schematic overview of the three most relevant apoptotic pathways.

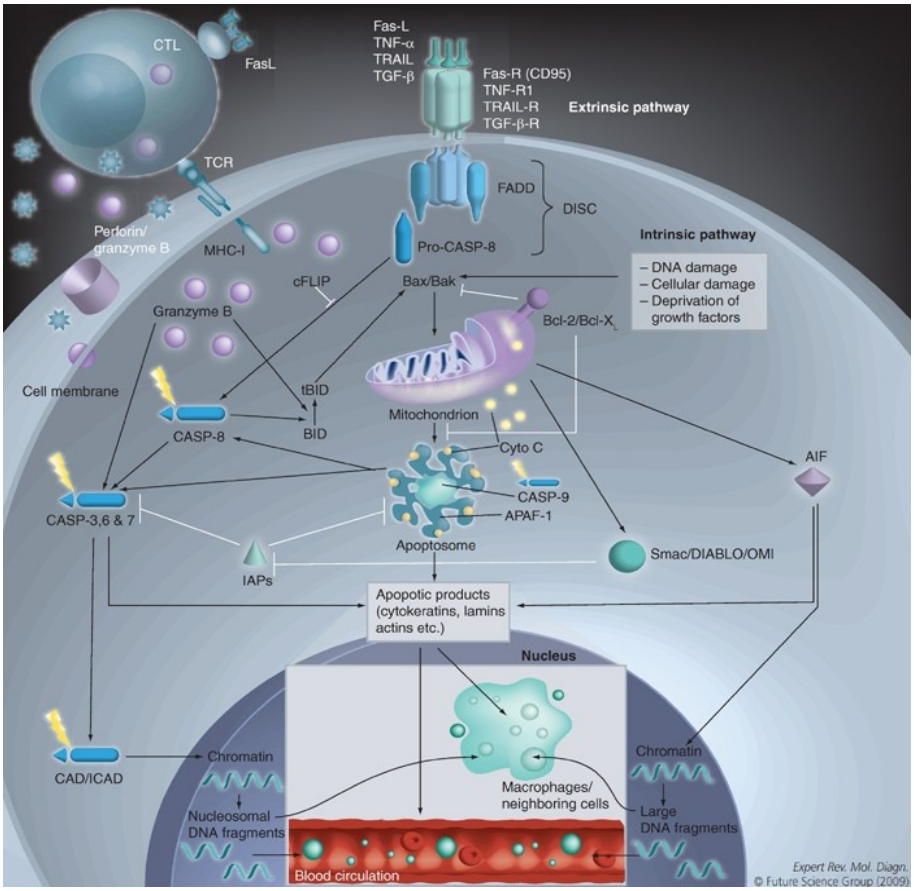

Figure 13: Schematic overview of the extrinsic, intrinsic, and perforin/granzyme apoptotic pathways (taken from www.medscape.com/viewarticle/703575_3)

3.3. The intrinsic pathway of apoptosis – when mitochondria become dangerous

The intrinsic pathway of apoptosis is characterized by mitochondrial damage and the involvement of several pro- and anti-apoptotic proteins. Most of these proteins belong to the well-known group of the B-cell leukemia/lymphoma 2 (Bcl-2) family. According to their Bcl-2 homology (BH) domains these proteins can be divided into three groups acting either as anti-apoptotic (four BH domains), pro-apoptotic (three BH domains), or as pro-apoptotic ligands (one BH domain) (Adams and Cory, 1998). Within the first group the best known representative is Bcl-2. Other members include Bcl-w, Bcl-XL, Bcl-x, Mcl-1, and BAG. Pro-apoptotic proteins of the Bcl-2 family are Bax, Bak, and Bok/Mtd, whereas BH3 only proteins contain Bid, Bad, Bik, Puma, and Noxa.

A crucial event during activation of the intrinsic pathway of apoptosis is the formation of the mitochondrial PTP, the dissipation of $\Delta\psi_m$, and subsequent release of pro-apoptotic proteins from the intermembrane space into the cytosol (Elmore, 2007). This permeabilization of mitochondria is mediated by the pro-apoptotic proteins Bax and Bak after oligomerization of these two proteins (Jourdain and Martinou, 2009). Bak is permanently localized to the outer membrane of mitochondria, whereas Bax is normally found in the cytosol and relocates to mitochondria during apoptosis. In response to DNA damage apoptosis is initiated as a consequence of high Bax levels or low Bcl-2 levels and mitochondrial permeabilization is dependent on the activation of caspase-2 (Vakifahmetoglu et al., 2006). During death receptor-mediated apoptosis Bax and Bak dimerize in response to caspase-8-mediated cleavage of Bid. Truncated Bid binds to Bax and Bak at mitochondria leading to activation and pore formation (Billen et al., 2008). Recently it was found that during ER stress, Bax/Bak are activated by Puma and Noxa (Li et al., 2006). Moreover it was shown that Bax/Bak is localized to the ER and organelle stress is accompanied by Ca^{2+} depletion and activation of caspase-12 (Scorrano et al., 2003).

As mentioned above, mitochondrial disruption goes “hand-in-hand” with the release of pro-apoptotic proteins which further trigger execution of apoptosis. Pro-apoptotic proteins from the mitochondrial intermembrane space can be divided into two groups. The first one consists of cytochrome *c*, Smac/DIABLO, and the serine protease HtrA2/Omi. The second group is constituted by apoptosis inducing factor (AIF), endonuclease G (EndoG), and CAD which resemble crucial enzymes in the executioner

phase of apoptosis (Elmore, 2007). Whereas Smac/DIABLO and HtrA2/Omi drive apoptosis by inhibiting the inhibitor of apoptosis proteins (IAPs) (Schimmer, 2004) cytochrome *c* is a key player in formation of the apoptosome by activation of the apoptosome proteins Apaf-1 and procaspase-9, thus initiating the caspase-dependent part of the intrinsic pathway of apoptosis (Hill et al., 2004). AIF, EndoG, and CAD are endonucleases which translocate into the nucleus and are responsible for DNA fragmentation and chromatin condensation (Elmore, 2007). In parallel to mitochondrial permeabilization one can often observe a collapse of $\Delta\psi_m$, although mitochondrial PTP formation can also occur without changes of $\Delta\psi_m$. For instance, cytochrome *c* release was already observed in the absence of $\Delta\psi_m$ (Kroemer and Reed, 2000).

Once released, cytochrome *c* first binds Apaf-1 leading to a conformational change of Apaf-1 in a dATP/ATP-dependent manner. Seven cytochrome *c*/Apaf-1 molecules oligomerize through interaction of their caspase recruitment domains and hence build a central recruitment platform for procaspase-9 which in turn leads to activation of the protease (Zou et al., 1999). This holoenzyme then catalyzes the activation of effector caspases such as caspase-3 and 7 (Jiang and Wang, 2004).

3.4. The perforin/granzyme pathway

This type of killing is mediated by cytotoxic T lymphocytes or natural killer cells and requires the combined actions of a membranolytic enzyme, perforin, and granule-associated granzymes A and B. Thereby, perforin permeabilizes the PM of the target cell which facilitates entry of the granzyme serine proteases. Granzyme A and B are responsible for initialing the events culminating in apoptosis. Granzyme A is able to activate caspase-independent pathways through DNA damage, while granzyme B is able to activate procaspase-10, cleave Bid and thereby triggers cytochrome *c* release, or can directly activate caspase-3 (Elmore, 2007).

3.5. Protein regulators and effectors of apoptosis

3.5.1. Caspases

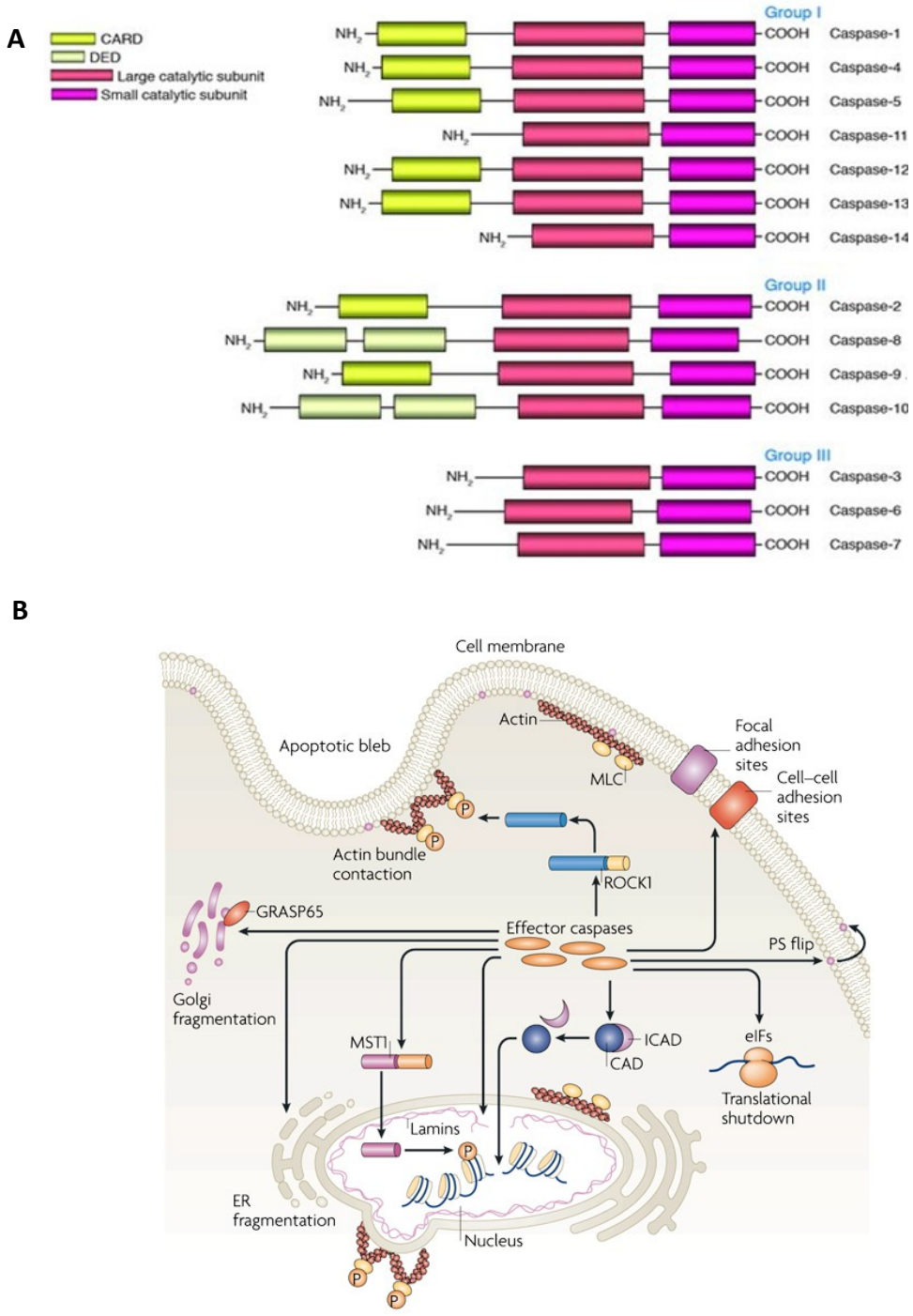

Figure 14: Structure of caspases that can be divided into three major groups (A) and their key cellular target structures (B) (taken from Lavrik et al., 2005 and Taylor et al., 2008)
Group I: inflammatory caspases; *Group II*: initiator caspases; *Group III*: executioner caspases
eIFs, translation initiation factors; *MLC*, myosin light chain

Caspases are a group of cysteine proteolytic enzymes that cleave after aspartic acid (*c*: cysteine; *aspase*: cleavage after aspartic acid) that resemble essential molecules in the apoptotic cascade (Alnemri et al., 1996). So far, 14 caspase members have been identified (Cohen, 1997). Thereby, one can differentiate between caspases that are important in the initiation phase of the apoptotic cascade and those that mainly act in the execution phase. Due to this specification, their substrate specificity, and their domain composition, caspases are divided into three subgroups (Thornberry, 1997) (***Figure 14 A***).

(i) Caspase-2, 8, 9, and 10 belong to the group of initiator caspases; (ii) caspase-3, 6, and 7 are active in the executioner phase of apoptosis as effector caspases; (iii) caspase-1, 4, 5, 11, 12, 13, and 14 are called inflammatory caspases which are involved in cytokine activation (Pop and Salvesen, 2009). Caspases are expressed as proenzymes (zymogens) where the N-terminal prodomain is followed by a large and a small subunit (***Fig. 14 A***). Most caspases are found enzymatically active as a homodimer where each homodimer consists of a small (10-13 kDa) and a large subunit (17-21 kDa). The formation of this tetrameric structure is initiated by the caspase prodomain (Nicholson, 1999). Initiator caspases exhibit autocatalytic cleavage activity which is important for self activation in the early stages of the apoptotic cascade (Stennicke and Salvesen, 1998). Once activated these enzymes can cleave other procaspases, rendering them enzymatically active, thus leading to initiation of a protease cascade and concomitant amplification of the apoptotic signal. To enhance autoproteolysis and concomitant activation of initiator caspases these enzymes depend on special recruitment platforms (e. g. DISC for caspase-8 and 10 (Peter and Krammer, 2003), the PIDDosome for caspase-2 (Tinel and Tschopp, 2004), and the formation of the apoptosome for caspase-9 (Martinon and Tschopp, 2007)). To ensure their activation initiator caspases contain death domains, death effector domains (DED), or caspase recruitment domains (CARD) for interaction with molecules of their recruitment platforms (Lavrik et al., 2005). Effector caspases are activated by initiator caspase-2, 8, 9, and/or 10 through enzymatic processing in which the large and the small subunits are separated from each other and the prodomain is removed (Yan and Shi, 2005). Executioner caspases, where caspase-3 is the most important one, are responsible for the cleavage of many cellular proteins such as poly (ADP-ribose) polymerase (PARP), cytokeratins, nuclear proteins (e. g. NuMA), and cytoskeletal proteins (e. g. fodrin, gelsolin) (Slee et al., 2001) (***Fig. 14 B***). In addition, executioner caspases can also act on other proteases and nucleases

thus rendering them enzymatically active. In this context, caspase-3 was previously shown to activate endonuclease CAD which is responsible for chromatin degradation by cleavage of its inhibitor ICAD (Sakahira et al., 1998).

In the group of inflammatory caspases, caspase-12 has an outstanding role in initiating ER-specific apoptosis and Aβ-mediated cytotoxicity and concomitant activation of executioner caspases (Hitomi et al., 2004; Nakagawa et al., 2000).

3.5.2. Other non-caspase proteases in apoptosis and regulation of PCD

In addition to caspases and granzymes, several other proteases can be involved in eliciting apoptosis. An important group of these proteases is represented by the calpain family. Calpains are neutral cysteine proteases and their activity strongly depends on the presence of Ca^{2+}. Calpains were recently shown to be involved in both, the initiation of apoptosis (Chen et al., 2006) as well as in the executioner phase (Villa et al., 1998). Fodrin, gelsolin, p53, PARP, and Bax were identified as typical substrates of these proteases (Goll et al., 2003; Kubbutat and Vousden, 1997; Wang, 2000; Wood et al., 1998). Another group of proteases that can be involved in apoptosis is resembled by the family of cathepsins which are also expressed as zymogens and can be divided into serine proteases (cathepsin A and G), cysteine proteases (cathepsin B, C, H, K, L, S, and T), and aspertate proteases (cathepsin D and E) (Schwartz, 1995). The most thoroughly characterized members are the lysosomal or endosomal enzymes cathepsin B and D. They are responsible for terminal degradation of proteins within these organelles but can also be translocated or released to the cytosol thus leading to cytochrome *c* relocation and dissipation of $\Delta\psi_m$ as response to oxidative stress (Roberg et al., 1999; Yap et al., 2006). Similar to calpains, cathepsins only exhibit weak cleavage activity towards procaspases but are activated by calpains during apoptosis in cortical neurons elicited by oxidative damage (Yap et al., 2006).

Negative regulation of apoptosis is maintained either by proteins of the Bcl-2 family as mentioned above or by the IAP family. These inhibitors include XIAP, c-IAP1, c-IAP2, NAIP, survivin, livin, and BIRC (Verhagen et al., 2001). IAPs can inhibit caspase-3, 7, and 9 by binding (Deveraux et al., 1997) or *via* ubiquitination and proteosomal degradation in case of caspase-3 and 7 (Huang et al., 2000). IAP-mediated negative regulation can be abolished

by negative regulators of IAPs such as Smac/DIABLO and Omi/HtrA2 (Liston et al., 2003). Caspase-8 was identified to fail in being recruited to the DISC in the presence of FLIPs (FADD-like ICE(FLICE)-inhibitory proteins) (Thome et al., 1997).

3.6. Malfunctioning of apoptosis

As would be expected for a central regulatory pathway of development, malfunctioning apoptosis results in disease. Forms of uncontrolled apoptosis were found in many neurodegenerative diseases such as AD, PD, Huntington's disease (HD), and MS but also in acute events such as stroke or brain trauma (Alam, 2003). Furthermore, increased apoptosis plays a crucial role in cardiovascular diseases, haematologic diseases, in AIDS, diabetes (type-I), and during inflammation (Rastogi et al., 2009). Elevated activities of caspase-8 and 9 have been observed in peripheral blood of AD patients as well as in brain tissue in AD or PD patients (Rastogi et al., 2009). Augmented activities of caspase-8 and 10 were found to play a crucial role in disease progression of HD (U et al., 2001). During *in vitro* studies, Aβ as well as Aβ activated astroglia were shown to kill primary neurons *via* nSMase-mediated generation of Cer (Jana and Pahan, 2004; Jana and Pahan, 2010a) and to induce toll-like receptor 2 signal transduction in microglia (Jana et al., 2008). Aβ is further assumed to induce apoptosis *via* increased FasL expression and induction of oxidative stress (Elmore, 2007). Patients suffering from diseases mentioned above benefit from anti-apoptotic therapies. These therapies include treatment with IAPs, synthetic caspase inhibitors, PARP inhibitors, inhibition of pro-apoptotic Bcl-2 family proteins, and stimulation of the protein kinase B (PKB)/Akt pathway (Elmore, 2007).

In contrast to excessive apoptosis, inadequate apoptotic events are associated with the development of cancer as well as with the establishment of autoimmune disorders by deficient removal of auto-aggressive T-cells or antibody-secreting B-cells, restenosis, and frequent viral infections (Rastogi et al., 2009). In case of cancer, tumors can establish due to resistance towards apoptosis which is triggered by overexpression of anti-apoptotic proteins of the Bcl-2 family, by downregulation of pro-apoptotic proteins, or expression of nonfunctional Fas (Elmore, 2007).

II. MATERIALS AND METHODS

1. MATERIALS

Cell culture supplies were from Gibco (Invitrogen, Vienna, Austria), PAA Laboratories (Linz, Austria), Bartelt (Graz, Austria), and Costar (Vienna). Fluorescent two-dimensional difference gel electrophoresis (2D-DIGE) cyanine (Cy) dyes (Cy2, Cy3, and Cy5), immobilized pH gradient strips (IPG strips, pH 3–10), and pharmalyte (pH 3-10) were from GE-Healthcare (Amersham Biosciences, Vienna). SM from chicken egg yolk, N-palmitoyl-D-*erythro*-sphingosylphosphorylcholine (SM(d18:1/16:0)), 1,2-dipalmitoyl-*sn*-glycero-3-phosphocholine (PC(16:0/16:0)), NaOCl (reagent hypochlorite), colchicine, 2,5-dihydroxy benzoic acid (DHB), Hank's buffered salt solution (HBSS), Met, oligomycin, propidium iodide (PI), lysopalmitoylphosphatidylcholine, 5,5',6,6'-tetrachloro-1,1',3,3'-tetraethyl-benzamidazolocarbocyanin iodide (JC-1), 3-(4,5-dimethyl-2-thiazolyl)-2,5-diphenyl-2H-tetrazolium bromide (MTT), chlorpromazine (CP), methyl-β-cyclodextrin (MβCD), genistein (GE), nystatin (NY), chelerythrine chloride (CHEL), nocodazole, brefeldin A, SMase from *Bacillus cereus*, carbonyl cyanide 4-(trifluoromethoxy)phenylhydrazone (FCCP), GW4869, desipramine, and N^6,2'-O-dibutyryladenosine 3',5' cyclic monophosphate (dbcAMP) were from Sigma (Vienna). Cellulose acetate was from Sartorius AG (Goettingen, Germany). 2',7'-dichlorofluorescin diacetate (H_2DCFDA), N-(4,4-difluoro-5,7-dimethyl-4-bora-3a,4a-diaza-*s*-indacine-3-pentanoyl)sphingosyl phosphocholine (BODIPY FL C_5-SM), N-(4,4-difluoro-5,7-dimethyl-4-bora-3a,4a-diaza-*s*-indacine-3-dodecanoyl)sphingosyl phosphocholine (BODIPY FL C_{12}-SM), N-(4,4-difluoro-5,7-dimethyl-4-bora-3a,4a-diaza-*s*-indacene-3-pentanoyl)sphingosine (BODIPY FL C_5-Cer = BODIPY-Cer), Blue DND-22, Blue-White DPX, CellMask Plasma Membrane Stain, HOECHST, DAPI, Lipofectamine 2000, and Alexa Fluor 488-labeled phalloidin were from Molecular Probes (Invitrogen, Vienna). N-[12-[(7-nitro-2-1,3-benzoxadiazol-4-yl)amino]dodecanoyl]-sphingosyl-1-phosphocholine (NBD-SM) and 10-(1-pyrene)decanoyl-sphingosyl-1-phosphocholine (PYRENE-SM) were a kind gift from Albin Hermetter (Graz University of Technology, Graz, Austria). Polyclonal rabbit anti-caspase-3 antibody (raised against human full-length caspase-3) and horse radish peroxidase (HRP)-

labeled goat anti-mouse IgG were from Santa Cruz (Santa Cruz Biotechnology, CA, USA). Polyclonal rabbit anti-PARP antibody (raised against a synthetic peptide corresponding to the caspase cleavage site in PARP) was from Cell Signaling (Cell Signaling Technology, MA, USA). Monolclonal anti β-actin and anti β-tubulin antibody, and HRP-labeled goat anti-rabbit IgG were from Sigma. Cy5-labeled goat anti-mouse antibody was from Jackson Dianova (Hamburg, Gemany). SuperSignal Western blot detection reagent, Ultra V blocking reagent, and BCA protein assay kit were from Pierce (Thermo Scientific, MA). SMPD3 siRNAs were from Quiagen (Hilden, Germany). Antibody Diluent was from Dako (Vienna). Precision Red (Reagent #2) Advanced protein assay was from Cytoskeleton (Denver, CO). MPO was from Planta Naturstoffe (Vienna). All other chemicals were from Sigma, Roth (Vienna), and Merck (Darmstadt, Germany).

2. METHODS

2.1. Cell culture and cell treatment

Catecholaminergic CATH.a cells were cultured in poly-L-lysine coated 75 cm^2 flasks containing 15 ml RPMI 1640 medium supplemented with 10% (v/v) horse serum (HS), 5% (v/v) fetal calf serum (FCS), 0.4% (v/v) HEPES buffer, 0.4% (w/v) sodium pyruvate, 0.4% (w/v) L-glutamine, and 1% penicillin/streptomycin at 37°C (5% CO_2). The split ratio of cells was 1:5 and passages below 30 were used for experiments.

Rat phaeochromacytoma (PC12) cells were cultured in collagen-coated 75 cm^2 flasks containing 15 ml RPMI 1640 medium supplemented with 10% (v/v) HS, 5% (v/v) FCS, 0.4% (v/v) HEPES buffer, 0.4% (w/v) sodium pyruvate, 0.4% (w/v) L-glutamine, and 50 µg/ml gentamycin at 37°C (5% CO_2). The split ratio of cells was 1:10 and passages below 30 were used for experiments.

2.2. Uptake studies of fluorescent SM in CATH.a or PC12 cells

PC12 cells were plated either in collagen-coated chamber slides or on collagen-coated cover slips (placed in 6 well plates) and were grown to 60% confluence before incubation with the respective fluorescent tracers. For steady-state labeling uptake experiments, PC12 cells were incubated with NBD-SM (2.5 µM) in serum-free culture medium for the indicated time periods at 37°C in the dark. Cells were then washed three times with ice-cold HBSS, mounted, and analyzed by laser fluorescence microscopy. For "pulse-chase" SM uptake experiments PC12 cells were cooled at 4°C (10 min). BODIPY-SM (2.5 µM) was added to serum-free culture medium and cells were pulsed for 30 min at 4°C (to prevent endocytosis) in the dark to allow insertion of BODIPY-SM into the PM. Following three washing steps with ice-cold HBSS, cells were chased for the indicated time periods at 37°C in the dark. Loosely bound fluorescent BODIPY-SM at the PM was removed by a so-called "back-exchange" (BE) step in which cells were washed with 5% FA-free BSA (DF-BSA) in ice-cold HBSS (6 times for 10 min on ice). Before fluorescence microscopy PC12 cells were washed two times with ice-cold HBSS and processed as described above.

Unlike otherwise noted, BODIPY-C_5-SM was used throughout all experiments and is designated as BODIPY-SM.

BODIPY-SM uptake in CATH.a cells (continuous and pulse-chase experiments) were performed identically as described above except that CATH.a cells were plated on poly-L-lysine-coated cover slips and that concentrations of BODIPY-SM were 1 µM only.

2.3. Colocalization experiments

PC12 cells plated on collagen-coated cover slips, were grown to 60% confluence before starting the experiments. To identify BODIPY-SM accumulating compartments, the cells were incubated with specific markers for lysosomes, ER, mitochondria, Golgi, or the PM, respectively.

PC12 cells were pulse-labeled with 2.5 µM BODIPY-SM as described above. After washing cells extensively with ice-cold HBSS, the cells were chased in the presence of the lysosomal tracker Blue DND-22 (70 nM), the ER selective probe Blue-White DPX (500 nM)

followed by a BE of PM-bound BODIPY-SM as described above. For mitochondrial visualization, PC12 cells were stably transfected with the mitochondrion selective tracer DsRed-Mito 2 days before labeling with BODIPY-SM. For PM staining, the cells were incubated in the presence of CellMask Plasma Membrane Stain (5 µg/ml) for 5 min at 37°C before the cells were pulse-labeled with BODIPY-SM as described above. PC12 nuclei were counterstained with HOECHST (5 µg/ml) for 10 min at 37°C before BE.

After BE, cells were washed 2 times with ice-cold HBSS, mounted and subjected to fluorescence microscopy. In case of PM staining, cells were washed extensively with HBSS after pulse-labeling with BODIPY-SM and were immediately analyzed by fluorescence microscopy without chasing the cells at 37°C and BE.

To visualize the Golgi apparatus PC12 cells were stained with BODIPY-Cer (2.5 µM) in the same way as it was described for BODIPY-SM. If not otherwise noted, chase duration was in all cases 30 min at 37°C and was followed by a BE. All incubation and staining steps were carried out in serum-free culture medium in the dark.

Co-localization experiments in CATH.a cells were performed exactly as described for PC12 cells. In some experiments, CATH.a nuclei were counterstained with HOECHST (5 µg/ml) for 10 min at 37°C before back extraction of PM-bound BODIPY-SM. Pretreatment with nocodazole (30 µM, final concentration) or brefeldin A (20 µg/ml, final concentration) was performed for 90 min in serum-free culture medium at 37°C. All subsequent incubation steps were carried out in the presence of nocodazole or brefeldin A.

2.4. Laser scanning microscopy

Fluorescence microscopy was performed on a Leica SP2 (Leica Lasertechnik GmbH, Heidelberg, Germany). Excitation wavelengths for detection of UV, green, red, and far-red fluorescing compounds were 405, 488, 543, and 647 nm, respectively. Fluorescence emission was recorded at 430-450 nm (UV), 500-535 nm (green), 555-620 nm (red), and 665-750 nm (far-red), respectively.

2.5. Differentiation of CATH.a cells

CATH.a cells were plated either in poly-L-lysine-coated 6 well plates or poly-L-lysine-coated 3.5 mm culture dishes and grown to 80% confluence. To induce differentiation cells were incubated in the presence of dbcAMP at the indicated concentrations for the indicated time periods in serum-free culture medium. The status of differentiation was monitored using phase contrast microscopy using neurite outgrowth as a measure.

2.6. Analysis of fluorescent lipid metabolism in CATH.a cells

CATH.a cells were plated either in poly-L-lysine-coated 6 well plates (steady-state labeling with BODIPY-SM) or poly-L-lysine-coated 3.5 mm culture dishes (pulse-chase experiments) and were grown to 80% confluence. Labeling with 1 µM BODIPY-SM, BODIPY-Cer, or PYRENE-SM was performed as described above. After the indicated time periods, cells were washed with ice-cold HBSS and were harvested by scraping in 500 µl of the same buffer followed by washing the culture dish with additional 500 µl of HBSS. After centrifugation at 1,500 *x g* for 5 min at 4°C the supernatant was removed and the cell pellet was stored at -80°C until used. In pulse-chase experiments the chase-medium was collected and lipids were extracted in $CHCl_3$/MeOH (2:1, v/v).

For lipid extraction from frozen CATH.a cell pellets, cells were resuspended in 300 µl sterile water (4°C) and were sonicated for 2 x 15 sec on ice. The cell extracts were vortexed vigorously and aliquots of 15 µl were taken for determination of the protein content which was performed in duplicates according to the Bradford assay (Bradford, 1976). One ml $CHCl_3$/MeOH (2:1, v/v) was added to the remaining cell suspension, lipids were extracted, the $CHCl_3$ phase was evaporated under a stream of N_2, and the dried lipid extracts were stored at -20°C until HPLC analysis for which lipids were dissolved in 60 µl ethanol. When cells were labeled with PYRENE-SM lipids were dissolved in 35 µl ethanol before HPLC analysis.

2.7. Sphingomyelinase assay

SMase activity in CATH.a cells was measured using a fluorescence assay as described (Loidl et al., 2002). CATH.a cell were plated in poly-L-lysine-coated 6 well plates and were grown to 80% confluence. For SMase inhibitor treatment, cells were washed with HBSS and incubated with desipramine or GW4869 in serum-free culture medium at the indicated concentrations for 1.5 h.

Subsequently, cells were washed twice with ice-cold HBSS and scraped in 500 µl of the same buffer followed by washing the culture dish with additional 500 µl of HBSS. After centrifugation at 1,500 *x g* for 5 min at 4°C the supernatant was removed and the cells were either suspended in 100 µl acid lysis buffer (250 mM sodium acetate, 0.2% Triton X-100, pH 5) for analyzing aSMase activity or in 100 µl neutral lysis buffer (20 mM HEPES, 10 mM $MgCl_2$, 0.1 mM Na_3VO_3, 0.1 mM Na_2MoO_4, 10 mM β-glycerophosphate, 750 µM ATP, 1 mM PMSF, 2 mM EDTA, 20 µg/ml aprotinin, 20 µg/ml leupeptin, 0.2% Triton X-100, pH 7.4) to measure neutral Mg^{2+}-dependent SMase activity. For activity determinations of neutral Mg^{2+}-independent SMases cthe ells were lysed in 100 µl neutral lysis buffer without $MgCl_2$. The samples were sonicated in a bath-type sonicator for 2 min and were then incubated for 1 h on ice (vortexing every 10 min). Cell debris were removed by centrifugation (15,000 *x g*, 4°C, 10 min) and 10 µl aliquots of the supernatant was used for determination of the protein content which was performed in duplicates according to the Precision Red (Reagent #2) Advanced protein assay.

BODIPY-SM was used as a fluorescent substrate to determine SMase activity. BODIPY-SM (1.5 nmol) was added per ml acid reaction buffer (250 mM sodium acetate, 1 mM EDTA, ph 5) to analyze aSMase activity. nSMase activity was determined in neutral reaction buffer (20 mM HEPES, 3.5 mM $MgCl_2$) to analyze Mg^{2+}-dependent nSMase activity, under vortexing. For activity determinations of neutral Mg^{2+}-independent SMases BODIPY-SM was added to neutral reaction buffer without $MgCl_2$. Reaction buffer (150 µl) was transferred into each well of a 96 well plate and 50 µl of the corresponding lysis buffer containing 10 µg protein (the final substrate concentration was 1.5 µM) were added. The plate was shaken on a rotary shaker (1,350 rpm) for 30 sec and reaction was allowed to proceed at 37°C for 40 min in the dark. Reaction was stopped by adding 800 µl

$CHCl_3$/MeOH (2:1, v/v) and lipids were extracted as described above. Dried lipid extracts were stored at -20°C until HPLC analysis for which lipids were dissolved in 250 µl ethanol.

Substrate and protein concentrations were set to a level on which a maximum of 20% of initial BODIPY-SM substrate was converted to BODIPY-Cer to ensure a linear relationship.

2.8. RNAi in CATH.a cells

CATH.a cells were plated in poly-L-lysine-coated 6 well plates and grown to 50% confluence. Transfection of cells with siRNA was performed using Lipofectamine 2000 reagent according to the manufacturer's suggestions. siRNAs used for SMPD3 knockdown were from Qiagen (product number: 2445407_60 and 2445407_70, respectively). Twenty-four h post transfection the cells were subjected to analysis of SMase activity.

2.9. CATH.a cell treatment with SMase from **B. cereus**

CATH.a cells were grown in poly-L-lysine-coated 3.5 mm culture dishes to 80% cell confluence. Pulse-labeling with 1 µM BODIPY-SM was performed as described above. After washing the cells extensively with ice-cold HBSS cells were chased in serum-free culture medium for 1 h to ensure homogenous distribution of the fluorescent lipid to BODIPY-SM accumulating compartments. Cells were then washed once with HBSS containing 5% DF-BSA and once with HBSS alone. Subsequently, cells were treated with bacterial SMase (150 mU/ml, final concentration) at 37°C in serum-free culture medium for the indicated time periods. Cells were washed in the same way as described above and were scraped in 500 µl ice-cold HBSS followed by washing the culture dish with additional 500 µl of the same buffer. After centrifugation at 1,500 *x g* for 5 min at 4°C the supernatant was removed and the cell pellet was stored at -80°C until lipid extraction.

For HPLC analysis, dried lipid extracts were dissolved in 60 µl ethanol.

2.10. Inhibition of clathrin- and caveolae-mediated endocytosis in CATH.a cells

2.10.1. HPLC analysis

CATH.a cells were grown in poly-L-lysine-coated 6 well plates to 80% confluence. Cells were then washed with HBSS and preincubation with inhibitors was performed according to (Puri et al., 2001) with slight modifications. (a) Chlorpromazine (CP) treatment: cells were incubated in the presence of 7.5 µg/ml (final concentration) CP for 30 min at 37°C. (b) Methyl-β-cyclodextrin (MβCD) treatment: cells were treated with 5 mg/ml (final concentration) MβCD for 30 min at 37°C to deplete PM Chol. (c) Genistein (GE) treatment: cells were incubated in the presence of 200 µM (final concentration) GE for 2 h at 37°C. (d) Nystatin (NY) treatment: cells were treated with 30 µg/ml (final concentration) NY for 30 min at 37°C. (e) Chelerythrine chloride (CHEL) treatment: cells were incubated in the presence of 1.5 µM (final concentration) CHEL for 1 h at 37°C. All preincubation steps were performed in serum-free culture medium followed by pulse-labeling with 1 µM BODIPY-SM as described above in the presence of the corresponding inhibitors (exception: MβCD was only present during preincubation of CATH.a cells). (f) Potassium (K^+) depletion: cells were washed with K^+-free buffer (20 mM HEPES, 140 mM NaCl, 1 mM $CaCl_2$, 1 mM $MgCl_2$, 1 mg/ml glucose, pH 7.4) and then incubated in K^+-free hypotonic buffer (K^+-free buffer diluted 1:1 with distilled water) for 5 min at 37°C. Subsequently, cells were washed three times with K^+-free buffer and incubated in the same buffer for 20 min at 37°C before pulse-labeling with BODIPY-SM which was essentially performed in K^+-free buffer instead of serum-free culture medium. Control experiments were performed in the same way except that all buffer solutions contained 10 mM KCl.

After a 30 min chase at 37°C cells were washed with ice-cold HBSS and PM-bound BODIPY-SM was BE to DF-BSA as described above except that BE solutions contained an inhibitor cocktail (5 mM NaN_3, 50 mM 2-deoxyglucose, 2 mM iodoacetate, 10 µM FCCP; final concentrations) to prevent intracellular trafficking. Essentially all washing and BE steps were performed under the presence of the respective endocytosis inhibitors. Following BE, cells were harvested by scraping in ice-cold HBSS as described above and cell pellets were stored at -80°C until lipid extraction.

For HPLC analysis, dried lipid extracts were dissolved in 60 µl ethanol.

2.10.2. Fluorescence microscopy

CATH.a cells were grown on poly-L-lysine-coated cover slips to 60% confluence before experimental start. Inhibitor studies were carried out exactly as described above except that cells were labeled with 2.5 µM BODIPY-SM. Where mentioned cells were immediately mounted and applied to LSM after the chase period without BE. LSM was performed as described above.

2.11. Recycling of BODIPY-SM in CATH.a cell

CATH.a cells were grown in poly-L-lysine-coated 3.5 mm culture dishes to 80% cell confluence. Pulse-labeling with 3 µM BODIPY-SM was performed as described above. After washing the cells extensively with ice-cold HBSS cells were chased in serum-free culture medium at 37°C for 5, 10, and 30 min, respectively. Subsequently, cells were BE with 5% DF-BSA in ice-cold HBSS as describe above followed by a second BE with 5% DF-BSA in HBSS (37°C) for another 60 min. Therefore, prewarmed chase medium was added to the cells (defined as chase time 0) and after 10, 20, 40, and 60 min, BE medium was collected and replaced by fresh prewarmed BE medium. After 60 min cells were washed with ice-cold HBSS and harvested by scraping in ice-cold HBSS as described above. Cell pellets were stored at -80°C until lipid extraction. For HPLC analysis, dried lipid extracts were dissolved in 60 µl ethanol.

Lipids from the chase medium were extracted in $CHCl_3$/MeOH (2:1, v/v) and the dried lipid extracts were stored at -20°C until HPLC analysis for which lipids were dissolved in 60 µl ethanol.

2.12. Assessment of BODIPY-SM endocytosis

CATH.a cells were grown in poly-L-lysine-coated 3.5 mm culture dishes to 80% cell confluence. Pulse-labeling with 2 µM BODIPY-SM was performed as described above. After

washing the cells extensively with ice-cold HBSS cells were chased in serum-free culture medium at 37°C for the indicated time periods. Subsequently, cells were washed with ice-cold HBSS and BODIPY-SM was BE from the PM in ice-cold HBSS containing 5% DF-BSA and an inhibitor cocktail (see endocytosis inhibition assay) to prevent intracellular trafficking (6 x 10 min on ice). Cells were harvested by scraping in ice-cold HBSS as described above. The cell pellets were stored at -80°C until lipid extraction. For HPLC analysis, dried lipid extracts were dissolved in 60 µl ethanol.

BE fractions were pooled and lipids were extracted in $CHCl_3$/MeOH (2:1, v/v) by stirring over night at 4°C in the dark on a rotating wheel followed by vortexing for 3 min. Dried lipid extracts were stored at -20°C until HPCL analysis for which lipids were dissolved in 500 µl ethanol and aliquots were transferred to inserts containing HPLC autosampler vials.

In some experiments, lipids were extracted from each BE fraction without pooling and subjected to HPLC analysis for which the dried lipid extracts were dissolved in 180 µl ethanol.

2.13. Other assays using BODIPY-SM

To test BE efficiency, BE was performed as described above directly after pulse-labeling with BODIPY-SM. Cells were processed as described and lipids were extracted from the pooled BE fractions identically as described above.

Do determine whether BODIPY-SM endocytosis or processing occurs during treatment of cells at 4°C, cells were incubated on ice for 30 min in the dark directly after pulse-labeling with BODIPY-SM which was followed by BE, harvesting of cells, and lipid extraction from cells and pooled BE fractions.

Stability of BODIPY-SM in serum-free culture medium was examined by addition of the fluorescent lipid to serum-free culture medium (0.4 µM, final concentration) in 6 well plates followed by incubation at 37°C for the indicated time periods. Lipids were extracted in $CHCl_3$/MeOH (2:1, v/v) and the dried extracts were stored at -20°C until HPLC analysis for which lipids were dissolved in 200 µl ethanol.

2.14. HPLC analysis

Table 1: Solvent gradient used for elution of BODIPY-labeled lipids

Time [min]	Flow rate [ml/min]	Solvent A[a] [%]	Solvent B[b] [%]	Solvent C[c] [%]
- 5.0	0.7	80	20	0
- 8.0	0.7	0	100	0
- 11.7	0.7	0	100	0
- 12.0	1.0	0	100	0
- 15.0	1.0	0	20	80
- 20.0	1.0	0	20	80
- 20.5	1.0	80	20	0
- 23.0	0.7	80	20	0

[a] **Solvent A:** MeOH : H_2O : Tris/HCl (0.5 M, pH 9) 96 : 4 : 3 (v/v)
[b] **Solvent B:** ACN
[c] **Solvent C:** MeOH : Tris/HCl (0.5 M, pH 9) 97 : 3 (v/v)

Table 2: Solvent gradient used for elution of PYRENE-labeled lipids

Time [min]	Flow rate [ml/min]	Solvent A[a] [%]	Solvent B[b] [%]	Solvent C[c] [%]
- 5.0	0.7	0	20	80
- 6.0	0.7	0	100	0
- 7.7	0.7	0	100	0
- 8.0	1.0	0	100	0
- 10.0	1.0	40	20	40
- 18.5	1.0	40	20	40
- 21.0	0.7	40	20	40
- 33.0	0.7	40	20	40
- 33.5	0.7	0	20	80
- 36.0	0.7	0	20	80

[a] **Solvent A:** MeOH : Tris/HCl (0.5 M, pH 9) 96 : 1 (v/v)
[b] **Solvent B:** ACN
[c] **Solvent C:** MeOH : Tris/HCl (0.5 M, pH 9) 97 : 3 (v/v)

HPLC analysis of fluorescent lipids was performed using a method that is based on the protocol of (He et al., 2003). Lipids were dissolved in ethanol and the suspension was transferred into 1.5 ml glass autosampler vials equipped with inserts. BODIPY-labeled lipids were separated by reversed-phase HPLC (Waters HPLC 2690 Seperations Module) on a Chromasil C18 reverse-phase column (150 x 4.6 mm, 5 µm particle size; Altmann Analytik, München, Germany) equipped with the corresponding guard column (5 x 4.6 mm, 5 µm particle size) at a flow rate of 0.7-1 ml/min. BODIPY- and PYRENE-labeled lipids were eluted using the gradients described in ***Table 1*** and ***2***. A Waters 474 fluorescence detector set to 505/540 nm (Ex/Em) was used to detect BODIPY-labeled lipids or at 343/378 nm (Ex/Em) for detection of PYRENE-labeled lipids. BODIPY-C_{12}-SM was used as internal standard and the product concentration was calculated according to linear regression analysis which was established from standard curves of the respective fluorescent lipids (BODIPY-C_5-SM, BODIPY-Cer, and PYRENE-SM, respectively).

2.15. Modification of brain lipids and SM by reagent HOCl

HOCl modification of SM(d18:1/16:0) was performed at a molar oxidant:SM ratio of 2.5:1. Liposomes were prepared by dispersing 2 mg SM in 1 ml H_2O using sonication (4 x 20 sec on ice). Following lipid extraction reaction products were analyzed by MALDI-TOF-MS as described below. Residual HOCl in the reaction mixture was quenched by addition of Met at an oxidant:Met ratio of 1:5 (35.6 mM, final concentration).

Female C57Bl/6 mice were killed by cervical dislocation. The brains were removed, weighed, snap frozen in liquid nitrogen, and homogenized in a mortar. Lipid extraction was performed as described (Goti et al., 2002) and lipids were stored at -80°C until used. HOCl-mediated brain lipid modification was performed with NaOCl (1, 10, and 50 µg/100 µg lipid) over night at room temperature (RT). Subsequently, lipids were extracted, dissolved in 1 ml $CHCl_3$/MeOH (1:1, v/v), and stored at -20°C until FT-ICR-MS analysis (see below).

2.16. Modification of SM by the MPO/H_2O_2/chloride system

SM liposomes (30 µg/ml) in phosphate buffer (50 mM, pH 5) supplemented with 140 mM NaCl were incubated in the presence of MPO (70 nM, final concentration) at 37°C for 30 min under rapid shaking. Reaction was started by addition of H_2O_2 (200 µM, final concentration; 8 additions of 25 µM H_2O_2 in 4 min intervals; (Bergt et al., 2000)) and stopped by removing cationic MPO using cellulose acetate. Subsequently, SM modification was allowed to proceed at RT in the dark for further 24 h. Lipid extraction was performed as described (Folch et al., 1957), the organic phase was evaporated to dryness, and stored at -20°C until MALDI-TOF-MS analysis. For measurements lipids were dissolved in 20 µl $CHCl_3$ and 1.5 µl aliquots were applied to a gold target plate (Applied Biosystems, Germany).

2.17. MALDI-TOF-MS

For lipid analysis, a 0.5 M DHB/methanol solution containing 0.1% trifluoroacetic acid (TFA) was used as matrix. Lipids dissolved in $CHCl_3$ were directly applied to a gold target plate as 1.5 µl droplets, followed by addition of 1 µl matrix solution. Subsequently, samples were allowed to crystallize at RT or under a warm gas stream. All MALDI-TOF mass spectra were acquired on a Voyager-*DE* STR BioSpectrometry workstation (Applied Biosystems). The system utilizes a pulsed nitrogen laser, emitting at 337 nm, which was operated in positive ion mode. The extraction voltage was 20 kV and the 'low mass gate' was turned on to prevent saturation of the detector by ions resulting from the matrix. For each mass spectrum, three single spectra recorded with more than 100 single laser shots were averaged. To enhance the spectral resolution, all spectra were measured in the reflector mode.

2.18. Fourier-transform ion cyclotron resonance mass spectrometry (LC-FT-MS)

Analysis was performed on an Accela U-HPLC coupled to a LTQ-FT Ultra hybrid mass spectrometer (Thermo Scientific). Lipid extracts were diluted (1:100) in acetonitrile (ACN)/2-propanol (5:2, v/v) containing 1% ammonia acetate, 0.1% formic acid, and 1 pmol/µl d-31 34:1 PC as internal standard. Lipid samples were separated on a Thermo Hypersil GOLD C18 column (100 x 1 mm, 1.9 µm particle size). Solvent A was water with 1% ammonia acetate and 0.1% formic acid, and solvent B was ACN/2-propanol (5:2, v/v) with 1% ammonia acetate and 0.1% formic acid. The gradient ran from 35% to 70% B in 4 min, then to 100% B in another 16 min with a hold for 10 min. The flow rate was 250 µl/min. Data acquisition was done by FT-MS full scan at a resolution of 100 k and < 2 ppm mass accuracy with external calibration. The spray voltage was set to 5000 V, capillary voltage to 35 V, and the tube lens was at 120 V. Capillary temperature was at 250°C. Peak areas were calculated by QuanBrowser for all lipid species, identified previously by exact mass (< 2 ppm) and retention time. Lipids were quantified by correlation with known amounts of internal standard.

2.19. Kinetic studies of SM modification with HOCl

Liposomes prepared from chicken egg yolk palmitoyl SM (2 mg/ml stock solution) in phosphate buffer (50 mM, pH 6.5) supplemented with 140 mM NaCl were diluted to the indicated concentrations and subsequently incubated with the indicated concentrations of reagent HOCl at 37°C for 10 sec (final volume of 250 µl). The NaOCl solution was diluted 1:1 with phosphate buffer (50 mM, 140 mM NaCl, pH 5) prior to addition to prevent a shift of the pH value. Reactions were stopped by addition of $CHCl_3$/MeOH (2:1, v/v) to extract lipids. After vortexing rigorously for 1 min PC(16:0/16:0) (3 µg/ml, final concentration) was added as internal standard before further vortexing for 1 min. The organic phase was removed and dried under a stream of N_2. Samples were redissolved in MeOH and analyzed by HPLC-ESI-MS (Aquity UPLC, Synapt HDMS Q-TOF, Waters, Manchester, UK), using a Waters C18 column (2.1 x 50 mm, 1.7 µm) and a gradient from H_2O/MeOH (1:1, v/v) to isopropanol. Extracted ion chromatograms of m/z 703.58 (SM) and m/z 734.57 (PC) were

integrated using the MassLynx Software (Waters). Reaction rates and second-order rate constants (k_2) were calculated by following the time-dependent decrease of the m/z 703.58 peak.

2.20. PC12 cell experiments with SM, HOCl-SM, and HOCl

PC12 cells were incubated in serum-free RPMI 1640 medium supplemented with 0.4% (v/v) HEPES buffer, 0.4% (w/v) sodium pyruvate, 0.4% (w/v) L-glutamine, and 50 µg/ml gentamycin in the absence or presence of SM, HOCl-SM, or reagent HOCl. SM(d18:1/16:0) (stock solution 2.85 mM), HOCl-modified SM(d18:1/16:0) (HOCl-SM, used within two days after modification), and reagent HOCl (aqueous stock solution, 832 mM, stored at 4°C) were applied to PC12 cells at indicated concentrations and time periods. HOCl-SM concentrations were calculated with the molecular weight of the SM(d18:1/16:0)-derived chlorohydrin which was identified as the dominant HOCl-modified lipid species.

2.21. Cell viability (MTT assay)

PC12 cells were plated in 96 well plates (20,000 cells per well; the cells were counted manually by a hemacytometer after trypsinization) and allowed to grow for 24 h before the cells were treated with SM, HOCl-SM, or reagent HOCl in serum-deprived medium at indicated concentrations and indicated time periods. MTT (1.2 mM, dissolved in serum-free medium, 100 µl per well) was added to cells and incubated for 3 h at 37°C under standard conditions. Cells were washed with PBS, and cell lysis was performed with 100 µl lysis solution (isopropanol/1 M HCl, 25:1 (v/v)) on a rotary shaker (1,200 rpm, 15 min; (Kratzer et al., 2007)). Absorbance was measured at 570 nm on a Victor 1420 multilabel counter and corrected for background absorption (650 nm).

2.22. Measurement of ROS

ROS formation was examined using fluorescent DCF (940 nmol N_2-dried H_2DCFDA were dissolved in 250 µl DMSO before application). Rather than being a radical species selective probe, DCFDA (after hydrolysis to dichlorofluorescein and internalization) is converted to fluorescent dichlorofluorescein by several reactive radical species and allows assessment of general oxidative stress (Halliwell and Whiteman, 2004). PC12 cells were plated in 12 well plates and grown to 80% confluence. Cells were washed two times with PBS and then incubated in the absence or presence of SM or HOCl-SM at 37°C at indicated concentrations for the indicated time periods. Incubations were stopped by washing cells two times with PBS and subsequently, H_2DCFDA dissolved in HBSS (12.5 µM) was added and cells were incubated for further 1 h at 37°C in the dark. Then, the plates were kept on ice for 10 min, washed two times with ice-cold PBS, and cell lysis was performed with 100 µl lysis solution (3% Triton X-100 in PBS) on a rotary shaker (1,350 rpm) at 4°C in the dark for 60 min. Afterwards, 30 µl absolute ethanol was added to each well and shaking was continued for another 15 min to ensure complete dissolving of deacetylated and oxidized DCF. The cell lysates were transferred to Eppendorf tubes and centrifuged to remove cellular debris (13,000 rpm, 4°C, 10 min). One hundred µl of the supernatant was transferred to black 96-well microtiter plates and fluorescence intensity (FI) was measured at 484/540 nm (Ex/Em) on a Victor 1420 multilabel counter (Wallac). An aliquot of the supernatant was used for estimation of protein concentration using the BCA assay.

2.23. JC-1 assay

To examine $\Delta\psi m$ of PC12 cells, the JC-1 assay was performed. JC-1 is a cationic, lipophilic, fluorescent dye that can easily enter the electronegative matrix of intact mitochondria. As a monomer, JC-1 exhibits green fluorescence. Concentration-dependent accumulation in mitochondria leads to formation of J-aggregates resulting in a shift from green to red fluorescence. Hence, mitochondrial depolimerization that occurs in early apoptotic cascade can be observed *via* decrease in red and increase in green fluorescence. To achieve optimal assay conditions for PC12 cells, concentration dependency and kinetics

of JC-1 uptake as well as sensitivity to FCCP, an uncoupler of the respiratory chain used for background correction, was determined first. Therefore, PC12 cells were plated in black 96 well plates (20,000 cells per well) and allowed to grow for 24 h. Medium was removed and cells were washed with PBS before addition of JC-1 (dissolved in serum-free medium, 100 µl per well) at indicated concentrations for indicated times at 37°C in the dark. Following two washing steps with PBS, cells were treated either with FCCP or an equivalent vehicle control, which were added 30 min after loading the cells with JC-1, at indicated concentrations for indicated times at 37°C in the dark. After 30 min PC12 cells were washed twice with PBS, fifty µl PBS were then added to each well and the FI read at 484/540 (excitation/emission) for detection of the green substrate, and 544/590 (excitation/emission) for detection of the red substrate on a Victor 1420 multilabel counter. The results were analyzed in terms of the ratio of red and green FIs. Therefore, results are not linked to the number of viable cells.

In all other assays SM, HOCl-SM, or reagent HOCl in serum-deprived medium was added at the indicated concentrations for the indicated time periods. Cells were then washed with PBS and incubated with JC-1 (2.5 µM) at 37°C in the dark for 30 min. After two washing steps with PBS cells were treated in parallel with either vehicle control or FCCP (5 µM) for 30 min at 37°C in the dark and then processed as described above.

2.24. Oxygraph measurements

To examine cellular oxygen flux and phosphorylation control in cell respiration Oxygraph-2k (OROBOROS) was used according to the protocol of Gnaiger (Hutter et al., 2006) with some modifications. Briefly, PC12 cells were trypsinized and afterwards resuspended in serum-free medium. The cell suspension (2.5 ml) was added into each Oxygraph-2k chamber at a concentration such that routine respiration yields a volume-specific oxygen flux of about 60 $pmol.s^{-1}.cm^{-3}$ (6 x 10^5 cells/ml), while rotation of the stirrers was maintained in the Oxygraph-2k. Chambers were then closed by fully inserting the stoppers, thereby extruding all gas bubbles. Residual cell suspension from the receptacle was siphoned off, respective substances were applied using a 25 µl syringe (Hamilton), and

oxygen flux was recorded for 6 h at 37°C in the absence or presence of HOCl-SM (66 µM). To block ATP synthesis, titration 1 µl oligomycin (5 mM) into each chamber was performed. When oxygen flux declined to a new steady state, titration of 1 µl FCCP (10 mM) was started into each chamber for total uncoupling of mitochondrial respiratory chain and continued till a plateau or even a slight inhibition of oxygen flux was reached. Subsequently, titration of 1 µl KCN (10 mM) was performed for background correction. Afterwards, values for aerobic activity of cells under routine culture conditions (C_r), the oligomycin-inhibited leak of respiration (C_{ro}), and the maximum stimulated respiration after treatment of cells with FCCP (C_{ru}) were used to calculate the relative routine rate ($\mathbf{j'_r} = C_r/C_{ru}$), oligomycin-inhibited respiration rate ($\mathbf{j'_{ro}} = C_{ro}/C_{ru}$), and phosphorylation control ratio ($\mathbf{j'_p} = (C_r-C_{ro})/(C_{ru})$).

2.25. Western blot analysis of caspase-3 activation and PARP cleavage

PC12 cells (80% confluency, 9 cm^2 culture plates) were incubated in the absence or presence of SM, HOCl-SM, reagent HOCl, or colchicine at indicated concentrations for indicated time periods. For protein isolation, the cells were washed with ice-cold PBS and then scraped in 70 µl lysis buffer (50 mM Tris/HCl pH 7.4, 1% NP-40, 150 mM NaCl, 1 mM Na_3VO_4, 1 mM NaF, 1 mM EDTA, 10 µM PMSF, aprotinin, leupeptin, pepstatin: 1 µg/ml each). After sonication (2 x 2 min on ice) cell debris were removed by centrifugation (13,000 rpm, 4°C, 10 min) and the protein content was determined using the BCA assay. Detergent protein extracts were diluted in sample buffer and boiled for 5 min at 95°C prior to SDS-PAGE. Proteins were separated by linear PAGE (150 V, reducing conditions) and electrophoretically transferred onto PVDF membranes (150 mA). To block nonspecific adsorption, membranes were incubated with 5% (w/v) non-fat milk powder in Tris-buffered saline Tween-20 (TBS-T). Polyclonal rabbit anti-caspase-3 antibody and polyclonal rabbit anti-PARP antibody (diluted 1:200 and 1:500, respectively, both in 5% (w/v) non-fat milk powder in TBS-T, incubation over night at 4°C) were used as primary antibody. Immunoreactive bands were visualized using HRP-conjugated goat anti-rabbit IgG (dilution

1:5,000 in 5% (w/v) non-fat milk powder in TBS-T, 2 h incubation) and subsequent SuperSignal development.

2.26. Sub-G1 population analysis

PC12 cells (80% confluency, 9 cm^2 culture plates) were incubated in the absence or presence of SM, HOCl-SM, reagent HOCl, or colchicine at indicated concentrations for indicated time periods. At indicated time points, both, control and treated cells were harvested (0.25% trypsin-EDTA), resuspended in 500 µl PBS (pH 7.4), fixed with 5 ml ice-cold MeOH, and stored at 4°C. Propidium iodide (PI) staining was done using DNA-Prep stain (PI = 50 µg/ml) and RNase (4 KU/ml; type III-A, bovine pancrease); (Hrzenjak et al., 2006)). Finally, the cells were analyzed on Coulter EPICS XL-MCL using System II/3.0 data analyzing software (Beckman Coulter).

2.27. Sample preparation for 2D-DIGE

Confluent PC12 cells on 75 cm^2 flasks were incubated for 24 h in the absence or presence of SM or HOCl-SM (47.5 µM), respectively. Cells were washed with sucrose (250 mM in 10 mM Tris/HCl, pH 7.4), then scraped in 100 µl lysis buffer (7 M urea, 2 M thiourea, 4% CHAPS, 30 mM Tris) and processed for 2D-DIGE. Cell lysates were sonicated (4 x 10 sec on ice) and centrifuged (13,000 rpm, 15°C, 10 min). Lysates from control, SM-, and HOCl-SM-treated cells were labeled using Cy dyes according to the manufacturer's recommendations. Protein lysates of control cells were labeled with Cy2, whereas protein lysates from SM- and HOCl-SM-treated cells were labeled with Cy3 or Cy5. The protein content was determined using the Bradford assay. Protein (50 µg) from cell lysates was labeled with 400 pmol of amine reactive Cy2, Cy3, or Cy5 N-hydroxysuccinamide (NHS) ester DIGE dyes (Amersham Biosciences), freshly dissolved in anhydrous dimethyl formamide. The labeling mixture was incubated on ice in the dark for 30 min. The reaction was quenched by addition of lysine (10 nmol) followed by incubation on ice for another 10

min. Each respective labeled protein sample was mixed with equal volumes of 2 x sample buffer containing 7 M urea, 2 M thiourea, 4% (w/v) CHAPS, 2% (w/v) DTT, and 2% (v/v) Pharmalyte (pH 3-10) and subsequently left on ice for 10 min. Afterwards, 600 µg of the corresponding unlabeled protein lysates were added to respective labeled protein samples, and the three samples were mixed prior to isoelectric focusing (IEF) on Immobiline IPG strips.

2.28. 2D-DIGE and Image Analysis

The IPG strips (24 cm, linear pH range of 3-10) were rehydrated over night in ceramic strip holders in 600 µl reswelling solution containing 1.95 mg of protein lysates from control, SM-, and HOCl-SM-treated cells (see above), 7 M urea, 2 M thiourea, 1% (w/v) CHAPS, 0.4% (w/v) DTT, 0.5% (v/v) Pharmalyte (pH 3-10), and 0.002% (v/v) Bromophenol blue. To prevent adverse IEF of proteins, at least 300 µl of reswelling solution were mixed with the merged protein lysates. IEF was carried out at 20°C with a maximum current set at 50 µA/strip using an Ettan IPGphor unit (Amersham Biosciences). After IEF (3 h at 150 V, 3 h at 300 V, 3 h at 600 V, remaining time at 8,000 V to reach a total of 50,000 Vh) strips were equilibrated in SDS equilibration buffer (6 M urea, 2% (w/v) SDS, 30% (v/v) glycerol, 50 mM (v/v) Tris/HCl, pH 8.8) either supplemented with 1% (w/v) dithiothreitol (first equilibration step, 15 min) or with 4.5% (w/v) iodoacetamide (second equilibration step, 15 min), each under gentle shaking. IPG strips were directly applied to self-cast SDS gels (12%). SDS-PAGE was carried out at 18°C (Ettan Dalt, Amersham Biosciences; 15 mA/gel). Fluorescence imaging was performed on a Typhoon 9400 scanner (Amersham Biosciences; excitation 488/532/633 nm, emission 520/580/670 nm for Cy2, Cy3, and Cy5, respectively). Statistical analysis and quantification of protein spots was carried out using the DeCyder-DIA software (Amersham Biosciences). Differentially expressed protein spots were manually picked and in gel tryptically digested. Fold-regulation is expressed as mean from three different gels run from three independent experiments.

2.29. LC-MS/MS analysis of tryptic digests

Peptide extracts were dissolved in 0.1% formic acid and separated on a nano-HPLC system. Seventy µl were injected and concentrated on the loading column (LC Packings C18 PepMapTM, 5 µm, 0.3 x 5 mm, 100 Å; LC Packings, Amsterdam, NL) for 5 min using 0.1% formic acid as isocratic solvent at a flow rate of 20 µl/min. The column was then switched into the nanoflow circuit, and the sample was loaded on the nanocolumn (LC-Packings C18 PepMap, 0.075 x 150 mm) at a flow rate of 300 nl/min and separated using a gradient from 0.3% formic acid and 5% ACN to 0.3% formic acid and 50% ACN over 60 min. The sample was ionized in a Finnigan nano-ESI ion source (Finnigan MAT, San Jose, USA) equipped with NanoSpray tips (PicoTipTM Emitter, New Objective, Woburn, MA, USA) and analyzed in a Thermo-Finnigan LCQ Deca XPplus ion trap mass spectrometer. The MS/MS data were analyzed by searching the National Center for Biotechnology Information (NCBI) public database with SpectrumMill version 2.7 (Agilent, Waldbronn, Germany). Acceptance parameters were at least three or more identified distinct peptides.

2.30. Clustering of identified proteins

Relative expression patterns (log_2(control/SM) and log_2(control/HOCl-SM)) for spots within one gel representing the same protein (Refseq protein identifier) were filtered for outliers (> upper quartile + 1.5*IQR (inter quartile range) or < lower quartile - 1.5*IQR). The median from the remaining values were averaged over 2 or 3 gels resulting in one expression value for each identified protein. Data were combined, grouped and visualized as heatmaps using Genesis (Sturn et al., 2002).

2.31. Ingenuity Pathway Analysis (IPA)

Differentially expressed proteins were analyzed using a free trial version of the IPA software to monitor possible global proteomic regulation in response to SM and HOCl-SM.

IPA (www.ingenuity.com; https://analysis.ingenuity.com) uses a knowledge base derived from the literature to relate gene products, based on their interaction and function. This software is designed to identify biological networks, global canonical pathways, and global functions. The identified proteins and their corresponding x-fold change and accession numbers were uploaded as .txt file into the Ingenuity software package. Ingenuity uses these data to navigate the Ingenuity Pathways Knowledge Base and extract overlapping networks between the candidate proteins. A score of better than 2 is usually attributed to a valid network (the score represent the log probability that this network was found by random chance).

2.32. Identification of cytoskeletal alterations in PC12 cells in response to SM/HOCl-SM treatment

2.32.1. Immunofluorescence

PC12 were grown in collagen-coated chamber slides to 80% confluence. After washing with PBS cells were incubated in serum-free culture medium in the absence or presence of SM or HOCl-SM at the indicated concentrations for 24 h at 37°C. Subsequently, cells were washed with PBS and the actin cytoskeleton was stained using Alexa Fluor 488-labeled phalloidin in a simultaneous fixation, permeabilization, and staining step according to the manufacturer's protocol. Subsequently, cells were washed three times with PBS and nonspecific absorption was blocked with Ultra V Blocking reagent. Blocking was followed by incubation with monoclonal mouse anti-β-tubulin antibody (diluted 1:200 in antibody diluent) for 1 h in the dark followed by four washing steps in PBS (5 min each). Cy5-labeled goat anti-mouse antibody (diluted 1:150 in antibody diluent) was used as secondary antibody (incubation for 1 h in the dark). Following 4 washing steps with PBS (5 min each) PC12 cell nuclei were counterstained with DAPI for 10 min in the dark. After extensive washing with PBS cells were mounted and subjected to immunofluorescence analysis.

2.32.2. Western blotting

Do compare intracellular actin- and tubulin content in PC12 cells after treatment with SM/HOCl-SM Western blot analysis were performed. Cells were grown in collagen-coated 6 well plates to 80% confluence. After washing with PBS cells were incubated in serum-free culture medium in the absence or presence of SM or HOCl-SM at the indicated concentrations for 24 h at 37°C. For protein isolation, the cells were washed with ice-cold PBS, scraped in lysis buffer, and protein extracts were processed as described above (analysis of caspase-3 activation and PARP cleavage). Linear PAGE, protein transfer onto PVDF membranes, and blocking nonspecific adsorption was performed as described. Monoclonal mouse anti-β-actin and anti-β-tubulin antibody (diluted 1:2,500 and 1:500, respectively, both in 5% (w/v) non-fat milk powder in TBS-T, 2 h incubation at RT) were used as primary antibody. Immunoreactive bands were visualized using HRP-conjugated goat anti-mouse IgG (dilution 1:5,000 in 5% (w/v) non-fat milk powder in TBS-T, 2 h incubation at RT) and subsequent SuperSignal development.

2.33. Statistical analysis

Data are presented as mean ± SD. ANOVA with Bonferroni correction (using the GraphPad Prism package) was used for analysis of statistical significance. All values of $p < 0.05$ were considered significant. For proteome analyses only spots that were regulated ≥ 2-fold (up or down; DeCyder software; GE-Healthcare) were picked and further processed for identification.

III. RESULTS

First Part

1. BACKGROUND

The SL family plays key role in cellular membrane organization and the initiation/execution of signaling events. SL are able to physically associate with each other and are able to engage in hydrogen bonding with Chol thereby generating highly-ordered and rigid lipid microdomains that alter the physical and biochemical properties of cellular membranes. Together with specialized proteins these microdomains form lipid rafts, structures that play essential roles in endocytosis, protein sorting and transport, and signaling (Neumann and van Meer, 2008).

Moreover, many SL have been identified as bioactive lipids that determine cell fate. They play key roles in inflammatory processes and can regulate cell proliferation, cell growth and survival, migration, senescence, and apoptosis (Hannun and Obeid, 2008). Among this diverse set of lipids, Cer and S1P are the most prominent SL involved in signaling pathways. S1P is a key regulator of proliferation, inflammation, and cell survival representing an anti-apoptotic lipid that can be considered as the “counterpart” of Cer. Cer itself is the most prominent pro-apoptotic lipid triggering differentiation, senescence, and regulation of cell growth and cell death. Cer can be generated *de novo* or by SM hydrolysis, mediated by either aSMase or nSMase. Because the cellular SM content is a magnitude higher than that of Cer, already small changes in the cellular SM pool can induce an enormous increase of Cer during activation of the apoptotic machinery.

SL are highly enriched in the brain. Especially GalCer and SM are located in the neuronal myelin sheath where they ensure proper neuronal function. However, SL were also shown to be involved in neurodegeneration. Neurodegenerative disorders are often accompanied by apoptotic cell death. A variety of studies highlighted the role of SM-derived Cer as inducer of neuronal, glial, and oligodendrocyte cell death during disease progression (Jana and Pahan, 2004; Jana and Pahan, 2010a; Jana and Pahan, 2010b).

Therefore, it is important to gain a detailed understanding of SL metabolism in neuronal tissue.

2. AIMS

The first part of my thesis aimed at examining uptake mechanisms of fluorescently-labeled SL derivates and clarifying intracellular trafficking and metabolism of these model lipids in a neuronal cell line (CATH.a). Special emphasis was placed on SM as this lipid is highly enriched in the CNS and represents the main precursor for the generation of pro-apoptotic Cer and other signaling SL species. During theses studies we examined:

i.) uptake of BODIPY-labeled SL in CATH.a cells

ii.) metabolism of BODIPY-SM and BODIPY-Cer in differentiated and undifferentiated CATH.a cells

iii.) contribution of a/nSMase to BODIPY-SM hydrolysis

3. AIM 1 – UPTAKE OF BODIPY-LABELED SL IN CATH.A CELLS

CATH.a is a catecholaminergic cell line of neuronal origin derived from transgenic mice harboring the SV40 T antigen oncogene under the transcriptional regulation of the rat tyrosine hydroxylase promoter. CATH.a cells express several markers specific for differentiated neurons thus representing an appropriate CNS neuronal model for the pulse-chase and steady-state labeling experiments described below.

3.1. Pulse-chase experiments

The first series of experiments was designated to study time-dependent uptake as well as localization and subcellular distribution of a fluorescent SM analogue in CATH.a cells by using the fluorescent lipid BODIPY-SM. This fluorescent tracer was used because the

BODIPY fluorophore exhibits higher photostability and fluorescence intensity compared to other fluorophores (e. g. NBD, PYRENE).

"Pulse-chase" experiments were performed in order to achieve adequate cell labeling already after short incubation time periods. Cells grown on glass cover slips were labeled (pulsed) with BODIPY-SM in serum-free medium at the indicated concentration for 30 min at 4°C to inhibit endocytosis and to allow the lipid to equilibrate with the PM-lipid pool. After washing, cells were incubated in serum- and label-free medium (chased) at 37°C for the indicated time periods and remaining fluorescent SM at the PM was removed by a back-exchange (BE) step where cells were washed extensively with 5% DF-BSA in HBSS at 4°C. Uptake and distribution of the fluorescent lipid was examined by laser scanning microscopy (LSM).

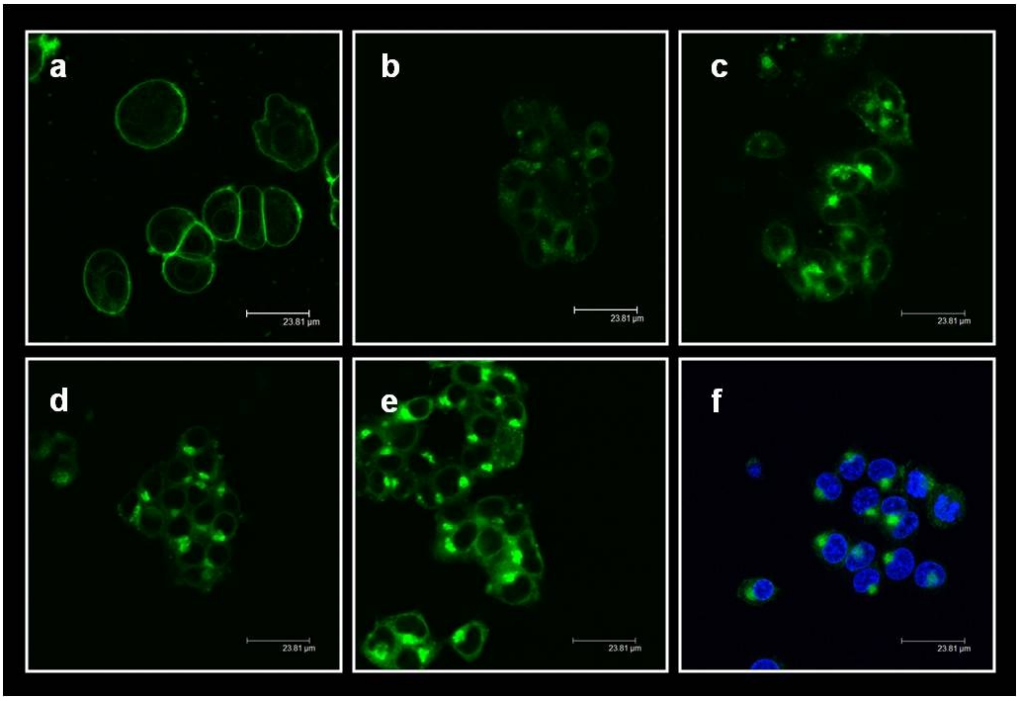

Figure 15: Uptake and subcellular localization studies of fluorescent BODIPY-SM in CATH.a cells by application of pulse-chase experiments. CATH.a cells, grown on poly-D-lysine-coated cover slips, were cooled at 4°C for 10 min and then pulse-labeled with BODIPY-SM (2.5 µM) in serum-free culture medium for 30 min at 4°C. Cells were washed extensively with HBSS and were chased in serum-free culture medium for (***b***) 5 min, (***c***) 15 min, (***d***) 30 min, (***e***) 60 min, or (***f***) 240 min at 37°C. Remaining BODIPY-SM at the PM was BE by washing the cells 6 times for 10 min with 5% DF-BSA in ice-cold HBSS at 4°C before subjecting cells to LSM. Cells in ***a*** were pulse-labeled with BODIPY-SM as described above, washed extensively with HBSS, and were immediately analyzed by fluorescence microscopy without chasing at 37°C and BE. Nuclei of CATH.a cells in ***f*** were counterstained with HOECHST (5 µg/ml) for 10 min at 37°C.

Results shown in ***Figure 15 a*** demonstrate incorporation of the majority of BODIPY-SM into the PM after pulse labeling for 30 min at 4°C. Efficient and rapid intracellular uptake of the fluorescent SM analogue already 5 min after chasing at 37°C was observed (***Fig. 15 b***). At early stages (< 10 min, ***Fig. 15 b***) BODIPY-SM was present in punctuated intracellular structures that most probably resemble early recycling endosomes which may transport BODIPY-SM and/or BODIPY-SM-derived BODIPY-Cer, generated *via* activation of SMases to late endosomes/lysosomes or the Golgi apparatus, which represents the point of intersection in SL synthesis and trafficking. Therefore, it is not surprising that at later time points (15 min – 240 min, ***Fig. 15 c – f***) SM is primarily localized at perinuclear regions resembling most probably the Golgi apparatus. Interestingly, accumulation of BODIPY-SM at pericentriole regions was not observed until a 15 min chase period but was still detectable after 30 min of incubation at 37°C. This suggests an ongoing recycling mechanism for BODIPY-SM within CATH.a cells following the secretory pathway. This pathway is characterized by recycling endosome-mediated transport of the lipid from the PM to the Golgi (maybe accompanied by SM degradation to Cer) followed by its transport back to the cell surface. These results parallel previous studies in which a recycling mechanism to the Golgi apparatus has been shown for endocytosed SM in CHO-K1 cells (Koval and Pagano, 1989). Due to the fact that SM should be localized in high amounts to the PM or to early/late endosomes or lysosomes, it is likely that most of internalized BODIPY-SM is hydrolyzed to BODIPY-Cer either *via* PM-bound nSMase or *via* aSMase that can localize to the PM and to lysosomes. BODIPY-Cer was previously shown to be a reliable marker for the Golgi apparatus (Marks et al., 2008) although the exact sorting pathways/mechanisms are not known. To elucidate intracellular localization of BODIPY-SM in more detail, co-localization experiments with organelle-selective, fluorescent probes were performed.

3.2. BODIPY-SM accumulating compartments

To identify BODIPY-SM accumulating compartments CATH.a cells were stained with specific markers for lysosomes, ER, Golgi, and the PM as described in ‘Materials and Methods’.

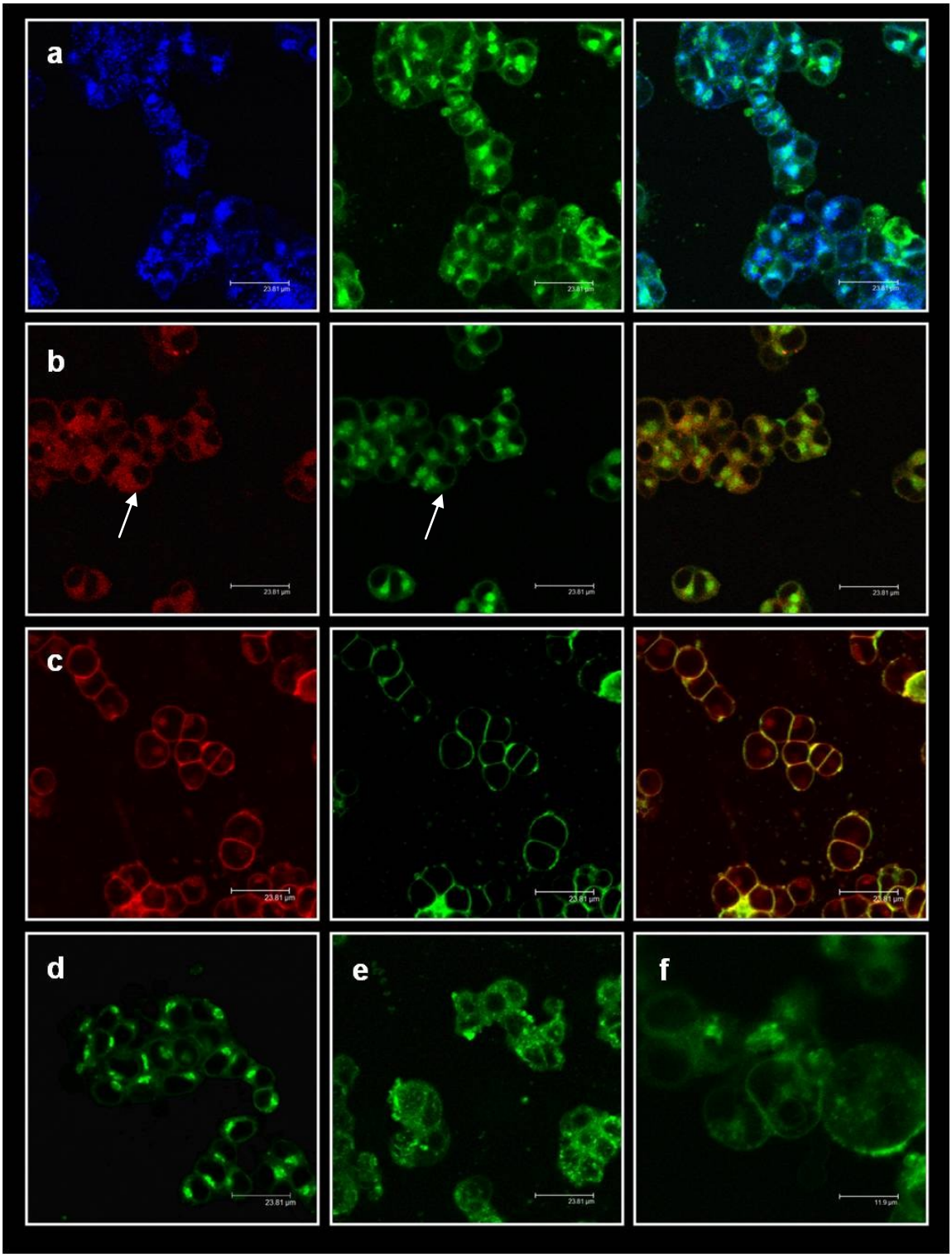

Figure 16: Colocalization studies of fluorescent BODIPY-SM with organelle-specific markers in CATH.a cells. CATH.a cells, grown on poly-L-lysine-coated cover-slips, were cooled at 4°C for 10 min and then pulse-labeled with BODIPY-SM (2.5 µM) for 30 min at 4°C. Cells were washed extensively with HBSS and were chased for 30 min at 37°C in the presence of the organelle specific markers LysoTracker Blue DND-22 (70 nM; ***a***) or ER-Tracker Blue-White DPX (500 nM; ***b***) followed by a BE as described. Cells in ***c*** were stained with CellMask Plasma Membrane Stain (5 µg/ml) for 5 min at 37°C prior to pulse-labeling with BODIPY-SM. After pulse-labeling cells were washed extensively with HBSS and were immediately analyzed by fluorescence microscopy without chase and BE.

Fluorescence images of both the BODIPY-SM and the organelle-specific probes were recorded from the same field of cells and then used to produce overlays from the double staining. In ***d*** CATH.a cells were stained with BODIPY-Cer (2.5 µM) in the same way as it was described for BODIPY-SM. In ***e*** and ***f*** cells were pretreated with nocodazole (30 µM) or brefeldin A (20 µg/ml) for 90 min at 37°C and were then stained with BODIPY-SM. All subsequent incubation steps in ***e*** and ***f*** were carried out in the presence of nocodazole or brefeldin A. If not noted otherwise, a 30 min chase period (37°C) was followed by BE. All incubation and staining steps were carried out in serum-free culture medium.

Interestingly, BODIPY-SM does not localize to lysosomes (***Figure 16 a***) after 30 min of incubation with the fluorescent lipid. Investigations of BODIPY-metabolism in CATH.a neurons (see Figure 20 below) as well as in PC12 cells (data not shown) using HPLC analysis revealed rapid hydrolysis of the tracer in both cell lines even after short chasing times. Therefore, BODIPY-Cer generation *via* activation of SMases is very likely to occur. Colocalization of BODIPY-SM and the lysosomal tracker in the Golgi apparatus (***Fig. 16 a***) is presumably due to partial mislocalization into this compartment. As it is evident, that BODIPY-SM is not transported to CATH.a lysosomes (at least not at the investigated time intervals) Cer generation presumably takes place at the PM.

In contrast to lysosomes we could detect partial delivery of BODIPY-labeled lipids to the ER (***Fig. 16 b***; white arrows). Under normal conditions only low concentrations of SM can be detected in the ER. Therefore it is likely that BODIPY-Cer, other SL species (generated *via* breakdown of BODIPY-SM), or other lipid classes (e. g. PL that gain excess to the BODIPY-labeled FA acyl chain) are responsible for ER staining. This is a reasonable explanation considering that the ER is the first site in both SL and PL synthesis. Many reactions in SL turnover are reversible, enabling degradation of complex SL (such as SM) and re-incorporation of the fluorescent FA acyl chain in newly synthesized PL in the ER.

Additionally we confirmed insertion of BODIPY-SM into the PM right after pulse-labeling at 4°C (***Fig. 16 c***). Obviously, SM inserts into the PM at low temperature without trafficking to other cellular compartments. Therefore, passive diffusion of BODIPY-SM can be ruled out because active endocytic processes as well as enzyme-based degradation of BODIPY-SM should not occur at these temperatures.

Furthermore CATH.a cells were labeled with the Golgi marker BODIPY-Cer. These experiments revealed the same subcellular distribution of the fluorescent tracer as observed with BODIPY-SM (***Fig. 16 d***). These results strengthen previous assumptions that a

significant amount of BODIPY-SM is rapidly hydrolyzed generating BODIPY-Cer that subsequently localizes to the Golgi.

Finally, it was demonstrated that uptake of BODIPY-SM is a microtubule-dependent process: Pretreatment of CATH.a cells with the microtubule-disrupting agent nocodazole (***Fig. 16 e***) resulted in accumulation of BODIPY-SM in punctuate structures within the cells. These ministacks result from Golgi fragmentation due to disruption of the microtubular network. These results were confirmed by Golgi disruption using brefeldin A (***Fig. 16 f***). In response to Golgi fragmentation PM and diffuse intracellular fluorescence was observed.

3.3. Uptake mechanism of BODIPY-SM in CATH.a cells

In the next set of experiments BODIPY-SM uptake was pharmacologically manipulated. The outcome of these (ant)agonists on intracellular BODIPY-SM trafficking and turnover was visualized by LSM and quantitatively analyzed by HPLC. CATH.a cells were treated with various inhibitors of clathrin- and caveolae-mediated endocytosis. To dissect clathrin-dependent pathways, chlorpromazine (CP) was used. This compound causes assembly of the clathrin lattice on endosomal membranes and prevents the assembly of coated pits at the PM (Wang et al., 1993). Caveolae-mediated endocytosis was inhibited with the cholesterol binding/depleting drugs methyl-β-cyclodextrin (MβCD) and nystatin (NY), or the Tyr kinase inhibitor genistein (GE).

Cells were preincubated in the presence or absence of the respective inhibitors at the indicated concentrations for 30 min (2 h in case of GE) at 37°C, before cells were pulse-labeled with BODIPY-SM at 4°C. After a 30 min chase at 37°C cells were analyzed by LSM either prior of after a BE step to DF-BSA.

To verify results obtained from immunofluorescence analysis and to get a closer insight into the kinetics of SM hydrolysis to Cer, HPLC analysis of cellular lipid extracts was performed. CATH.a cells were treated with endocytosis inhibitors, pulse-labeled with BODIPY-SM, cellular lipids were extracted and the cell-associated BODIPY-SM and BODIPY-Cer concentrations were quantitated by peak area comparison with external standards.

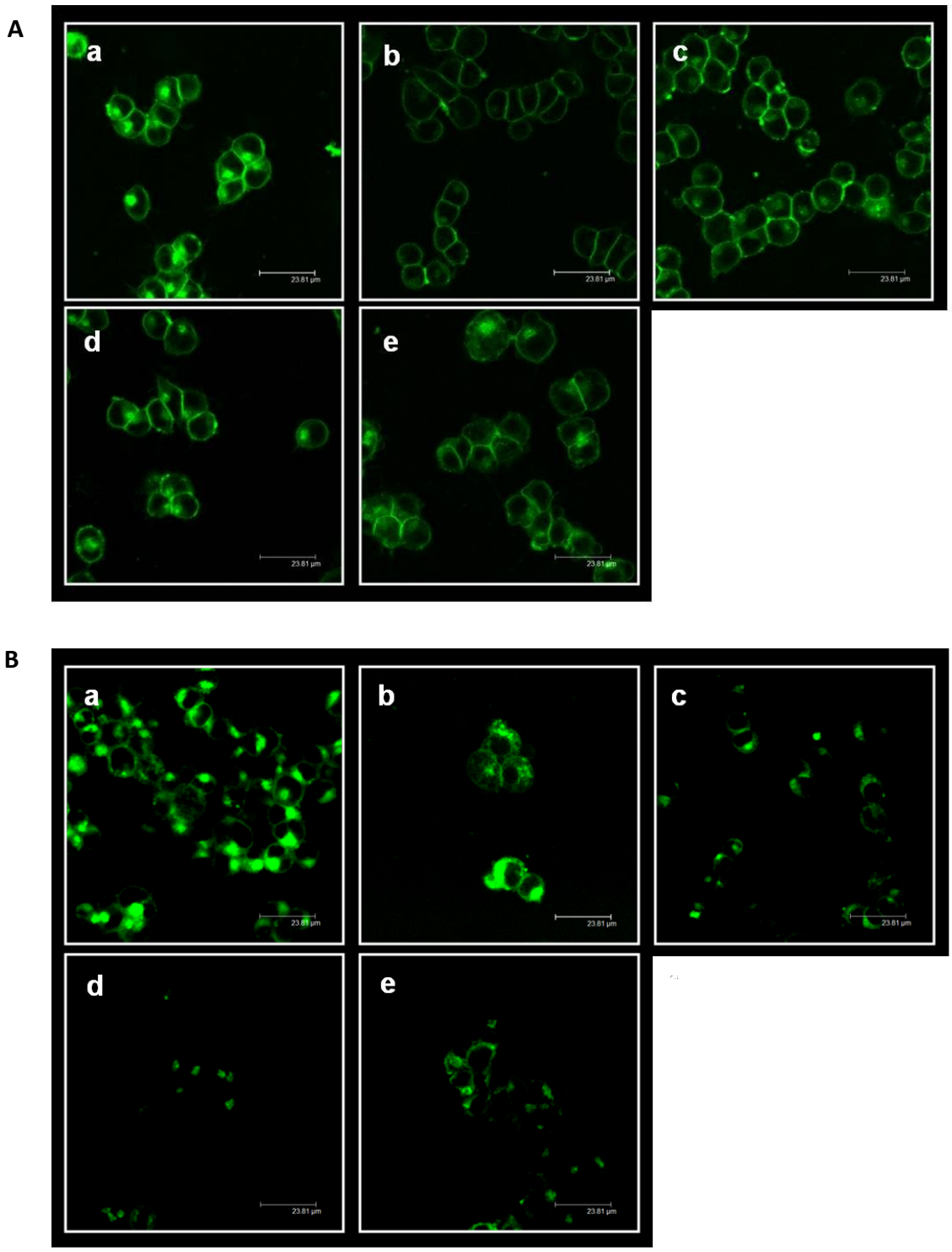

Figure 17: Effects of inhibitors of clathrin- and caveolae-mediated endocytosis on BODIPY-SM uptake by CATH.a neurons. LSM analysis was performed prior (A) or after (B) a BE to DF-BSA. CATH.a cells, grown on poly-L-lysine-coated cover slips, were preincubated in the absence (***a***) or presence of CP (7.5 µg/ml, ***b***), MβCD (5 mg/ml, ***c***), NY (30 µg/ml, ***d***), or GE (200 µM, ***e***) for 30 min at 37°C (2 h in case of GE preincubation). Cells were then washed two times with ice-cold HBSS. Cells were allowed to cool down at 4°C for 10 min before they were pulse-labeled with BODIPY-SM (2.5 µM) for 30 min at 4°C. Cells were washed extensively with HBSS and were chased for 30 min at 37°C. All incubation steps were performed in the presence of respective inhibitors except for MβCD which was present only during the preincubation period. All micrographs were recorded with the same laser intensity.

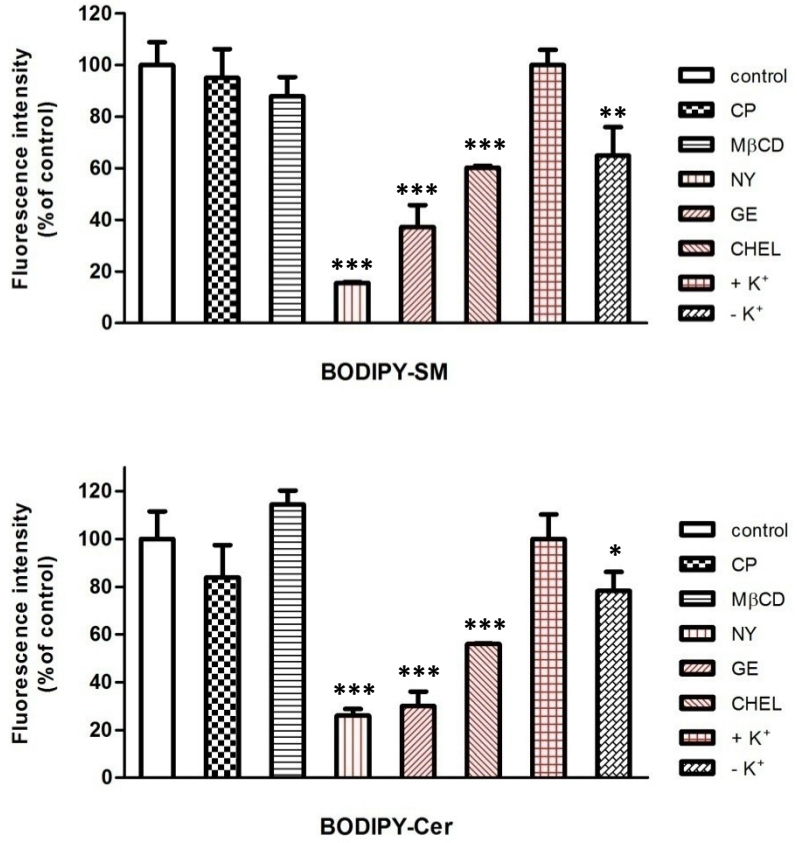

Figure 18: Uptake and conversion of BODIPY-SM in CATH.a cells using inhibitors of clathrin- and caveolae-mediated endocytosis. CATH.a cells, grown on poly-L-lysine-coated 6 well plates, were preincubated in the absence or presence of either CP (7.5 µg/ml), MβCD (5 mg/ml), NY (30 µg/ml), GE (200 µM), or CHEL (1.5 µM) for 30 min at 37°C (2 h for GE, 1 h for CHEL). K^+ depletion was performed using hypotonic K^+-free buffer as described in 'Materials and Methods'. Cells were then washed two times with ice-cold HBSS. Cells were allowed to cool down at 4°C for 10 min before they were pulse-labeled with BODIPY-SM (1 µM) for 30 min at 4°. Cells were washed extensively with HBSS and were chased for 30 min at 37°C. Subsequently, cells were washed again with HBSS and were BE with 5% -DF-BSA in ice-cold HBSS (6 times, 10 min each). Essentially all incubation steps were performed in the presence of respective inhibitors except for MβCD which was only present during the preincubation period. Cells were harvested by scraping in ice-cold HBSS, and lipids were extracted in $CHCl_3$/MeOH 2:1. Dried lipids were dissolved in ethanol and subjected to HPLC analysis as described in 'Materials and Methods'. Concentrations of cell-associated lipids were calculated by regression analysis of FI values which were normalized to the internal standard and total cell protein. Results are expressed as fluorescence intensity in % of control, and represent mean ± SD (n = 3). * $p < 0.05$; ** $p < 0.005$; *** $p < 0.001$.

In addition to pharmacological antagonists K^+ depletion was used to inhibit clathrin-adapter interactions at the PM (Hansen et al., 1993). Finally cells were treated with the selective (but not isoform-specific) PKC inhibitor chelerythrine (CHEL) to suppress caveolae-mediated endocytosis.

Results shown in ***Figure 17 and 18*** suggest that the majority of BODIPY-SM endocytosis proceeds *via* a caveolae-dependent pathway. Caveole are small (50-80 nm) invaginations of the PM that are enriched in SL and Chol and perform a number of different signalling functions. Especially Chol sequestration within the PM using the polyene antibiotic NY inhibited uptake of BODIPY-SM without affecting cell viability. Immunofluorescence analysis after treatment with NY revealed that SM is mainly localized to the PM after a 30 min chase at 37°C and accumulates in the Golgi to a lower degree as observed in control cell (***Fig. 17 A*** (***a*** and ***d***)). Moreover, recording uptake after BE of membrane bound BODIPY-SM showed markedly reduced intracellular fluorescence in CATH.a cells incubated in the presence of NY. HPLC analysis revealed that BODIPY-SM by NY-treated cells was < 20% as compared to control cells (***Fig. 18***). Interestingly, treatment with the Chol depleting agent MβCD was almost without effect on BODIPY-SM endocytosis in CATH.a cells. In contrast to results obtained by HPLC immunofluorescence analysis revealed ≈ 50% reduced fluorescence (***Fig. 17 B*** (***a*** and ***c***)). Treatment of CATH.a cells in the presence of the PKC and *src* inhibitors CHEL and GE provoked a significant decrease of BODIPY-SM uptake to approx. 60 and 40% of control cells as demonstrated by immunofluorescence and HPLC analysis (***Fig. 17 B*** and ***Fig. 18***).

In contrast to caveolae-mediated endocytosis, BODIPY-SM uptake *via* clathrin-coated pits was less pronounced. However, K^+ depletion inhibited BODIPY-SM uptake in CATH.a cells to 70% of control values, whereas CP was more or less without effect (***Fig. 18***). It was previously reported that K^+ depletion interferes with the organization of the cortical actin cytoskeleton which may account for altered lipid uptake (Rajasekaran et al., 2001). Although CP was without effect on net uptake of BODIPY-SM immunofluorescence analysis suggested altered intracellular trafficking in response to this antagonist (***Fig. 17 B*** (***b***)). In contrast to control cells, CP-treated cells accumulated BODIPY-SM in punctuate structures throughout the cytoplasm. Moreover, HPLC analysis showed reduced levels of cell-associated Cer after CP incubation. This might be explained by the fact that CP is an inhibitor of aSMase (Lin et al., 2011) which would suggest that BODIPY-SM-derived BODIPY-Cer is responsible for Golgi staining.

Taken together, studies using inhibitors of clathrin- and caveolar endocytosis demonstrated that BODIPY-SM is predominately taken up *via* caveolae-mediated endocytosis in CATH.a cells. A significant amount of BODIPY-SM was rapidly converted to

BODIPY-Cer during the pulse-chase studies described above. Therefore these studies should be performed with metabolically stable fluorescently-tagged SM analogues.

4. AIM 2 – BODIPY-SM METABOLISM IN CATH.A CELLS

4.1. Generation of external standard curves

After analysis of BODIPY-SM uptake routes in CATH.a cells using pulse-chase experiments and LSM intracellular hydrolysis of BODIPY-SM to BODIPY-Cer and synthesis of BODIPY-SM from BODIPY-Cer was investigated. In order to get an idea about the kinetics of SM hydrolysis versus SM synthesis CATH.a cells were labeled with fluorescent SM or Cer analogues. Uptake and metabolism of the lipids was quantitatively analyzed by HPLC applying steady-state (tracer present throughout the whole incubation time) or pulse-chase labeling protocols.

During these studies BODIPY-labeled SM and Cer as well as PYRENE-labeled SM analogues were used. To calculate absolute concentrations of these fluorescent lipids, external HPLC calibration curves with known amounts of standards were established (***Figure 19***).

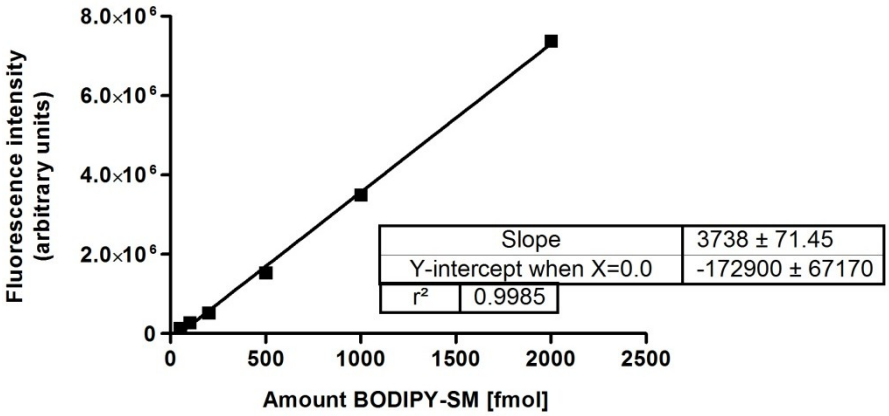
Fluorescence intensity (arbitrary units)
8.0×10⁶
6.0×10⁶
4.0×10⁶
2.0×10⁶
0
0
500
1000
1500
2000
2500
Amount BODIPY-SM [fmol]
Slope
3738 ± 71.45
Y-intercept when X=0.0
-172900 ± 67170
r²
0.9985

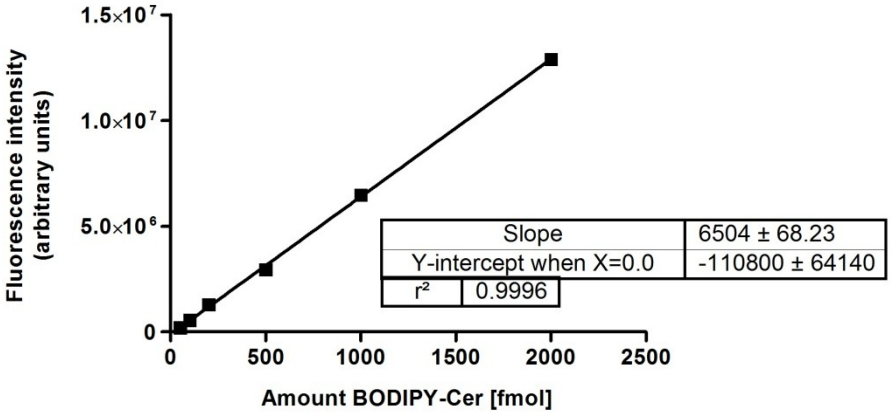
Fluorescence intensity (arbitrary units)
1.5×10⁷
1.0×10⁷
5.0×10⁶
0
0
500
1000
1500
2000
2500
Amount BODIPY-Cer [fmol]
Slope
6504 ± 68.23
Y-intercept when X=0.0
-110800 ± 64140
r²
0.9996

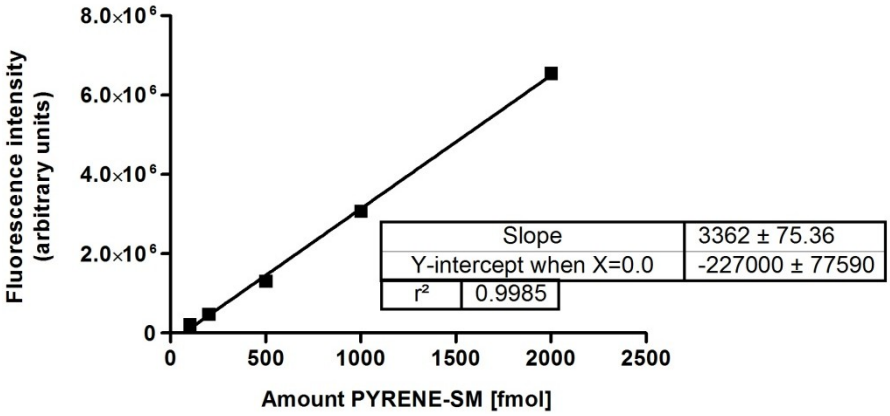
Fluorescence intensity (arbitrary units)
8.0×10⁶
6.0×10⁶
4.0×10⁶
2.0×10⁶
0
0
500
1000
1500
2000
2500
Amount PYRENE-SM [fmol]
Slope
3362 ± 75.36
Y-intercept when X=0.0
-227000 ± 77590
r²
0.9985

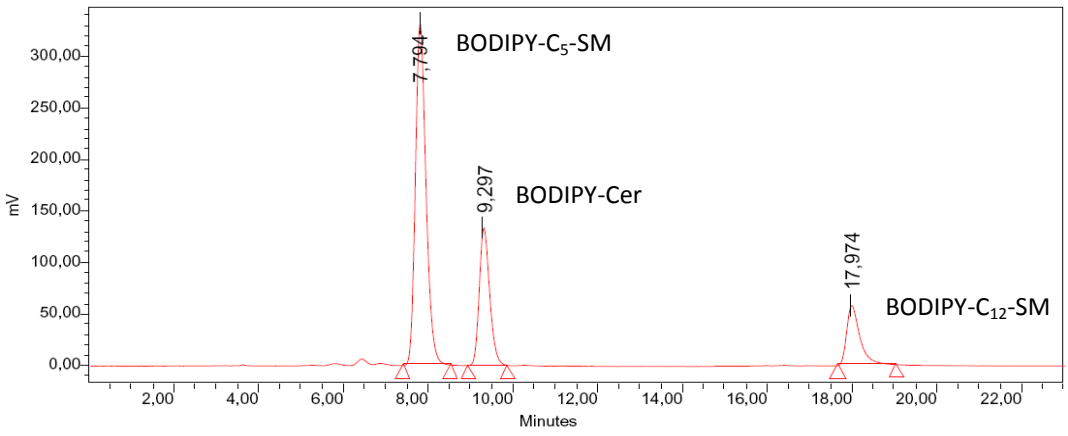
mV
300,00
250,00
200,00
150,00
100,00
50,00
0,00
7,794
BODIPY-C5-SM
9,297
BODIPY-Cer
17,974
BODIPY-C12-SM
2,00
4,00
6,00
8,00
10,00
12,00
14,00
16,00
18,00
20,00
22,00
Minutes

Figure 19: External standard curves for BODIPY-SM, BODIPY-Cer, and PYRENE-SM quantitation. Calibration curves were established by HPLC analysis of different concentrations of respective standards. Chromatographic conditions and gradient elution programs are described in 'Materials and Methods'. All measurements were performed in duplicates. A typical elution profile of BODIPY-SL is shown below the calibration curves.

4.2. Steady-state labeling experiments

During steady-state labeling experiments, cells were incubated in the presence of BODIPY-SM, BODIPY-Cer, or PYRENE-SM for the indicated time periods at 37°C. Cells were harvested and cellular lipid extracts were subjected to HPLC analysis to quantitate the cellular BODIPY-SM and Cer concentrations.

Results shown in ***Figure 20 A*** revealed BODIPY-SM uptake by CATH.a cells in a time-dependent manner. Already after 10 min, a significant proportion (approx. 20%) of BODIPY-SM was hydrolyzed to BODIPY-Cer. At the end of the experiment BODIPY-Cer concentrations even exceeded the concentration of the initially added tracer (BODIPY-SM) indicating efficient BODIPY hydrolysis. Due to the rapid formation of BODIPY-Cer it might be reasonable to assume that a fraction of BODIPY-SM is subjected to SMase-dependent hydrolysis already at the PM.

Also BODIPY-Cer uptake by CATH.a cells increased in a time-dependent manner albeit at slower rates as observed for BODIPY-SM, particularly at early time points (5 – 60 min; ***Fig. 20 B***). In addition it should be emphasized that the kinetics of SM synthesis from Cer by SMS is approx. 2-fold slower as compared to SM hydrolysis catalyzed by SMase.

Although less polar than other fluorescent lipids (e. g. NBD-labeled SL) short-chain BODIPY-labeled BODIPY-SM and BODIPY-Cer are no exact tracers of their natural counterparts with respect to assembly in raft and non-raft phases (van Meer and Liskamp, 2005).

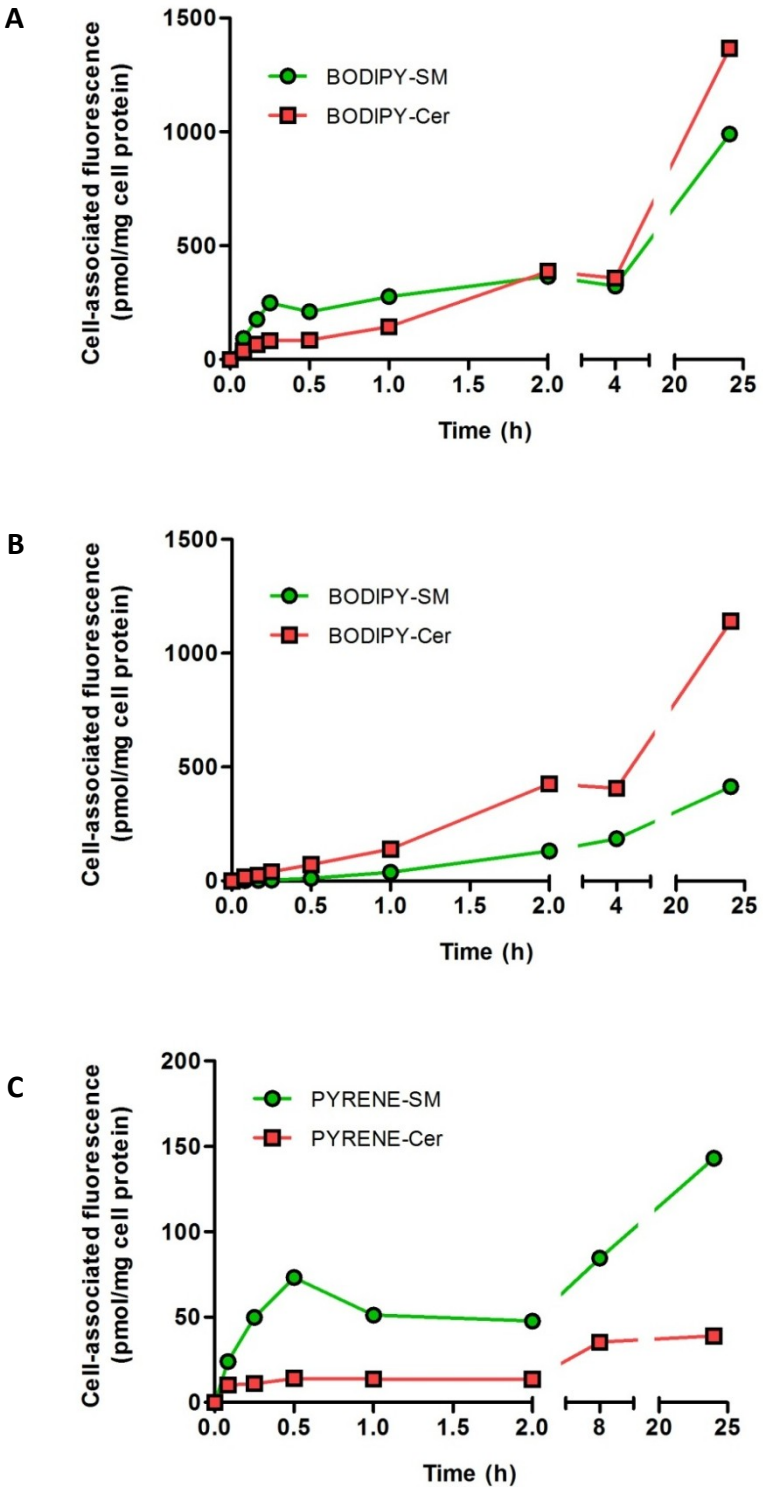

Figure 20: Uptake and metabolism of fluorescent SM and Cer analogues in CATH.a cells during steady-state labeling with the respective tracers. CATH.a cells, grown on poly-L-lysine-coated 6 well plates, were labeled with BODIPY-SM (***A***), BODIPY-Cer (***B***), or PYRENE-SM (***C***; 1 µM each), for the indicated time periods at 37°C. Cells were washed with HBSS, scraped in ice-cold HBSS, and lipids were extracted in $CHCl_3$/MeOH 2:1. Dried lipids were dissolved in ethanol and subjected to HPLC analysis as described in 'Materials and Methods'. Concentrations of cell-associated lipids were calculated by peak are comparison with the established external standard curve for the analyte under investigation. Extraction efficacy was calculated by peak area comparison with an internal standard (BODIPY-C_{12}-SM).

Therefore uptake of a PYRENE-labeled SM derivative was investigated in CATH.a cells. The combination of the highly hydrophobic PYRENE moiety and a longer (C10) FA acyl residue results in a SM derivate with physiochemical properties that are closer to natural SM as compared to BODIPY-SM. This was reflected by significantly different uptake kinetics for the PYRENE-labeled SM analogue compared to BODIPY-SM: After a 24 h incubation the concentrations of the PYRENE-labeled lipids are almost an order of magnitude lower as compared to the BODIPY-labeled analogue (***Fig. 20 C***). These results suggest slower incorporation of PYRENE-SM into the PM as compared to BODIPY-SM presumably representing the rate-limiting step in lipid uptake. Furthermore, less SM hydrolysis to Cer was observed during steady-state labeling. The reason(s) for these observations are currently not clear, however, it is plausible that BODIPY-SM represents a better substrate for a/nSMase and/or PYRENE-SM hydrolysis at the PM is less efficient.

4.3. Pulse-chase studies

To get an indication about the time-dependent metabolism of a known amount of PM-located SM in CATH.a cells pulse-chase studies and subsequent HPLC analyses of cell and medium lipids were performed.

As shown in ***Figure 21 A*** (left panel) cells acquired approx. 280 nmol BODIPY-labeled lipids, from these SM contributed approx. 230 nmol while the remaining is made up by BODIPY-Cer. This indicates that BODIPY-SM hydrolysis is an extremely fast process. During the 24 h time period BODIPY-SM was hydrolyzed at a rate of approx. 6 pmol/h. Surprisingly, SM hydrolysis was not accompanied by a concomitant equimolar increase in cellular BODIPY-Cer levels. To get an indication for potential release of analytes into the cellular supernatant medium lipids were analyzed (***Fig. 21 A***, right panel). These analyses revealed that approx. 65 and 60% of SM and Cer were recovered from the cellular supernatant. Importantly, the largest contribution to medium fluorescence was contributed by a currently unidentified analyte. This compound eluated early (2 min, ***Fig. 21 C***) and before SM and Cer indicating rather polar properties, probably a galactosylated SM species.

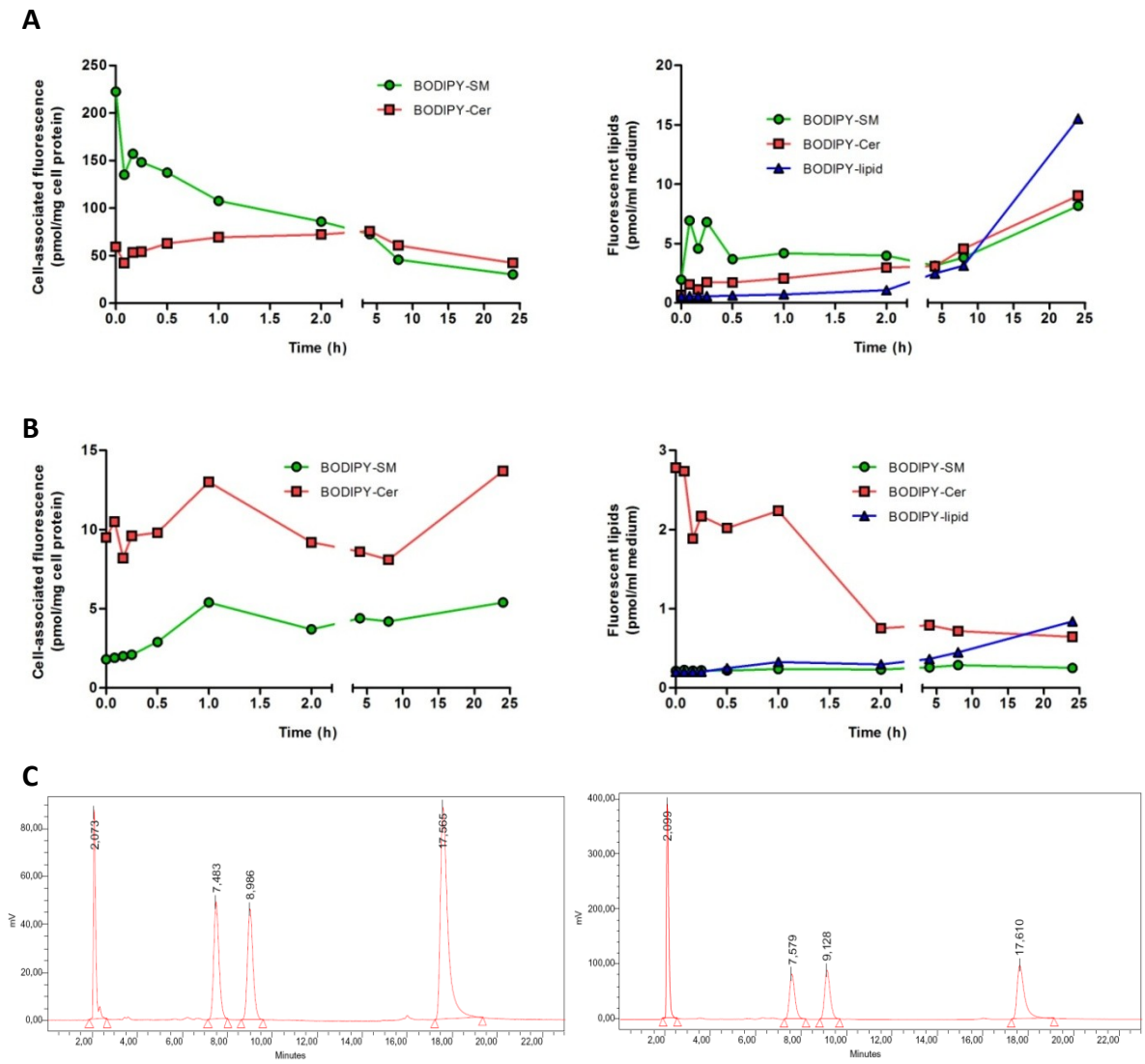

Figure 21: Uptake and metabolism of BODIPY-SM and BODIPY-Cer in CATH.a cells after pulse-labeling. CATH.a cells, grown on poly-L-lysine-coated 3.5 mm culture dishes, were cooled down at 4°C for 10 min and were then pulse-labeled with BODIPY-SM (***A***) or BODIPY-Cer (***B***; 1 µM each) in serum-free culture medium for 30 min at 4°C. Cells were washed with HBSS and were chased in serum-free culture medium at 37°C for the indicated time periods. Cells were scraped in ice-cold HBSS, and lipids were extracted in $CHCl_3$/MeOH 2:1. At each time-point medium was collected and lipids were extracted as described. Dried lipids were dissolved in ethanol and subjected to HPLC analysis as described in 'Materials and Methods'. Concentrations of cell-associated lipids were calculated by peak are comparison with the established external standard curve for the analyte under investigation. Extraction efficacy was calculated by peak area comparison with an internal standard (BODIPY-C_{12}-SM). (***C***) Elution profiles of cellular supernatant-derived BODIPY-SL after 4 (left panel) and 24 h (right panel).

When CATH.a cells were labeled with BODIPY-Cer less efficient uptake as compared to SM was observed (***Fig. 21 B***) most probably a result of less effective incorporation into the PM. Furthermore BODIPY-Cer concentrations were not significantly altered within the 24 h incubation ranging between 7 and 14 pmol/mg cell protein), and the BODIPY-SM content slightly increased from approx. 2 to 5 pmol/mg cell protein. Also during these

experiments low concentrations (0.2 - 3 pmol/ml medium) of fluorescent SM, Cer, and the unidentified polar analyte were detectable in the cellular supernatant.

Data in ***Figure 22*** show the conversion rates of BODIPY-SM to BODIPY-Cer and *vice versa* after incubation of CATH.a cells with the respective tracer.

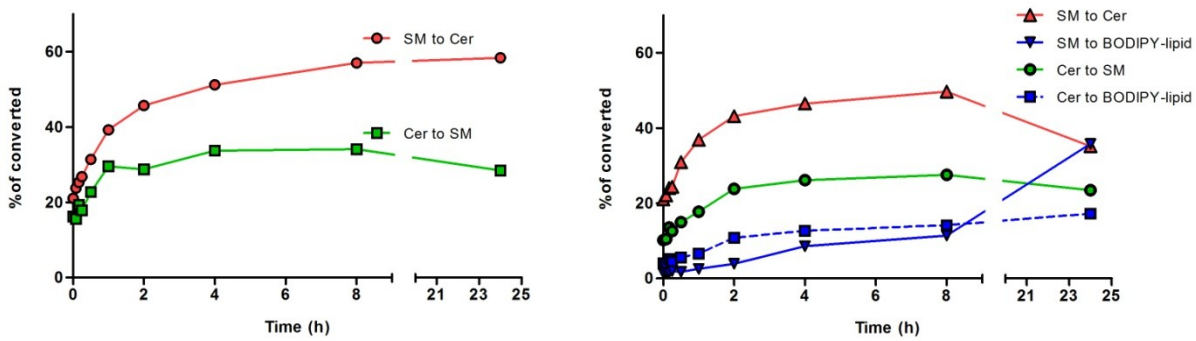

Figure 22: Conversion rates of BODIPY-SM and BODIPY-Cer into other SL. Absolute values used for calculation were taken from Figure 21. Results are expressed as % of conversion of the respective parent fluorescent lipid. Left graph: cellular lipids; right graph: lipids from cells and cellular supernatant.

From these data it is obvious that SM generation and hydrolysis are time-dependent processes starting immediately after pulse labeling. It is important to note that approx. 20% of fluorescent SL are already converted to the corresponding metabolite when starting the chase period. This indicates that SMases and SMS are enzymatically active even at low temperatures. Conversion reaches a plateau after 1 (SM synthesis from Cer) and 4 h (SM hydrolysis to Cer) start of the chase. Analysis of lipids present intracellularly and in the cellular supernatant (***Fig. 22***, right panel) revealed that after 24 h BODIPY-SM is converted to almost equal amounts to BODIPY-Cer and the unidentified polar SL species that is secreted into the culture medium. Similar results were obtained after labeling with BODIPY-Cer, though interconversion was considerably slower and less effective.

4.4. Localization of BODIPY-labeled SL

To determine the ratio of intracellular and PM-located BODIPY-labeled SM and BODIPY-SM-derived BODIPY-Cer two strategies were applied: First, BODIPY-SM at the PM was subjected to hydrolysis by exogenously added SMase from *B. cereus*. Second, intracellular concentrations of BODIPY-labeled SL were determined after pulse-chase experiments followed by BE of PM-bound BODIPY-labeled lipids to DF-BSA.

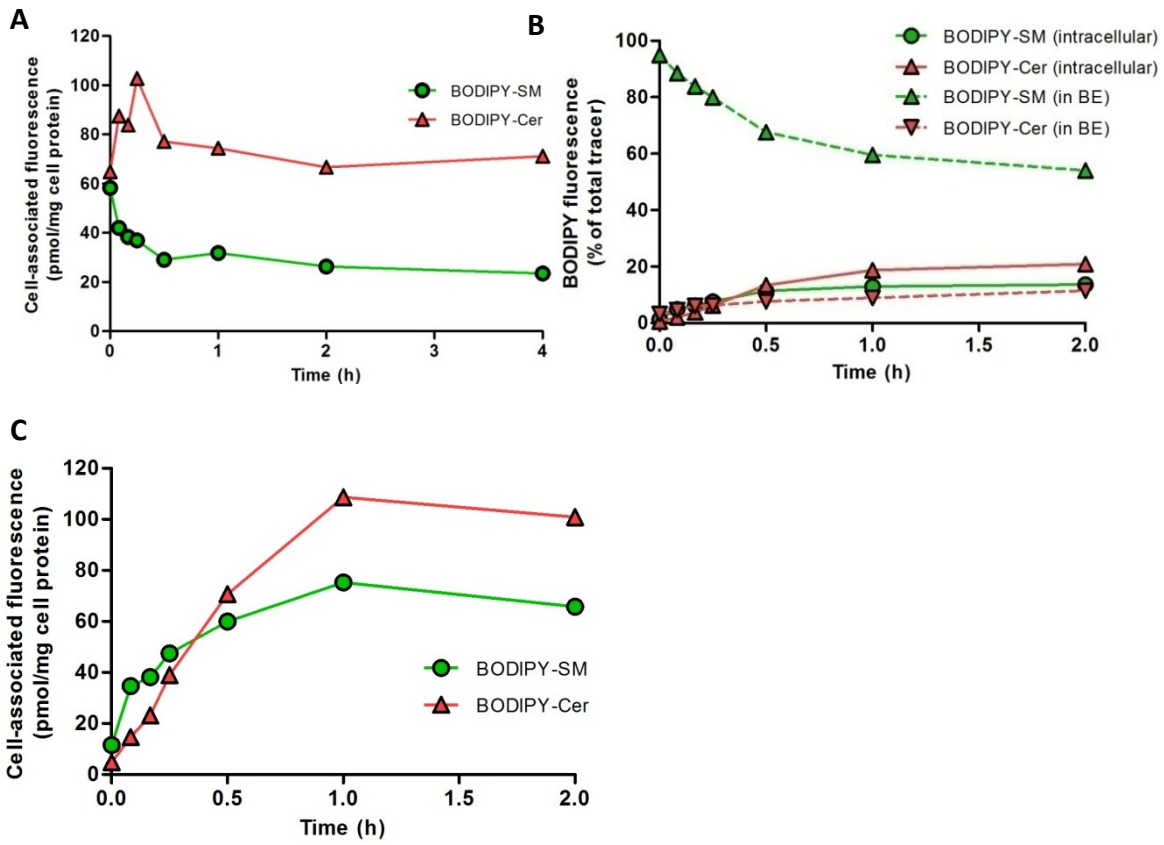

Figure 23: Determination of intracellular and PM-located BODIPY-SM. CATH.a cells, grown on poly-L-lysine-coated 3.5 mm culture dishes, were cooled down at 4°C for 10 min and were then pulse-labeled with BODIPY-SM (2 µM) in serum-free culture medium for 30 min at 4°C. (***A***) Cells were washed extensively with HBSS and were chased in serum-free culture medium at 37°C for 1 h to allow BODIPY-SM internalization. Following washing with HBSS, cells were subjected to *B. cereus* SMase treatment in serum-free culture medium at 37°C for the indicated time periods. (***B***) After pulse-labeling cells were washed extensively with HBSS and were chased in serum-free culture medium at 37°C for the indicated time periods before BE of PM-located BODIPY-labeled lipids to DF-BSA. BE fractions were pooled and lipids were extracted as described in 'Materials and Methods'. In both experiments cells were harvested by scraping in ice-cold HBSS, and lipids were extracted in $CHCl_3$/MeOH 2:1. Dried lipids were dissolved in ethanol and subjected to HPLC analysis as described in 'Materials and Methods'. Concentrations of cell-associated lipids were calculated by peak area comparison with the established external standard curve for the analyte under investigation. Extraction efficacy was calculated by peak area comparison with an internal standard (BODIPY-C_{12}-SM).

Since SMase from *B. cereus* is not internalized by eukaryotic cells only SM localized in the extracellular leaflet of the PM is accessible to hydrolysis. Treatment of BODIPY-SM-labeled CATH.a cells with bacterial SMase and subsequent HPLC analysis of lipid extracts revealed that loaded cells contained 60 and 65 pmol/mg cell protein of SM and Cer, respectively. Treatment with *B. cereus* SMase reduced the BODIPY-SM concentrations down to 20 pmol/mg cell protein, indicating that approx. 65% are accessible to SMase-dependent hydrolysis (***Figure 23 A***). The situation for BODIPY-Cer is slightly different: The relatively high BODIPY-Cer content at time 0 is most likely due to conversion by cellular SMase activity during the 60 min equilibration period before the actual hydrolysis experiment was started by addition of bacterial SMase.

When *B. cereus* SMase was added we have observed a transient increase in Cer concentrations (from 65 to 105 pmol/mg cell protein) within the first 15 min which then leveled off again to the initial value. This is most likely a reflection of cellular Cer efflux to the supernatant or Cer conversion to other SL species.

The next set of experiments was designed to confirm results obtained with bacterial SMase treatment. Therefore, cells were pulse-labeled with BODIPY-SM, washed, and supplemented with fresh medium. At the indicated time points cells were applied to a 60 min BE of PM-associated BODIPY-lipids to DF-BSA at 4°C. Concentrations of BODIPY-SM and BODIPY-Cer in cells or the BE medium were quantitated by HPL. These experiments demonstrated that approx. 34% of BODIPY-fluorophores were recovered from intracellular compartments (***Fig. 23 B***). This fraction was constituted by 60% BODIPY-Cer and 40% BODIPY-SM. The remaining fluorescence was detected in the BE medium where BODIPY-SM contributed to 83 and BODIPY-Cer to 17% of BODIPY fluorescence. These results clearly confirm data obtained by exogenous SMase treatment. Absolute values for cell-associated fluorophores are shown in ***Fig. 23 C***.

4.5. SM recycling to the PM

BODIPY-SM undergoes rapid metabolism in CATH.a cells. Therefore, the recycling kinetics of BODIPY-SM to the PM was investigated.

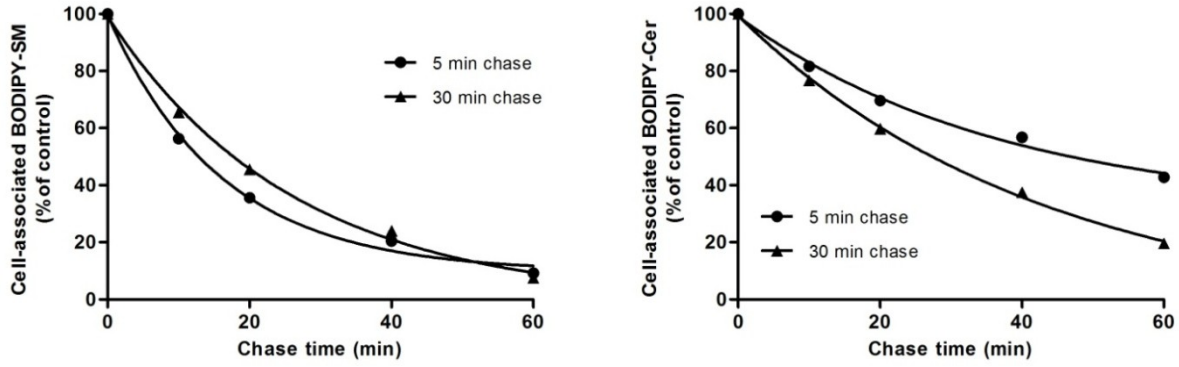

Figure 24: Determination of recycling kinetics of intracellular BODIPY-SM to the PM. CATH.a cells, grown on poly-L-lysine-coated 3.5 mm culture dishes, were cooled down at 4°C for 10 min and were then pulse-labeled with BODIPY-SM (3 µM) in serum-free culture medium for 30 min at 4°C. Cells were washed extensively with HBSS and were chased in serum-free culture medium at 37°C for the indicated time periods. Following BE of membrane-bound BODIPY-SM cells were again chased in prewarmed BE medium for up to 1 h. After the indicated time periods chase medium was collected and replaced by fresh BE medium. After 60 min cells were harvested by scraping in ice-cold HBSS and lipids from cells and chase medium were extracted in $CHCl_3$/MeOH 2:1. Dried lipids were dissolved in ethanol and subjected to HPLC analysis as described in 'Materials and Methods'. Concentrations of cell-associated lipids were calculated by peak area comparison with the established external standard curve for the analyte under investigation. Extraction efficacy was calculated by peak area comparison with an internal standard (BODIPY-C_{12}-SM).

Results shown in ***Figure 24*** demonstrate that originally intracellular BODIPY-SM is efficiently recycled to the PM from intracellular compartments and becomes accessible to BE mediated by extracellular DF-BSA. After a 5 min chase, lipids were rapidly transported to the PM presumably through early/recycling endosomes. In contrast, after chasing for 30 min BODIPY-SM recycling was slightly delayed. Obviously, BODIPY-SM is localized to different intracellular compartments after different chase periods out of which the fluorescent lipid exhibits different recycling kinetics to the PM. For BODIPY-Cer (***Fig. 24***, right panel) qualitatively comparable observations were made: After a 5 min chase approx. 50% of the fluorescent lipid was removed by BE. This value increased to 80% after a 30 min chase period. Also these results indicate efficient recycling of intracellular BODIPY-Cer to the PM which is accessible towards uptake by extracellular DF-BSA.

4.6. BODIPY-SM metabolism in differentiated CATH.a cell

It was previously shown that CATH.a cells can undergo PKA-mediated differentiation when treated with corticotrophin-releasing factor (CRF) or PKA agonists such as dbcAMP (Cibelli et al., 2001). In order to test if CATH.a differentiation alters BODIPY-SM uptake and metabolism pulse-chase studies were performed in differentiated CATH.a cells.

To induce differentiation in CATH.a neurons, cells were treated with dbcAMP. Results obtained from phase contrast microscopy revealed CATH.a differentiation into neurite containing cells upon dbcAMP treatment. Differentiation followed a concentration-dependent manner which reached a plateau when concentrations of 2 µM dbcAMP were applied to cells (data not shown). Interestingly, differentiation was a time-dependent process in which a maximum of differentiation was observed after 24 h incubation (***Fig. 25 b*** and ***d***). Treatment which dbcAMP up to four days with change of differentiation medium every 24 h did not further increased the degree of CATH.a differentiation (data not shown).

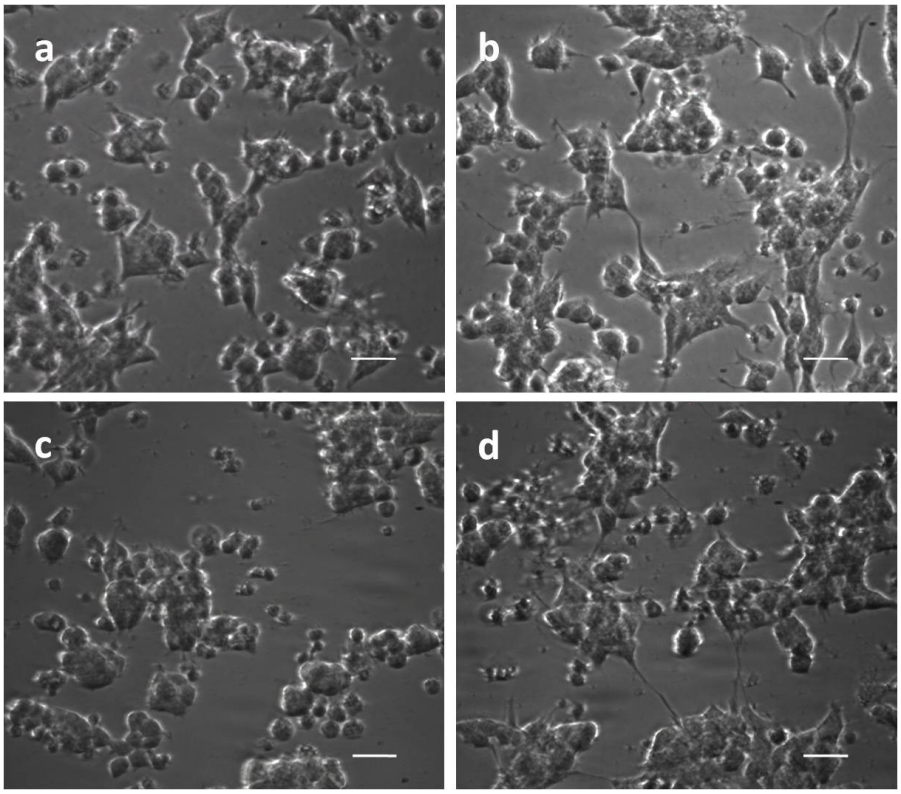

Figure 25: Differentiation of CATH.a cells. CATH.a cells, grown on poly-L-lysine-coated 6 well plates were incubated in the absence (***a*** and ***c***) or presence (***b*** and ***d***) of dbcAMP (2 mM) in serum-free culture medium for 24 (***a*** and ***b***) or 48 h (***b*** and ***d***) at 37°C. Differentiation was followed by phase contrast microscopy.

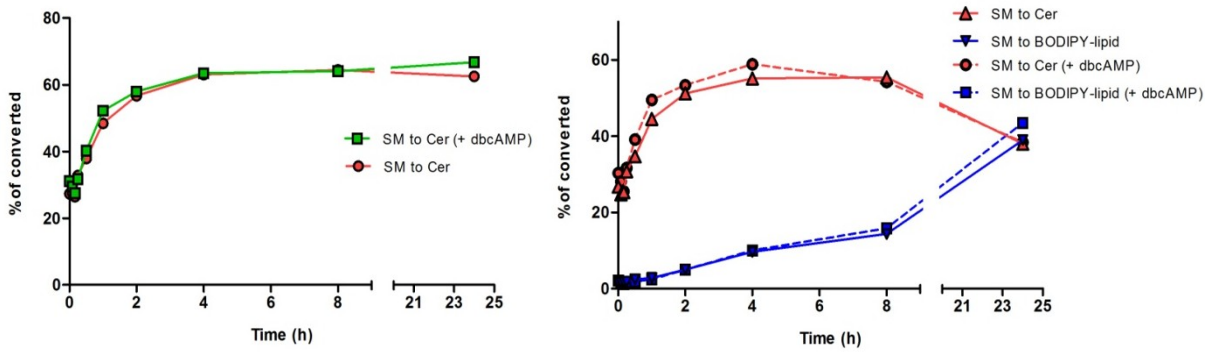

Figure 26: Metabolism of fluorescent BODIPY-SM in differentiated and undifferentiated CATH.a cells after pulse-labeling. CATH.a cells, grown on poly-L-lysine-coated 3.5 mm culture dishes, were washed with HBSS and incubated in the absence or presence of dbcAMP (1 µM) in serum-free culture medium at 37°C for 24 h. Subsequently, cells were cooled down at 4°C for 10 min and were then pulse-labeled with BODIPY-SM (1 µM) in serum-free culture medium for 30 min at 4°C. Cells were washed extensively with HBSS and were chased in serum-free culture medium at 37°C for the indicated time periods. Cells were harvested by scraping in ice-cold HBSS, and lipids were extracted in $CHCl_3$/MeOH 2:1. At each time-point medium was collected and lipids were extracted as described. Dried lipids were dissolved in ethanol and subjected to HPLC analysis as described in 'Materials and Methods'. Concentrations of cell-associated lipids were calculated by peak are comparison with the established external standard curve for the analyte under investigation. Extraction efficacy was calculated by peak area comparison with an internal standard (BODIPY-C_{12}-SM). Left graph: cellular lipids; right graph: lipids from cells and cell supernatant

As observed in previous pulse-chase metabolic studies BODIPY-SM is rapidly hydrolyzed to BODIPY-Cer in CATH.a cells in which Cer generation reached a plateau after 2 h chasing at 37°C (60% of intracellular BODIPY-SM was converted to Cer; ***Figure 26***, left panel). Taken lipid export to the culture medium into account HPLC analysis exhibited that approx. 40% of initial BODIPY-SM was equally converted to Cer and another BODIPY-SM-derived lipid species (***Fig. 26***, right panel) which is almost identical with results shown above (***Fig. 22***, right panel).

5. AIM 3 – CONTRIBUTION OF a/nSMASE TO BODIPY-SM HYDROLYSIS

5.1. SMase activity in CATH.a cells

As evident from our previous results, BODIPY-SM undergoes rapid hydrolysis to BODIPY-Cer due to SMase activity. A major question still was whether aSMase, nSMase, or both enzymes contribute to SM degradation. Therefore, basal activities of these enzymes were determined in differentiated and undifferentiated CATH.a cells as well as in the absence or presence of pharmacological aSMase and nSMase inhibitors.

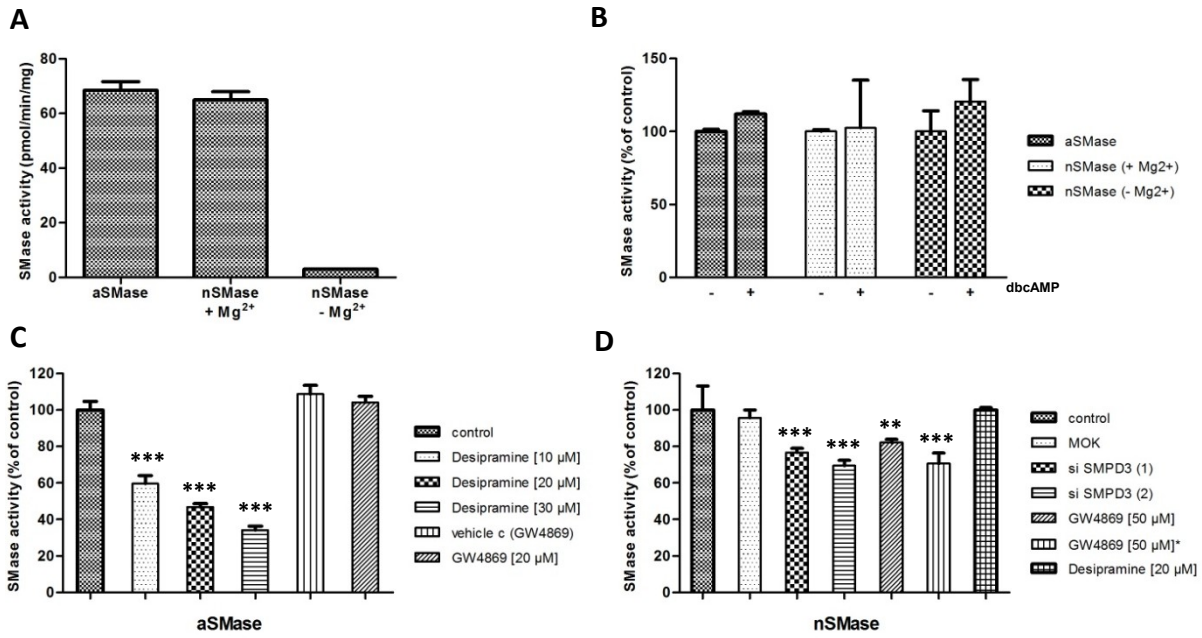

Figure 27: SMase activity in differentiated and undifferentiated CATH.a cells in the absence or presence of SMase inhibitors and after RNAi. CATH.a cells, grown on poly-L-lysine-coated 6 well plates, were lysed in acid lysis buffer for determination of aSMase or neutral lysis buffer for determination of nSMase activity followed by determination of SMase activity as described in 'Materials and Methods'. (***A***) Basal activity in CATH.a cells. (***B***) CATH.a cells were preincubated in the absence (-) or presence (+) of dbcAMP for 24 h to induce differentiation. (***C*** and ***D***) Pretreatment with desipramine or GW4869 was performed for 90 min in serum-free culture medium at 37°C. SMPD3 siRNA silencing was performed as described in 'Materials and Methods'. After incubation of cell lysates with BODIPY-SM as substrate, reaction was stopped by addition of $CHCl_3$/MeOH 2:1. Dried lipid extracts were dissolved in ethanol and subjected to HPLC analysis as described in 'Materials and Methods'. Concentrations of cell-associated lipids were calculated by peak area comparison with the established external standard curve for the analyte under investigation. Extraction efficacy was calculated by peak area comparison with an internal standard (BODIPY-C_{12}-SM). Data represent the means ± SD (n = 3). ** $p < 0.005$; *** $p < 0.001$.
* Protein lysates (instead of intact CATH.a cells) were incubated with GW4869 30 min before substrate addition

Measurements of aSMase and nSMase activity showed that both enzymes exhibit similar reaction kinetics in CATH.a cells when BODIPY-SM was used as a substrate (***Figure 27 A***). These experiments revealed BODIPY-SM conversion rates of approx. 70 pmol/min/mg cell protein which is in good agreement with other studies that investigated SMase activities in various cell lines using fluorescent substrates (Levade et al., 1995).

Many cells contain Mg^{2+}-independent SMases. Therefore, experiments were performed in the absence or presence of Mg^{2+} in lysis and reaction buffer. In CATH.a cells Mg^{2+}-independent SMase activity was more or less undetectable which clearly demonstrates the dependence of nSMase on Mg^{2+} ions (***Fig. 27 A***). In addition these results confirm that aSMase activity does not interfere with nSMase measurement under the experimental conditions applied. As would be expected from data shown in ***Fig. 26***, SMase activities were not altered in differentiated CATH.a cells (***Fig. 27 B***).

To test the potency of the aSMase inhibitor desipramine and the nSMase competitive inhibitor GW4869 CATH.a cells were treated with the respective inhibitors before determination of SMase activities. As shown in ***Fig. 27 C*** desipramine resulted in inhibition of aSMase activity in a concentration-dependent manner. Treatment with the lysosomotropic compound exhibited IC_{50} values of 20 µM whereas higher concentrations (30 µM) decreased aSMase activity by 70%. Desipramine treatment did not affect nSMase activity in CATH.a cells (***Fig. 27 D***). In contrast to the aSMase inhibitor desipramine, GW4869 is a less potent inhibitor of nSMase activity (***Fig. 27 D***). Treatment with this inhibitor did not alter nSMase activity up to 30 µM (data not shown) and concentrations of 50 µM resulted in approx. 20% enzyme inhibition. To exclude the possibility that the antagonist is not taken up by cells, GW4869 was added directly to protein extracts 30 min before addition of the substrate buffer. Using this protocol also only slight inhibition (approx. 30%) of nSMase was observed.

To achieve significant downregulation of nSMase activity we performed RNAi using two different SMPD3 siRNAs. However, also RNAi decreased nSMase activity only to approx. 70 and 75%, respectively. To achieve better SMPD3 silencing we are currently optimizing the siRNA transfection protocol of CATH.a cells.

5.2. Contribution of aSMase to BODIPY-SM hydrolysis

To determine if aSMase is involved in BODIPY-SM degradation CATH.a cells were treated with desipramine before pulse-labeling with BODIPY-SM.

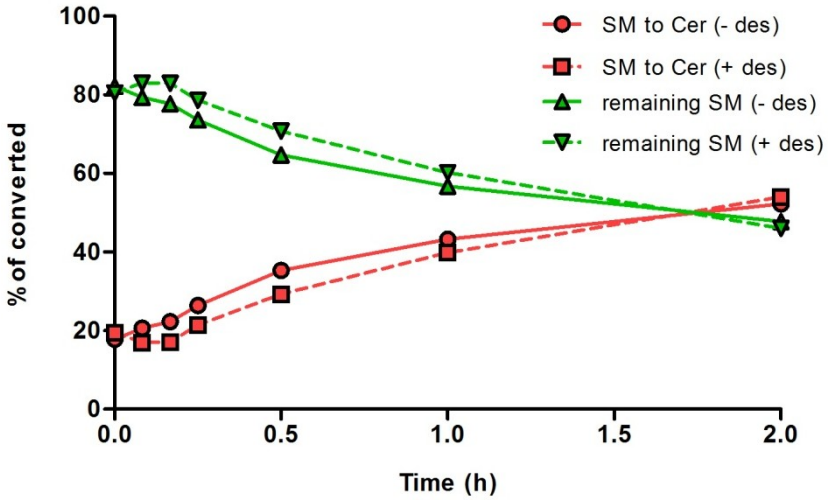

Figure 28: BODIPY-SM hydrolysis in desipramine-treated CATH.a cells. CATH.a cells, grown on poly-L-lysine-coated 3.5 mm culture dishes, were washed with HBSS and were preincubated in the absence or presence of desipramine (30 µM) in serum-free culture medium at 37°C for 90 min. Subsequently, cells were cooled down at 4°C for 10 min and were then pulse-labeled with BODIPY-SM (1 µM) in serum-free culture medium for 30 min at 4°C. Cells were washed extensively with HBSS and were chased in serum-free culture medium at 37°C for the indicated time periods. Cells were harvested by scraping in ice-cold HBSS, and lipids were extracted in $CHCl_3$/MeOH 2:1. At each time-point medium was collected and lipids were extracted as described. Dried lipids were dissolved in ethanol and subjected to HPLC analysis as described in 'Materials and Methods'. Concentrations of cell-associated lipids were calculated by peak area comparison with the established external standard curve for the analyte under investigation. Extraction efficacy was calculated by peak area comparison with an internal standard (BODIPY-C_{12}-SM).

As BODIPY-SM is rapidly hydrolyzed to BODIPY-Cer a metabolic process starting already at the PM we wanted to examine which SMases contribute to the degradation of the fluorescent lipid. Desipramine was shown to significantly inhibit aSMase activity. Results after treatment of CATH.a cells with desipramine coupled to pulse-chase experiments using BODIPY-SM revealed that aSMase seems to be only slightly involved in BODIPY-SM hydrolysis (***Figure 28***). Cells were chased up to 2 h because previous experiments showed that after this time period BODIPY-SM degradation reaches steady-state kinetics. At early stages (up to 1 h chasing) Cer generation was slightly delayed in desipramine-treated cells. These results suggest that nSMase provides the major contribution to SM hydrolysis in CATH.a cells.

Second Part

1. BACKGROUND

MS is characterized by actively demyelinating plaques in response to inflammatory events mediated by resident and immune cells transmigrated across the BBB from the periphery. One of the key oxidant-producing enzymes is MPO that is expressed in neutrophils (5% of total cell protein content), monocytes (1% of total cell protein content), as well as in resident macrophages in the CNS. MPO was recently shown to be linked to acute and progressive (neurodegenerative) CNS diseases like e. g. brain stroke (Breckwoldt et al., 2008), AD (Green et al., 2004), PD (Choi et al., 2005), or MS (Chen et al., 2008). In the presence of physiological Cl^- concentrations, MPO can generate HOCl that modifies DNA, proteins, and lipids. Under physiological conditions, MPO contributes to host defense but sustained MPO activation, as present during chronic inflammation, leads to oxidative/chlorinative tissue damage.

The CNS is an organ that is rich on SL (15% of total lipids; (O'Brien and Sampson, 1965)). Especially the myelin sheath of neurons contains high amounts of SM. Since MPO was shown to be abundantly present in demyelinating lesions of MS animal models, we tested the hypothesis that this enzyme is involved in oxidative/chlorinative modification of SM species. The ability of oxidized/chlorinated lipid species to display cytotoxic effects towards neurons might be of central importance for disease progression in several neurological disorders involving an inflammatory component.

2. AIMS

The aim of the second part of my thesis was to examine the impact of the MPO derived oxidant HOCl on unsaturated SM species that are indispensable for normal function of the CNS. Therefore the project aimed to:

i.) study the uptake of fluorescently-labeled SM analogues in dopaminergic PC12 cells

ii.) investigate the accessibility of SM towards HOCl modification and to identify and characterize SM-derived oxidation products

iii.) define the impact of exogenously added SM and HOCl-SM on viability parameters of PC12 cells

iv.) study alterations in the PC12 cell proteome in response to SM and HOCl-SM

3. AIM 1 – UPTAKE OF FLUORESCENT NBD- AND BODIPY-SM IN PC12 CELLS

3.1. Steady-state labeling with NBD-SM

The first series of experiments was aimed to study cellular SM uptake as well as localization and distribution of the lipid in PC12 cells using the fluorescent tracer NBD-SM, another fluorescent analogue of SM. Cells were continuously labeled with NBD-SM and uptake and distribution of this fluorescent lipid was followed by fluorescence microscopy.

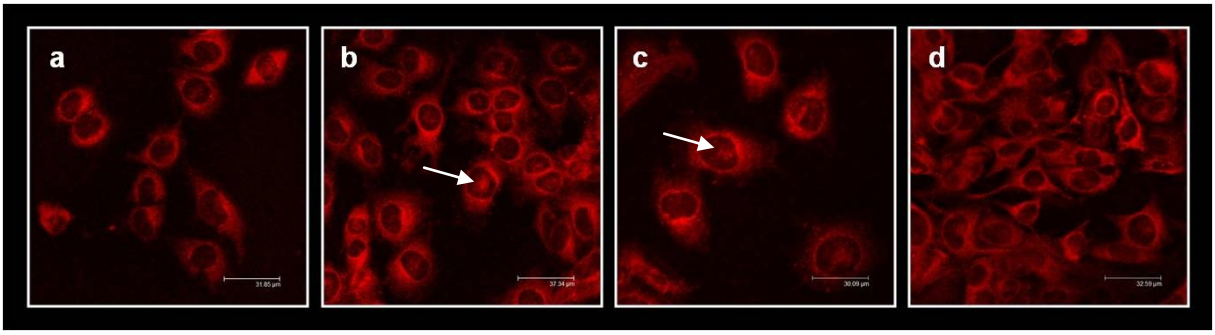

Figure 29: Uptake and localization studies of fluorescent NBD-SM in PC12 cells. PC12 cells were grown on collagen-coated chamber slides and were labeled with NBD-SM (2.5 µM) in serum-free culture medium for (***a***) 30 min, (***b***) 60 min, or (***c*** and ***d***) 120 min at 37°C. Cells were then washed three times with HBSS and subjected to fluorescence microscopy.

Results shown in ***Figure 29*** demonstrate efficient and rapid cellular uptake of NBD-labeled SM in PC12 cells similar to what was observed after labeling CATH.a cells with BODIPY-SM. After 30 min of incubation (***Fig. 29 A***) NBD-SM was already distributed throughout the cell with a preferred localization around the nucleus, presumably in the Golgi apparatus and/or the ER. In addition, NBD-SM was found to accumulate at pericentriole regions of the cells (white arrows) indicative for transport of the fluorescent SM (or the NBD-SM-derived Cer) to recycling endosomes. These results are in line with previous studies in where a recycling mechanism to early endosomes and the Golgi apparatus has been shown for endocytosis of SM (Pagano et al., 1999; Takahashi et al., 2007). Longer incubation times (1 and 2 h; ***Fig. 29 B, C*** and ***D***) did not significantly alter uptake efficacy or subcellular localization of NBD-SM.

3.2. Pulse-chase studies

To investigate time-dependent uptake as well as subcellular distribution of fluorescent SM analogues in more detail, pulse-chase studies with BODIPY-SM were applied in a similar manner as performed in CATH.a cells.

Similar to formerly observed in CATH.a cells, pulse-chase experiments revealed a time-dependent uptake of fluorescent SM into PC12 cells. As shown in ***Figure 30 a*** pulse labeling at 4°C for 30 min resulted in efficient accumulation of BODIPY-SM in the PM. After 5 min of a 37°C chase period, fluorescent BODIPY-SM or BODIPY-SM-derived BODIPY-Cer accumulated in punctuated structures within the cells (***Fig. 30 b***). In addition, a portion of the lipid already reached the Golgi apparatus (white arrows) that is tightly associated with the PC12 nucleus. Golgi labeling by BODIPY-labeled SL is even more pronounced after chasing 15 min at 37°C although BODIPY-SM enriched endosomes are still visible (***Fig. 30 c***).

Whereas an increase in fluorescence intensity can be observed when CATH.a neurons were chased for 15 min instead of 5 min at 37°C, hardly any differences in fluorescence intensity are obtained at longer chasing time periods (***Fig. 30 c – f***).

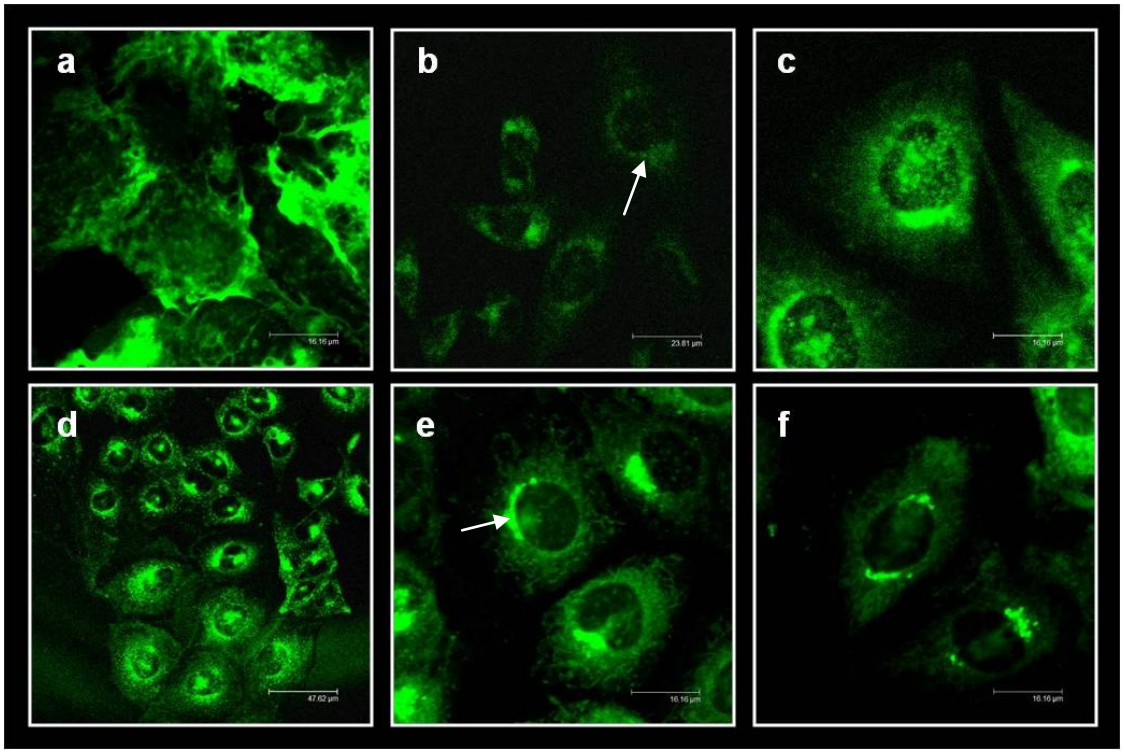

Figure 30: Uptake and localization studies of fluorescent BODIPY-SM in PC12 cells by pulse-chase experiments. PC12 cells, grown on collagen-coated cover-slips, were cooled-down at 4°C for 10 min and then pulse-labeled with BODIPY-SM (2.5 µM) in serum-free culture medium for 30 min at 4°C. Cells were washed extensively with HBSS and were chased in serum-free culture medium for (***b***) 5 min, (***c***) 15 min, (***d***) 30 min, (***e***) 60 min, or (***f***) 240 min at 37°C. Remaining BODIPY-SM at the PM was BE by washing the cells 6 times for 10 min with 5% DF-BSA in ice-cold HBSS at 4°C and cells were processed as described in 'Materials and Methods'. Cells in ***a*** were pulse-labeled with BODIPY-SM as described above, washed extensively with HBSS, and were immediately analyzed by fluorescence microscopy without chasing at 37°C and BE.

Moreover, the predominant Golgi labeling remains unaltered at longer time points. These results suggest rapid uptake of fluorescent BODIPY-SM which is presumably accompanied with its degradation to BODIPY-Cer as it was observed in CATH.a cells.

3.3. BODIPY-SM accumulating compartments

In order to investigate BODIPY-SM accumulating compartments in PC12 cells, colocalization studies were performed as described for CATH.a cells.

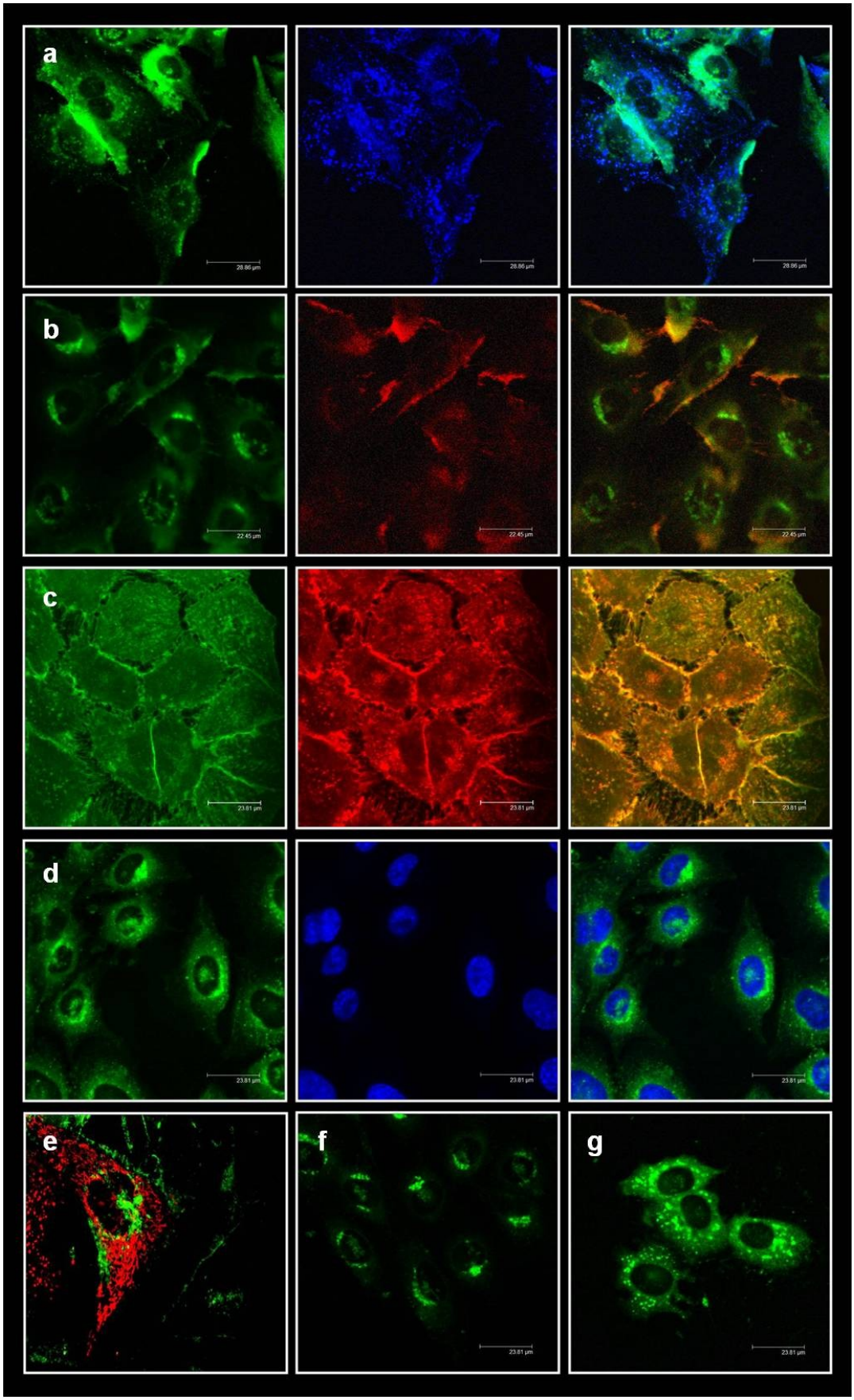
a
b
c
d
e
f
g

Figure 31: Colocalization studies of fluorescent BODIPY-SM with organelle-specific markers in PC12 cells. PC12 cells, grown on collagen-coated cover-slips, were pulse-labeled with BODIPY-SM (2.5 µM) for 25 min at 4°C. Cells were washed extensively with HBSS and were chased for 30 min at 37°C in the presence of the organelle specific markers LysoTracker Blue DND-22 (70 nM; ***a***) or ER-Tracker Blue-White DPX (500 nM; **b**) followed by a BE. Cells in ***c*** were stained with CellMask Plasma Membrane Stain (5 µg/ml) for 5 min at 37°C before cells were pulse-labeled with BODIPY-SM as described above. After pulse-labeling cells were washed extensively with HBSS and were immediately analyzed by fluorescence microscopy without chasing at 37°C and BE. Fluorescence images of both the BODIPY-SM and the organelle-specific probes were recorded from the same field of cells and then used to produce overlays from the double-staining. In ***d*** PC12 cells nuclei were counterstained with HOECHST (5 µg/ml) before BE. In ***e*** PC12 cells were stably transfected with the mitochondrion selective tracer DsRed-Mito. 2 days after transfection PC12 cells were labeled with BODIPY-SM as described above and analyzed by LSM (no BE). In ***f*** PC12 cells were stained with BODIPY-Cer (2.5 µM) in the same way as it was described for BODIPY-SM. In ***g*** PC12 cells were treated with nocodazole (33 µM) for 90 min at 37°C and were then stained with BODIPY-SM. All subsequent incubation steps were carried out in the presence of nocodazole. If not otherwise noted, duration of chasing in all cases was 30 min at 37°C and was followed by a BE. All incubation and staining steps were carried out in serum-free culture medium.

In contrast to what has been found in CATH.a cells, some PC12 lysosomes contained BODIPY-SM (white arrows) suggesting uptake of the lipid *via* the degradative endocytic pathway (***Figure 31 a***). However, BODIPY-labeled SL only partially accumulated in the ER (***Fig. 31 b***) and were absent in PC12 mitochondria (***Fig. 31 e***), identically to what was observed in CATH.a cells. Staining the PM indicated BODIPY-SM insertion in the lipid bilayer after pulse-labeling (***Fig. 31 c***). Additionally, localization of BODIPY-SM to PC12 nuclei could be ruled out which confirmed pericentriolar localization of the fluorescent lipid (***Fig. 31 d***). Similar to BODIPY-SM, BODIPY-Cer also localized to the Golgi (***Fig. 31 f***). Disruption of this organelle provoked accumulation of BODIPY-SM in Golgi-derived ministacks (***Fig. 31 g***).

4. AIM 2 – INVESTIGATION OF THE ACCESSIBILITY OF SM TOWARDS HOCl MODIFICATION AND IDENTIFICATION AND CHARACTERIZATION OF SM-DERIVED OXIDATION PRODUCTS

4.1. Modification of SM by reagent HOCl and identification and characterization of SM derived oxidation products

Next, the oxidative effect of reagent HOCl on SM was investigated. For these experiments, chicken egg yolk derived SM which contains SM(d18:1/16:0) as predominant

SM species (93% d18:1 of total long-chain base and 68% 16:0 of total FA acyl residue; (Ramstedt et al., 1999)). SM modification was carried out in water using a 2.5-fold molar excess of HOCl (7.12 mM) over SM. SM micelles were generated by sonication and incubation with HOCl was performed over night before the extent of modification was estimated using MALDI-TOF-MS.

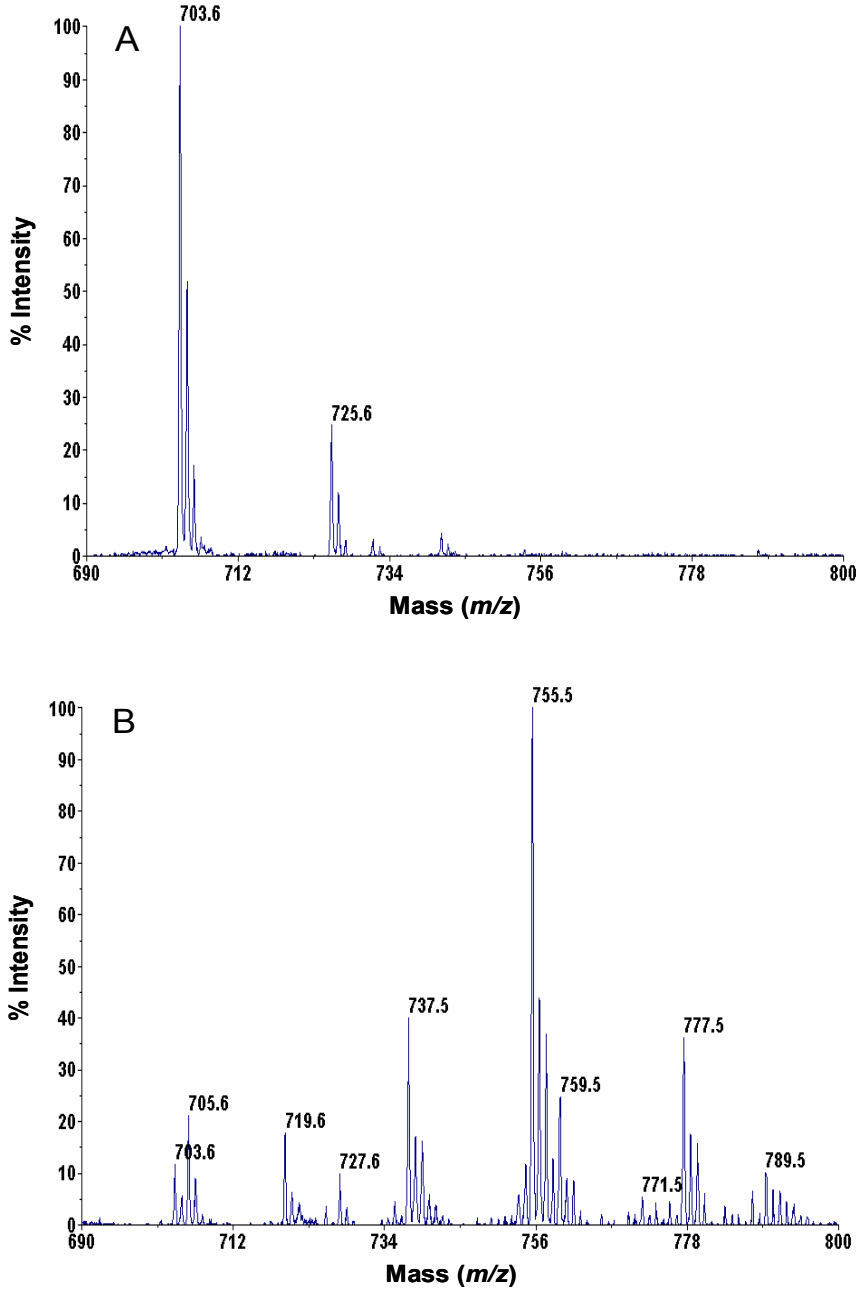

Figure 32: MALDI-TOF analysis of SM and HOCl-modified SM. *SM from chicken egg yolk was modified with reagent HOCl as described in 'Materials and Methods'. Following modification, lipids were extracted and analyzed by MALDI-TOF-MS using DHB as matrix as described in 'Materials and Methods'. Representative spectra of the predominant SM subspecies SM(d18:1/16:0) before (**A**) and after (**B**) HOCl modification are shown.*

Figure 32 A shows that untreated SM from chicken egg yolk exhibits two major peaks at 703.6 Da and 725.6 Da, corresponding to the respective protonated form (+ H^+) and the sodium adduct (+ Na^+) which is in agreement with previous studies showing that PC and SM tend to form sodium adducts when analyzed in the positive ion mode by MALDI-TOF-MS, even after lipid extraction (Schiller et al., 2004). Moreover, neither potassium adducts (m/z = 742.7 Da) nor other native SM species present in chicken egg yolk-derived SM (e. g. SM(d18:1/18:0) with m/z = 731.7 Da) could be detected by MALDI-TOF-MS.

In response to treatment of chicken egg yolk-derived SM with reagent HOCl (***Fig. 32 B***), one major peak (shifted by 52 Da) appeared at m/z = 755.5 Da that corresponds to the newly formed SM(d18:1/16:0) mono-chlorohydrin. Beside the detection of the respective sodium adduct at 777.5 Da HOCl-mediated SM modification led to the generation of a monochlorinated derivate of the SM(d18:1/16:0) chlorohydrin, detected at 737.5 (+ H^+) and 759.5 Da (sodium adduct). The formation of unsaturated adducts of chlorohydrins after HOCl treatment was previously also described for unsaturated PC (Spalteholz et al., 2004). The peak at 719.6 Da represents formation of a SM(d18:1/16:0) epoxide and peaks at 771.6 and 789.6 are indicative of mixed chlorohydrins/chloramide species as the SM amide group also represents a target for HOCl oxidation.

In parallel to chlorohydrin/chloramide formation almost no native SM(d18:1/16:0) with a mass of 703.6 Da was detected. This is indicative of an almost complete modification achieved by addition of a 2.5-fold molar excess of reagent HOCl. In response to HOCl modification the presence of SM(d18:0/16:0) at 705.6 (+ H^+) and 727.6 Da (+ Na^+) could be detected. This SM species contains a saturated long-chain base thus rendering the lipid resistant to chlorohydrin formation initiated by HOCl.

The mass assignment of respective native and chlorinated/oxidizes SM species that are shown in ***Fig. 32 A*** and ***B*** are summarized and listed in ***Table 3*** and the proposed structures, chemical formulas, and corresponding m/z values of native and chlorinated SM species are displayed in ***Figure 33***.

Table 3: Assignment of molecular ions produced by modification of SM(d18:1/16:0) with HOCl

SM species	*m/z*
SM(d18:1/16:0) $+H^+$	703.6
SM(d18:0/16:0) $+H^+$	705.6
SM(d18:1/16:0) epoxide $+H^+$	719.6
SM(d18:1/16:0) $+Na^+$	725.6
SM(d18:0/16:0) $+Na^+$	727.6
SM(d18:1/16:0) chlorohydrin $-H_2O$ $+H^+$	737.5 / 737.6
SM(d18:1/16:0) chlorohydrin $+H^+$	755.5 / 755.6
SM(d18:1/16:0) chlorohydrin $-H_2O$ $+Na^+$	759.5 / 759.6
SM(d18:1/16:0) chlorohydrin chloramide $-H_2O$ $+H^+$	771.5 / 771.6
SM(d18:1/16:0) chlorohydrin $+Na^+$	777.5 / 777.6
SM(d18:1/16:0) chlorohydrin chloramide $+H^+$	789.5 / 789.6

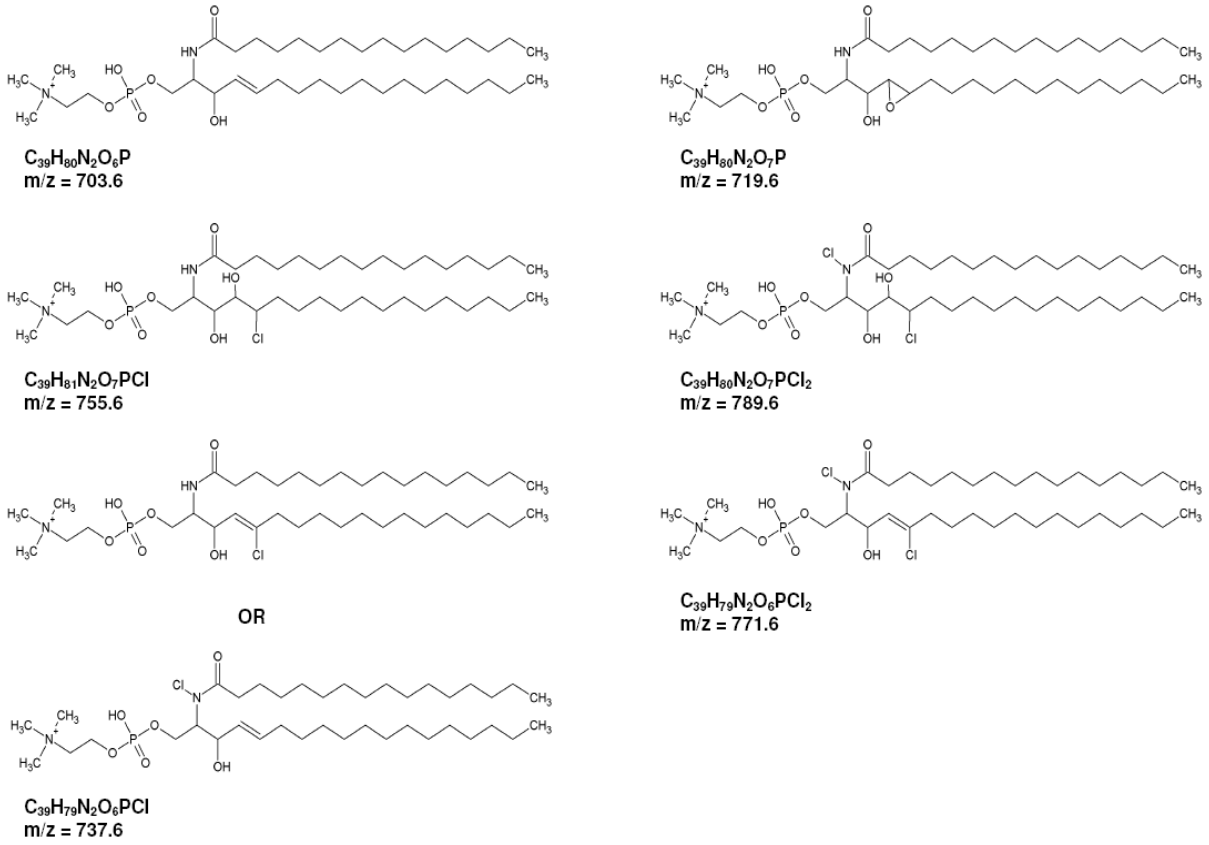

Figure 33: Proposed structures and resulting masses of SM(d18:1/16:0) before and after HOCl modification

4.2. Modification of SM by the MPO/H_2O_2/Cl^- system

After having proven the accessibility of SM towards HOCl modification it was tested whether SM can also be modified by the MPO/H_2O_2/Cl^- system under physiological conditions. Hence, 30 µg SM were dispersed in phosphate buffer (50 mM, 140 mM NaCl, pH 5) by sonication and incubated in the presence of 70 nM MPO at 37°C for 30 min under rapid shaking. Reaction was started by addition of H_2O_2 (200 µM, final concentration). After removal of MPO the reaction was allowed to proceed for further 12 h before extent of modification was estimated using MALDI-TOF-MS.

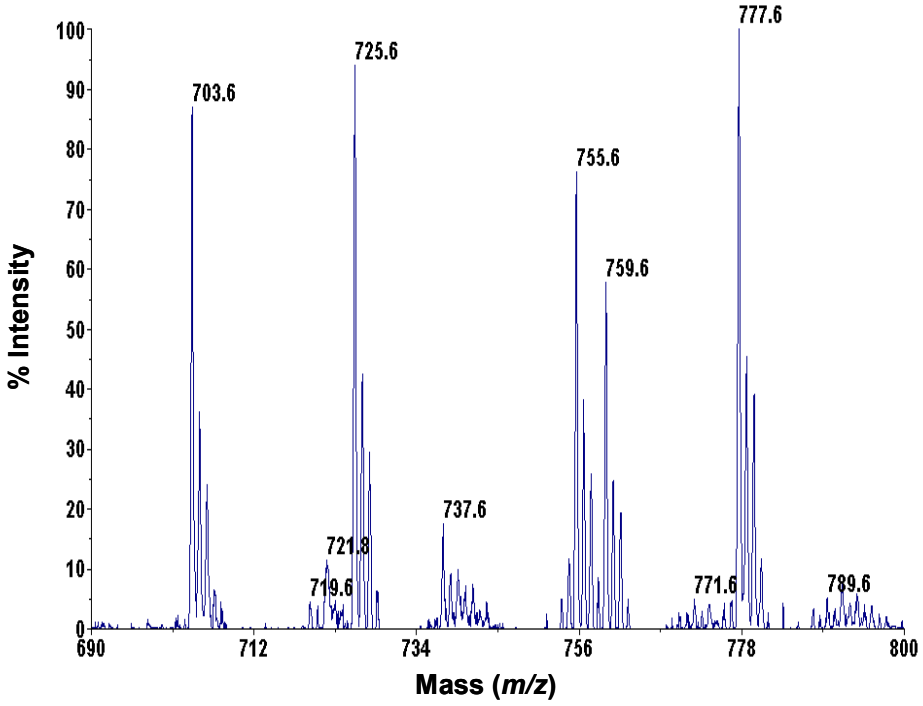

Figure 34: MALDI-TOF-MS analysis of SM modified by the MPO/H_2O_2/Cl^- system. SM from chicken egg yolk was modified in phosphate buffer by HOCl generated by MPO sing H_2O_2 and Cl^- as substrates. Following modification, lipids were extracted and analyzed by MALDI-TOF-MS using DHB as matrix as described in 'Materials and Methods'. A representative spectrum of the predominant SM subspecies SM(d18:1/16:0) after modification by the MPO/H_2O_2/Cl^- system is shown.

In contrast to the experiments where SM was treated with reagent HOCl, experimental conditions where SM(d18:1/16:0) was almost quantitatively modified (see ***Fig. 32 B***), a significant proportion of unmodified SM(d18:1/16:0) was still detectable when HOCl was generated enzymatically (***Figure 34***; peak at 703.6 Da). However, formation of

the SM(d18:1/16:0) epoxide (719.6 Da), the SM mono-chlorohydrin (755.6 and 777.6 Da), as well as generation of the less saturated, monochlorinated adduct (737.6 and 759.6 Da) and mixed chlorohydrin/chloramide species of SM(d18:1/16:0) was clearly occurring under these more physiological conditions. The respective structures, chemical formulas, corresponding m/z values, and mass assignments (shifted by 0.1 Da in case of the chlorinated SM species compared to reagent HOCl modification) are shown and listed in ***Fig. 33*** and ***Tab. 3***.

4.3. Modification of mouse brain lipids with reagent HOCl

To elucidate potential lipotoxic effects of MPO-generated HOCl in acute and progressive CNS diseases we next aimed to establish the accessibility of SM to HOCl modification in a physiologically relevant lipid matrix. Serving as an *in vitro* model for HOCl-derived oxidative damage, total mouse brain lipids were exposed to reagent HOCl. For this purpose, frozen brains of female C57Bl/6 mice were homogenized in liquid nitrogen, lipids were extracted according to a modified Folch procedure (Goti et al., 2002) and the resulting lipid extracts were incubated in the presence of increasing HOCl:lipid ratios. After a second extraction, lipids were analyzed by FT-ICR-MS.

These analyses revealed SM(d18:1/18:0) (*N*-(octadecanoyl)-sphing-4-enine-1-phosphocholine) and SM(d18:1/24:1) (*N*-(tetracosenoyl)-sphing-4-enine-1-phosphocholine) as the predominant molecular species (mean 950 and 420 nmol/g wet tissue) in the brain SM fraction (***Figure 35 A***). The corresponding N-hexadecanoyl-, N-octadecenoyl-, and N-eicosanoyl-species were present in minor amounts contributing to approx. 20 nmol/g wet brain. This assignment reflects the typical brain-SM abundance where SM(d18:1:18:0) is mainly found in the gray matter whereas SM(d18:1/24:1) is more or less exclusively localized to the white matter. Modification of mouse total brain lipids with reagent HOCl resulted in depletion of these SM species in a HOCl-concentration-dependent manner.

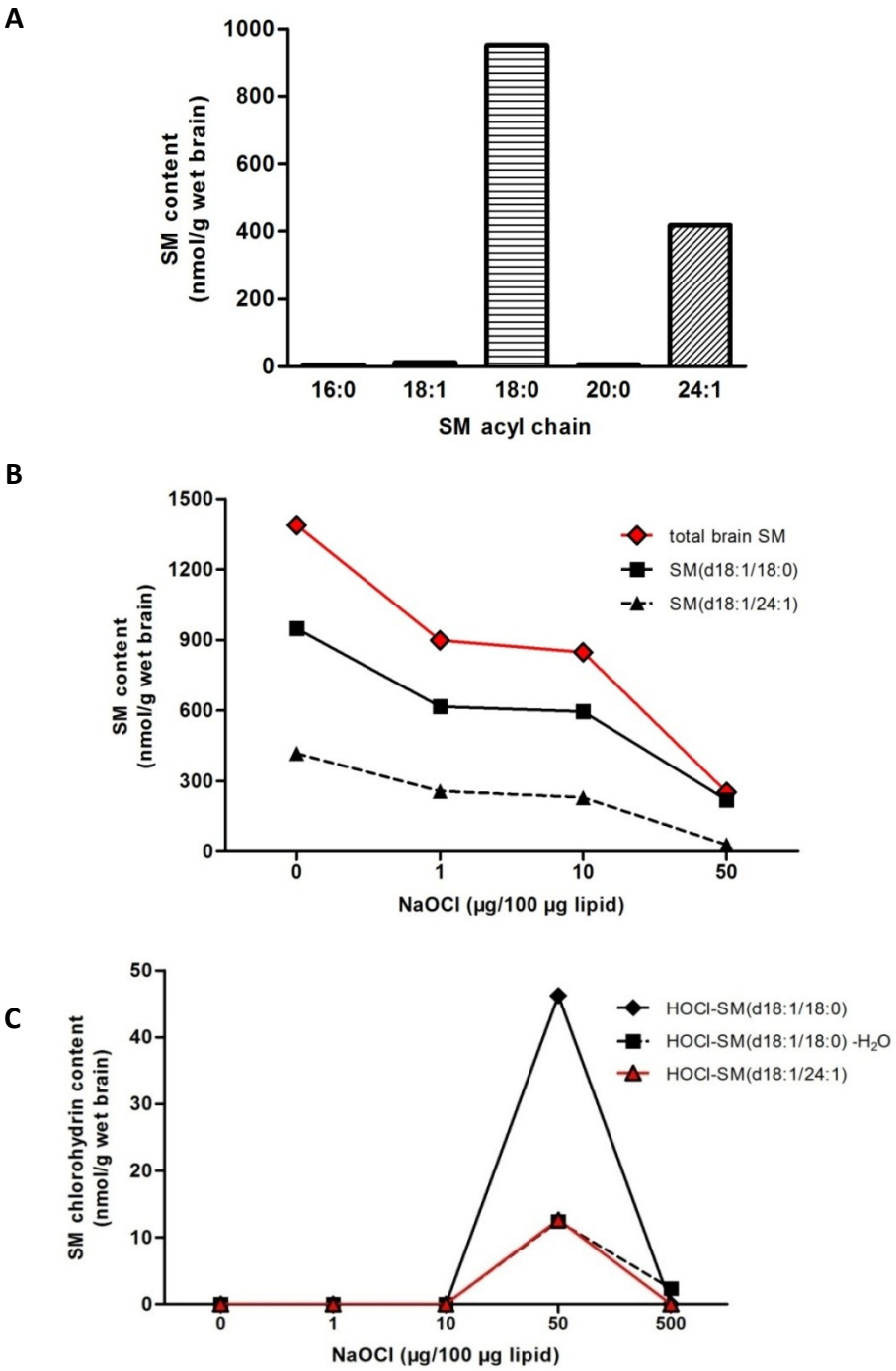

Figure 35: FT-ICR-MS analysis of native and HOCl-modified mouse brain lipids. C57Bl/6 mice were killed by cervical dislocation, brains were removed, homogenized in liquid nitrogen, and lipids were extracted using a modified Folch extraction. Extracts were dried under a stream of nitrogen and defined amounts were modified at the indicated NaOCl concentrations. After another extraction step lipids were dissolved in $CHCl_3$/MeOH (1:1, v/v) and analyzed by a hybrid linear ion trap FT-ICR-MS in positive ESI mode as described in 'Materials and Methods'. Results are mean values of duplicate determinations.

(***A***) Composition of native mouse brain SM.

(***B***) Total, SM(d18:1/16:0), and SM(d18:1/24:1) content in mouse brain lipid samples prior and after HOCl modification at the indicated ratios.

(***C***) Generation of SM chlorohydrin species derived from mouse brain SM following HOCl modification at the indicated ratios.

Of note, 1 µg NaOCl per 100 µg lipid (corresponding to an equimolar NaOCl concentration over brain lipids) resulted in the depletion of approx. 40% of the original SM content indicating that this lipid subspecies is highly sensitive towards HOCl modification. A 50-fold molar excess of HOCl over brain lipids resulted in nearly complete disappearance of SM(d18:1/18:0) and (d18:1/24:1) (***Fig. 35 B***) which was accompanied by an transient generation of the respective chlorinated SM species. We could detect formation of SM(d18:1/18:0) and (d18:1/24:1) mono-chlorohydrins and a less saturated, monochlorinated derivate (described above) of SM(d18:1/18:0) (***Fig. 35 C***). However, the formation of HOCl-SM in murine total brain lipids was only detectable when high concentration of reagent HOCl were applied to the lipid matrix (50 µg/100 µg brain lipid that corresponds to a 50-fold molar excess of reagent HOCl over brain lipids). Of note, the loss of native brain SM species did not correlate with gain of new, HOCl-modified SM species. Interestingly, application of higher NaOCl concentration (500 µg/100 µg brain lipid corresponding to a 500-fold molar excess of reagent HOCl over brain lipids) to mouse brain lipids did not induce increased conversion and/or accumulation of SM chlorohydrins but prevented detection of chlorinated SM. This could be explained by abstraction of the FA acyl residue from the Sph backbone due to introduction of the chlorohydrin group as it was already described for PC chlorohydrins which may also account for the discrepancies of the amounts of decreasing native SM and accompanied HOCl-SM generation.

4.4. Determination of second-order rate constants for HOCl-mediated SM modification

To get an indication of the susceptibility of SM to HOCl modification, rate constants for the reaction of SM(d18:1/16:0) with reagent HOCl were determined. In these studies SM liposomes were treated for 10 sec with reagent HOCl. Reactions were stopped by addition of $CHCl_3$/MeOH (2:1, v/v), lipids were extracted according to (Folch et al., 1957), and the decrease of SM(d18:1/16:0) was determined by HPLC-ESI-MS using PC(16:0/16:0) as internal standard. Experimental conditions, reaction rates, and the resulting rate constants are given in ***Table 4***.

Table 4: Second-order rate constants at pH 6.5 (37°C) for the reaction of SM with NaOCl. SM(d18:1/16:0) samples were incubated for 10 seconds with reagent NaOCl, extracted in $CHCl_3$/MeOH (2:1, v/v), dried under nitrogen, redissolved in methanol, and analyzed by LC-ESI-MS as described in Material and Methods. PC(16:0/16:0) was used as internal standard. All experiments were performed in triplicates.

NaOCl (mol/L)	**SM_0 [a] (mol/L)**	**SM_t [b] (mol/L)**	**SM_{mod} [c] (mol/L)**	**Rate [d] (mol L^{-1} s^{-1})**	**k_2 [e] (L mol^{-1} s^{-1})**
4.00×10^{-3}	1.20×10^{-3}	4.04×10^{-4}	7.96×10^{-4}	7.96×10^{-5}	16.58
4.00×10^{-3}	2.00×10^{-3}	1.14×10^{-4}	1.86×10^{-3}	1.86×10^{-4}	23.20
4.00×10^{-3}	2.84×10^{-3}	1.05×10^{-3}	1.79×10^{-3}	1.79×10^{-4}	15.78
2.84×10^{-3}	2.84×10^{-3}	1.21×10^{-3}	1.64×10^{-3}	1.64×10^{-4}	20.23
5.69×10^{-3}	2.84×10^{-3}	2.99×10^{-5}	2.82×10^{-3}	2.82×10^{-4}	17.46
					18.7 ± 3.05 (mean ± SD)

[a] **SM_0** = initial [SM]
[b] **SM_t** = [SM] after 10 sec incubation in the presence of NaOCl
[c] **$[SM_{mod}]$** = $[SM_0] - [SM_t]$
[d] **rate** = $[SM_{mod}]/10$
[e] ***k_2*** = rate /($[SM_0]$ [NaOCl])

These experiments (performed at pH 6.5) revealed a second-order rate constant (k_2) of 18.7 ± 3.05 L mol^{-1} s^{-1} (mean ± SD). This is in a comparable range as reported for the reaction of plasmalogens with HOCl (55 ± 7 L mol^{-1} s^{-1}; (Skaff et al., 2008)). Plasmalogens belong to the ether lipid subfraction and contain a vinyl ether linkage on the sn-1 position that is highly susceptible to HOCl modification. This lipid species is readily modified by MPO *in vivo* (Thukkani et al., 2003) and the products, α-chloro-fatty aldehydes (e. g. 2-ClHDA), are important *in vivo* biomarkers for MPO activity. Therefore, HOCl-SM can also be assumed to be generated *in vivo* when HOCl is present.

5. AIM 3 – DEFINING THE IMPACT OF EXOGENOUSLY ADDED SM AND HOCl-SM ON VIABILITY PARAMETERS OF PC12 CELLS

5.1. Impact of native and HOCl-modified SM on PC12 cell viability

The next set of experiments aimed to characterize the impact of HOCl-modified SM on neuronal viability parameters. Therefore, MTT cell viability assays were performed in which PC12 cells which were treated with SM, HOCl-SM, or HOCl at the indicated concentrations for the indicated time periods.

During these experiments it became evident that HOCl-SM in contrast to SM induces cell death. As shown in ***Figure 36 A*** native SM (applied as water dispersed micelles) did not cause significant cytotoxicity to PC12 cells. Even in the presence of the highest concentrations of SM (498 µM) only a slight reduction of formazan crystal formation (20 and 26%, respectively) was observed after 12 and 24 h. At earlier time points SM had hardly any impact on cellular viability of PC12 cells. In contrast to SM, HOCl-SM severely decreased cell viability of PC12 cells already after 1 h of incubation with the HOCl-modified lipid (24% at 199 µM; ***Fig. 36 B***). This rapid and extensive loss in viability – following a time- and concentration-dependent manner – was dramatically increased after longer incubation times of PC12 cells with HOCl-SM. Treatment over 12 or 24 h resulted in PC12 cell death at low HOCl-SM concentration of 33 µM (19 and 30%, respectively) with IC_{50} values of approx. 80 (12 h) and 50 µM (24 h). The potent oxidant HOCl alone also significantly induced time- and concentration-dependent cell death in PC12 cells (***Fig. 36 C***) with IC_{50} values of approx. 280 (1 h), 170 (12 h), and 90 µM (24 h). Interestingly, the cytotoxic effects of HOCl were more prominent at shorter times of treatment compared to those of HOCl-SM (92% cell death at concentrations of 400 µM HOCl after 1 h of incubation), whereas HOCl-SM induced cell death more efficiently at longer incubation times starting at 12 h of treatment compared to the oxidant (the IC_{50} values of HOCl-SM are almost 2-fold lower compared to those of the strong oxidant HOCl; see above). Furthermore, HOCl at concentrations of 500 µM provoked complete cell death which was not observed in PC12 cells treated with similar concentrations of HOCl-SM.

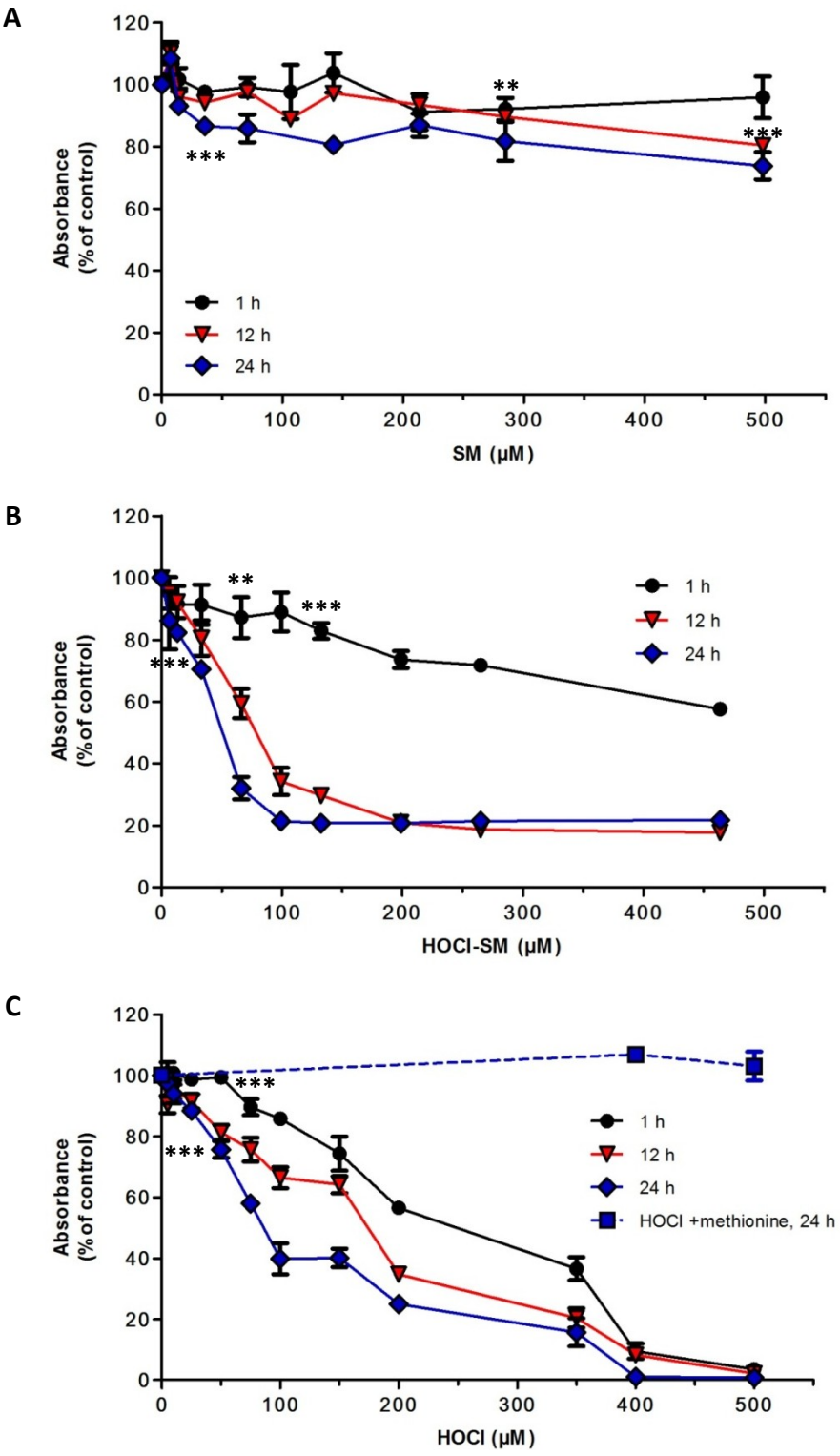

Figure 36: Viability of SM-, HOCl-SM-, and HOCl-treated PC12 cells. Viability of PC12 cells was examined using the MTT cell viability assay. Cells were incubated in the absence or presence of SM (***A***), HOCl-SM (***B***), or HOCl (***C***) at the indicated concentrations for the indicated time periods. Results are expressed as absorbance as % of control and represent the means ± SD (n = 3). ** $p < 0.005$; *** $p < 0.001$. For clarity p values are shown only for the first data point reaching significance.

Met, which was used as a scavenger for remaining HOCl after SM modification completely inhibited loss of cell viability in PC12 cells when the amino acid was added 2 hours before experimental start in a 5-fold molar excess over HOCl over 24 hours (***Fig. 36 C***, dashed line). The generated Met sulfoxide as well as Met was without effect on cell viability up to 1 mM. These data indicate that only HOCl-SM but not Met sulfoxide exerts cytotoxicity to PC12 cells.

5.2. Impact of SM and HOCl-SM on ROS generation in PC12 cells

To get insight into mechanisms that contribute to the cytotoxic properties of HOCl-SM intracellular ROS formation was analyzed in PC12 cells. Therefore, cells were incubated in the absence or presence of SM and HOCl-SM at the indicated concentrations for the indicated time periods. ROS generation was followed using the fluorescent probe DCFDA that was applied to PC12 cells after the lipid treatment. Oxidized DCF was extracted after cell lysis and fluorescence intensities were measured.

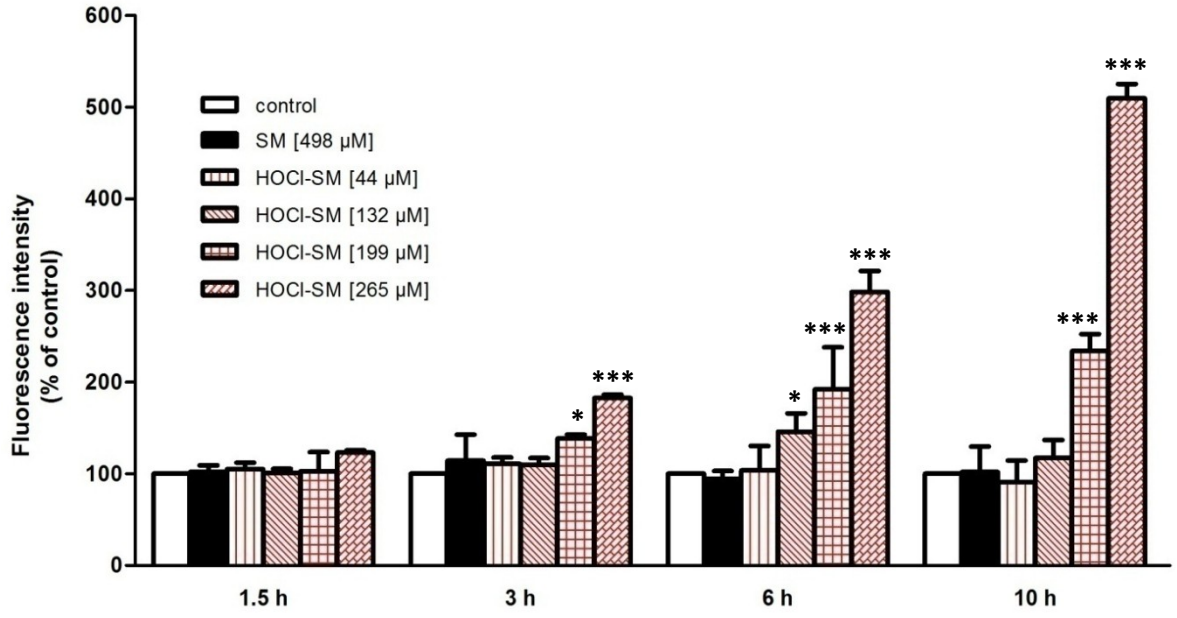

Figure 37: ROS formation in SM- and HOCl-SM-treated PC12 cells. Generation of ROS in PC12 cells was examined in assays using the fluorescent tracer DCFDA. Cells were incubated in the absence or presence of SM or HOCl-SM at the indicated concentrations for the indicated time periods. DCFDA was added to the cells in HBSS (12.5 µM) and after 1 h deacetylated and oxidized DCF was extracted by cell lysis using a 3% Triton X-100 solution. Fluorescence intensities were read at 484/540 nm (Ex/Em) as described in 'Materials and Methods'. Results are expressed as fluorescence intensity as % of control and represent the means ± SD (n = 3). * $p < 0.05$; *** $p < 0.001$.

Results of these experiments shown in ***Figure 37*** revealed that HOCl-SM concentrations >44 µM significantly induced deacetylation and oxidation of the fluorescent tracer DCFDA indicative of formation of intracellular ROS. Especially higher concentrations of the HOCl-modified lipids (199 and 265 µM, respectively) resulted in strongly enhanced fluorescence. In this process, ROS generation followed a time-dependent manner. Whereas ROS formation was not detectable after 1 h at all applied HOCl-SM concentrations, longer incubation times of 3 h (1.3- and 1.8-fold over baseline) and 6 h (1.9- and threefold over baseline) resulted in increased fluorescence at HOCl-SM concentrations of ≥ 200 µM. The highest level of intracellular ROS at these concentrations was measured after 10 h (2.5- and 5-fold over baseline) indicating radical induced cell damage/stress. As expected, unmodified SM was without effect on ROS formation in PC12 cells, even at very high concentrations of almost 500 µM. These experiments strongly suggest that HOCl-SM-induced ROS formation might play a key role in reduced cell viability of HOCl-SM-treated PC12 cells. Importantly, the possibility that HOCl-SM itself could function as a radical generator, was ruled out by incubation of HOCl-SM with DCFDA, resulting in no detectable increase in fluorescence (data not shown).

5.3. HOCl-SM induces morphological changes, damage, and dysfunction of PC12 mitochondria

In most cases, intracellular ROS formation is the consequence of mitochondrial dysfunction. To investigate whether SM or HOCl-SM impairs mitochondrial function changes of the $\Delta\psi$m were examined. $\Delta\psi$m is generated by the flux of positive charges across the inner membrane of mitochondria and contributes to most of the energy that is stored in the proton motive force which drives phosphorylation of ADP to ATP. Therefore, assays using the lipophilic, fluorescent mitochondrial tracker JC-1 were performed. In contrast to damaged mitochondria, JC-1 forms J-aggregates in functional mitochondria which exhibit orange/red fluorescence. The amount of JC-1 uptake into mitochondria hence depends on $\Delta\psi$m.

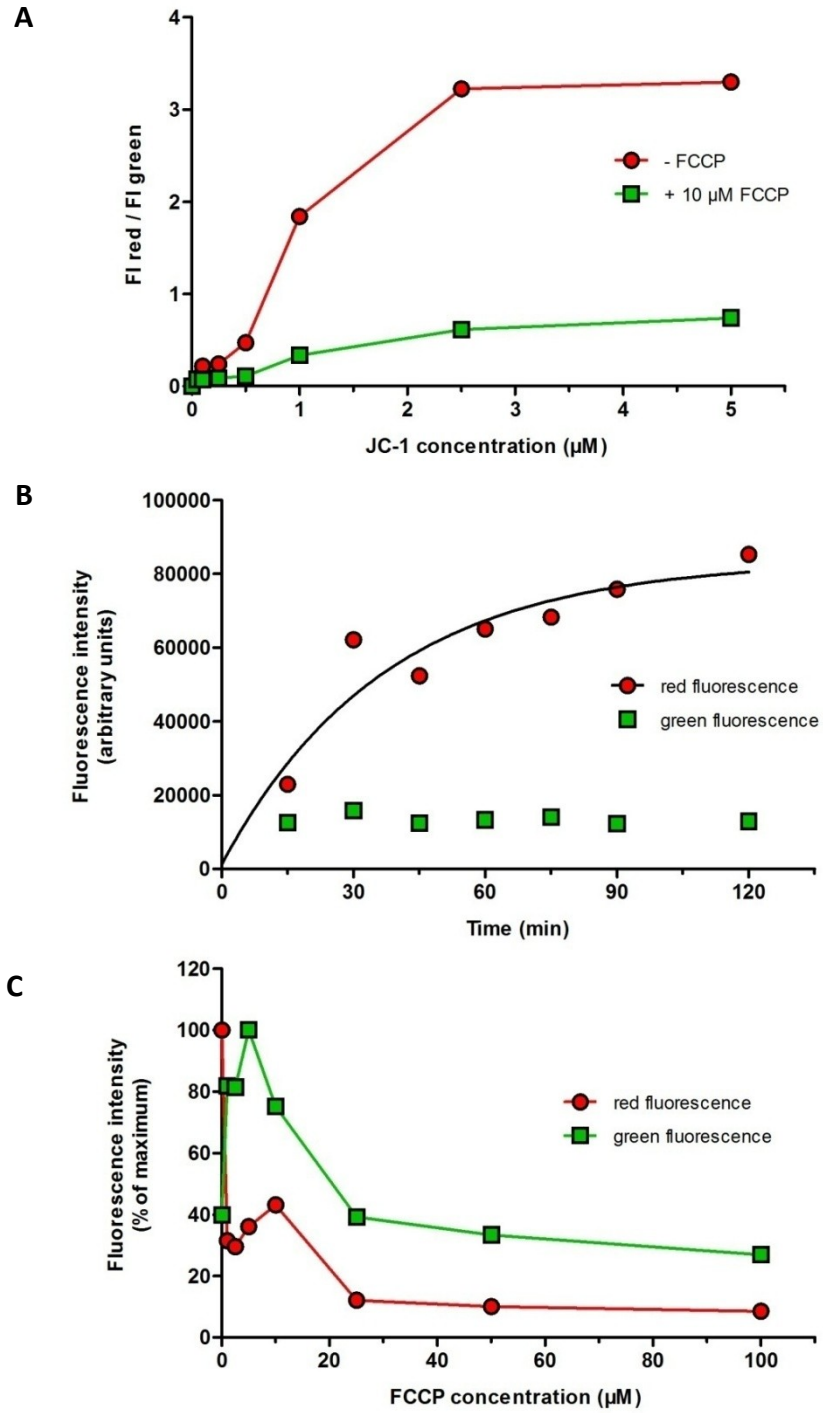

Figure 38: Optimization of JC-1 assay parameters in PC12 cells. A Dose-response as a function of the loading concentration of JC-1 in PC12 cells treated with or without FCCP. Cells were incubated in the presence of JC-1 at the indicated concentrations for 30 min at 37°C. FCCP treatment was performed 15 min prior dye loading. Results were calculated by division of red fluorescence by green fluorescence. ***B*** Kinetics of JC-1 uptake was determined by incubation of PC12 cell with 2.5 µM JC-1 at 37°C for the indicated time periods. ***C*** Sensitivity of $\Delta\psi$m of PC12 cells to FCCP was tested by incubation of the cells with 2.5 µM JC-1 (60 min) followed by treatment with FCCP at the indicated concentrations for 30 min at 37°C. Red and green fluorescence intensities were measured as described in 'Materials and Methods' and are expressed as % of the maximum.

To achieve optimal assay conditions for PC12 cells in terms of dye concentration, dye uptake kinetics, and FCCP titering cells were treated with the indicated concentrations of JC-1 and/or FCCP (a protonophore used to dissipate $\Delta\psi m$) for the indicated time periods and fluorescence intensities were measured.

These experiments revealed that the intensity of emitted red fluorescence by PC12 cells strongly correlate with the concentration of JC-1 used (***Figure 38 A***). Starting from concentrations of 1 µM JC-1, the cells sufficiently emitted red fluorescence (red/green ratio ~ 2). Lower loading concentrations of the dye were not sufficient to allow quantification of $\Delta\psi m$. JC-1 loading followed a saturation curve character in which concentrations higher than 2.5 µM did not increase formation of J-aggregates. Therefore, this concentration of the lipophilic dye was used in the following series of experiments. Treatment with FCCP did not cause a significant increase in green fluorescence but almost abolished formation of J-aggregates indicated by more intense green than red fluorescence. This effect was more or less independent from the loading concentration of JC-1.

Results of ***Fig. 38 B*** demonstrate the time course for JC-1 uptake in PC12 cells by increase of red and green fluorescence. Accumulation of the dye in mitochondria leading to formation of J-aggregates is a rather slow process in which an incubation time of 30 min was the minimum to detect significant discrepancies between red and green fluorescence. However, emission of red light increases with time up to 120 min (endpoint of measurement) whereas green fluorescence reaches a plateau after 15 min. A JC-1 loading time of 30 min was used for following experiments.

To test if J-aggregates are sensitive towards FCCP treatment, PC12 cells that were incubated with 2.5 µM JC-1 for 60 min were treated with different concentrations of the protonophore (***Fig. 38 C***). Interestingly, concentration of FCCP up to 5 µM efficiently reduced emission of red light which was accompanied by increased green fluorescence, indicative for JC-1 deaggregation in mitochondria as a consequence of $\Delta\psi m$ dissipation. In contrast, concentrations of the respiratory chain uncoupler of 25 µM and higher not only decreased red- but also green fluorescence. It is, therefore likely, that low FCCP concentrations provoke a collapse of $\Delta\psi m$, whereas higher concentrations impact on the plasma membrane potential ($\Delta\psi p$), thus leading to JC-1 efflux from PC12 cells. Under the

experimental conditions applied treatment with 5 µM FCCP was used for PC12 $\Delta\psi m$ dissipation and background correction.

Following the setup of optimal assay conditions, $\Delta\psi m$ was examined in PC12 cells treated with SM, HOCl-SM, or HOCl at the indicated concentrations for the indicated time periods.

JC-1 assays shown in ***Figure 39*** support results that were obtained by measurements of cell viability and intracellular ROS formation. HOCl-SM was shown to promote a time- and concentration-dependent rapid and substantial collapse of $\Delta\psi m$ in PC12 cells: IC_{50} values were 100 (1 h), 50 (12 h), and 25 µM (24 h) (***Fig. 39 B***). The dissipation of $\Delta\psi m$ followed similar characteristics as observed during measurement of cell viability of HOCl-SM-treated PC12 cells though the collapse of $\Delta\psi m$ displayed a more rapid event compared to loss of viability. Obviously, $\Delta\psi m$ collapse is the first event in this cascade of cell death, followed by generation of intracellular ROS which then leads to apoptotic or necrotic cell death. Interestingly, concentrations of 66 µM HOCl-SM are well able to interfere with mitochondrial function and to induce cell death but are not sufficient to generate extensive amounts of intracellular ROS. This suggests an important role of HOCl-SM itself in PC12 cell death. In general mitochondria seem to be affected earlier and at lower concentrations of applied HOCl-SM compared to cell viability measurements using the MTT assay.

SM alone showed less pronounced effects on $\Delta\psi m$ compared to HOCl-SM (***Fig. 39 A***). After 1 h of incubation no detectable dissipation of $\Delta\psi m$ could be observed. However, longer incubation times also resulted in a significant decrease of $\Delta\psi m$ with IC_{50} concentrations of 140 and 70 µM (12 and 24 h, respectively). These values are substantially lower compared to those after HOCl-SM treatment. Loss of mitochondrial function in response to SM treatment started 5 h after lipid addition (data not shown) and did coincide neither with ROS formation nor with reduced cell viability (see above).

Reagent HOCl also strongly induced mitochondrial dysfunction, although in a more linear way compared to SM or HOCl-SM with IC_{50} values of approx. 300 µM (1 and 24 h; ***Fig. 39 C***).

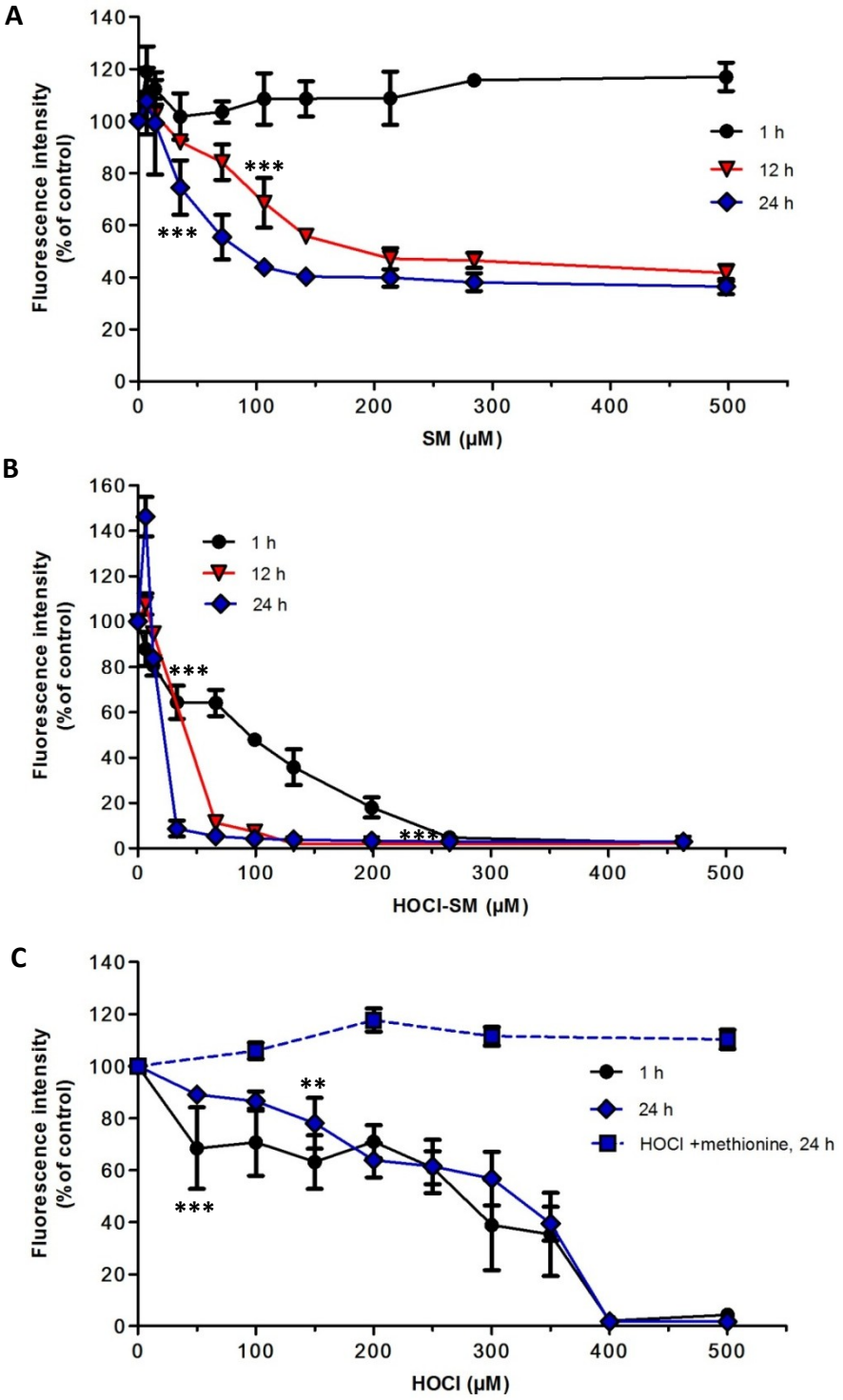

Figure 39: Δψm of SM-, HOCl-SM-, and HOCl-treated PC12 cells. Δψm of PC12 cells was examined using the JC-1 assay. Cells were incubated in the absence or presence of SM (***A***), HOCl-SM (***B***), or HOCl (***C***) at the indicated concentrations for the indicated time periods. Results were calculated by division of red fluorescence by green fluorescence after background correction using fluorescence values after FCCP treatment and are expressed as fluorescence intensity as % of control and represent the means ± SD (n = 3). ** $p < 0.005$; *** $p < 0.001$. For clarity p values are shown only for the first data point reaching significance.

Beside the fact that there are hardly any time-dependent differences in $\Delta\psi$m after HOCl incubation of PC12 cells it is interesting to note that there are slight differences between viability parameters and mitochondrial dysfunction in HOCl-treated PC12 cells (compare ***Fig. 36 C*** and ***Fig. 39 C***). Rather than this, determination of $\Delta\psi$m after HOCl treatment carried out even lower IC_{50} concentrations for cell viability compared to $\Delta\psi$m which was not observed after PC12 cell treatment with SM or HOCl-SM. Addition of Met in a 5-fold molar excess over HOCl completely abolished dissipation of $\Delta\psi$m up to concentrations of 500 µM HOCl (***Fig. 39 C***, dashed line).

Mitochondrial function of SM- and HOCl-SM-treated PC12 cells was studied in more detail using the Oxygraph-2k. PC12 cells were treated in parallel with either 66 µM HOCl-SM or water as vehicle control and oxygen flux was recorded for 6 hours before oligomycin was added to inhibit ATP synthase. Residual respiration is, therefore, mainly caused by the proton leak. When oxygen flux declined to a new steady state, FCCP was applied for total uncoupling of mitochondrial respiratory chain, thus indicating the potential maximum of respiration. Subsequently, values for aerobic activity of cells under routine culture conditions (C_r), the oligomycin-inhibited leak of respiration (C_{ro}), and the maximum stimulated respiration after treatment of cells with FCCP (C_{ru}) were used to calculate oxygen flux ratios which include the relative routine rate ($\mathbf{j'_r} = C_r/C_{ru}$), oligomycin-inhibited respiration rate ($\mathbf{j'_{ro}} = C_{ro}/C_{ru}$), and phosphorylation control ratio ($\mathbf{j'_p} = (C_r-C_{ro})/(C_{ru})$).

A lower respiration after uncoupling respiratory chain with FCCP – illustrating maximal respiratory capacity – compared to basal respiration at experimental start point (***Figure 40***, C_r 0 h - C_r 6 h) in case of HOCl-SM-treated PC12 cells suggest/point towards partial cell death of these cells during this time period. Apparently, PC12 cells are more susceptible to HOCl-SM when treated trypsinized in suspension compared to cells adhered to collagen-coated culture flasks. Nevertheless, the relative routine rate indicates a higher value of electron transport capacity that is utilized in the routine respiratory state for HOCl-SM-treated cells (73 and 53%, respectively) in which a higher percentage of electron transport capacity is related to non-phosphorylating respiration, demonstrated by values of oligomycin-inhibited respiration rate (43 and 16%, respectively).

These two values are combined in the phosphorylation control ratio, showing that in HOCl-SM-treated PC12 cells a lower percentage of total (uncoupled) electron transport capacity is functionally related to the control of respiration by phosphorylation compared to control cells (30 and 37%, respectively). Taken together, results of JC-1 assays and of oxygen flux measurements strongly indicate necrotic cell death as well as mitochondrial dysfunction in PC12 cells in course of HOCl-SM treatment.

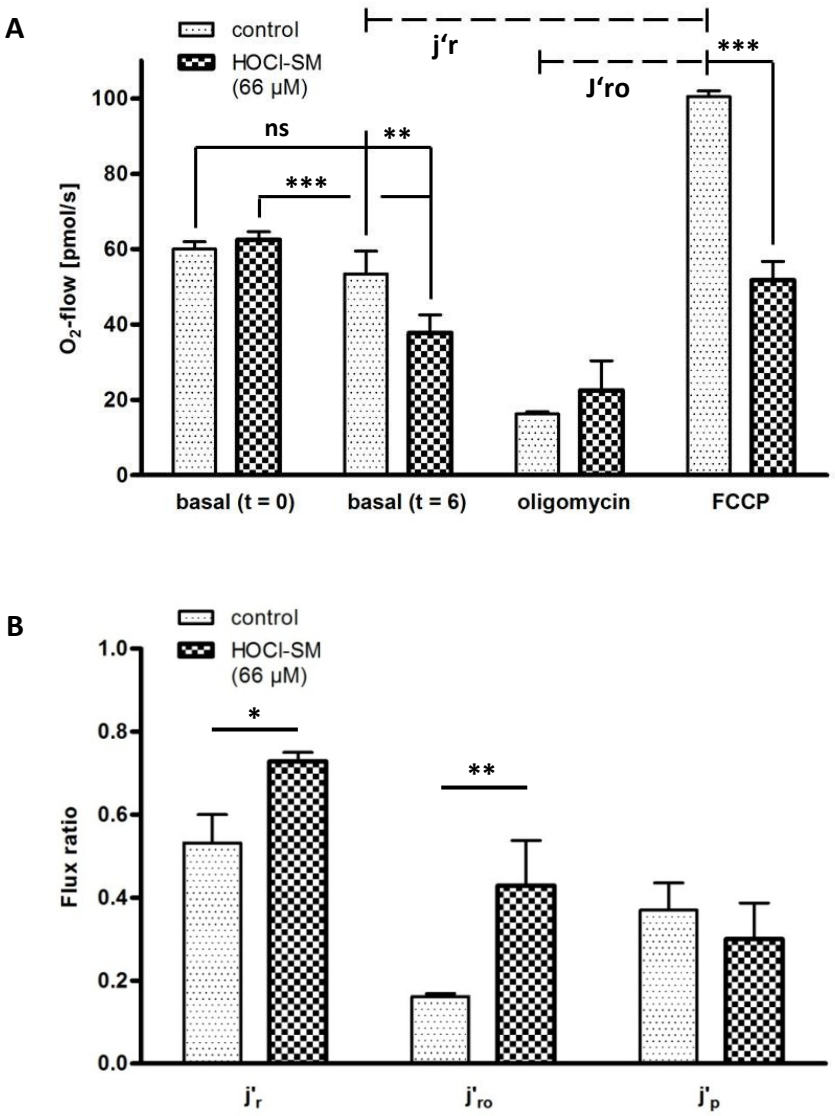

Figure 40: Investigation of mitochondrial dysfunction* via *oxygen flux measurement and determination of phosphorylation control in cellular respiration in PC12 cells. Mitochondrial activity of PC12 cells was analyzed by determination of cellular respiration using OROBOROS Oxygraph-2k. Trypsinized cells were resuspended in serum-free medium and incubated in the absence or presence of 66 µM HOCl-SM. Oxygen flux was recorded for 6 hours and respiration of intact cells was measured under routine conditions (C_r), after inhibition of ATP synthase (C_{ro}), and after uncoupling to maximum flux (C_{ru}). Results are expressed as cellular oxygen flow [pmol s^{-1}] (***A***) or as oxygen flux ratios (j'_r), (j'_{ro}), and (j'_p) (***B***) and represent the means ± SD (n = 3). * $p < 0.05$; *** $p < 0.001$.

5.4. Hypochlorite-modified SM induces apoptosis in PC12 cells

Decreased cell viability due to mitochondrial dysfunction and/or generation of ROS is very often accompanied by apoptotic cell death. HOCl-modified FFA provoke cell lysis of red blood cells (Carr et al., 1997a) and PC chlorohydrins induce activation of caspase-3 in myeloid cells (Dever et al., 2006). Therefore, the next set of experiments aimed to distinguish between apoptotic and necrotic cell death in PC12 cells treated with HOCl-SM. Hence, immunoblotting was performed to detect cleavage of procaspase-3 and PARP (a downstream target of caspase-3) which are typical hallmarks of the apoptotic cascade. In addition to Western blotting, Pi staining coupled to FACS analysis was performed in PC12 cells, incubated in the absence or presence of SM, HOCl-SM, or reagent HOCl, respectively.

As shown in ***Figure 41*** exogenously added HOCl-SM induced autocatalytic cleavage of procaspase-3 (32 kDa) to active caspase-3 (17 kDa; corresponding to the large subunit) at concentrations of 132 to 265 µM. This was accompanied by caspase-3-mediated cleavage of intact PARP (118 kDa) to the catalytically inactive 89 kDa peptide fragment. Also PARP cleavage was observed at HOCl-SM concentrations of >66 µM. At the highest concentration of HOCl-SM used (265 µM) neither caspase-3 nor PARP cleavage was detected although decrease in PC12 cell viability was found to follow a concentration-dependent manner (see ***Fig. 36 B***). In contrast to HOCl-SM neither unmodified SM nor reagent HOCl induced apoptosis in PC12 cells.

In line with data shown in ***Fig. 41*** SM at even 498 µM was without effect on sub-G1 population that appears because of alcohol mediated extraction of low abundance DNA in apoptotic cells (***Figure 42 B*** and ***C***). Similar to SM, HOCl-SM at 66 µM did not render PC12 cells apoptotic as already shown by immunoblotting. In contrast, HOCl-SM concentrations of 132 and 199 µM induced formation of sub-G1 peaks (17.5 and 13.8% apoptotic cells, respectively; ***Fig. 42 A – C***), whereas at higher concentrations the number of viable and apoptotic cells was below detection limit which was also observed when cells were treated with 600 µM HOCl alone. Once more these results suggest a caspase independent cell death in HOCl treated PC12 cells.

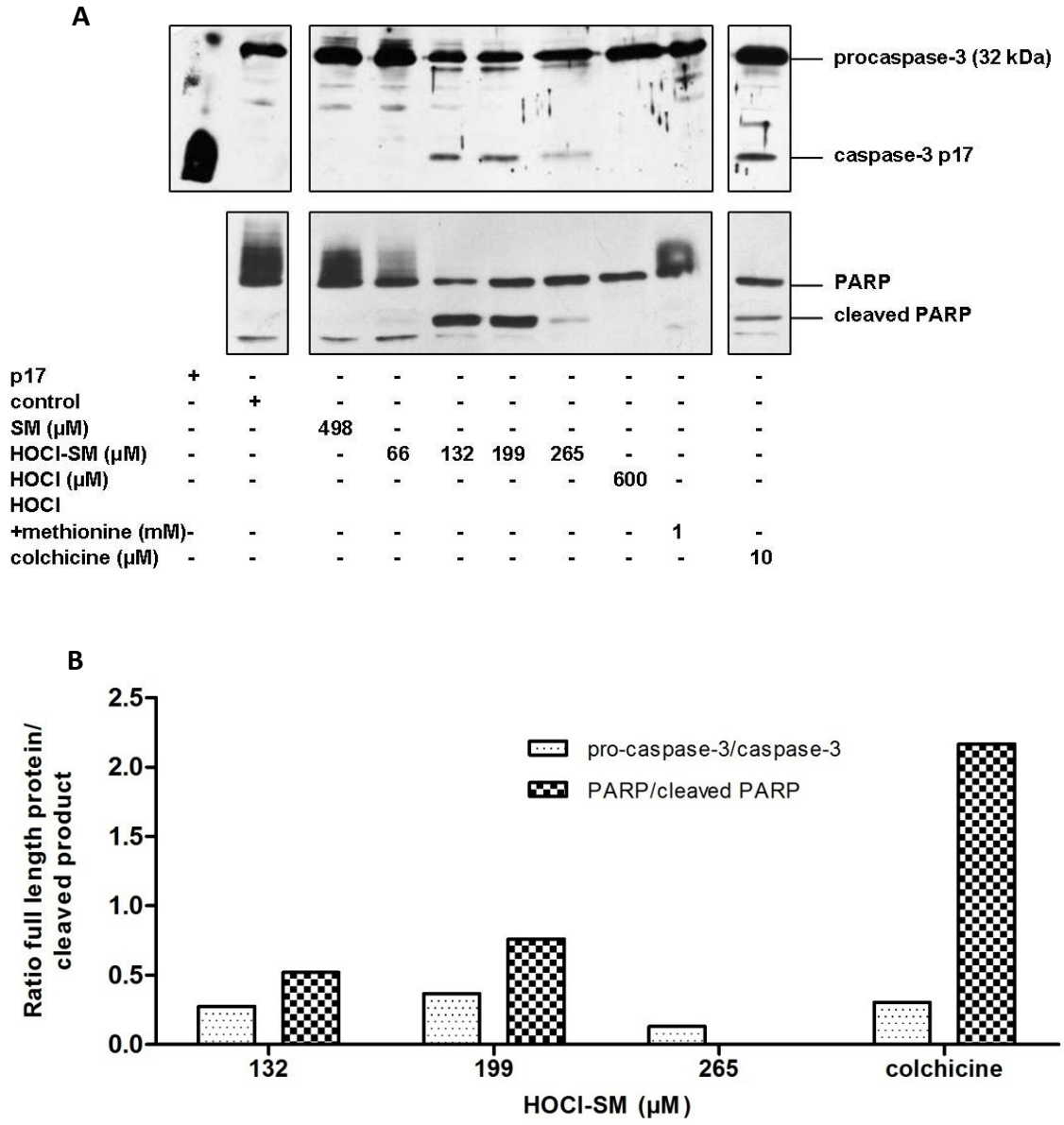

Figure 41: Induction of the apoptotic cascade in PC12 cells in response to HOCl, SM, or HOCl-SM treatment analyzed by Western blotting. PC12 cells were incubated in the absence or presence of SM, HOCl-SM, or HOCl at the indicated concentrations for 13 h. Cell treatment with colchicine (10 µM) served as positive control and was performed for 24 h. Protein lysates (40 µg/lane) were either run on 12% (caspase-3 activation), or 8% (PARP cleavage) SDS gels and were transferred onto PVDF membranes for subsequent detection using anti-caspase-3 and anti-PARP primary antibody. X-ray films showing caspase-3 and PARP cleavage after immunoblotting (***A***) were analyzed densitometrically and blotted as reversed optical density (***B***).

A

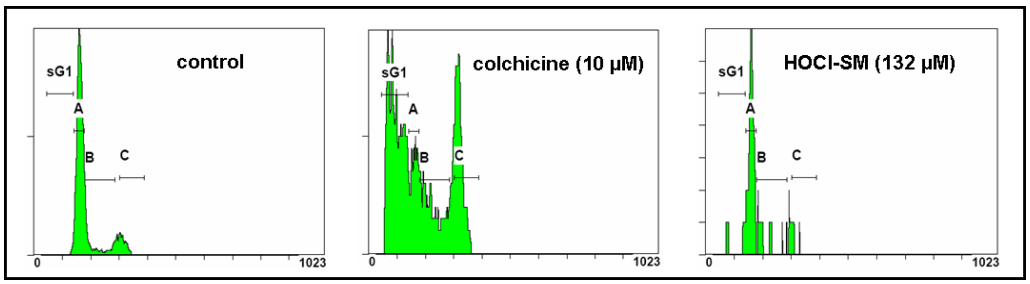

B

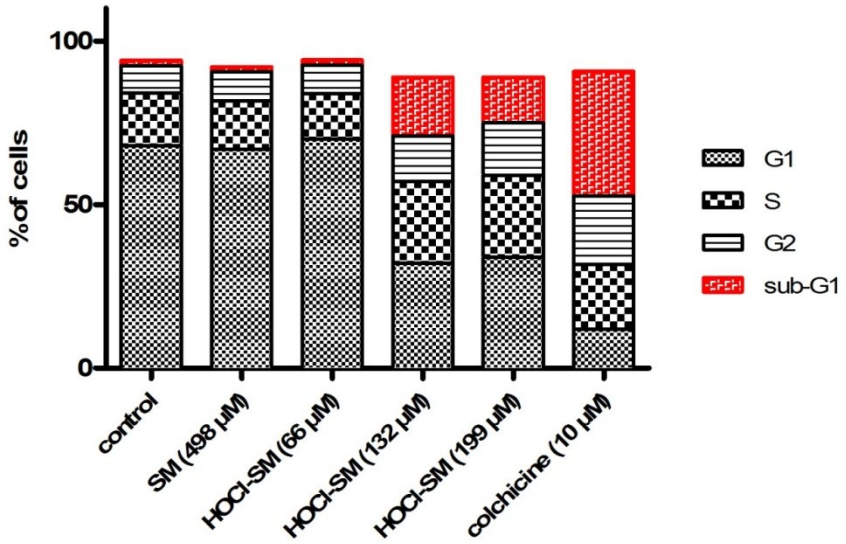

C

sample	sub-G1 (%)
control	1.7
SM (498 µM)	1.5
(66 µM)	1.7
HOCl-SM (132 µM)	17.5
(199 µM)	13.8
colchicine (10 µM)	38.0

Figure 42 Detection of PC12 cell apoptosis as response to SM or HOCl-SM treatment by degraded-DNA-based Pi stain coupled to FACS analysis. PC12 cells were incubated in the absence or presence of SM, HOCl-SM, or colchicine (positive control) at the indicated concentrations for 13 h (SM and HOCl-SM) or 24 h (colchicine), respectively. Subsequently, cells were trypsinized from the culture plates, fixed in ice-cold methanol, and stained with Pi before FACS analysis. Apoptotic cells appear below G1 phase (sub-G1 peak) (***A***). Results in ***B*** show PC12 cells in different stages of the cell cycle and are expressed as % of cells and represent mean values from duplicate experiments. The values of cells in sub-G1 are summarized in ***C***.

When cells were preincubated with the HOCl scavenger Met (molar ratio Met:HOCl = 5:1) sub-G1 peak formation was at control levels (data not shown). Also incubation of PC12 cells with colchicine induced a significant increase of sub-G1 cells (38% apoptotic cells). Interestingly, colchicine treatment provoked a more dominant formation of sub-G1 peaks compared to HOCl-SM treatment. Taken together Western blot and cell cycle analysis strongly suggest apoptotic PC12 cell death in response to HOCl-SM treatment. At the highest concentrations used cell death is most probably due to necrosis or aponecrosis/necroptosis rather than apoptosis.

6. AIM 4 – STUDYING ALTERATIONS IN THE PC12 CELL PROTEOME IN RESPONSE TO SM AND HOCl-SM

6.1. Identification of differentially regulated proteins in PC12 cells alter SM or HOCl-SM treatment

To identify alterations in the proteome as a consequence of treatment of PC12 cells with SM or HOCl-SM, a 2D-DIGE/LC-ESI-MS proteomic approach was performed. In these experiments a triple labeling strategy with Cy dyes was applied where protein lysates from control cells were minimally labeled with Cy2 and protein lysates of SM- and HOCl-SM-treated cells (47.5 µM SM/HOCl-SM; 24 h) were labeled with Cy3 and Cy5, respectively. The labeled lysates were pooled and separated by two-dimensional gel electrophoresis. Using the DeCyder software differentially expressed spots (> 2-fold regulation) corresponding to differentially regulated proteins identified after the gel scan were picked manually and subjected to in-gel trypsin digests. Subsequently, tryptic peptides were analyzed by nanoLC-ESI-MS analysis.

Results obtained from three different gels demonstrate that 82 proteins with a minimum coverage of at least three identified peptides were found to show differences in their expression pattern after PC12 cell treatment with either SM or HOCl-SM. Pictures of three individual gel images after fluorescent scanning illustrating the position of the corresponding picked spots are shown in ***Figure 43***.

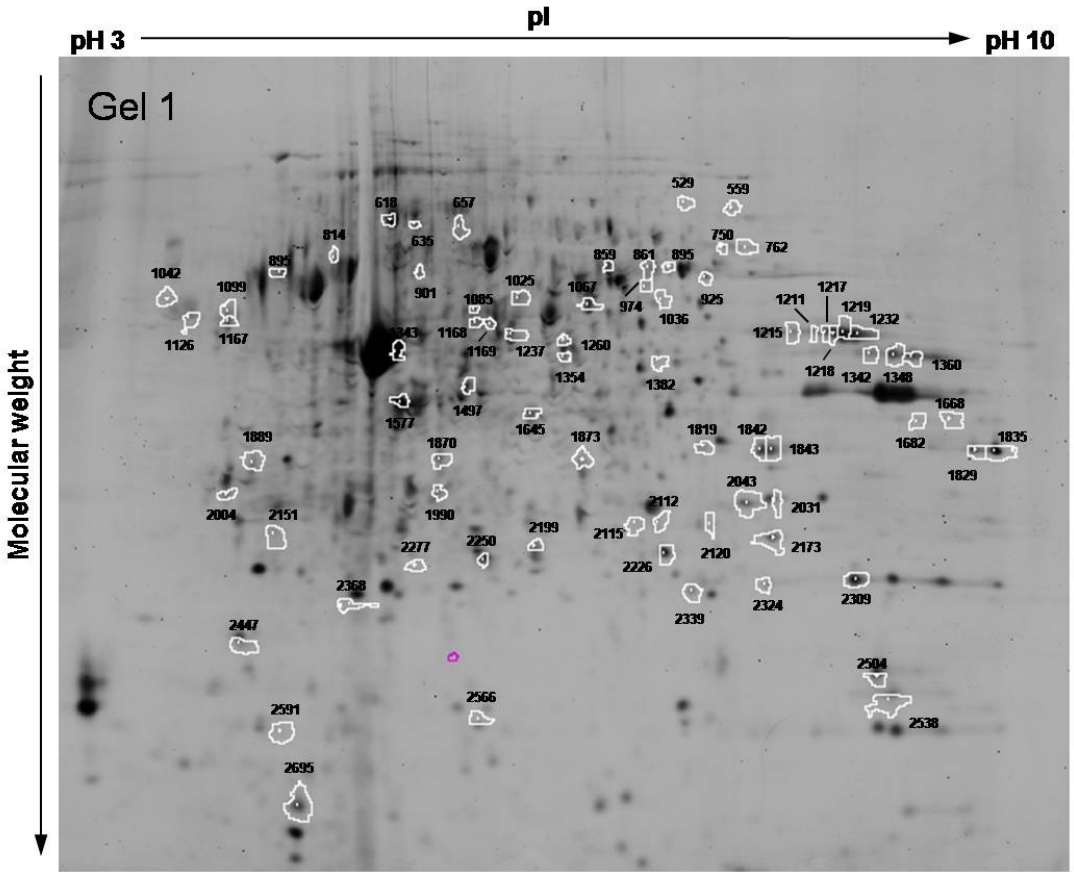
pI
pH 3
pH 10
Molecular weight
Gel 1

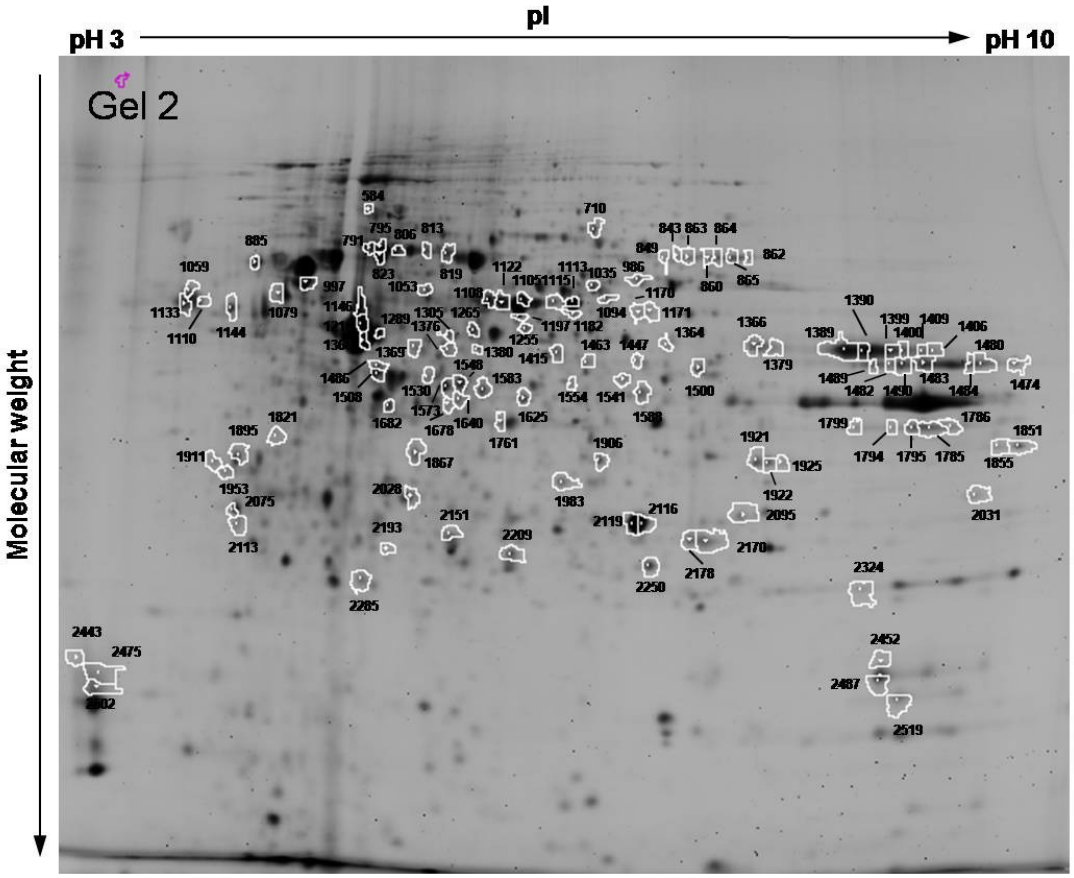
pI
pH 3
pH 10
Molecular weight
Gel 2

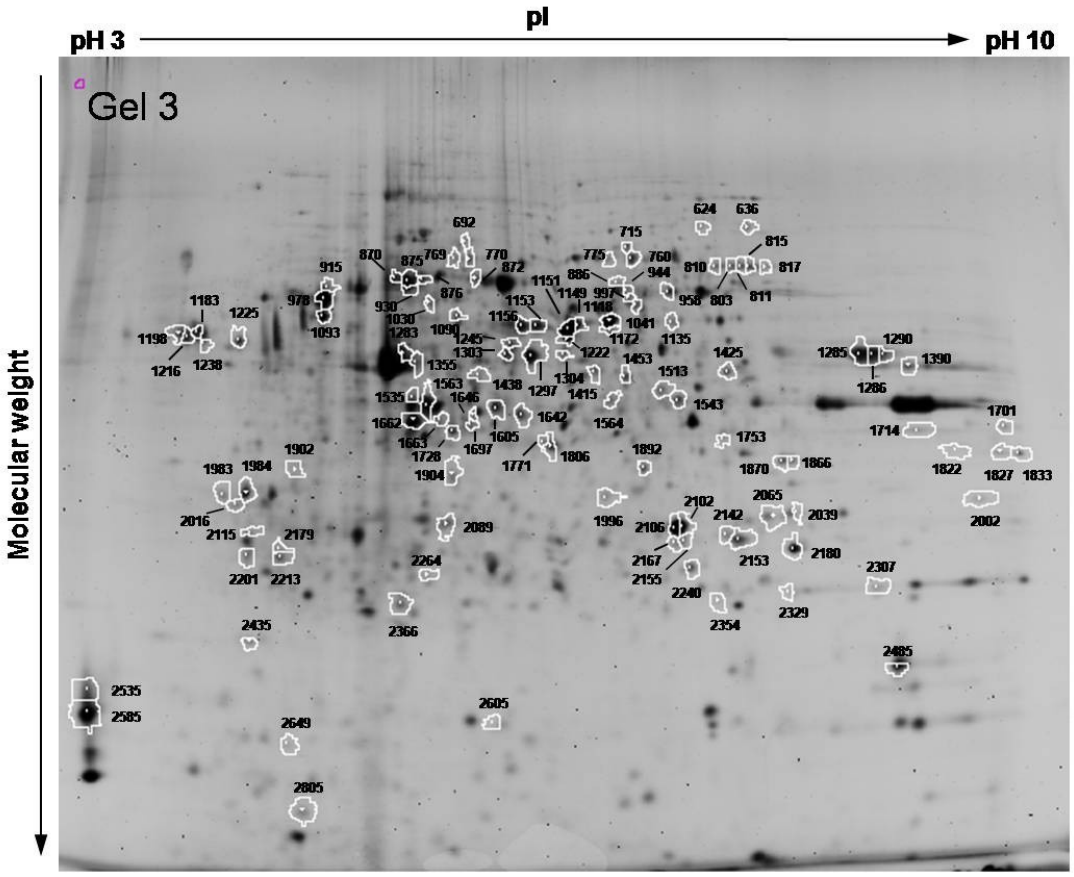

Figure 43: Changes in protein expression in response to SM and HOCl-SM treatment (1). PC12 cells were plated on 75 cm^2 flasks and incubated in the absence or presence of SM and HOCl-SM as described in 'Materials and Methods'. After 24 h incubation, protein lysates from control, SM-, and HOCl-SM-treated cells were minimally labeled (according to the manufacturer's recommendations) using Cy2, Cy3, and Cy5, respectively. After addition of the corresponding unlabeled protein extracts the three samples were pooled and separated on pH 3-10 IPG strips in the first dimension. The second dimension was run on self-cast 12% SDS-PAGE gels at 18°C. Following laser scanning of the corresponding gels on a Typhoon 9400 scanner, 2-fold differentially expressed proteins were identified using the DeCyder software. Grey scale images of the 2D-DIGE gels from three individual experiments (termed Gel 1 – 3) are shown. Spot numbers are identical to the numbering used in ***Tables 5*** and ***6***.

Each gel image additionally shows the spot numbers of differentially expressed proteins. Up- and down-regulated proteins that were identified in at least two individual gels were used for data set analyzation and are summarized in table form (***Table 5:*** proteins regulated in response to SM; ***Table 6:*** proteins regulated in response to HOCl-SM) which provide information on spot number, number of acquired spectra, distinct identified peptides, MS/MS search score, percentage amino acid coverage, theoretical and experimental molecular weight (MW), theoretical and experimental isoelectric point (pI), and x-fold regulation.

Table 5: Proteins regulated in response to SM

Upregulated proteins in response to SM

Gel 1
Gel 2
Gel 3

Protein name	RefSeq/UniProt accession number	Spot	Spectra	Distinct peptides	Distinct summed MS/MS search score	% AA coverage	MW theor. (Da)	MW exper. (Da)	pI theor.	pI exper.	Regulation control - SM (Cy2/Cy3)
leucine aminopeptidase 3	NP_001011910 Q68FS4	859	41	10	148.65	23	56150.4	63956	6.78	6.95	3.08
		1035	108	18	341.73	44	56150.4	58930	6.78	6.75	2.3
		997	134	18	334.9	44	56150.4	58020	6.78	6.9	2.41
PREDICTED: similar to Fascin, isoform 2	NP_001094276 B5DEI1	859	17	9	114.02	17	54550.3	63956	6.44	6.95	3.08
		710	12	6	92.13	15	54550.3	71581	6.44	6.75	2.04
		1035	88	17	304.05	40	54550.3	58930	6.44	6.75	2.3
		997	131	23	395.38	52	54550.3	58020	6.44	6.9	2.41
aldehyde dehydrogenase family 3, member A1	NP_114178 P11883	859	14	6	74.2	13	50338.9	63956	6.33	6.95	3.08
		1035	107	15	270.5	29	50338.9	58930	6.33	6.75	2.3
		944	58	13	210.95	38	50338.9	60793	6.33	6.9	2
		997	24	7	115.62	13	50338.9	58020	6.33	6.9	2.41
proteasome (prosome, macropain) subunit, alpha type 1	NP_058974 P18420	1873	17	6	77.37	24	29517.7	36654	6.14	6.7	3.79
		1983	178	14	231.29	57	29517.7	32124	6.14	6.55	2.38
		1996	89	14	220.22	58	29517.7	31383	6.14	6.75	2.29
superoxide dismutase 2	NP_058747 P07895	2309	39	5	84.93	29	24683.2	25859	8.96	8.7	4.78
		2324	11	5	81.41	22	24683.2	25859	8.96	7.95	2.21
		2324	87	7	122.4	32	24683.2	22813	8.96	8.6	3.73
		2307	62	7	110.97	23	24683.2	23534	8.96	8.65	4.83
peroxiredoxin 1	NP_476455 Q63716	2324	57	9	145.33	45	22109.5	25859	8.27	7.95	2.21
		2324	32	10	156.35	49	22109.5	22813	8.27	8.6	3.73
		2307	4	4	55.49	19	22109.5	23534	8.27	8.65	4.83
PREDICTED: similar to aldehyde dehydrogenase family 7, member A1	NP_695212 Q64057	859	10	6	73.19	13	58749	63956	7.99	6.95	3.08
		1035	12	6	100.17	15	58749	58930	7.99	6.75	2.3
Glutathione transferase omega-1 (GSTO 1-1)	NP_001007603 Q9Z339	1873	15	6	79.17	23	27669.1	36654	6.25	6.7	3.79
		1983	50	9	137.4	40	27669.1	32124	6.25	6.55	2.38
acidic ribosomal phosphoprotein P0	NP_071797 P19945	1497	16	7	104.94	30	34215.7	45457	5.91	5.95	2.02
		1682	14	4	72.25	13	34215.7	40884	5.91	5.35	3.2
dihydrofolate reductase	NP_569084 Q920D2	2339	44	8	128.14	45	21638.2	24733	6.77	7.45	2.4
		2354	34	8	123	42	21638.2	22636	6.77	7.55	2.04
lectin, galactose binding, soluble 1	NP_063969 P11762	2695	91	8	139.31	58	14856.9	13258	5.14	4.8	3.25
		2805	127	9	151.26	58	14856.9	11505	5.14	4.7	2.6
phosphoglycerate kinase 1	NP_445743 P16617	1211	15	6	77.82	15	44538.7	53124	8.02	8.4	2.93
		1215	33	9	146.5	26	44538.7	53124	8.02	8.25	2.9
		1217	54	13	182.16	41	44538.7	53124	8.02	8.5	2.7
		1218	14	7	86.5	20	44538.7	53520	8.02	8.65	2.61
		1219	181	20	329.08	60	44538.7	53520	8.02	8.7	2.66
		1232	56	12	174.54	33	44538.7	53520	8.02	8.9	2.38
		1497	69	15	252.11	52	44538.7	45457	8.02	5.95	2.02
		1646	95	17	299.66	39	44538.7	40567	8.02	5.8	2.07
septin 6	NP_001100678 B3GNI4	974	14	5	75.88	13	49782	62085	6.24	7.2	2.36
		1041	79	15	257.93	43	49782	55807	6.24	7.05	3.66
eukaryotic translation initiation factor 4A1, isoform CRA_a	NP_955404 Q6P3V8	1146	16	8	132.63	22	44607.4	55807	5.61	5.15	2.45
		1283	38	13	215.35	35	44607.4	50439	5.61	5.3	2.89

Cathepsin D precursor	NP_599161 P24268	1369 1376	47 35	9 5	159.52 80.59	28 14	44681 44681	48139 48139	6.66 6.66	5.55 5.75	2.4 2.94
		1438	47	9	157.51	29	44681	45588	6.66	5.85	2.26
MYG1 protein	NP_001005545 Q641W2	1376	19	6	105.97	15	42889	48139	6.02	5.75	2.94
		1438	41	12	228.53	38	42889	45588	6.02	5.85	2.26
PREDICTED: similar to transcriptional activator protein Pur-alpha	NP_001017503 Q68A21	1376	6	3	41.95	9	33018	48139	6.2	5.75	2.94
		1438	7	4	56.79	11	33018	45588	6.2	5.85	2.26
heterogeneous nuclear ribonucleoprotein C	NP_001020804 Q4V8K6	1821	6	3	49.77	12	32857.2	36952	4.86	4.55	5.47
		1902	20	6	98.68	22	32857.2	33658	4.86	4.6	2.85
phosphatidylethanolamine binding protein	NP_058932 P31044	2285	61	7	123.81	39	20801.5	23717	5.47	7.15	4.7
		2366	82	10	169.74	53	20801.5	22286	5.47	5.3	3.04
voltage dependent anion channel (Vdac1)	NP_112643 Q9Z2L0	1851	64	12	216.24	61	31966	35820	8.35	9.7	2.1
		1827	57	11	197.03	50	31966	36381	8.35	9.55	2.02
		1833	26	7	126.51	35	31966	36381	8.35	9.6	2.19
tyrosine 3-monooxygenase/tryptophan 5-monooxygenase activation protein	NP_113791 P62260	1953	322	18	349.5	80	29121.9	33658	4.55	4.25	3.73
		2016	152	18	309.97	69	29121.9	30185	4.55	4.2	3.43
Peroxiredoxin 2	NP_058865 P35704	2285	7	4	61.95	19	21797.8	23717	5.34	5.15	4.7
		2366	5	3	46.92	17	21797.8	22286	5.34	5.3	3.04

Downregulated proteins in response to SM

Gel 1
Gel 2
Gel 3

Protein name	RefSeq/UniProt accession number	Spot	Spectra	Distinct peptides	Distinct summed MS/MS search score	% AA coverage	MW theor. (Da)	MW exper. (Da)	pI theor.	pI exper.	Regulation control - SM (Cy2/Cy3)
gamma-butyrobetaine,2-oxoglutarate dioxygenase	NP_742059 P54001	657	31	14	183.32	30	60924.5	71488	5.7	5.9	-3.31
		819	5	4	55.57	8	60924.5	65711	5.7	5.7	-2.18
		770	84	15	259.52	28	60924.5	66741	5.7	5.8	-2.99
PREDICTED: similar to Alpha-enolase (NNE) (Enolase 1)	NP_036686 P04764	1025	7	4	51.11	7	53924	58505	5.81	6.3	-2
		1067	93	14	226.25	38	53924	56794	5.81	6.8	-2.2
		1237	19	6	83.13	18	53924	52731	5.81	6.25	-2.08
		1105	351	22	402.48	53	53924	57571	5.81	6.25	-2.31
		1108	222	22	395.45	49	53924	56243	5.81	6.05	-2.89
		1113	113	19	333.56	46	53924	56243	5.81	6.65	-2.21
		1115	51	11	180.93	20	53924	56243	5.81	6.5	-2.06
		1122	310	20	361.67	45	53924	56243	5.81	6.15	-2.83
		1182	216	22	388.9	53	53924	54520	5.81	6.6	-2.86
		1197	320	23	425.03	53	53924	54520	5.81	6.25	-3.17
		1118	191	20	340.08	46	53924	54946	5.81	6.8	-2.59
		1149	134	19	332.31	49	53924	54097	5.81	6.6	-2.61
		1151	258	20	361.38	52	53924	53262	5.81	6.5	-2.8
		1153	211	21	379.23	53	53924	53262	5.81	6.25	-2.52
		1156	139	17	317.71	39	53924	53262	5.81	6.15	-2.75
		1222	104	21	362.86	55	53924	50439	5.81	6.5	-2.47
calreticulin	NP_071794 P18418	1042	12	5	72.94	14	47995.7	58506	4.33	3.8	-5.22
		1110	6	3	41.75	7	47995.7	56682	4.33	4	-2.01
		1133	11	3	43.09	7	47995.7	55807	4.33	3.9	-3.08
		1198	15	3	52.09	8	47995.7	52034	4.33	3.8	-6.29
calumenin isoform a	NP_071980 Q3MID6	1126	45	13	180.61	39	37063.9	55133	4.49	3.95	-3
		1059	26	8	135.37	19	37063.9	58930	4.49	3.95	-3.28
		1110	85	14	236.23	42	37063.9	56682	4.49	4	-2.01
		1133	199	19	345.44	48	37063.9	55807	4.49	3.9	-3.08
		1183	144	18	345.34	52	37063.9	52849	4.49	3.95	-3.75
		1216	116	18	335.94	55	37063.9	51630	4.49	3.9	-3.22
		1238	50	11	200.77	36	37063.9	50049	4.49	4	-3.31

aldolase C	NP_036629 P09117	1382	6	4	50.99	14	39284	50061	6.67	7.25	-2.22
		1500	8	4	62.08	12	39284	46303	6.67	7.5	-3.12
		1425	82	13	241.73	40	39284	46664	6.67	7.6	-2.45
heterogeneous nuclear ribonucleoprotein A2/B1	NP_001098083 A7VJC2	1668-2	40	12	163.06	36	37477.9	41583	8.97	9.3	-3.02
		1785	15	5	80.97	14	37477.9	37824	8.97	8.85	-4.86
		1795	3	3	51.36	11	37477.9	37824	8.97	8.6	-4.17
		1799	62	11	199.38	39	37477.9	37824	8.97	9	-2.95
		1701	62	15	229.19	46	37477.9	39020	8.97	9.5	-2.61
triosephosphate isomerase 1	NP_075211 P48500	2112	71	12	216.83	58	31011.7	30901	5.56	7.35	-2.28
		2115	31	8	144.38	38	31011.7	30446	5.56	7.15	-2.95
		2120	107	12	209.32	58	31011.7	29997	5.56	7.55	-7.45
		2170	406	16	313.3	70	31011.7	26653	5.56	7.55	-4
		2153	193	13	248.7	55	31011.7	27282	5.56	7.7	-5.67
		2167	109	10	195.53	41	31011.7	27071	5.56	7.3	-2.32
Protein disulfide-isomerase precursor (Prolyl 4-hydroxylase subunit beta)	NP_037130 P04785	895	46	11	156.95	22	56951.6	63013	4.82	4.6	-2.36
		885	26	10	170.99	20	56951.6	64195	4.82	4.4	-3.93
dipeptidylpeptidase 7	NP_114179 Q9EPB1	895	6	3	45.61	6	55114.6	63013	4.86	4.6	-2.36
		885	15	5	90.99	10	55114.6	64195	4.86	4.4	-3.93
TAR DNA binding protein	NP_001011979 -	1169	4	3	42.43	9	44518	53919	6.26	6.05	-2.85
		1260	14	5	59.04	11	44518	53124	6.26	6.7	-2.15
		1380	56	10	182.71	24	44518	48139	6.26	6	-2.24
ERO1-like	NP_612537 Q8R4A1	657	10	4	60.9	10	54115.8	71488	6.1	5.9	-3.31
		819	50	13	222.51	29	54115.8	65711	6.1	5.7	-2.18
vimentin	NP_112402 P31000	814	49	17	231.54	38	53733	65883	5.06	5	-2.49
		895	51	13	201.59	28	53733	63013	5.06	4.6	-2.36
		885	6	3	50.07	6	53733	64195	5.06	4.4	-3.93
lactate dehydrogenase A	NP_058721 P04642	1668	27	8	107.02	28	36450.7	41583	8.45	9.3	-3.02
		1785	351	20	356.85	65	36450.7	37824	8.45	8.85	-4.86
		1795	162	13	223.53	40	36450.7	37824	8.45	8.6	-4.17
		1799	128	16	276.72	51	36450.7	37824	8.45	9	-2.95
far upstream element (FUSE) binding protein 1	NP_001032742 Q32PX7	529	31	10	147.43	20	67197.4	78730	7.18	7.45	-2.04
		559	24	7	101.19	13	67197.4	76996	7.18	7.8	-2.27
		624	102	17	306.64	30	67197.4	74420	7.18	7.4	-2.05
		636	152	20	348.21	36	67197.4	74420	7.18	7.7	-2.01
PREDICTED: similar to pyruvate kinase 3	NP_445749 P11980	762	10	4	50.77	7	57877.3	68883	7.57	8.05	-3.17
		750	77	14	235.25	35	57877.3	68883	7.57	7.7	-3.67
		863	39	11	171.98	25	57877.3	64912	7.57	7.35	-2.47
		861	12	6	75.1	13	57877.3	64912	7.57	7.2	-2.72
		811	46	15	251.36	32	57877.3	65201	7.57	7.65	-2.52
		815	39	11	167.5	24	57877.3	65201	7.57	7.75	-2.56
		817	110	19	351.75	41	57877.3	65201	7.57	7.85	-2.93
calumenin isoform b	NP_001029070 Q3MID6	1042	22	8	119.4	27	37148	58506	4.43	3.8	-5.22
		1198	120	15	285.82	46	37148	52034	4.43	3.8	-6.29
tropomyosin 3, gamma isoform 2	NP_001029242 Q63607	1889	33	8	112.93	28	33280.8	36382	4.73	4.4	-2.04
		1984	4	3	33.93	10	33280.8	31383	4.73	4.25	-2-32
glutathione S-transferase, mu 2	NP_803175 P08010	2173	53	11	141.97	48	25702.8	29120	6.91	8.1	-2.34
		2180	152	20	364.39	78	25702.8	26653	6.91	8.1	-2.44
Adenosine kinase (Adenosine 5'-phosphotransferase)	NP_037027 Q64640	1169	19	9	137.53	32	40133.9	53919	5.72	6.05	-2.85
		1303	7	4	61.2	14	40133.9	48894	5.72	6.1	-2.36
ErbB3-binding protein 1	NP_001004206 Q6AYD3	1169	7	3	43.29	8	43657	53919	6.41	6.05	-2.85
		1172	93	16	284.02	42	43657	52440	6.41	6.8	-2.48
		1222	10	4	72.83	10	43657	50439	6.41	6.5	-2.47
		1303	13	5	81.45	12	43657	48894	6.41	6.1	-2.36

similar to Pol(yrC)-binding protein 1 (predicted)	NP_001013241 Q6AYU5	1382	41	7	100.06	29	35512.7	50061	7.03	7.25	-2.22
		1425	15	5	80.5	20	35512.7	46664	7.03	7.6	-2.45
malate dehydrogenase, mitochondrial	NP_112413 P04636	1668-2	3	3	36.24	10	35683.8	41583	8.93	9.3	-3.02
		1701	3	3	39.88	10	35683.8	39020	8.93	9.5	-2.61
tumor protein D52	NP_001099891 -	2151	19	7	101.04	34	24268.9	29555	4.68	4.6	-5.28
		2213	46	9	162.31	37	24268.9	25636	4.68	4.05	-5.39
procollagen-proline, 2-oxoglutarate 4-dioxygenase, alpha II polypeptide	NP_001101745 -	819	33	8	141.83	16	60867.4	65711	5.69	5.7	-2.18
		770	7	3	48.61	6	60867.4	66741	5.69	5.8	-2.99
M2 pyruvate kinase	NP_445749 P11980	843	196	26	503.44	55	57781.2	64696	7.15	7.4	-2.2
		860	115	15	261.82	27	57781.2	64696	7.15	7.3	-2.86
		862	134	23	426	52	57781.2	64696	7.15	7.85	-3.47
		863	197	24	456.1	49	57781.2	64696	7.15	7.45	-2.91
		864	228	25	479.42	51	57781.2	64696	7.15	7.7	-2.43
		865	185	22	423.56	45	57781.2	64696	7.15	7.75	-2.61
		803	48	13	198.16	31	57781.2	65201	7.15	7.6	-2.96
		810	47	16	284.42	37	57781.2	65201	7.15	7.45	-3.25
		958	84	18	327.71	41	57781.2	60332	7.15	7.15	-2.34
		1090	67	18	312.3	45	57781.2	55375	7.15	5.7	-2.86
catalase	NP_036652 P04762	843	19	11	172.15	27	59757.5	64696	7.07	7.4	-2.2
		860	86	16	285.62	35	59757.5	64696	7.07	7.3	-2.86
		863	27	11	182.63	25	59757.5	64696	7.07	7.45	-2.91
		864	41	13	220.61	29	59757.5	64696	7.07	7.7	-2.43
		803	12	7	104.2	18	59757.5	65201	7.07	7.6	-2.96
		810	7	3	57.59	7	59757.5	65201	7.07	7.45	-3.25
		811	19	7	116.07	16	59757.5	65201	7.07	7.65	-2.52
actin, alpha 1, skeletal muscle, isoform CRA_a	NP_062085 P68136	1182	17	3	53.58	8	51496.2	54520	5.91	6.6	-2.86
		1153	5	3	45.18	8	51496.2	53262	5.91	6.25	-2.52
heterogeneous nuclear ribonucleo-protein; type A/B hnRNP p40AIF-C1	NP_112620 Q9QX81	1463	48	7	132.84	23	36233	46664	6.48	6.7	-2.02
		1453	91	9	161.55	25	36233	45588	6.48	6.9	-2.81
poly(rC) binding protein 2	NP_001013241 Q6AYU5	1463	18	4	71.02	13	38580.3	46664	6.33	6.7	-2.02
		1554	10	3	53.7	9	38580.3	43509	6.33	6.6	-2.15
		1453	22	5	88.31	17	38580.3	45588	6.33	6.9	-2.81
calponin 3, acidic	NP_062232 P37397	1508	25	8	138.73	29	36434.9	45588	5.47	5.25	-3.12
		1535	11	5	93.24	17	36434.9	42506	5.47	5.4	-3.39
Aspartate aminotransferase, cytoplasmic (Transaminase A)	NP_036703 P13221	1500	36	11	168.02	29	46429	46303	6.73	7.5	-3.12
		1425	56	14	239.8	40	46429	46664	6.73	7.6	-2.45
cathepsin B preproprotein	NP_072119 Q6IN22	1508	14	5	83.28	15	37544.4	45588	5.47	5.25	-3.12
		1563	5	3	49.69	11	37544.4	42506	5.47	5.5	-2.07
replication factor C (activator 1) 4	NP_001099339 B4F778	1554	52	13	222.79	38	39957.2	43509	6.21	6.6	-2.15
		1564	17	6	91.77	18	39957.2	41203	6.21	6.9	-2.02
annexin A1	NP_037036 P07150	1588	503	25	434.78	71	38829.7	42506	6.96	7.1	-2.1
		1625	62	15	252.26	44	38829.7	41849	6.96	6.3	-3.43
		1543	262	26	443.52	72	38829.7	42506	6.96	7.25	-2.09
		1564	42	11	178.16	34	38829.7	41203	6.96	6.9	-2.02
		1642	21	7	114.46	22	38829.7	40567	6.96	6.15	-2.81
PREDICTED: similar to methionine adenosyltransferase II, beta	NP_001037747 Q5U2R0	1588	19	6	109.42	24	37374.9	42506	6.46	7.1	-2.1
		1543	5	3	56.68	14	37374.9	42506	6.46	7.25	-2.09
lactate dehydrogenase B	NP_036727 P42123	1640	8	3	54.87	12	36612.6	41203	5.7	5.8	-2.05
		1728	10	4	57.09	9	36612.6	38120	5.7	5.6	-2.73
pyrroline-5-carboxylate reductase 1	NP_001099327 B2RYR3	1906	42	8	143.32	27	32226.5	34186	6.36	6.8	-2.14
		1892	82	15	281.6	54	32226.5	34186	6.36	7.05	-2.72
galectin 3	NP_114020 P08699	2031	25	4	71.88	16	27229.7	30659	8.92	9.4	-2.09
		2002	23	8	128.67	35	27229.7	31383	8.92	9.3	-2.02

phosphoglycerate mutase type B subunit	NP_445742 P25113	2116 2119	95 207	13 15	243.66 295.67	63 65	28846.2 28846.2	27926 27926	7.07 7.07	7.15 7.05	-2.96 -2.61
		2102 2106	41 179	7 12	126.74 231.21	37 52	28846.2 28846.2	28809 28364	7.07 7.07	7.3 7.25	-2.72 -2.36
phosphomannomutase 2	NP_001100443 B5DF46	2116	84	9	153.72	39	27708.9	27926	6.9	7.15	-2.96
		2102	37	10	165.77	44	27708.9	28809	6.9	7.3	-2.72
enoyl Coenzyme A hydratase, short chain, 1, mitochondrial	NP_511178 P14604	2116 2119	6 57	3 8	53.88 144.85	16 34	31516.6 31516.6	27926 27926	8.4 8.4	7.15 7.05	-2.96 -2.61
		2106	83	10	176.71	38	31516.6	28364	8.4	7.25	-2.36
Ppib protein	NP_071981 P24368	2487	57	11	190.42	46	23802.7	17375	9.5	8.75	-2.17
		2485	32	9	154.3	43	23802.7	18635	9.5	8.8	-2.23
transaldolase	NP_113999 Q9EQS0	1583 1625 1640	56 66 30	11 14 7	202.91 255.69 116.78	31 37 21	37476.3 37476.3 37476.3	42838 41849 41203	6.57 6.57 6.57	6 6.3 5.8	-3.07 -3.43 -2.05
		1642	36	12	201.57	32	37476.3	40567	6.57	6.15	-2.81
cofilin 1	NP_058843 P45592	2487	11	2	39.75	15	18532.6	17375	8.22	8.75	-2.17
		2485	11	3	58.15	27	18532.6	18635	8.22	8.8	-2.23

Table 6: Proteins regulated in response to HOCl-SM

Upregulated proteins in response to HOCl-SM

Gel 1
Gel 2
Gel 3

Protein name	RefSeq/UniProt accession number	Spot	Spectra	Distinct peptides	Distinct summed MS/MS search score	% AA coverage	MW theor. (Da)	MW exper. (Da)	pI theor.	pI exper.	Regulation control - HOCl-SM (Cy2/Cy5)
voltage dependent anion channel (Vdac1)	Q9Z2L0 NP_112643	1829 1835	25 81	9 11	120.82 178.52	38 51	31966 31966	37479 37479	8.35 8.35	9.45 9.6	2.54 2.61
		1851 1855	64 83	12 12	216.24 209.38	61 54	31966 31966	35820 35820	8.35 8.35	9.7 9.55	2.97 2.59
		1822 1827 1833	21 57 26	6 11 7	101.37 197.03 126.51	24 50 35	31966 31966 31966	36381 36381 36381	8.35 8.35 8.35	9.15 9.55 9.6	2.91 2.67 2.85
calcyclin binding protein	Q6AYK6 NP_001004208	2043	19	5	60.1	20	26541.3	32070	7.64	7.9	2.96
		2095	113	13	224.51	41	26541.3	28586	7.64	7.8	3.93
		2065	5	3	32.28	8	26541.3	29489	7.64	6.95	3.7
adenylate kinase 2 isoform a	NP_112248 P29410	2043	29	7	101.9	29	26392.7	32070	7.01	7.9	2.96
		2095	72	9	151	43	26392.7	28586	7.01	7.8	3.93
proteasome (prosome, macropain) subunit, alpha type 4	NP_058977 P21670	2031	9	3	39.44	13	29498	31832	7.58	8.1	3.74
		2039	17	5	66.87	18	29498	29719	7.58	8.1	3.65
expressed in non-metastatic cells 1, protein (NM23A)	NP_612557 Q05982	2566	48	10	164.21	67	17192.8	17320	5.96	5.95	7
		2605	16	6	90.61	46	17192.8	15223	5.96	6	6.12
heterogeneous nuclear ribonucleoprotein C	NP_001020804 Q4V8K6	1821	6	3	49.77	12	32857.2	36952	4.86	4.55	2.44
		1902	20	6	98.68	22	32857.2	33658	4.86	4.6	2.11
L-3-hydroxyacyl-Coenzyme A dehydrogenase	NP_476534 Q9WVK7	1855	12	5	82.59	14	34448	35820	8.83	9.55	2.59
		1822 1827	13 31	4 6	63.01 106.46	11 14	34448 34448	36381 36381	8.83 8.83	9.15 9.55	2.91 2.67
PREDICTED: similar to calmodulin 1	NP_114175 P62161	2443 2475 2502	12 11 13	2 2 2	32.16 36.79 35.83	20 20 20	14440.4 14440.4 14440.4	19678 18781 17241	4.36 4.36 4.36	3.15 3.4 3.4	5.07 6.22 2.24
		2535	14	3	52.49	21	14440.4	17241	4.36	3.15	4.73
Heat shock protein beta-1 (HSP 27)	NP_114176 P42930	2151 2193	363 85	13 11	220.57 188.31	57 51	22892.8 22892.8	27282 26038	6.12 6.12	5.75 5.3	2.37 2.11
		2264	17	4	50.16	17	22892.8	24277	6.12	5.5	2.05

Downregulated proteins in response to HOCl-SM

Gel 1
Gel 2
Gel 3

Protein name	RefSeq/UniProt accession number	Spot	Spectra	Distinct peptides	Distinct summed MS/MS search score	% AA coverage	MW theor. (Da)	MW exper. (Da)	pI theor.	pI exper.	Regulation control - HOCl-SM (Cy2/Cy5)
lactate dehydrogenase A	NP_058721 P04642	1682	61	14	198.24	51	36450.7	41583	8.45	9.05	-2.29
		1785	351	20	356.85	65	36450.7	37824	8.45	8.85	-3.6
		1786	160	18	321.47	63	36450.7	37824	8.45	9.15	-3.72
		1794	167	19	333.91	65	36450.7	37824	8.45	9.3	-3.05
		1795	162	13	223.53	40	36450.7	37824	8.45	8.6	-3.59
		1799	128	16	276.72	51	36450.7	37824	8.45	9	-2.46
		1714	98	18	278.12	63	36450.7	39020	8.45	8.95	-3.51
cofilin 1	NP_058843 P45592	2504	4	3	39.6	17	18532.6	18933	8.22	8.9	-2.52
		2487	11	2	39.75	15	18532.6	17375	8.22	8.75	-2.76
		2485	11	3	58.15	27	18532.6	18635	8.22	8.8	-2.7
cofilin 1	NP_058843 P45592	2538	42	7	123.05	42	18532.6	18108	8.22	8.95	-2.36
		2519	69	10	188.49	51	18532.6	16454	8.22	8.9	-2.78
proteasome (prosome, macropain) subunit, beta type, 9	NP_036840 Q6MGA6	2447	15	3	54.04	14	23343.6	21321	4.89	4.3	-2.48
		2438	14	3	50.07	16	23343.6	19832	4.89	4.3	-2.12
ornithine aminotransferase	NP_071966 P04182	1255	63	12	195.86	28	48332.9	51630	6.53	6.25	-2.79
		1304	72	15	261.81	43	48332.9	48894	6.53	6.5	-2.23
non-catalytic region of tyrosine kinase adaptor protein 1	NP_001100321 B2RZ33	1255	37	11	176.31	29	42876.7	51630	6.07	6.25	-2.79
		1304	9	5	80.29	14	42876.7	48894	6.07	6.5	-2.23
adenylosuccinate synthetase, non muscle	NP_001099445 -	1255	10	6	96.11	14	50085.4	51630	5.98	6.25	-2.79
		1304	4	4	57.85	12	50085.4	48894	5.98	6.5	-2.23
Aspartate aminotransferase, cytoplasmic (Transaminase A)	NP_036703 P13221	1500	36	11	168.02	29	46429	46303	6.73	7.5	-3.65
		1425	56	14	239.8	40	46429	46664	6.73	7.6	-2.15
voltage dependent anion channel (Vdac1)	NP_112643 Q9Z2L0	1922	12	4	71.46	15	32577.8	33921	8.3	8	-3.57
		1866	9	4	59.53	17	32577.8	34722	8.3	8.05	-3.07
voltage-dependent anion channel 2	NP_112644 P81155	1922	7	4	54.95	14	31746	33921	7.44	8	-3.57
		1925	12	5	76.83	21	31746	33921	7.44	8.1	-2.62
		1753	18	6	105.27	24	31746	38120	7.44	7.6	-2.16
hypertrophic agonist responsive protein B64, isoform CRA_c	NP_001094010 Q711G3	2028	49	10	158.99	48	28004.4	31139	5.64	5.25	-2.65
		2089	15	5	68.97	18	28004.4	28586	5.64	5.7	-2.84
phosphoglycerate mutase type B subunit	NP_445742 P25113	2116	95	13	243.66	63	28846.2	27926	7.07	7.15	-3.51
		2119	207	15	295.67	65	28846.2	27926	7.07	7.05	-3.24
		2102	41	7	126.74	37	28846.2	28809	7.07	7.3	-2.98
		2106	179	12	231.21	52	28846.2	28364	7.07	7.25	-2.73
phosphomannomutase 2	NP_001100443 B5DF46	2116	84	9	153.72	39	27708.9	27926	6.9	7.15	-3.51
		2102	37	10	165.77	44	27708.9	28809	6.9	7.3	-2.98
enoyl Coenzyme A hydratase, short chain, 1, mitochondrial	NP_511178 P14604	2116	6	3	53.88	16	31516.6	27926	8.4	7.15	-3.51
		2119	57	8	144.85	34	31516.6	27926	8.4	7.05	-3.24
		2106	83	10	176.71	38	31516.6	28364	8.4	7.25	-2.73
pyrroline-5-carboxylate reductase-like	NP_001011993 Q5PQJ6	2178	22	6	108.36	22	28878.7	26653	6.59	7.45	-2.44
		2142	35	5	89.21	18	28878.7	27495	6.59	7.6	-2.18
Ppib protein	NP_071981 P24368	2487	57	11	190.42	46	23802.7	17375	9.5	8.75	-2.76
		2485	32	9	154.3	43	23802.7	18635	9.5	8.8	-2.7

Ppib protein	NP_071981 P24368	2487	57	11	190.42	46	23802.7	17375	9.5	8.75	-2.76
		2485	32	9	154.3	43	23802.7	18635	9.5	8.8	-2.7
phosphoglycerate kinase 1	NP_445743 P16617	1364	89	19	341.2	57	44538.7	49276	8.02	7.25	-2.35
		1366	75	16	281.76	44	44538.7	49276	8.02	7.9	-3.38
		1379	21	6	111.69	14	44538.7	48515	8.02	8.05	-3.26
		1389	211	23	398.37	58	44538.7	48894	8.02	8.5	-4.47
		1390	201	22	361.81	48	44538.7	48894	8.02	8.6	-4.27
		1399	93	20	325.27	43	44538.7	48894	8.02	8.75	-5.66
		1400	106	20	344.16	52	44538.7	48894	8.02	8.9	-6.31
		1406	71	15	298.54	45	44538.7	48894	8.02	9.2	-3.26
		1409	119	22	400.43	61	44538.7	48894	8.02	9.05	-3.16
		1573	40	12	213.36	32	44538.7	43172	8.02	5.7	-3.05
		1285	370	29	522.86	76	44538.7	49661	8.02	8.5	-2.48
		1286	330	30	532.92	79	44538.7	49661	8.02	8.6	-2.75
		1290	26	10	146.36	23	44538.7	49661	8.02	8.7	-2.76
aldolase A, isoform CRA_e	NP_036627 P05065	1474	76	14	239.73	38	45086.5	47396	8.03	9.7	-3.97
		1480	63	9	158.5	20	45086.5	47396	8.03	9.5	-4.54
		1482	102	15	278.53	41	45086.5	47396	8.03	8.75	-3.34
		1483	140	17	310.68	50	45086.5	47396	8.03	9.1	-2.77
		1484	103	12	222.09	36	45086.5	47396	8.03	9.4	-4.43
		1489	112	13	238.66	38	45086.5	47396	8.03	8.6	-3.97
		1490	35	12	213.56	34	45086.5	47396	8.03	8.9	-4.57
		1286	52	11	196.58	32	45086.5	49661	8.03	8.6	-2.75
		1390	66	10	172	26	45086.5	47396	8.03	8.8	-2.05
similar to Pol(yrC)-binding protein 1 (predicted)	NP_001013241 Q6AYU5	1447	10	5	77.88	22	35512.7	47396	7.03	7.1	-3.03
		1425	15	5	80.5	20	35512.7	46664	7.03	7.6	-2.15
aldolase C	NP_036629 P09117	1500	8	4	62.08	12	39284	46303	6.67	7.5	-3.65
		1425	82	13	241.73	40	39284	46664	6.67	7.6	-2.15
Malate dehydrogenase 1, NAD (soluble)	NP_150238 O88989	1761	85	10	169.62	28	36484.3	38717	5.92	6.15	-2.41
		1771	44	10	139.48	30	36484.3	36952	5.92	6.35	-2.64
		1806	54	6	101.41	17	36484.3	35820	5.92	6.4	-4.06
guanine nucleotide binding protein, beta polypeptide 2-like 1	NP_570090 P63245	1921	66	12	204.85	41	35095	34186	7.6	7.9	-2.97
		1922	104	14	241.83	51	35095	33921	7.6	8	-3.57
		1925	84	13	221.74	43	35095	33921	7.6	8.1	-2.62
		1866	81	13	233.8	48	35095	34722	7.6	8.05	-3.07
		1870	82	12	206.44	45	35095	34722	7.6	8	-3.29
triosephosphate isomerase 1	NP_075211 P48500	2178	80	11	213.97	50	31011.7	26653	5.56	7.45	-2.44
		2142	70	13	239.12	55	31011.7	27495	5.56	7.6	-2.18
protease (prosome, macropain) 28 subunit, alpha	NP_058960 Q6P9V7	2028	31	9	144.51	37	28635.1	31139	5.63	5.25	-2.65
		2089	14	5	62.13	20	28635.1	28586	5.63	5.7	-2.84

Changes in protein expression in response to SM or HOCl-SM are summarized in ***Fig. 44 A*** and are presented as heat maps in which the values are expressed as $\log_2$ of fold regulation. Out of the 82 identified proteins we found 21 up- and 42 down-regulated after treatment of PC12 cells with SM. In contrast, incubation of cells with exogenously added HOCl-SM induced upregulation of 9 proteins and downregulation of 22 proteins. Out of these, a total of 12 proteins were identified to be coregulated by SM and HOCl-SM (2 up and 10 down; ***Fig. 44 A***).

A

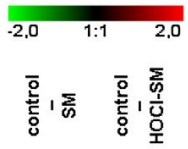

NP_001020804	heterogeneous nuclear ribonucleoprotein C (Hnrnpc)
NP_112643	voltage-dependent anion channel 1 (Vdac1)
NP_058747	superoxide dismutase 2, mitochondrial (Sod2)
NP_058865	peroxiredoxin 2 (Prdx2)
NP_058932	phosphatidylethanolamine binding protein 1 (Pebp1)
NP_113791	tyrosine 3-monooxygenase/tryptophan 5-monooxygenase activation protein, beta polypeptide (Ywhab)
NP_476455	peroxiredoxin 1 (Prdx1)
NP_001007603	glutathione S-transferase omega 1 (Gsto1)
NP_001100678	septin 11 (Sept11)
NP_063969	lectin, galactose binding, soluble 1 (Lgals1)
NP_058974	proteasome (prosome, macropain) subunit, alpha type 1 (Psma1)
NP_955404	eukaryotic translation initiation factor 4A1 (Eif4a1)
NP_695212	aldehyde dehydrogenase family 1, subfamily A3 (Aldh1a3)
NP_001005545	melanocyte proliferating gene 1 (Myg1)
NP_001017503	purine rich element binding protein B (Purb)
NP_001011910	leucine aminopeptidase 3 (Lap3)
NP_071797	acidic ribosomal phosphoprotein P0 (Arbp)
NP_001094276	similar to Fascin (LOC683788)
NP_114178	aldehyde dehydrogenase 3 family, member A1 (Aldh3a1)
NP_599161	cathepsin D (Ctsd)
NP_569084	dihydrofolate reductase (Dhfr)
NP_612557	expressed in non-metastatic cells 1 (Nme1)
NP_114175	calmodulin 1 (Calm1)
NP_058977	proteasome (prosome, macropain) subunit, alpha type 4 (Psma4)
NP_001004208	calcyclin binding protein (Cacybp)
NP_112248	adenylate kinase 2 (Ak2)
NP_476534	hydroxyacyl-Coenzyme A dehydrogenase (Hadh)
NP_114176	heat shock protein 1 (Hspb1)
NP_036840	proteosome (prosome, macropain) subunit, beta type 9 (Psmb9)
NP_001011993	pyrroline-5-carboxylate reductase-like (Pycrl)
NP_001099445	adenylosuccinate synthetase, non muscle (Adss)
NP_001100321	non-catalytic region of tyrosine kinase adaptor protein 1 (Nck1)
NP_071966	ornithine aminotransferase (Oat)
NP_112644	voltage-dependent anion channel 2 (Vdac2)
NP_001094010	isoamyl acetate-hydrolyzing esterase 1 homolog (Iah1)
NP_058960	proteasome (prosome, macropain) 28 subunit, alpha (Psme1)
NP_150238	malate dehydrogenase 1, NAD (soluble) (Mdh1)
NP_570090	guanine nucleotide binding protein (G protein), beta polypeptide 2 like 1 (Gnb2l1)
NP_036627	aldolase A (Aldoa)
NP_114020	lectin, galactose binding, soluble 3 (Lgals3)
NP_001032742	far upstream element (FUSE) binding protein 1 (Fubp1)
NP_001099339	replication factor C (activator 1) 4 (Rfc4)
NP_001037747	similar to methionine adenosyltransferase II, beta (MGC94725)
NP_001029242	tropomyosin 1, alpha (Tpm1)
NP_001011979	TAR DNA binding protein (Tardbp)
NP_037036	annexin A1 (Anxa1)
NP_036727	lactate dehydrogenase B (Ldhb)
NP_112620	heterogeneous nuclear ribonucleoprotein A/B (Hnrpab)
NP_803175	glutathione S-transferase, mu 2 (Gstm2)
NP_001099327	pyrroline-5-carboxylate reductase 1 (Pycr1)
NP_036686	enolase 1, alpha non-neuron (Eno1)
NP_001101745	procollagen-proline, 2-oxoglutarate 4-dioxygenase (proline 4-hydroxylase), alpha II polypeptide (P4ha2)
NP_072119	cathepsin B (Ctsb)
NP_037027	adenosine kinase (Adk)
NP_001004206	proliferation-associated 2G4 (Pa2g4)
NP_062085	actin, alpha 1, skeletal muscle (Acta1)
NP_612537	ERO1-like (S. cerevisiae) (Ero1l)
NP_445749	pyruvate kinase, muscle (Pkm2)
NP_742059	procollagen-proline, 2-oxoglutarate 4-dioxygenase (proline 4-hydroxylase), alpha 1 polypeptide (P4ha1)
NP_036652	catalase (Cat)
NP_112413	malate dehydrogenase 2, NAD (mitochondrial) (Mdh2)
NP_113999	transaldolase 1 (Taldo1)
NP_037130	prolyl 4-hydroxylase, beta polypeptide (P4hb)
NP_114179	dipeptidylpeptidase 7 (Dpp7)
NP_112402	vimentin (Vim)
NP_071980	calumenin (Calu)
NP_001098083	heterogeneous nuclear ribonucleoprotein A2/B1 (Hnrnpa2b1)
NP_062232	calponin 3, acidic (Cnn3)
NP_071794	calreticulin (Calr)
NP_001099891	tumor protein D52 (Tpd52)
NP_001029070	calumenin (Calu)
NP_058843	cofilin 1, non-muscle (Cfl1)
NP_071981	peptidylprolyl isomerase B (Ppib)
NP_001013241	poly(rC) binding protein 2 (Pcbp2)
NP_036629	aldolase C (Aldoc)
NP_511178	enoyl Coenzyme A hydratase, short chain, 1, mitochondrial (Echs1)
NP_445742	phosphoglycerate mutase 1 (Pgam1)
NP_036703	glutamate oxaloacetate transaminase 1, soluble (Got1)
NP_001100443	phosphomannomutase 2 (Pmm2)
NP_075211	triosephosphate isomerase 1 (Tpi1)
NP_058721	lactate dehydrogenase A (Ldha)

B

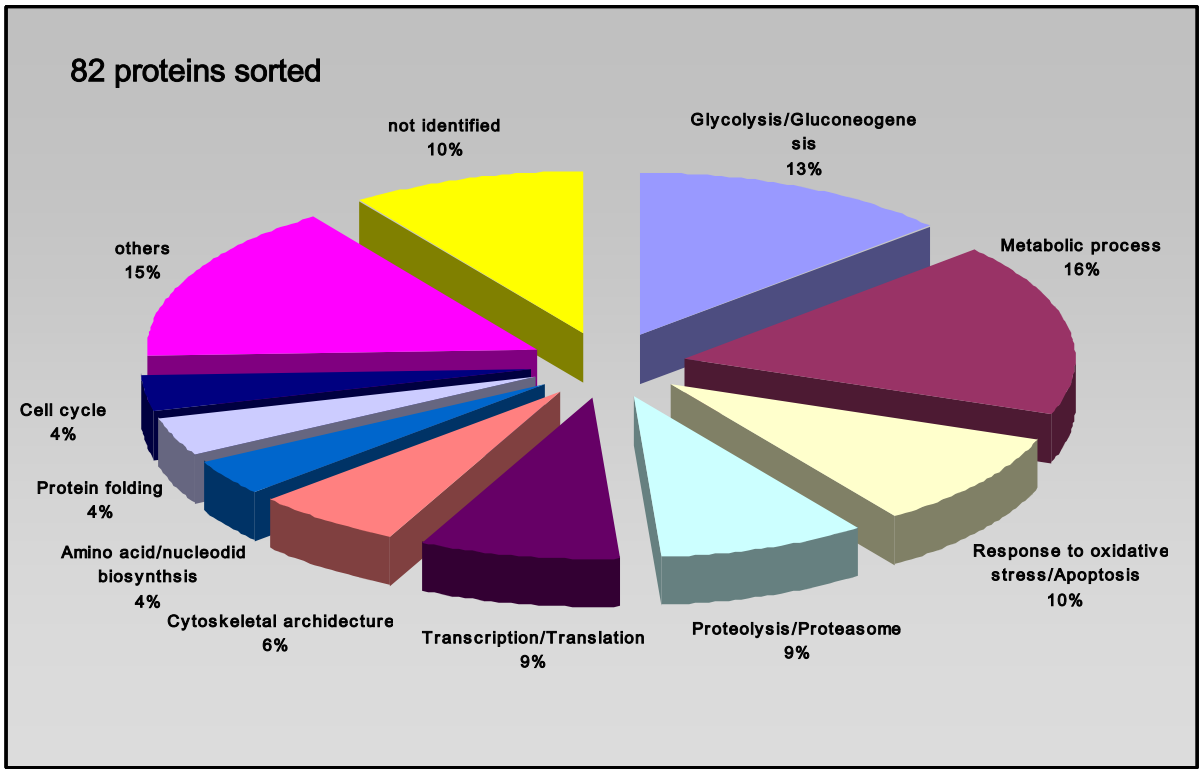

C

GO term	GO term in dataset
Upregulation ***(21 dataset entries)***	
response to oxidative stress/apoptosis	6
transcription/translation	3
proteolysis	2
Downregulation ***(42 dataset entries)***	
metabolism	9
glycolysis/gluconeogenesis	8
cytoskeletal architecture	4
transcription/translation	4
protein folding	3

GO term	GO term in dataset
Upregulation ***(9 dataset entries)***	
metabolic process	4
response to oxidative stress/apoptosis	2
Downregulation ***(22 dataset entries)***	
glycolysis/gluconeogenesis	6
metabolism	6
proteolysis	3
cell migration	2

Figure 44: Changes in protein expression in response to SM and HOCl-SM (3). Following 2D-DIGE 2-fold differentially expressed proteins were identified using the DeCyder software, manually picked, digested, and analyzed by nanoLC-ESI-MS as described in 'Materials and Methods'. MS data were analyzed by searching the NCBI database using SpectrumMill version 2.7, and $\log_2$ expression patterns of proteins (control vs. SM and control vs. HOCl-SM) identified in two or three individual gels were calculated and averaged.

(***A***) Combined data visualized as heat maps.

(***B***) Differentially expressed proteins grouped according to their biological process.

(***C***) Most representative up- and down-regulated biological processes including the number of identified proteins in course of SM (left panel) and HOCl-SM treatment (right panel).

The identified differentially expressed proteins were further grouped in their functional classes according to their *Gene Ontology* (GO) terms and sorted according to the biological process in which those are involved using the online platform ***g:Profiler*** (http://biit.cs.ut.ee/gprofiler/). ***Fig. 44 B*** shows that many of the differentially expressed proteins are involved energy (glycolysis and gluconeogenesis) and other metabolic processes (29% of differentially expressed proteins) as well as in response to oxidative stress (10% of differentially expressed proteins). Other representative biological processes are proteolysis, transcription and translation, and architecture of the cytoskeleton which contain 9%, 9%, and 6% of identified proteins, respectively. In case of the 21 proteins that are upregulated in response to SM, the main part is involved in response to oxidative stress (29% corresponding to 6 proteins; ***Fig 44 D***). In case of downregulated proteins 21% of proteins (9 proteins out of 42 identified) cover metabolic processes and 19% (8 proteins) take part in glycolysis and gluconeogenisis. Interestingly, most of the downregulated proteins (n = 22) in response to HOCl-SM are also involved in energy metabolic processes (27 % corresponding to 6 proteins). Therefore, it is not surprising that the main part of co-downregulated proteins also belong to this biological process. Upregulated proteins as a function of HOCl-SM treatment correspond to metabolic processes and response to oxidative stress (44% and 22%, respectively).

6.2. Pathway analysis of differentially expressed proteins in PC12 cells course of treatment with SM or HOCL-SM

In order to examine potential relationship between proteins that show differences in their expression pattern after SM or HOCl-SM treatment of PC12 cells, hypothetical protein networks covering these proteins were generated using a free trial version of ***Ingenuity Pathway Analysis*** (IPA) (www.ingenuity.com; https://analysis.ingenuity.com). IPA builds such hypothetical networks by comparing the proteins with each other followed by including not identified proteins from the database needed to complete meaningful biological networks. These input proteins that map to the networks are called focus proteins. Network generation ranked by score is optimized for inclusion of as many proteins from the input expression profile as possible and aims for highly interrelated networks, which are likely to represent significant biological functions.

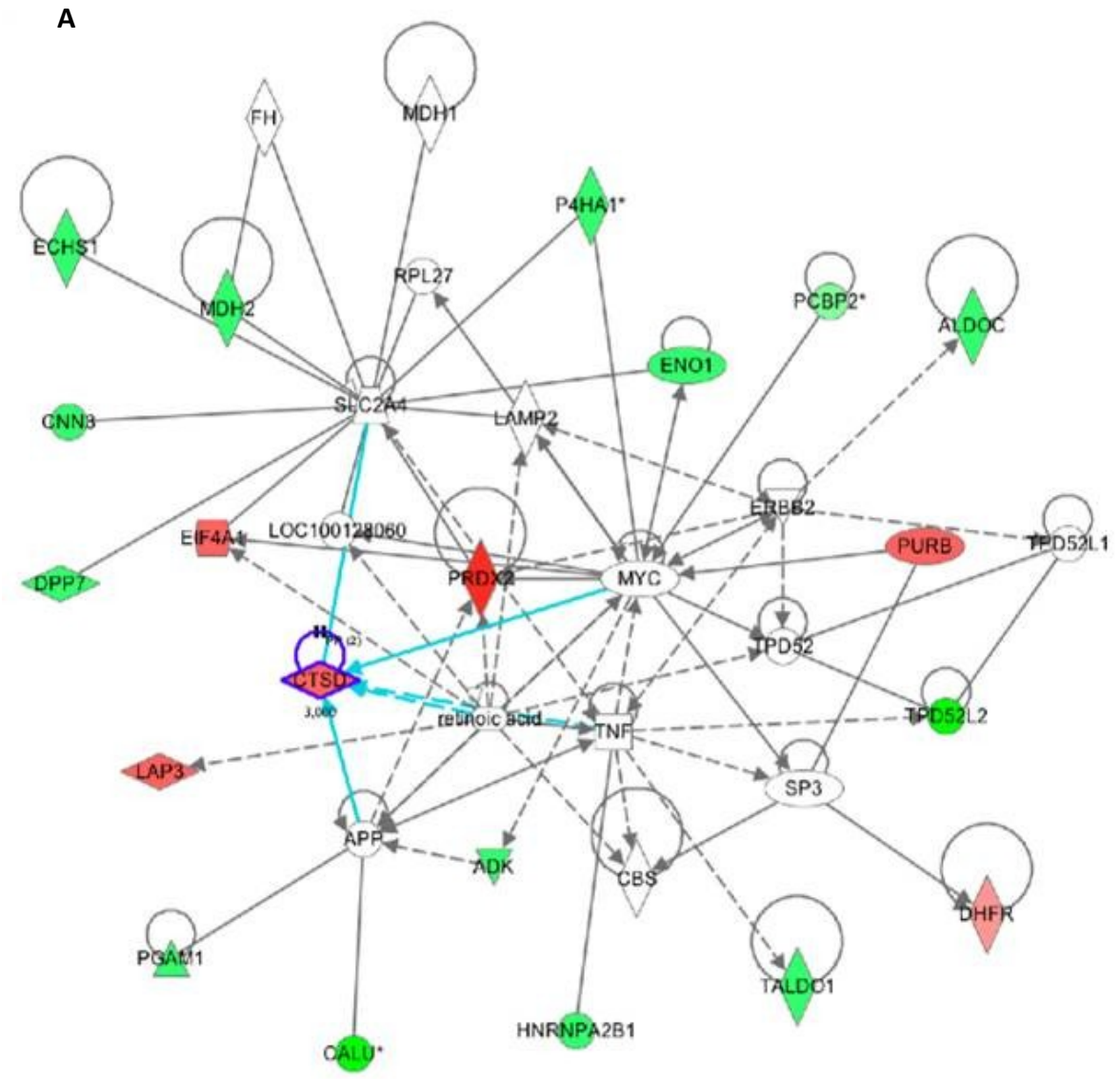

ADK, Adenosine kinase; ALDOC, Fructose-bisphosphate aldolase C (brain-type aldolase); APP, Amyloid beta A4 protein; CALU, Calumenin; CBS, Cystathionine beta-synthase; CNN3, Calponin-3; CTSD, Cathepsin D; DHFR, Dihydrofolate reductase; DPP7, Dipeptidylpeptidase 2; ECHS1, Enoyl-CoA hydratase, mitochondrial; EIF4A1, Eukaryotic initiation factor 4A-I; ENO1, Alpha-enolase; ERBB2, Receptor tyrosine-protein kinase erbB-2; HNRNPA2B1, Heterogeneous nuclear ribonucleoproteins A2/B1; LAMP2; Lysosomeassociated membrane glycoprotein 2; LAP3, Cytosol aminopeptidase; MDH1, Malate dehydrogenase, cytoplasmic; MDH2, Malate dehydrogenase, mitochondrial; MYC, N-myc proto-oncogene protein; P4HA1, Prolyl 4-hydroxylase subunit alpha-1 PCBP2, PCBP2 protein; PGAM1, Phosphoglycerate mutase 1; PRDX2, Peroxiredoxin-2; PURB, Transcriptional activator protein Pur-beta; RPL27, 60S ribosomal protein L27; SLC2A4, Solute carrier family 2, facilitated glucose transporter member 4 (Glucose transporter type 4, insulin-responsive); SP3, Transcription factor Sp3; TALDO1, Transaldolase; TNF, Tumor necrosis factor; TPD52, Tumor protein D52; TPD52L1, Tumor protein D53 (Tumor protein D52-like 1)

B

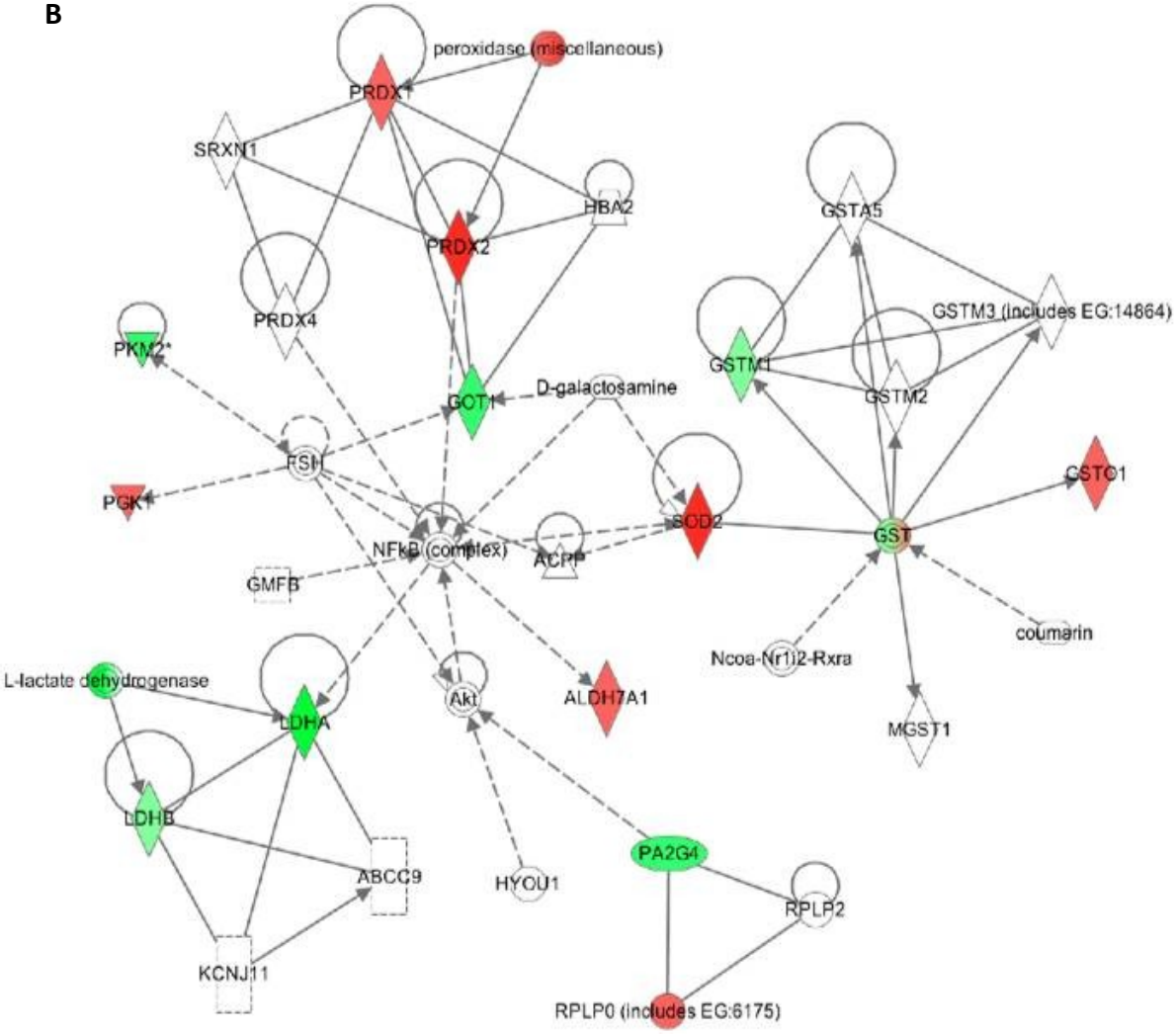

ABCC9, ATP-binding cassette transporter sub-family C member 9 (Sulfonylurea receptor 2); ACPP, Acid phosphatases; ALDH7A1, Alpha-aminoadipic semialdehyde dehydrogenase; Akt, RAC-alpha serine/threonine-protein kinase (AKT, protein kinase B): FSH, Folliclestimulating hormone; GMFB, GMFB protein (Glia maturation factor, beta); GOT1, Aspartate aminotransferase, cytoplasmic; GST, Glutathione S-transferase; GSTA5, Glutathione S-transferase A5; GSTM1, Glutathione S-transferase Mu 1; GSTM2, Glutathione S-transferase Mu 2; GSTM3, Glutathione S-transferase Mu 3; GSTO1, Glutathione S-transferase omega-1; HYOU1, Hypoxia up-regulated protein 1; KCNJ11, ATP-sensitive inward rectifier potassium channel 11; LDHA, L-lactate dehydrogenase A chain; LDHB, L-lactate dehydrogenase B chain; MGST1, Microsomal glutathione S-transferase 1; Ncoa-Nr112-Rxra, Nuclear receptor coactivator-Retinoic acid receptor RXR-alpha NFKB, Nuclear factor NF-kappa-B complex; PA2G4, Proliferation-associated protein 2G4; PGK2, Phosphoglycerate kinase 2; PKM2, Pyruvate kinase isozymes M1/M2; PRDX1, Peroxiredoxin-1 PRDX2, Peroxiredoxin-2; PRDX4, Peroxiredoxin-4; RPLP0, 60S acidic ribosomal protein P0; RPLP2, 60S acidic ribosomal protein P2; SRXN1, Sulfiredoxin-1

C

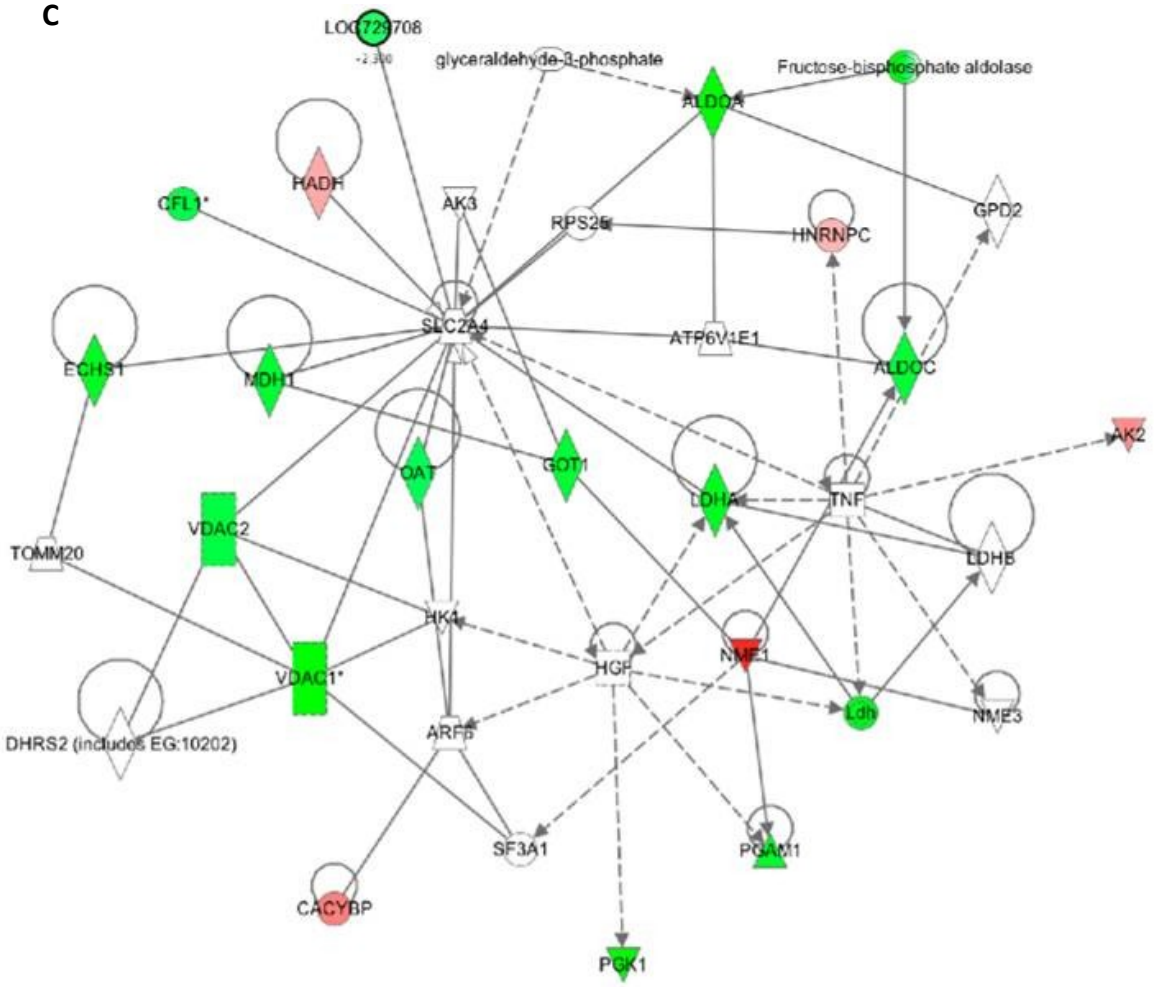

AK2, Adenylate kinase 2, mitochondrial; AK3, GTP:AMP phosphotransferase mitochondrial; ALDOA, Fructose-bisphosphate aldolase A; ALDOC, Fructose-bisphosphate aldolase C; ARF6, ADP-ribosylation factor 6; ATP6V1E1, V-type proton ATPase subunit E 1; CACYBP, Calcyclin-binding protein; CFL1, Cofilin-1; DHRS2, Dehydrogenase/reductase member 2; ECHS1, Enoyl-CoA hydratase, mitochondrial; GOT1, Aspartate aminotransferase, cytoplasmic; GPD2, Glycerol-3-phosphate dehydrogenase, mitochondrial; HADH, 3-hydroxyacyl-CoA dehydrogenase type-2; HGF, Hepatocyte growth factor; HK1, Hexokinase-1; HNRNPC, Heterogeneous nuclear ribonucleoproteins C1/C2; Ldh, L-lactate dehydrogenase; LDHA, L-lactate dehydrogenase A chain LDHB, L-lactate dehydrogenase B chain; LOC729708, PREDICTED: similar to Triosephosphate isomerase (TIM) (Triose-phosphate isomerase) isoform 1; MDH1, Malate dehydrogenase 1, mitochondrial; NME3, Nucleoside diphosphate kinase 3; NME1, Nucleoside diphosphate kinase A OAT, Ornithine aminotransferase; PGAM1, Phosphoglycerate mutase 1; PGK1, Phosphoglycerate kinase 1; RPS25, 40S ribosomal protein S25; SF3A1, Splicing factor 3 subunit 1; SLC2A4, Solute carrier family 2, facilitated glucose transporter member 4 (Glucose transporter type 4, insulin-responsive); TNF, Tumor necrosis factor; TOMM20, Mitochondrial import receptor subunit TOM20 homolog; VDAC1, Voltage-dependent anionselective channel protein 1; VDAC2, Voltage-dependent anion-selective channel protein 2

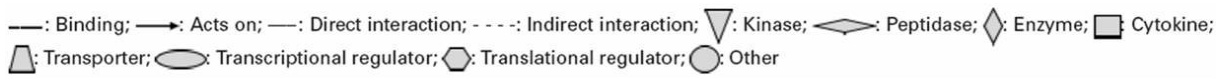

Figure 45: IPA based protein networks of differentially regulated proteins in SM and HOCl-SM-treated PC12 cells. Networks of interacting proteins were generated through Ingenuity Pathway Analysis. Proteins identified (displayed as abbreviated gene names) were connected with interaction partners known from the literature and information stored in the Ingenuity Pathways Knowledge Base. Protein names are listed right below each respective figure. Upregulated proteins are shown in red, downregulated in green. Solid lines represent direct interaction and dashed lines indirect interaction. Meanings of other symbols are shown above. Most meaningful networks covering the highest score are shown (two networks generated from protein regulation in response to SM (***A*** and ***B***) and one network generated in response to HOCl-SM (***C***)).

(***A***) Network A contained 15 identified proteins (out of 34 molecules present in the network) identified proteins and involved top functions in Energy Production, Molecular Transport, and Nucleic Acid Metabolism (score = 44)

(***B***) Network B contained 16 identified proteins (out of 35 molecules present in the network) and involved top functions in Small Molecule Biochemistry, Molecular Transport, and Free Radical Scavenging (score = 26)

(***C***) Network C contained 21 identified proteins (out of 35 molecules present in the network) and involved top functions in Carbohydrate Metabolism, Energy Production, and Molecular Transport (score = 48)

Figure 45 A and ***B*** show the 2 pathways that reached the highest scores during IPA of proteins regulated in response to PC12 cell treatment with SM. The highest score of 44 (indicating that there is a chance of $1:10^{44}$ of another randomly occurring network containing the same numbers of focus genes) was obtained for the pathway "Energy Production, Molecular Transport, and Nucleic Acid Metabolism" that mapped 20 (out of 35) proteins identified to be differentially expressed after SM treatment (***Fig. 45 A***). In this network SLC2A4 is a major hub and we have identified eight focus genes (ECSH1, MDH2, CNN3, EIF4A1, PRDX2, ENO1, and ALDOC) in the immediate neighborhood of SLC2A4, which is identical to insulin-sensitive GLUT4. This network was followed by the pathway "Small Molecule Biochemistry, Molecular Transport, Free Radical Scavenging" with a score of 26 (16 differentially expressed proteins out of 34; ***Fig. 45 B***).

Within the latter network, several upregulated proteins are products of genes that are under the control of Nrf2. Among these are PRDX1 and PRDX2, SOD, and GSTO1 conferring cellular protection against oxidative damage. Hence, this might be a reasonable explanation for the absence of intracellular ROS formation in PC12 cells incubated in the presence of SM as well as for cell survival of these cells in course of SM treatment.

For HOCl-SM the highest score was obtained for "Carbohydrate Metabolism, Energy Production, Molecular Transport" (score = 48; ***Fig. 45 C***), followed by "Cell-Mediated

Immune Response, Cellular Growth and Proliferation, Hematological System Development and Function" (score = 15; data not shown). Also in this network SLC2A4 (insulin-sensitive GLUT4) is a central hub, though not identified during our proteomic analyses. However, out of the total 35 interaction partners in this network 20 focus genes were identified in our proteome approach. Some of them are direct interactors of GLUT4 (ECHS1, HADH, MDH, VDAC 1 and 2, OAT, AAT, and ALDOA). Of the regulated proteins within this network five (HADH, CACYBP, HNRNPC, AK2, and NME1) were upregulated while all the other enzymes/transporters related to glycolysis (e. g. PGK1, ALDOA, ALDOC, MDH1, LDHA, PGAM1, and TPI1) energy production, and molecular transport were downregulated, clearly indicating severe interference of HOCl-SM with cellular energy homeostasis (this is also observed to a lesser extent in SM-treated PC12 cells). Such a cellular status of energy deprivation is as a typical hallmark in many neurodegenerative disorders (Hoyer et al., 2005).

6.3. SM and HOCl-SM induce alterations of the PC12 actin/tubulin cytoskeleton

A substantial proportion (6%; ***Fig. 44 C***) of identified and differentially expressed proteins is involved in assembly, organization, and maintenance of the actin/tubulin cytoskeleton suggesting changes in PC12 cell morphology and motility as a response to SM or its chlorohydrins. Proteins that regulate the maintenance and dynamics of the cytoskeleton (e. g. actin, vimentin, cofilin) were shown to be generally downregulated in SM-treated cells. These observations strongly suggest that SM and probably also HOCl-SM induce alterations in the cytoskeletal architecture, resulting in altered cell motility and/or altered cell morphology.

To obtain experimental evidence we performed immunofluorescence studies and Western blot analysis in SM- or HOCl-SM-treated PC12 cells (24 h incubation). For immunofluorescence the cells were fixed in formaldehyde and stained for their actin- (using rhodamine-labeled phalloidin) and tubulin (anti-tubulin antibody and Cy5-labeled secondary antibody) cytoskeleton.

Results obtained from immunofluorescence studies (***Figure 46 A***) revealed that SM and HOCl-SM-treated PC12 cells showed differences in organization of their cytoskeleton and displayed significant morphological alterations when compared to control cells. SM-stimulated cells generally exhibited a more condensed cell shape (***Fig. 46 A*** (***b***)).

With respect to their actin cytoskeleton, SM and HOCl-SM-treated cells displayed distinct alterations compared to control cells (i. e. less intracellular actin fibres). In addition the formation of a so called cortical cytoskeleton was observed, especially in HOCl-SM-treated cells (***Fig. 46 A*** (***c*** and ***d***)) which might be an indication for lower cell motility due to HOCl-SM treatment.

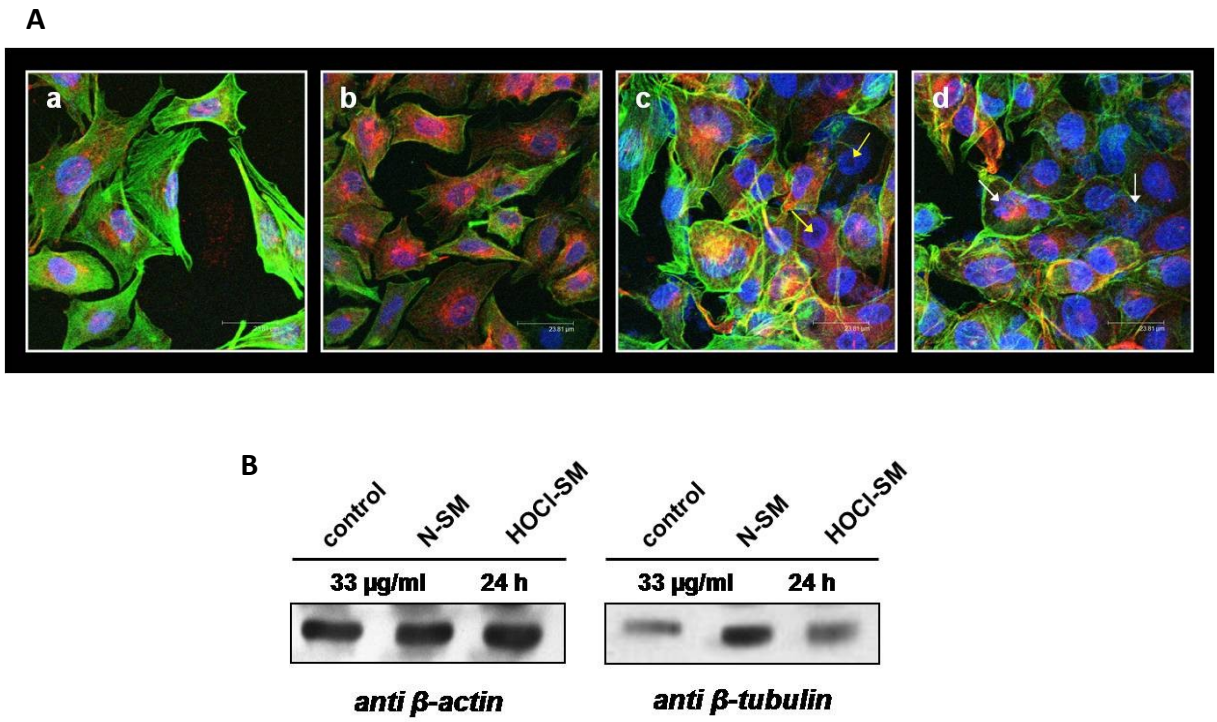

Figure 46: Alterations of the PC12 cytoskeleton as response to SM or HOCl-SM treatment. PC12 cells were either grown on collagen-coated chamber slides or 6-well plates, incubated in the absence (***a***) or presence of SM (213 µM, ***b***) or HOCl-SM (66 µM ***c***; 99 µM ***d***) at the indicated concentrations for 24 h, and subsequently subjected to immunofluorescence (***A***) or Western blot analysis (***B***), respectively, as described in 'Materials and Methods'.
(***A***) PC12 cells treated with or without SM or HOCl-SM were washed with PBS, fixed in 3.7% formaldehyde solution in PBS, and were double-stained with Alexa Fluor 488-labeled phalloidin (stains actin cytoskeleton; green) and with an anti-β-tubulin antibody and a Cy5-labeled secondary antibody (red). Nuclei were counterstained with DAPI.
(***B***) After incubation of PC12 cells in the absence or presence of SM or HOCl-SM, proteins were scraped in RIPA buffer and protein lysates (40 µg/lane) were run on 10% SDS gels and transferred onto PVDF membranes for subsequent detection using anti-β-actin and anti-β-tubulin primary antibody.

Western blot analyses revealed that the overall cellular actin content was not changed in response to SM or HOCl-SM (***Fig. 46 B***). Concerning the microtubular network, immunofluorescence results displayed upregulation of tubulin in SM-treated cells. This upregulation as a consequence of incubation with SM could be also detected during Western blot analysis (***Fig. 46 A*** and ***B***). Comparing control and HOCl-SM-treated PC12 cells no significant differences in intracellular tubulin organization or in tubulin levels was observed. However, similar to SM stimulation HOCl-SM incubated PC12 cells tended to be smaller in size compared to untreated control cells. In addition these cells exhibited a rounder cell shape (presumably caused by the establishment of the cortical actin cytoskeleton) and preferred to grow together in bigger clumps compared to untreated and SM-treated cells.

In addition it could be shown that a certain number cells already underwent the apoptotic cascade when incubated at concentrations of 66 and 99 µM HOCl-SM. Typical hallmarks of PCD cell death observed here were nuclear pore formation, an early marker in apoptosis (***Fig. 46 A*** (***c***); yellow arrows) and fragmentation of PC12 nuclei (***Fig. 46 A*** (***d***); white arrows). Taken together these experimental data strengthen results obtained from the proteomic approach by clearly indicating profound alterations in organization of the PC12 cell actin/tubulin cytoskeleton in course of SM/HOCl-SM treatment.

IV. DISCUSSION

1. SL METABOLISM IN CATH.A CELLS

SL are an important class of lipids in eukaryotic cells. Beside their ability to influence membrane structure and dynamics they are central regulators of endocytic, sorting, and transport processes. Many SL are potent signaling molecules which regulate cell homeostasis. Cer, S1P, and Sph, which act as lipid second messengers determine cell proliferation, differentiation, senescence, growth arrest, and apoptosis. Therefore, imbalances in intracellular SL levels are associated with a number of pathophysiological conditions. Mutations in genes that contribute to hydrolysis of complex SL lead to accumulation of these lipids within the cell and subsequently to SL storage diseases. Elevated levels of Cer can render cells apoptotic which accounts for cell death in many diseases. In brain, where SL are highly enriched dysregulated Cer generation was shown to account for neuronal loss in neurodegenerative disorders (France-Lanord et al., 1997; Jana and Pahan, 2004; Jana and Pahan, 2010b) and are, therefore, implicated in disease progression. Among the diverse class of SL SM is of special interest as it plays a crucial role in the generation of bioactive lipid second messengers. SM represents a precursor for Cer synthesis, which is the branching point for generation of other signaling lipids or complex SL. Therefore, changes in the cellular SM pool are accompanied by altered concentrations of other SL species which strongly depend on the kinetics of the involved enzymes.

Cer homeostasis is a potential therapeutic target in neurodegenerative disorders. Therefore it is substantial to understand mechanisms that govern SL turnover in neuronal cells. In the first part of this thesis I have investigated SM and Cer uptake and intracellular trafficking in CATH.a cells by pharmacologically and biophysically interfering with homeostatic pathways. Fluorescently-labeled SM and Cer analogues were used in these studies.

Results obtained during the first part of my thesis revealed efficient SM uptake and metabolism in CATH.a cells. Due to the facts that short-chain SL are present in mammalian cells and that metabolic enzymes exhibit similar substrate specificity for fluorescent SL

analogues compared to radioactively-labeled lipids, BODIPY- and PYRENE-labeled SM/Cer were used for these experiments (Karasawa et al., 1999; Loidl et al., 2002). Results obtained from immunofluorescence analyses demonstrate insertion of BODIPY-SM into the PM of CATH.a cells at 4°C. The fluorescent lipid was subject to rapid endocytosis after chasing the cells at 37°C. First staining was observed in punctuated intracellular structures, which presumably represent early and/or recycling endosomes. This parallels previous studies in which fluorescently-labeled SM were visible in these compartments after a short incubation period at 37°C (Koivusalo et al., 2007; Koval and Pagano, 1989; Puri et al., 2001). At later time periods, fluorescence was mainly found at the PM and around the perimeter of the nucleus, which was identified as the Golgi apparatus in colocalization experiments. Quantitative analysis of the intracellular SM content revealed that cell-associated BODIPY-SM is localized up to 65-85% to the extracellular leaflet of the PM. Extensive Golgi staining is likely due to accumulation of BODIPY-SM-derived BODIPY-Cer in this compartment as this fluorescent lipid exhibits high affinity for the Golgi (Babia et al., 2001). BODIPY-SM localization to the Golgi might provide only a minor contribution to the intensive staining. Golgi staining was observed after a 5 min chase indicating that BODIPY-SM hydrolysis might partially occur at the PM. nSMase is expressed at comparable mRNA levels in all murine tissues (except spleen) but high enzymatic activity is observed only in the brain (Tomiuk et al., 1998). As nSMase is believed to be PM-associated this enzyme might contribute to SM degradation at the PM. However, as a *bona-fide* enzyme, nSMase activation normally depends on various stimuli (e. g. TNFα, IF-1β, nerve growth factor (NGF), interferon γ) leading to cell death, differentiation, or inflammation (Luberto et al., 2002; Nikolova-Karakashian et al., 2008; Tepper et al., 2000). Therefore, the question remains if incubation with SM is sufficient to activate the membrane-bound enzyme since overexpression of nSMase in HEK cells did not alter rates of SM hydrolysis (Tomiuk et al., 1998). As transport of BODIPY-SM to intracellular compartments does not occur at low temperatures, I suggest that the contribution of lysosomal aSMase to BODIPY-SM hydrolysis should play a minor role in SM degradation. This is supported by our colocalization experiments where BODIPY-SM was almost undetectable in the lysosomal compartment. However, recent studies identified trafficking of lysosomal aSMase to the outer leaflet of the PM in response to a variety of stimuli (e. g. UV radiation, FasL/CD95, Ca^{2+} entry after cell wounding; (Charruyer et al., 2005; Tam et al., 2010; Zeidan and Hannun, 2007)).

Although it is not entirely clear whether translocation of aSMase to the PM is a regulated process or if the PM is just a second cellular compartment where aSMase is located under physiological conditions it is plausible that PM-localized aSMase contributes to BODIPY-SM hydrolysis. In addition sSMase was suggested to be involved in SM metabolism at the extracellular leaflet of the PM (Milhas et al., 2010). The activity of this Zn^{2+}-dependent enzyme was not assessed in our studies.

When CATH.a cells were treated with the lysosomotropic compound desipramine a concentration-dependent decrease in aSMase activity was observed. However, BODIPY-SM uptake in the presence of this inhibitor was only slightly affected. A decrease in Cer generation was most pronounced following a 1 h chase at 37°C which might be an indication that aSMase might contribute to BODIPY-SM hydrolysis at the PM. In addition part of BODIPY-SM could undergo hydrolysis in lysosomes. However, the possibility that other SMases contribute to BODIPY-SM hydrolysis in CATH.a cells cannot be excluded on basis of the present findings. RNAi of nSMase experiments will help us to examine if this enzyme or another aSMase is involved in this process. If BODIPY-SM hydrolysis also occurs in intracellular compartments apart from lysosomes remains to be elucidated. Studies in PC12 cells demonstrated localization of nSMase to the Golgi (Hofmann et al., 2000) which supports the idea that part of BODIPY-SM is hydrolyzed at this organelle. Additionally, recent studies have shown that nSMase can translocate from the PM or the Golgi to early endosomes. These findings implicate that nSMase activity could contribute to BODIPY-SM hydrolysis in several compartments analyzed during the present study (Milhas and Hannun, unpublished data).

In addition to the Golgi and lysosomes we have also observed accumulation of BODIPY-tagged lipids in the ER. As mentioned above, BODIPY-SM-derived BODIPY-Cer rather than the *de novo* synthesized PL might account for ER staining because under physiological conditions SM is only present in minor amounts in the ER. During metabolism of BODIPY-SM CATH.a cells synthesized an unidentified polar BODIPY-labeled lipid species that might represent GlcCer, GalCer, or a more complex GSL. GalCer and, unlike to other cells, GlcCer synthesis in neurons takes place in the ER (van Echten and Sandhoff, 1989). These data suggest that BODIPY-Cer generated *via* SMase activity reaches the ER, which is the site for GlcCer and/or GalCer synthesis.

To elucidate uptake mechanisms for BODIPY-SM in CATH.a cells studies with specific inhibitors of clathrin- and caveolae-mediated endocytosis were performed. Although K^+ depletion, which inhibits formation of clathrin-coated pits, slightly reduced BODIPY-SM uptake, pronounced inhibition of BODIPY-SM uptake by antagonists of the caveolar pathway strongly suggests that this is quantitatively the more important route. Cytoskeletal alterations due to K^+ depletion might account for decreased uptake of the fluorescent SM analogue (Altankov and Grinnell, 1993; Rajasekaran et al., 2001). Unchanched intracellular BODIPY-SM levels after CP treatment give this theory further support. Additionally, other studies that examined uptake mechanisms of SL in various cell lines revealed cavolea-mediated endocytosis of complex GSL (e. g. LacCer, GalCer, globoside; (Sharma et al., 2004; Sharma et al., 2003; Singh et al., 2003)).

In contrast, studies that investigated uptake of fluorescently-labeled SM analogues are quite controversial. Whereas some groups suggested SM uptake in clathrin-coated pits and caveolae (Puri et al., 2001), other studies highlight the role of SM stereochemistry in cellular uptake. These studies showed that BODIPY-labeled naturally occurring D-*erythro*-SM (used in our studies) is internalized *via* a NY-sensitive, CP-insensitive mechanism in human skin fibroblasts, whereas the stereoisomer L-*threo*-SM is taken up *via* a CP-sensitive mechanism, similar to what was observed with stereoisomers of BODIPY-labeled LacCer (Marks et al., 2008; Singh et al., 2006). Moreover, we could demonstrate that BODIPY-SM trafficking to the Golgi is a microtubule dependent process. When we treated cells with nocodazole we could indeed identify uptake of the tracer into the cell cytoplasm, but Golgi targeting was hindered. Similar results were obtained by another group after studying uptake and trafficking of LacCer and GM_1 globoside in human skin fibroblasts (Choudhury et al., 2002). In summary, our studies suggest that caveolar endocytosis is mainly responsible for uptake of BODIPY-SM in CATH.a cells. However, it is noteworthy, that we have observed that a significant proportion of BODIPY-SM was already hydrolyzed to Cer. Thus, in fluorescence microscopy, it would be important to use a fluorescent, metabolically stable SM analogue in order to rule out labeling of intracellular compartments with SM-derived metabolites. Therefore, we synthesized a non-degradable FITC-labeled SM analogue according to (Darroch et al., 2005) which will be used for endocytosis inhibitor experiments in future studies.

As mentioned above, uptake of BODIPY-SM is a rapid process. HPLC analysis after continuous labeling of CATH.a cell with either BODIPY-SM or BODIPY-Cer revealed that BODIPY-SM uptake exhibited faster kinetics compared to BODIPY-Cer. As both molecules contain a C5 FA acyl residue and the same fluorophore, BODIPY-Cer appears to be less effectively inserted into the PM. This might be explained by its higher hydrophobicity due to the lack of the PC headgroup compared to SM. Some studies reported that BODIPY-labeled SM does not reflect properties of their natural counterparts as they physically change the property of the attached FA acyl chain and, therefore, do not partition into ordered domains of membrane models (Kuerschner et al., 2005; van Meer and Liskamp, 2005). Since PYRENE-labeled lipids physically better mimic their natural counterparts, steady-state experiments were also performed with PYRENE-labeled SM. These results revealed significant slower uptake kinetics of this fluorescent lipid in CATH.a cells. According to what was observed during steady-state labeling with BODIPY-Cer the higher degree in hydrophobicity of the PYRENE-SM might account for a less efficient incorporation into the PM. Additionally, approx. 60% of BODIPY-SM were converted to Cer after 24 h incubation, whereas only 20% of PYRENE-SM were found hydrolyzed at that time. This indicates that more hydrophilic SM-analogues might display better substrates for SMases in CATH.a cells. Considering that fluorescently-tagged Cer can undergo spontaneous transbilayer movement and can gain access to cellular compartments by passive diffusion even at low temperatures (Kok et al., 1995; Koval and Pagano, 1989) rapid SM hydrolysis might additionally account for increased cell-associated fluorescence in CATH.a cells labeled with BODIPY fluorophores. In other cell lines (e. g. HaCaT keratinocytes, human smooth muscle cells) it was demonstrated that fluorescently-labeled SM analogues have similar SMase affinity as compared to their radioactive derivates, indicating that the fluorophore has relatively little effect on substrate properties (Loidl et al., 2002; Wanner et al., 2004).

Pulse-chase studies confirmed results obtained during steady-state labeling with BODIPY-SL. We could demonstrate that BODIPY-SM uptake and metabolism of the tracer occurs more rapidly compared to BODIPY-Cer. This was confirmed by the presence of higher BODIPY-Cer concentrations in the cellular supernatant as compared to BODIPY-SM during pulse-chase studies at 4°C. Interestingly, a significant amount of BODIPY-SM and BODIPY-Cer was already metabolized after pulsing the cells at 4°C. This indicates that

SMase and SMS are enzymatically active even at low temperatures, which was also suggested previously (Andrieu et al., 1995; Kok et al., 1995).

Probing of the PM and intracellular SM pool with exogenously added DF-BSA revealed that BODIPY-SM is fully accessible to BE. Therefore, it can be assumed that BODIPY-SM is synthesized from BODIPY-Cer, however, the lipid is neither able to reach the cytoplasm nor the inner leaflet of the PM at low temperatures. These findings indicate that SM endocytosis is an energy-dependent process that cannot occur at low temperatures. In contrast Cer is able to reach intracellular compartments by diffusion at low temperatures. BE of PM-associated BODIPY-SM directly after pulse-labeling or after 30 min incubation at 4°C demonstrated that less than 1% of BODIPY-SM entered the cells. SM synthesis was previously described to proceed at the *cis*- or *trans*-Golgi compartments, strongly depending on the cell line under investigation (Sadeghlar et al., 2000). However, recent studies demonstrated SMS2 activity at the PM (Huitema et al., 2004; Subathra et al., 2011; Tani and Kuge, 2009) which might account for BODIPY-SM generation at low temperatures in our studies.

Turnover of BODIPY-labeled SL in CATH.a cells revealed that SMase activity exhibits significantly faster reaction kinetics than SMS. These findings are supported by studies that showed rapid NBD-SM hydrolysis in neurons but slow conversion of NBD-Cer to NBD-SM (Kilkus et al., 2008). In contrast other groups report higher BODIPY-Cer turnover rates compared to BODIPY-SM hydrolysis (Wanner et al., 2004). However, SM/Cer turnover was identified to be strongly dependent on the respective cell line as oligodendrocytes, in contrast to neurons, show remarkably preference for SM-synthesis (Kilkus et al., 2008).

As mentioned above, BODIPY-SM and BODIPY-Cer turnover was accompanied by synthesis of a yet unidentified polar BODIPY-SM species. Previous studies showed that BODIPY-SM is not interconverted to other lipid species (e. g. PL) after cellular uptake (Wanner et al., 2004). Results of our studies demonstrated rapid hydrolysis of BODIPY-SM to BODIPY-Cer, which reached a plateau after approx. 2 h. However, hydrolysis of SM did not stop at this time but proceeded for 24 h. Analysis of the conversion profiles of BODIPY-SM revealed that after 2 h of incubation with the tracer, cells started to synthesize the polar BODIPY-labeled SL species. This was accompanied by exocytosis to the cellular supernatant as this lipid was not identified intracellularly after HPLC analysis.

Comparable observations were made after CATH.a labeling with BODIPY-Cer. Conversion rates revealed rapid SM synthesis, though less pronounced than BODIPY-SM hydrolysis by SMases. CATH.a cells incubated with BODIPY-Cer also showed more rapid synthesis of the polar SL species, which is presumably due to direct availability of Cer. At longer time periods (24 h) BODIPY-Cer conversion to this polar lipid was less efficiently than from BODIPY-SM. This points towards a potential role of polar SL species synthesis to be involved in a detoxification process. As intracellular Cer concentrations are higher in CATH.a cells labeled with BODIPY-SM than in cells which were supplemented directly with BODIPY-Cer enhanced conversion of BODIPY-Cer to the polar lipid species might rescue cells from apoptosis elicited by high Cer concentrations.

As discussed above, this polar SL presumably represents a glycosylated SL species, most probably GlcCer, GalCer, or even a more complex GSL. Many studies highlightened the importance of GSL during axonal growth (Harel and Futerman, 1993; Schwarz and Futerman, 1997) which might be a possible explanation for increased synthesis of these lipids in CATH.a cells. Surprisingly, in dbcAMP-differentiated CATH.a cells synthesis of the polar SL species was neglectable. A potential synthesis of common myelin SL (e. g. GalCer, cerebroside sulfate; (Boggs et al., 2008)) might be seen controversial due to the fact that under physiological conditions oligodendrocytes supply neurons with myelin (de Vries and Hoekstra, 2000).

Investigations of PM-localization of BODIPY-SM and BODIPY-Cer highlighted that approx. 60-80% of added BODIPY-SM is localized to the extracellular leaflet of the lipid bilayer findings consistent with previous studies (Slotte and Ramstedt, 2007; Tepper et al., 2000). This strengthens the hypothesis that intracellular compartments accumulate mostly BODIPY-SM-derived BODIPY-Cer, which was also apparent during fluorescence microscopy performed during the present study. The remaining SM is found intracellularly in the inner leaflet of the PM, endosomes, and Golgi (Holthuis et al., 2001). In contrast, BODIPY-SM-derived BODIPY-Cer mainly remained intracellularly. SM recycling from intracellular compartments to the PM occurs very fast. Depleting the PM-associated BODIPY-SM pool by BE followed by treatment of CATH.a cells in BE medium at 37°C revealed that 80% of intracellular BODIPY-SM were recycled to the extracellular leaflet of the PM within 60 min. Interestingly, application of different chase time periods exhibited differences in recycling

kinetics of the tracer. Following a 5 min chase after which most of BODIPY-SM should be localized to early/recycling endosomes BODIPY-SM was more efficiently recycled to the PM than following a 30 min chase after which BODIPY-SM already remained in intracellular compartments like the Golgi.

When looking at differentiated CATH.a cells no significant differences in SM metabolism compared to undifferentiated cells were observed. Studies performed in differentiated PC12 cells that were labeled with a fluorescent Cer analogue revealed that NGF treatment (leading to differentiation) of PC12 cells resulted in rapid conversion of this Cer pool to SM in a time-dependent manner (Piccinotti et al., 2000). After 24 h the Cer-derived SM content in differentiated cells was 2 - 4-fold increased. Also endogenous SM was shown to accumulate 2-fold.

Increased SM synthesis was also shown to be important during neuronal maturation. During this period SM is required for formation of protein-lipid complexes, a prerequisite to target randomly distributed GM_1 ganglioside in immature neurons to the axon of mature neurons (Ledesma et al., 1999). However, SMase activity was not altered in PC12 cells in response to NGF treatment (Dobrowsky et al., 1995). These observations could indicate that SM synthesis rather than metabolism is affected during neuronal differentiation.

Taken together we could demonstrate that fluorescent SL analogues are rapidly metabolized in CATH.a cells. BODIPY-SM undergoes rapid hydrolysis already at the PM in line with results reported for NBD-SM (Kok et al., 1995). A model for SM uptake, trafficking and sorting in CATH.a neurons is displayed in ***Figure 47*** and suggests that BODIPY-Cer is able to passively diffuse to intracellular compartments leading to Golgi and ER accumulation (Koval and Pagano, 1989). ER/Golgi localization of BODIPY-Cer results in generation of polar SL, which are immediately secreted into the cellular supernatant. Most of remaining SM remains at the PM whereas the remaining part is internalized to intracellular compartment *via* early endosomal trafficking as shown for NBD-SM or is recycled back to the PM *via* recycling endosomes. Endocytosed BODIPY-SM is transported directly to intracellular compartments of SL synthesis (Golgi) bypassing lysosomal degradation. This is in agreement with other studies that showed that PYRENE- and NBD-labeled short chain SM analogues efficiently recycle to the PM after endocytosis and can

directly target the Golgi (Koivusalo et al., 2007; Kok et al., 1995). Results from the former study clearly reveal a major contribution of the FA acyl chain length on intracellular sorting and trafficking of SM. PYRENE-labeled long chain SM analogues that are endocytosed with the same efficiency than the short chain SM reach early/recycling endosomes but are then sorted to late endosomes/lysosomes where they are subject to aSMase hydrolysis. In this respect, BODIPY-C_5-SM used in our study might not completely resemble properties of naturally occurring SM, which are more hydrophobic and contain longer FA acyl chains. However, the study provides a good overview about SM uptake, trafficking, and metabolism in a neuronal cell line.

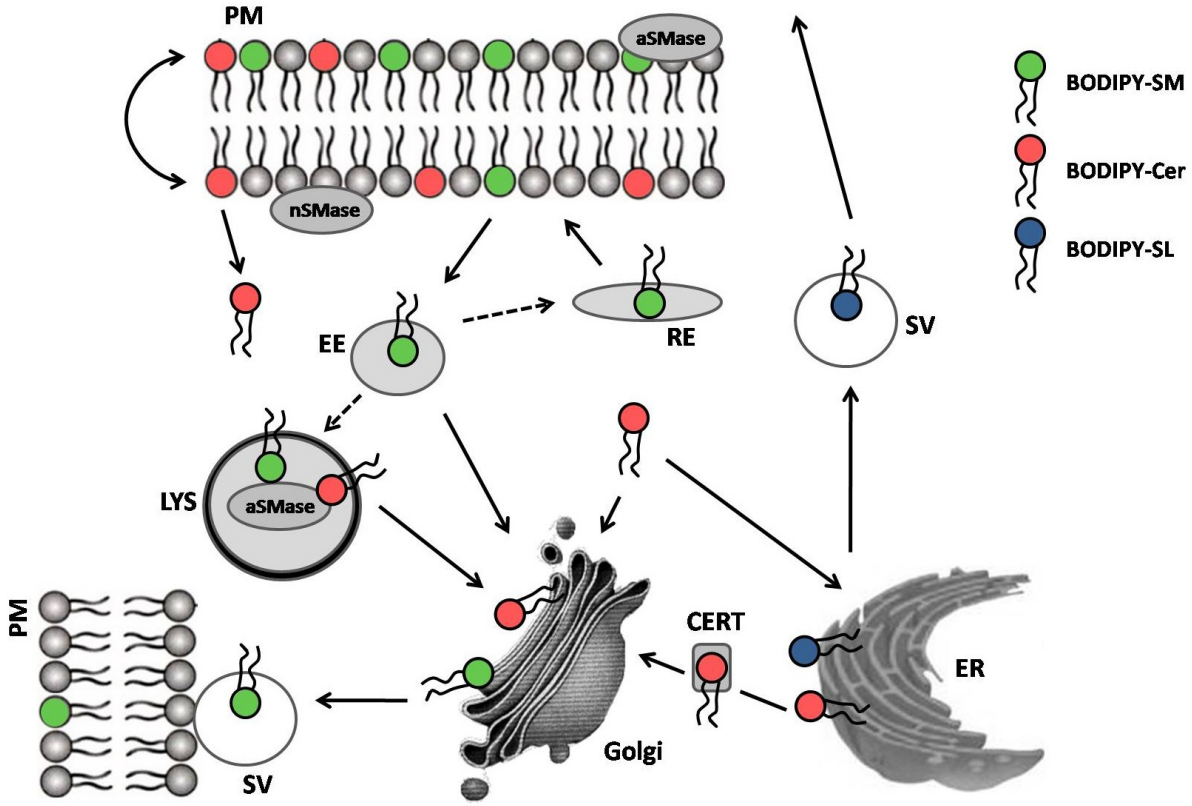

Figure 47: Schematic overview of uptake, trafficking, and sorting of BODIPY-labeled SL species in CATH.a cells.
EE, early endosome; *RE*, recycling endosome; *LYS*, lysosome; *SV*, secretory vesicle

2. CYTOTOXICITY OF HOCl-MODIFIED SM

Activated neutrophils are the first immune cells that are recruited from the peripheral blood to sites of infection and/or inflammation, followed by monocytes. Neutrophils account for generation and the release of reactive species and, therefore, account for bacterial killing. However, sustained activation of neutrophils at site of infection lead to oxidative modification of surrounding cells and tissue and thus, is accompanied by tissue damage. One of the key oxidant producing enzymes that is highly expressed in neutrophils and also to a lesser degree in monocytes is MPO. The heme-containing enzyme can bind halide and pseudohalide ions (Cl^-, Br^-, or SCN^-), other small ions such as NO, NO_2^-, azide (N_3^-), or CN^-, or larger organic substrates (Tyr, polyphenoles) and induces their one- or two-electron oxidation using H_2O_2 as substrate which is accompanied with generation of a variety of reactive species that account for oxidative damage. Among these reactive species, HOCl is generated in the presence of physiological Cl^- concentrations and it was shown previously, that 45% of H_2O_2 consumed by MPO results in HOCl formation (Pattison and Davies, 2006). The primary MPO-oxidant is able to oxidize other substrates such as ions (e. g. SCN^-) or macromolecules like proteins, lipids, or nucleic acids. As formation of reactive oxidants and concomitant oxidation of secondary targets is beneficial in terms of bacterial killing when MPO is released into the phagolysosome or, in smaller amounts, in the extracellular space of activated phagocytes, sustained MPO activation as present in diseases that are accompanied with chronic inflammation exhibits adverse effects to the surrounding tissue. For instance, HOCl modification can render enzymes and proteins unfunctional generate cytotoxic molecules such as chloramines, reactive chloro-aldehydes, or chlorohydrins, interfere with cellular processes such as replication and transcription, or initiate lipid peroxidation. Therefore, MPO and secondary MPO-derived products such as 5-chlorouracil, 3-chloro-Tyr, and 2-chloro-fatty aldehydes are excellent biomarkers for detection of chronic inflammation in diseases such as atherosclerosis, glomerulosclerosis, diabetes, cancer, lung injury, and neurodegenerative disorders. In addition elevated levels of these biomarkers are also found in course of disease progression of more acute events such as stroke, cardiac dysfunction, or ischemia/reperfusion (Klebanoff, 2005; Malle et al., 2007).

In CNS-related diseases, MPO levels and activity were found elevated both in acute events such as brain stroke and traumatic injury (Biagas et al., 1992; Breckwoldt et al., 2008) and neurodegenerative disorders that are accompanied by chronic inflammation (Chen et al., 2008; Choi et al., 2005; Green et al., 2004). Interestingly, these studies suggest microglial cells and astrocytes besides invaded activated neutrophils to be the major sites of MPO expression in the brain. Although promyelomonocytes lose their ability to express MPO during their transformation into resident macrophages, it was previously shown that certain types of these cells still contain MPO. These MPO-rich macrophage populations were found also in atherosclerotic lesions, circulating blood, and brain, as already mentioned above (Arnhold and Flemmig, 2010). Therefore, proteins and especially unsaturated lipids that are highly enriched in the brain are susceptible targets for MPO-mediated oxidation/modification.

The aim of the second part of this study was the investigation of potential lipotoxic effects of HOCl-modified SM in a neuronal background. SM is highly enriched in the brain and intramolecular double bounds as well as amide linkages display potential targets for HOCl generated *via* the MPO/H_2O_2/Cl^- system. In addition, alterations on the proteom level after treatment of PC12 neurons with or without SM or HOCl-SM were examined. The results summarized previously (Nusshold et al., 2010) revealed that HOCl modification of chicken egg-yolk-derived SM (which mainly contains SM(d:18:1/16:0)) generated a variety of chlorinated SM species with high neurotoxic properties. These SM chlorohydrins/chloramides severely impaired cell viability, resulted in dissipation of $\Delta\psi m$, affected the actin/tubulin cytoskeleton, and induced the apoptotic machinery. In addition, incubation of PC12 cells in the presence of SM or HOCl-SM downregulated the expression of glycolytic enzymes downstream of fructose 1,6-bisphosphate whereas SM but not HOCl-SM induced several proteins involved in the Nrf2-mediated oxidative stress response.

SM(d18:1/16:0) was chosen as a model SM in our studies because it contains a single double bound in the Sph backbone and an amide group both representing the only potential targets for HOCl modification. Oxidative modifications were analyzed using MALDI-TOF-MS. When reagent HOCl was used as oxidant the predominant chlorinated SM species were the SM(d18:1/16:0) chlorohydrin and an unsaturated, monochlorinated species. The conversion of these unsaturated chlorohydrins have been identified already a long time ago after treatment of PC liposomes with HOCl although the decrease in mass of

34 Da was originally misinterpreted by the formation of a glycol moiety (Arnhold et al., 2001). In these studies the authors suggested that the glycols originate after aqueous attack on PC epoxides that were also found to be generated as a consequence of HOCl treatment. More recently, isotopic labeling using ^{18}O-labeled water and HOCl, and ^{37}Cl-labeled HOCl revealed that HOCl attack on double bonds of FA acyl residues leads to formation of positively charged carbenium ions which can then either yield saturated or unsaturated chlorohydrins depending on addition of H_2O-derived OH^- or removal of H^+ on the carbenium intermediate (Spalteholz et al., 2004). Although not experimentally verified in our present studies we conclude that a comparable pathway is responsible for generation of unsaturated, chlorinated SM species and that conversion of SM-derived glycols can be ruled out. In addition we did not try to analyze the occurrence of the two possible positional isomers of the SM chlorohydrin (depending on the site of addition of Cl^+ and OH^- on the double bond in the Sph backbone) as it was already shown for oleic acid and esterified oleate (Spickett, 2007).

In addition to chlorohydrin formation LysoPL conversion following HOCl treatment was observed in PAPC, PSPC, and also, to a minor degree in POPC liposomes which was explained by a weakening of the ester bond due to introduction of electron-attracting substitutes upon chlorohydrin formation (Arnhold et al., 2002). Although the double bond in SM(d18:1/16:0) is close to both the amide and the phosphodiester bond which could favor weakening of these intramolecular linkages as observed for ester bonds in PC liposomes (Arnhold et al., 2002), formation of SM-derived LysoPL after HOCl modification could not be identified using MALDI-TOF-MS. Therefore, we suggest that SM is not that susceptible towards generation of LysoPL upon HOCl treatment as ester bond containing PL molecules are.

Whereas the PC headgroup is rather inert towards HOCl modification (k_2(PC headgroup) = 2 x 10^{-2} L mol^{-1} sec^{-1}), the amide group that links the FA acyl residue to the Sph backbone represents another potential target for HOCl oxidation that was previously shown to exhibit similar second-order reaction kinetics than aliphatic double bonds (k_2(amide/double bond) = 10 and 9 L mol^{-1} sec^{-1}) (Pattison et al., 2003). Interestingly, our studies suggested that formation of mixed SM chlorohydrins/chloramide species only contribute to a fraction of HOCl-SM species out of which SM chlorohydrins and unsaturated, monochlorinated derivates predominate significantly. Moreover, we were not

able to detect formation of SM chloramides that still contain the unoxidized double bond in the Sph backbone. Hence, it can be argued that the double bond in SM(d18:1/16:0) exhibits a higher second-order reaction constant towards HOCl compared to the SM amide group and thus chlorohydrin formation is favored. Although this contradicts previous studies that examined reaction rates of HOCl with FA acyl double bonds and SM amides using computational modeling. However, these modeling studies were performed with the upper limit of experimentally determined accessible amide groups and, therefore, reaction of HOCl with SM amides can be estimated to be lower (Pattison et al., 2003). This theory is strengthened under consideration that amide groups of small cyclic and uncharched molecules react more readily with HOCl compared to that of linear and charged ones (Pattison and Davies, 2001).

Determinations of the reaction rate of multilamellar SM(18:1/16:0) liposomes with HOCl revealed a second-order rate constant of 18.7 ± 3.05 L mol^{-1} sec^{-1} that is in the range of that of plasmalogens incubated with the oxidant (55 ± 7 L mol^{-1} sec^{-1}) and to that of previous studies which investigated the kinetics of HOCl with aliphatic double bonds (5 - 50 L mol^{-1} sec^{-1}) (Arnhold et al., 1995; Skaff et al., 2008; Winterbourn et al., 1992). The reaction kinetics of unilamellar SM with HOCl can be estimated to be even higher than our calculated values for multilamellar SM liposomes. This is due to the fact that the reaction of HOCl with multilamellar egg PC liposomes is a magnitude of six lower compared to unilamellar liposomes. This was explained by a reduced ability of HOCl to diffuse into the liposome core as the environment becomes more apolar. Regarding these values, a second-order reaction constant in the range of at least 10^2 L mol^{-1} sec^{-1} for HOCl towards unilamellar SM liposomes seems to be reasonable as SM exhibits two instead of only one potential targets for HOCl modification as compared to SOPC. Furthermore, an acidic pH as obtained at inflammatory sites increases the amount of HOCl compared to its less reactive anion OCl^- and should, therefore, additionally increase the reactivity of HOCl towards SM.

Interestingly, we were also able to detect SM-derived epoxides which arise due to dehalogenation of SM chlorohydrins. The exact reason for epoxide formation as it was already observed after HOCl treatment of Chol is still unclear as epoxidation of halohydrins normally only occurs under alkaline conditions (Spickett, 2007). If a hitherto unknown mechanism or ionization during MALDI-TOF-MS analysis accounts for SM epoxide conversion remains to be elucidated.

Similarly oxidized lipid species were also found after SM modification with the MPO/H_2O_2/Cl^- system. The reason for incomplete enzymatic SM modification (approx. 2/3 of SM was oxidized) is presumably due to self-modification of the protein moiety of MPO. The one-electron donor H_2O_2 that exhibits a high second-order rate constant for reaction with MPO compound I but slow reaction kinetics with MPO compound II (***Fig. 7***) can also interfere with generation of HOCl due to accumulation of inactive compound II which is unable to oxidize halides (Arnhold and Flemmig, 2010; Furtmuller et al., 2000; Jantschko et al., 2003). Indeed H_2O_2 concentrations of > 100 µM efficiently block HOCl conversion (Malle et al., 2007). However, it is very unlikely that excessive H_2O_2 accounts for incomplete SM modification in our study as the oxidant was added step-wise to prevent accumulation of compound II and its recycling to ferric MPO, favored by addition of ascorbic acid that exhibits high reaction kinetics towards compound II (Bolscher et al., 1984), was ineffective (data not shown).

Analysis of SM species present in C57Bl/6 mouse brain lipid extracts revealed the presence of C18:1 SM containing C16:0, C18:0, C18:1, C20:0, and C24:1 FA acyl chains. C18:0 and C24:1 are the most abundant molecular species, similar to what was reported for SM composition of human and bovine brain, of rat cerebellar granule cells, and of rat cortical neurons (Ramstedt et al., 1999; Staellberg-Stenhagen and Svennerholm, 1965; Tyurin et al., 2008; Valsecchi et al., 2007). C18:0 containing SM is thereby mainly enriched in the gray matter, whereas C24:1 containing SM is predominately found in the white matter. Of note, SM in total mouse brain lipid extracts were also susceptible towards HOCl oxidation (***Fig. 35 B*** and ***C***). Application of 50 µg reagent HOCl per 100 µg lipids resulted in complete conversion of SM(d18:1/24:1) and the remaining SM (approx. 300 nmol/g wet brain) more or less exclusively consisted of unmodified SM(d18:1/180). Application of higher HOCl concentrations diminished unmodified SM below the detection limit. Interestingly, modification of SM did not coincide with the level of generated SM chlorohydrins. Under normal conditions, chlorohydrins, especially when derived from SM can be considered to be relatively stable molecules. However, in a complex lipid matrix, other lipid moieties harbor HOCl-susceptible groups such as the amine-containing headgroups from PE and PS which are preferentially targeted by HOCl. Generated chloramines can breakdown into N-centered radical which can induce further lipid peroxidation thus leading to profound lipid modification. Hence, application of HOCl

concentrations where the level of generated SM chlorohydrins is rather low, chlorohydrin modification by other reactive lipid species generated in course of HOCl-treatment my additionally decrease their concentration below the detection limit. Not until incubation of brain lipids at higher HOCl concentrations which raise the level of generated SM chlorohydrins, these oxidized lipids become detectable. Similar to what was observed after HOCl modification of egg yolk SM, chlorohydrins predominated over the unsaturated, monochlorinated species.

HOCl and HOCl-modified lipids are potent inducers of apoptosis/cell death (Yap et al., 2007). HOCl-modified lipids were recently identified to exhibit cytotoxicity in various cell lines and to be excellent biomarkers under severe and chronic inflammatory conditions which presumably can amplify disease progression (Spickett, 2007). In the present study, HOCl-SM provoked dissipation of $\Delta\psi_m$, concomitant generation of ROS, and severely impacted on PC12 cell respiration. A collapse of $\Delta\psi_m$ is very often accompanied by apoptotic cell death though it is not yet completely clear at which state of the apoptotic cascade loss of $\Delta\psi_m$ occurs and whether this event is actually necessary for induction of the PCD (Ly et al., 2003). However, a decrease of $\Delta\psi_m$ is mostly accompanied with formation of the PTP, which in turn is a major contributor to disease progression of neurodegenerative disorders (Knott et al., 2008; Norenberg and Rao, 2007). PTP formation leads to the release of many mitochondrial pro-apoptotic factors such as cytochrome *c*, AIF, and Smac/Diablo thereby triggering formation of the apoptosome and activation of the caspase cascade (Ly et al., 2003). PTP was shown to occur in response to HOCl in hepatocytes and isolated mitochondria, resulting in consumption of intracellular GSH and subsequent production of ROS, chromatin condensation, procaspase-3 processing (Whiteman et al., 2005). Dissipation of $\Delta\psi_m$ was observed to follow a time- and concentration-dependent manner in response to HOCl-SM treatment in PC12 cells. Similar results were observed in the human promonocytic cell line U937 as well in peripheral blood monocytes when incubated in the presence of HOCl-LDL (Ermak et al., 2008; Vicca et al., 2003). In these studies, oxidized LDL provoked a significant collapse of $\Delta\psi_m$ in U937 cells right after 30 min of incubation (reminiscent to what was observed after PC12 cell treatment with HOCl-SM) which was followed by cytochrome *c* release and ROS formation, PS externalization, and concomitant activation of caspase-9 and caspase-3. Furthermore, the oxidized lipoproteins elicited

alterations in expression rates of proteins belonging to the Bcl-2 superfamiliy thus highlighting the involvement of mitochondria in HOCl-LDL induced cell death. Overexpression of Bcl-2 in U937 cells abolished most of the cellular effects mentioned above. Similar results were obtained in studies where bovine aortic endothelial cells were treated with Cu^{2+}-oxidized LDL (Zmijewski et al., 2005). Experiments demonstrated that Cu^{2+}-oxidized LDL enhanced ROS formation in these cells which was due to mitochondrial irritation visualized by an increased intramitochondrial ROS level and dissipation of $\Delta\psi_m$. In inhibitor studies these authors could identify mitochondrial complex II as the key player involved in Cu^{2+}-oxidized LDL induced ROS generation. Also other studies using different cell lines reported that HOCl-LDL- and Cu^{2+}-oxidized LDL-mediated cell death is executed by the mitochondrial pathway of apoptosis (Chen et al., 2004; Vicca et al., 2000).

Chlorohydrins, LysoPL, and α-chloro-fatty aldehydes, generated during HOCl-treatment were identified to cause cellular cytotoxicity (Dever et al., 2006; Thukkani et al., 2005; Thukkani et al., 2003; Vissers et al., 2001). Recent studies demonstrate that apoptosis rather than necrosis is responsible for cell death. Treatment of porcine brain capillary endothelial cells with 2-ClHDA, a chloroaldehyde that is generated during HOCl-mediated attack of plasmalogens, resulted in decreased $\Delta\psi_m$, concomitant ROS formation, and procaspase-3 cleavage suggesting mitochondrial apoptotic cell death (Uellen et al., unpublished data). Cholesterol-, FFA-, and PL chlorohydrins were originally considered to elicit their cytotoxicity mainly by causing cell lysis as they were assumed to destabilize the PM, since they introduce polar groups in the hydrophobic environment of the lipid bilayer. Recently, FFA chlorohydrins were shown to provoke cytotoxicity in human endothelial cells and low µM concentrations of PC chlorohydrins induced ROS formation in PMA-stimulated splenocytes as well as ATP depletion and caspase-3 activation in myeloid cells (Dever et al., 2003; Dever et al., 2006; Dever et al., 2008; Vissers et al., 2001). At higher PC chlorohydrin concentrations caspase activity was undetectable and, therefore, the authors suggested necrosis to account for cell death. Most of these cellular events were also found in HOCl-SM-treated PC12 cells. Incubation with HOCl-SM induced a rapid collapse of $\Delta\psi_m$ and mitochondrial fragmentation (data not shown), followed by ROS formation and impaired respiration, and subsequent cleavage of procaspase-3 and apoptotic cell death. Insofar, it is very likely that HOCl-modified SM causes mitochondrial dysfunction that is followed by PTP formation and release of pro-apoptotic proteins that induce apoptosis. Similar as observed

in human myeloid cells (Dever et al., 2006) treated with PC chlorohydrins induction of apoptosis was only evident when PC12 cells were incubated in the presence of relatively high concentrations (130 to 270 µM) of HOCl-SM. Concentrations below and above did not lead to caspase-3 activation. In addition, HOCl-SM concentrations mentioned above only induced partial cleavage of the procaspase-3 pool whereas MTT assays demonstrated reduced cell viability by 80%. These discrepancies suggest that HOCl-SM treatment does not only induce apoptosis in PC12 cells but cell death is rather a necroptotic/aponecrotic event which covers both, apoptotic and necrotic features (i. e. damage of cell and organelle membranes). Presumably, insertion of the more polar HOCl-SM always partially causes membrane destabilization. However, at high concentrations these modified lipids may immediately destabilize PC12 membranes and, therefore, cause cell lysis before HOCl-SM can elicit its cytotoxicity to the cell. At lower concentrations cells in which (membrane) damage is beyond repair die due to necrosis whereas other cells undergo apoptosis.

Up to now the question by which mechanism HOCl-modified SM elicits its apoptotic/cytotoxic potential remains. Studies indicate that oxidation products of arachidonic acid (e. g. hydroperoxyeicosatetraenoic acid, HNE, or MDA) induce apoptosis in vascular smooth muscle cells (Kalyankrishna et al., 2002). Recent studies highlightened the role of oxidized PL in induction of the apoptotic machinery. POVPC and PGPC were shown to induce apoptosis in vascular smooth muscle cells due to activation of aSMase (Loidl et al., 2003). Mitogen-activated protein kinases, c-Jun N-terminal kinase, and p38, which are downstream targets of aSMase were phosphorylated in response to oxidized PL. Inhibition of aSMase activity was accompanied with suppression of caspase-3 activation (Fruhwirth et al., 2006) suggesting a potential role of Cer in this apoptotic pathway. Furthermore, azelaoyl-PC which is abundant in oxidized LDL was identified to trigger the intrinsic pathway of apoptosis *via* mitochondrial damage (Chen et al., 2007). Moreover, endogenously oxidized PL were shown to induce apoptosis. Cytochrome *c*-oxidized cardiolipin was demonstrated as a central molecule being responsible for the release of pro-apoptotic factors during early stages of the intrinsic apoptotic pathway (Kagan et al., 2005). Previously it was shown that typical events of the apoptotic cascade are closely linked to PL oxidation. For instance, PS externalization, which is important for recognition and concomitant phagocytosis of apoptotic cells by macrophages requires PS oxidation (Hazen, 2008; Kagan et al., 2004). Other studies also revealed that apoptosis is linked to oxidation

of PC, PS, and PE (Arroyo et al., 2002). Interestingly, it was found that apoptotic cells generally contain elevated level of oxidized PL (Chang et al., 2004).

However, since HOCl-SM treatment provoked rapid dissipation of $\Delta\psi_m$, mitochondrial fragmentation, and energy deprivation in PC12 cells it is obvious that this chlorinated lipid or HOCl-SM-derived metabolites directly target mitochondria, which then elicits apoptosis in PC12 cells. Considering studies that showed activation of aSMase in response to treatment with oxidized PL (Fruhwirth et al., 2006; Loidl et al., 2003) a similar reaction mechanism might account for energy deprivation and apoptosis in this study. Results from the first part of this thesis show rapid BODIPY-SM hydrolysis at the PM and/or intracellular compartments in CATH.a cells after disturbing SM-Cer homeostasis by incubation with this tracer. Hence it is likely that naturally occurring SM(d18:1/16:0) induces SM turnover in PC12 cells. Cer can promote the apoptotic machinery either by acting on enzymes and proteins (e. g. PP2A phosphorylation, cytochrome *c* oxidation, cathepsin D activation; (Ghafourifar et al., 1999; Heinrich et al., 1999; Lin et al., 2006)) or by direct interference with mitochondria (e. g. mitochondrial PTP formation, disruption of inner and outer mitochondrial membrane, targeting of respiratory chain complexes; (Colombini, 2010; Gudz et al., 1997; Novgorodov et al., 2005)). However, although we could detect dissipation of $\Delta\psi_m$ after SM treatment, mitochondrial irritation was not sufficient to render PC12 cells apoptotic in contrast to what was observed after PC12 treatment with HOCl-SM. Whether HOCl-SM-derived chlorinated Cer is a more potent pro-apoptotic lipid than unmodified Cer is currently unclear. Studies that showed disruption of the mitochondrial membranes due to insertion of Cer might favor this idea. As discussed earlier, chlorinated lipids are considered to introduce hydrophilic groups into membrane lipid bilayers leading to membrane perturbation and rupture. Hydrophilic lipids might be subject to faster PM insertion kinetics than more apolar lipids (more efficient PM insertion of the hydrophilic BODIPY-SM than apolar PYRENE-SM). Presumably, Cer generated from exogenously applied SM targets the membrane of mitochondria which, however, is not sufficient to induce apoptosis. In contrast, Cer chlorohydrins could severely damage the outer and/or the inner membrane of mitochondria leading to mitochondrial fragmentation, energy deprivation, and the release of pro-apoptotic proteins. Another open question is whether SMases display other substrate specificity toward HOCl-SM. It might be possible that HOCl-SM is more efficiently converted to the corresponding Cer than unmodified SM,

which would provoke a more pronounced increase in intracellular Cer concentrations. Another possibility that can account for induction of apoptosis in HOCl-SM-treated PC12 cells is substrate specific activation of SMases as shown for oxidized PL (Fruhwirth et al., 2006).

Recently energy deprivation was reported in cells treated with small chlorohydrin molecules. Several studies identified 3-Cl-propanediol, also termed *S*-α-chlorohydrin (ACH), as an inhibitor of glyceraldehyde-3-phosphate dehydrogenase (GAPDH) and triosephosphate isomerase (Jelks and Miller, 2001; Romero et al., 1997; Sheline and Choi, 1998). Treatment with ACH induced energy deprivation-dependent cell death in cultured cortical neurons, rat astrocytes, and brain microvessel endothelial cells (Brown et al., 2011; Romero et al., 1997; Sheline and Choi, 1998; Willis et al., 2007), disruption of the redox state in primary astrocyte cultures (Skamarauskas et al., 2007), ROS-dependent apoptosis in mouse melanoma cells (Park et al., 2010), dysfunction of the BBB (Willis et al., 2007), and microglial activation (Lynch et al., 2004) which further emphasize the neurotoxicity of chlorohydrins. Energy deprivation plays a central role in neurodegenerative diseases (Hoyer et al., 2005). Recently it was revealed that cancer cells switch from oxidative phosphorylation to glycolysis for ATP production during hypoxia thus hindering them to undergo the apoptotic cascade. Similarly is was observed that neurons also switch to glycolysis to maintain ATP production and synthesize antioxidant molecules to survive during oxidative stress (Hedskog et al., 2011). Since small chlorohydrin molecules were shown to induce energy deprivation by inhibition of glycolytic enzymes (see above) this might allow us to speculate that SM chlorohydrins also target these enzymes. Cer targeting of mitochondria and energy deprivation would suggest a possible combination that accounts for PC12 cell death during HOCl-SM treatment. Thereby, SM-derived Cer might target mitochondria leading to oxidative stress (dissipation of $\Delta\psi_m$ in SM- and HOCl-SM-treated PC12 cells). SM-treated PC12 cells can overcome this problem by switching energy production to glycolysis. However, as chlorohydrins might inhibit glycolytic enzymes in PC12 cells, energy production can be severely impaired which results, in combination with ROS formation, in cell death. This might account for differences in cell viability in SM- and HOCl-SM-treated PC12 cells.

Results obtained after identification of differentially expressed proteins in control, SM-, and HOCl-SM-treated cells further support this theory. Many enzymes that contribute to energy metabolism were identified to be downregulated compared to control cells which points towards energy deprivation in HOCl-SM-treated PC12 cells. Moreover it was suggested that astrocytes play a critical role in energy homeostasis in neurons *via* a pathway termed the neuron-astrocyte lactate shuttle (Pellerin et al., 2007). After neuronal activation astrocytes increase their glycolytic rates and generate lactate, which is then transported to neurons where it is converted back to pyruvate (by means of lactate dehydrogenase (LDH)) and enters oxidative phosphorylation (Kasischke et al., 2004). Downregulation of glycolytic enzymes by HOCl-SM and (partially) by SM observed during this *in vitro* study would impair neuronal oxidative glycolysis during the initial phase and probably also nonoxidative glycolysis in astrocytes. Downregulation of LDH as observed here would also decrease lactate oxidation and ATP production, a prerequisite for glutamate recycling. In combination these are classical markers of energy deprivation as observed in many neurological diseases.

PC12 treatment with unmodified SM also provoked downregulation of a few enzymes that contribute to energy metabolism. This raises the question by which mechanism(s) SM and HOCl-SM can induce changes in the expression pattern of these enzymes apart from directly inhibiting their enzymatic activity. Once more the SM-Cer pathway could be of central importance in this process. In LPS-treated rats it was demonstrated that the inflammatory response results in impaired cardiac glycolysis and a net reduction of glycogen biosynthesis, effects abolished by pharmacological inhibition of ceramidase (Tessier et al., 2003). *In vitro* studies have demonstrated that Cer inhibits activation of Akt, antagonizes insulin-dependent glucose transport (Summers et al., 1998), and suppresses phosphorylation of insulin receptor substrate-1 (Kanety et al., 1996). In neurons inhibition of hexokinase activity (*via* inhibition of Akt) was reported in response to C2-ceramide (Arboleda et al., 2007). Finally, analysis of alterations in gene expression accompanying C2-ceramide-induced apoptosis in PC12 cells revealed significantly decreased (3-fold) expression of aldolase C expression at the mRNA level (Decraene et al., 2002), which is consistent with our proteome findings (downregulation of aldolase C by SM and HOCl-SM between 2.2- and 3.5-fold).

However, also with regard to protein expression, some distinct differences between SM and HOCl-SM became apparent. Whereas SM induced the expression of peroxiredoxins 1 and 2 (PRDX1 and 2), mitochondrial superoxide dismutase 2, proteasome subunit α type-1, and glutathione S-transferase ω-1 (which are all involved in Nrf2-mediated oxidative stress response), this type of response was not observed with HOCl-SM. Interestingly, a recent report identified erythrocyte peroxiredoxin 2 as a target for HOCl-dependent oxidation (Stacey et al., 2009). Taken together the induction of the protective Nrf2 response might be a plausible explanation for the absence of intracellular ROS generation in SM-treated PC12 cells and supports suggestions mentioned above.

Differences in protein expression in SM- and HOCl-SM-treated PC12 cells were also identified for cytoskeletal proteins. HOCl-SM-treated cells exhibited preferred clumping as well as the establishment of a cortical actin ring, which might be due to a lower motility in response to cell stress or represent a protective mechanism. Such a cortical actin cytoskeleton was shown to be important in proper barrier function in endothelial cells (Singleton et al., 2010) and was identified to be established under certain kinds of cell stress. Studies that suggested decreased activity of cofilin to play a role in maintenance of the cortical actin ring under hypertonic conditions (Di Ciano-Oliveira et al., 2006) would fit to our results as we found cofilin more then 2-fold downregulated in HOCl-SM-treated cells. In terms of hyperosmotic stress RhoA-kinase activation was shown to account for actin remodeling by shortening of stress fibers accompanied with predominance of cortical F-actin staining (Miranda et al., 2010). In yeast cortical actin-derived oxidation-induced actin bodies protect cells from oxidative stress (Farah et al., 2011).

Studies from the first part of this thesis revealed caveolae-mediated endocytosis of BODIPY-SM. Choudhury and colleagues (Choudhury et al., 2002) could show that BODIPY-labeled GSL are similarly endocytosed and that Golgi targeting of the fluorescent lipids depends on microtubules. Additionally disruption of microtubules with nocodazole selectively interfered with the apical transport of NBD-SM from the Golgi to the PM (Vanmeer and Vanthof, 1993). These authors concluded that microtubules might maintain the Golgi close to the PM or act as tracks for SM-containing vesicles. Therefore, upregulation of tubulin due to exogenouslyadded SM seems to indicate an important function of microtubules in maintenance of lipid sorting and trafficking.

Taken together results point towards a potent role of HOCl-SM in neurotoxicity (a model is shown in ***Figure 48***). Under inflammatory conditions MPO-derived HOCl-SM can oxidatively modify SM leading to formation of SM chlorohydrin/chloramide species that elicit ROS formation in PC12 cells. Concomitantly, mitochondrial irritation provokes defective oxidative phosphorylation, induces caspase-3 and PARP cleavage, and decreases cell viability. These events are not observed in PC12 cells incubated in the presence of unmodified SM. However, both lipids were shown to be potent lipid modulators of protein expression in neuronal cells driving downregulation of glycolytic enzymes and LDH in PC12 cells. Chronic inflammation as observed in neurodegenerative diseases is accompanied by energy deprivation, sustained MPO activation, and generation of reactive species. These observations as well as the high SM content in neuronal tissue highlight a potential role of HOCl-SM in disease progression.

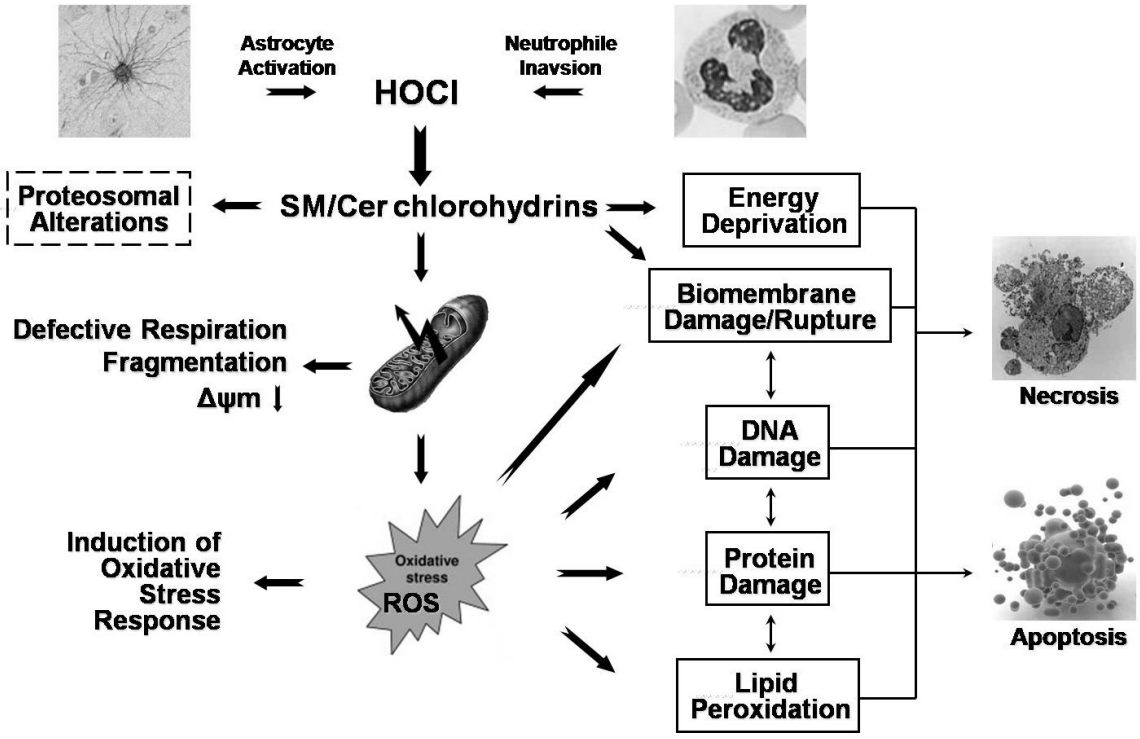

Figure 48: Proposal of generation of HOCl-modified SM and its potential lipotoxic effects.

V. REFERENCES

Adams, J.M., and S. Cory. 1998. The Bcl-2 protein family: arbiters of cell survival. *Science*. 281:1322-1326.

Agner, K. 1950. Studies on peroxidative detoxification of purified diphtheria toxin. *J Exp Med*. 92:337-347.

Alam, J.J. 2003. Apoptosis: target for novel drugs. *Trends Biotechnol*. 21:479-483.

Albert, C.J., J.R. Crowley, F.F. Hsu, A.K. Thukkani, and D.A. Ford. 2001. Reactive chlorinating species produced by myeloperoxidase target the vinyl ether bond of plasmalogens: identification of 2-chlorohexadecanal. *J Biol Chem*. 276:23733-23741.

Alnemri, E.S., D.J. Livingston, D.W. Nicholson, G. Salvesen, N.A. Thornberry, W.W. Wong, and J. Yuan. 1996. Human ICE/CED-3 protease nomenclature. *Cell*. 87:171.

Altankov, G., and F. Grinnell. 1993. Depletion of intracellular potassium disrupts coated pits and reversibly inhibits cell polarization during fibroblast spreading. *J Cell Biol*. 120:1449-1459.

Amtmann, E., and M. Zoller. 2005. Stimulation of CD95-induced apoptosis in T-cells by a subtype specific neutral sphingomyelinase inhibitor. *Biochem Pharmacol*. 69:1141-1148.

Andrieu, N., R. Salvayre, J.P. Jaffrezou, and T. Levade. 1995. Low temperatures and hypertonicity do not block cytokine-induced stimulation of the sphingomyelin pathway but inhibit nuclear factor-kappa B activation. *J Biol Chem*. 270:24518-24524.

Anliker, B., and J. Chun. 2004. Lysophospholipid G protein-coupled receptors. *J Biol Chem*. 279:20555-20558.

Aratani, Y., F. Kura, H. Watanabe, H. Akagawa, Y. Takano, K. Suzuki, M.C. Dinauer, N. Maeda, and H. Koyama. 2002. Critical role of myeloperoxidase and nicotinamide adenine dinucleotide phosphate-oxidase in high-burden systemic infection of mice with Candida albicans. *J Infect Dis*. 185:1833-1837.

Aratani, Y., F. Kura, H. Watanabe, H. Akagawa, Y. Takano, K. Suzuki, N. Maeda, and H. Koyama. 2000. Differential host susceptibility to pulmonary infections with bacteria and fungi in mice deficient in myeloperoxidase. *J Infect Dis*. 182:1276-1279.

Arboleda, G., T.J. Huang, C. Waters, A. Verkhratsky, P. Fernyhough, and R.M. Gibson. 2007. Insulin-like growth factor-1-dependent maintenance of neuronal metabolism through the phosphatidylinositol 3-kinase-Akt pathway is inhibited by C2-ceramide in CAD cells. *Eur J Neurosci*. 25:3030-3038.

Arenz, C., M. Thutewohl, O. Block, H. Waldmann, H.J. Altenbach, and A. Giannis. 2001. Manumycin A and its analogues are irreversible inhibitors of neutral sphingomyelinase. *Chembiochem*. 2:141-143.

Arnhold, J., and J. Flemmig. 2010. Human myeloperoxidase in innate and acquired immunity. *Arch Biochem Biophys*. 500:92-106.

Arnhold, J., A.N. Osipov, H. Spalteholz, O.M. Panasenko, and J. Schiller. 2001. Effects of hypochlorous acid on unsaturated phosphatidylcholines. *Free Radic Biol Med*. 31:1111-1119.

Arnhold, J., A.N. Osipov, H. Spalteholz, O.M. Panasenko, and J. Schiller. 2002. Formation of lysophospholipids from unsaturated phosphatidylcholines under the influence of hypochlorous acid. *Biochim Biophys Acta*. 1572:91-100.

Arnhold, J., O.M. Panasenko, J. Schiller, A. Vladimirov Yu, and K. Arnold. 1995. The action of hypochlorous acid on phosphatidylcholine liposomes in dependence on the content of double bonds. Stoichiometry and NMR analysis. *Chem Phys Lipids*. 78:55-64.

Arroyo, A., M. Modriansky, F.B. Serinkan, R.I. Bello, T. Matsura, J. Jiang, V.A. Tyurin, Y.Y. Tyurina, B. Fadeel, and V.E. Kagan. 2002. NADPH oxidase-dependent oxidation and externalization of

phosphatidylserine during apoptosis in Me2SO-differentiated HL-60 cells. Role in phagocytic clearance. *J Biol Chem*. 277:49965-49975.

Ashkenazi, A., and V.M. Dixit. 1998. Death receptors: signaling and modulation. *Science*. 281:1305-1308.

Babia, T., M.D. Ledesma, R. Saffrich, J.W. Kok, C.G. Dotti, and G. Egea. 2001. Endocytosis of NBD-sphingolipids in neurons: exclusion from degradative compartments and transport to the Golgi complex. *Traffic*. 2:395-405.

Bainton, D.F., J.L. Ullyot, and M.G. Farquhar. 1971. The development of neutrophilic polymorphonuclear leukocytes in human bone marrow. *J Exp Med*. 134:907-934.

Batista, L.F., B. Kaina, R. Meneghini, and C.F. Menck. 2009. How DNA lesions are turned into powerful killing structures: insights from UV-induced apoptosis. *Mutat Res*. 681:197-208.

Baumann, N., and D. Pham-Dinh. 2001. Biology of oligodendrocyte and myelin in the mammalian central nervous system. *Physiol Rev*. 81:871-927.

Becher, A., and R.A. McIlhinney. 2005. Consequences of lipid raft association on G-protein-coupled receptor function. *Biochem Soc Symp*:151-164.

Bergt, C., K. Oettl, W. Keller, F. Andreae, H.J. Leis, E. Malle, and W. Sattler. 2000. Reagent or myeloperoxidase-generated hypochlorite affects discrete regions in lipid-free and lipid-associated human apolipoprotein A-I. *Biochem J*. 346 Pt 2:345-354.

Biagas, K.V., M.W. Uhl, J.K. Schiding, E.M. Nemoto, and P.M. Kochanek. 1992. Assessment of posttraumatic polymorphonuclear leukocyte accumulation in rat brain using tissue myeloperoxidase assay and vinblastine treatment. *J Neurotrauma*. 9:363-371.

Bianco, F., C. Perrotta, L. Novellino, M. Francolini, L. Riganti, E. Menna, L. Saglietti, E.H. Schuchman, R. Furlan, E. Clementi, M. Matteoli, and C. Verderio. 2009. Acid sphingomyelinase activity triggers microparticle release from glial cells. *EMBO J*. 28:1043-1054.

Billen, L.P., A. Shamas-Din, and D.W. Andrews. 2008. Bid: a Bax-like BH3 protein. *Oncogene*. 27 Suppl 1:S93-104.

Birbes, H., S. El Bawab, Y.A. Hannun, and L.M. Obeid. 2001. Selective hydrolysis of a mitochondrial pool of sphingomyelin induces apoptosis. *FASEB J*. 15:2669-2679.

Birbes, H., C. Luberto, Y.T. Hsu, S. El Bawab, Y.A. Hannun, and L.M. Obeid. 2005. A mitochondrial pool of sphingomyelin is involved in TNFalpha-induced Bax translocation to mitochondria. *Biochem J*. 386:445-451.

Boggs, J.M., W. Gao, and Y. Hirahara. 2008. Myelin glycosphingolipids, galactosylceramide and sulfatide, participate in carbohydrate-carbohydrate interactions between apposed membranes and may form glycosynapses between oligodendrocyte and/or myelin membranes. *Biochim Biophys Acta*. 1780:445-455.

Boldin, M.P., T.M. Goncharov, Y.V. Goltsev, and D. Wallach. 1996. Involvement of MACH, a novel MORT1/FADD-interacting protease, in Fas/APO-1- and TNF receptor-induced cell death. *Cell*. 85:803-815.

Bolscher, B.G., G.R. Zoutberg, R.A. Cuperus, and R. Wever. 1984. Vitamin C stimulates the chlorinating activity of human myeloperoxidase. *Biochim Biophys Acta*. 784:189-191.

Bradford, M.M. 1976. A rapid and sensitive method for the quantitation of microgram quantities of protein utilizing the principle of protein-dye binding. *Anal Biochem*. 72:248-254.

Breckwoldt, M.O., J.W. Chen, L. Stangenberg, E. Aikawa, E. Rodriguez, S. Qiu, M.A. Moskowitz, and R. Weissleder. 2008. Tracking the inflammatory response in stroke in vivo by sensing the enzyme myeloperoxidase. *Proc Natl Acad Sci U S A*. 105:18584-18589.

Breslow, D.K., and J.S. Weissman. 2010. Membranes in balance: mechanisms of sphingolipid homeostasis. *Mol Cell*. 40:267-279.

Brown, A.M., J. Skamarauskas, T. Lister, A. Madjd, and D.E. Ray. 2011. Differential susceptibility of astrocytic and neuronal function to 3-chloropropanediol in the rat inferior colliculus. *J Neurochem*. 116:996-1004.

Brown, D.A., and J.K. Rose. 1992. Sorting of GPI-anchored proteins to glycolipid-enriched membrane subdomains during transport to the apical cell surface. *Cell*. 68:533-544.

Camoletto, P.G., H. Vara, L. Morando, E. Connell, F.P. Marletto, M. Giustetto, M. Sassoe-Pognetto, P.P. Van Veldhoven, and M.D. Ledesma. 2009. Synaptic vesicle docking: sphingosine regulates syntaxin1 interaction with Munc18. *PLoS One*. 4:e5310.

Carr, A.C., J.J. van den Berg, and C.C. Winterbourn. 1996. Chlorination of cholesterol in cell membranes by hypochlorous acid. *Arch Biochem Biophys*. 332:63-69.

Carr, A.C., M.C. Vissers, N.M. Domigan, and C.C. Winterbourn. 1997a. Modification of red cell membrane lipids by hypochlorous acid and haemolysis by preformed lipid chlorohydrins. *Redox Rep*. 3:263-271.

Carr, A.C., C.C. Winterbourn, J.W. Blunt, A.J. Phillips, and A.D. Abell. 1997b. Nuclear magnetic resonance characterization of 6 alpha-chloro-5 beta-cholestane-3 beta,5-diol formed from the reaction of hypochlorous acid with cholesterol. *Lipids*. 32:363-367.

Chalfant, C.E., K. Rathman, R.L. Pinkerman, R.E. Wood, L.M. Obeid, B. Ogretmen, and Y.A. Hannun. 2002. De novo ceramide regulates the alternative splicing of caspase 9 and Bcl-x in A549 lung adenocarcinoma cells. Dependence on protein phosphatase-1. *J Biol Chem*. 277:12587-12595.

Chang, M.K., C.J. Binder, Y.I. Miller, G. Subbanagounder, G.J. Silverman, J.A. Berliner, and J.L. Witztum. 2004. Apoptotic cells with oxidation-specific epitopes are immunogenic and proinflammatory. *J Exp Med*. 200:1359-1370.

Charruyer, A., S. Grazide, C. Bezombes, S. Muller, G. Laurent, and J.P. Jaffrezou. 2005. UV-C light induces raft-associated acid sphingomyelinase and JNK activation and translocation independently on a nuclear signal. *J Biol Chem*. 280:19196-19204.

Chatterjee, S. 1999. Neutral sphingomyelinase: past, present and future. *Chem Phys Lipids*. 102:79-96.

Chen, J., J.L. Mehta, N. Haider, X. Zhang, J. Narula, and D. Li. 2004. Role of caspases in Ox-LDL-induced apoptotic cascade in human coronary artery endothelial cells. *Circ Res*. 94:370-376.

Chen, J.W., M.O. Breckwoldt, E. Aikawa, G. Chiang, and R. Weissleder. 2008. Myeloperoxidase-targeted imaging of active inflammatory lesions in murine experimental autoimmune encephalomyelitis. *Brain*. 131:1123-1133.

Chen, M.J., Y.W. Yap, M.S. Choy, C.H. Koh, S.J. Seet, W. Duan, M. Whiteman, and N.S. Cheung. 2006. Early induction of calpains in rotenone-mediated neuronal apoptosis. *Neurosci Lett*. 397:69-73.

Chen, R., L. Yang, and T.M. McIntyre. 2007. Cytotoxic phospholipid oxidation products. Cell death from mitochondrial damage and the intrinsic caspase cascade. *J Biol Chem*. 282:24842-24850.

Chen, Y., Y. Liu, M.C. Sullards, and A.H. Merrill, Jr. 2010. An introduction to sphingolipid metabolism and analysis by new technologies. *Neuromolecular Med*. 12:306-319.

Choi, D.K., S. Pennathur, C. Perier, K. Tieu, P. Teismann, D.C. Wu, V. Jackson-Lewis, M. Vila, J.P. Vonsattel, J.W. Heinecke, and S. Przedborski. 2005. Ablation of the inflammatory enzyme myeloperoxidase mitigates features of Parkinson's disease in mice. *J Neurosci*. 25:6594-6600.

Choudhury, A., M. Dominguez, V. Puri, D.K. Sharma, K. Narita, C.L. Wheatley, D.L. Marks, and R.E. Pagano. 2002. Rab proteins mediate Golgi transport of caveola-internalized glycosphingolipids and correct lipid trafficking in Niemann-Pick C cells. *J Clin Invest*. 109:1541-1550.

Cibelli, G., P. Corsi, G. Diana, F. Vitiello, and G. Thiel. 2001. Corticotropin-releasing factor triggers neurite outgrowth of a catecholaminergic immortalized neuron via cAMP and MAP kinase signalling pathways. *Eur J Neurosci*. 13:1339-1348.

Clarke, C.J., T.G. Truong, and Y.A. Hannun. 2007. Role for neutral sphingomyelinase-2 in tumor necrosis factor alpha-stimulated expression of vascular cell adhesion molecule-1 (VCAM) and intercellular adhesion molecule-1 (ICAM) in lung epithelial cells: p38 MAPK is an upstream regulator of nSMase2. *J Biol Chem*. 282:1384-1396.

Claus, R.A., A.C. Bunck, C.L. Bockmeyer, F.M. Brunkhorst, W. Losche, R. Kinscherf, and H.P. Deigner. 2005. Role of increased sphingomyelinase activity in apoptosis and organ failure of patients with severe sepsis. *FASEB J*. 19:1719-1721.

Claus, R.A., M.J. Dorer, A.C. Bunck, and H.P. Deigner. 2009. Inhibition of sphingomyelin hydrolysis: targeting the lipid mediator ceramide as a key regulator of cellular fate. *Curr Med Chem*. 16:1978-2000.

Coetzee, T., N. Fujita, J. Dupree, R. Shi, A. Blight, K. Suzuki, and B. Popko. 1996. Myelination in the absence of galactocerebroside and sulfatide: normal structure with abnormal function and regional instability. *Cell*. 86:209-219.

Cohen, G.M. 1997. Caspases: the executioners of apoptosis. *Biochem J*. 326 (Pt 1):1-16.

Colombini, M. 2010. Ceramide channels and their role in mitochondria-mediated apoptosis. *Biochim Biophys Acta*. 1797:1239-1244.

Cuvillier, O., D.S. Rosenthal, M.E. Smulson, and S. Spiegel. 1998. Sphingosine 1-phosphate inhibits activation of caspases that cleave poly(ADP-ribose) polymerase and lamins during Fas- and ceramide-mediated apoptosis in Jurkat T lymphocytes. *J Biol Chem*. 273:2910-2916.

Darroch, P.I., A. Dagan, T. Granot, X. He, S. Gatt, and E.H. Schuchman. 2005. A lipid analogue that inhibits sphingomyelin hydrolysis and synthesis, increases ceramide, and leads to cell death. *J Lipid Res*. 46:2315-2324.

Daugherty, A., J.L. Dunn, D.L. Rateri, and J.W. Heinecke. 1994. Myeloperoxidase, a catalyst for lipoprotein oxidation, is expressed in human atherosclerotic lesions. *J Clin Invest*. 94:437-444.

Dbaibo, G.S., D.K. Perry, C.J. Gamard, R. Platt, G.G. Poirier, L.M. Obeid, and Y.A. Hannun. 1997. Cytokine response modifier A (CrmA) inhibits ceramide formation in response to tumor necrosis factor (TNF)-alpha: CrmA and Bcl-2 target distinct components in the apoptotic pathway. *J Exp Med*. 185:481-490.

de Vries, H., and D. Hoekstra. 2000. On the biogenesis of the myelin sheath: cognate polarized trafficking pathways in oligodendrocytes. *Glycoconj J*. 17:181-190.

Decraene, C., B. Brugg, M. Ruberg, E. Eveno, C. Matingou, F. Tahi, J. Mariani, C. Auffray, and G. Pietu. 2002. Identification of genes involved in ceramide-dependent neuronal apoptosis using cDNA arrays. *Genome Biol*. 3:RESEARCH0042.

Delgado, A., J. Casas, A. Llebaria, J.L. Abad, and G. Fabrias. 2007. Chemical tools to investigate sphingolipid metabolism and functions. *ChemMedChem*. 2:580-606.

Dever, G., L.J. Stewart, A.R. Pitt, and C.M. Spickett. 2003. Phospholipid chlorohydrins cause ATP depletion and toxicity in human myeloid cells. *FEBS Lett*. 540:245-250.

Dever, G., C.L. Wainwright, S. Kennedy, and C.M. Spickett. 2006. Fatty acid and phospholipid chlorohydrins cause cell stress and endothelial adhesion. *Acta Biochim Pol*. 53:761-768.

Dever, G.J., R. Benson, C.L. Wainwright, S. Kennedy, and C.M. Spickett. 2008. Phospholipid chlorohydrin induces leukocyte adhesion to ApoE-/- mouse arteries via upregulation of P-selectin. *Free Radic Biol Med*. 44:452-463.

Deveraux, Q.L., R. Takahashi, G.S. Salvesen, and J.C. Reed. 1997. X-linked IAP is a direct inhibitor of cell-death proteases. *Nature*. 388:300-304.

Di Ciano-Oliveira, C., A.C. Thirone, K. Szaszi, and A. Kapus. 2006. Osmotic stress and the cytoskeleton: the R(h)ole of Rho GTPases. *Acta Physiol (Oxf)*. 187:257-272.

Dickson, R.C., R.L. Lester, and M.M. Nagiec. 2000. Serine palmitoyltransferase. *Methods Enzymol*. 311:3-9.

Dickson, R.C., C. Sumanasekera, and R.L. Lester. 2006. Functions and metabolism of sphingolipids in Saccharomyces cerevisiae. *Prog Lipid Res*. 45:447-465.

Dobrowsky, R.T., G.M. Jenkins, and Y.A. Hannun. 1995. Neurotrophins induce sphingomyelin hydrolysis. Modulation by co-expression of p75NTR with Trk receptors. *J Biol Chem*. 270:22135-22142.

Dodelet-Devillers, A., R. Cayrol, J. van Horssen, A.S. Haqqani, H.E. de Vries, B. Engelhardt, J. Greenwood, and A. Prat. 2009. Functions of lipid raft membrane microdomains at the blood-brain barrier. *J Mol Med*. 87:765-774.

Doehner, W., A.C. Bunck, M. Rauchhaus, S. von Haehling, F.M. Brunkhorst, M. Cicoira, C. Tschope, P. Ponikowski, R.A. Claus, and S.D. Anker. 2007. Secretory sphingomyelinase is upregulated in chronic heart failure: a second messenger system of immune activation relates to body composition, muscular functional capacity, and peripheral blood flow. *Eur Heart J*. 28:821-828.

Domigan, N.M., T.S. Charlton, M.W. Duncan, C.C. Winterbourn, and A.J. Kettle. 1995. Chlorination of tyrosyl residues in peptides by myeloperoxidase and human neutrophils. *J Biol Chem*. 270:16542-16548.

Elmore, S. 2007. Apoptosis: a review of programmed cell death. *Toxicol Pathol*. 35:495-516.

Ermak, N., B. Lacour, T.B. Drueke, and S. Vicca. 2008. Role of reactive oxygen species and Bax in oxidized low density lipoprotein-induced apoptosis of human monocytes. *Atherosclerosis*. 200:247-256.

Erridge, C., and C.M. Spickett. 2007. Oxidised phospholipid regulation of Toll-like receptor signalling. *Redox Rep*. 12:76-80.

Farah, M.E., V. Sirotkin, B. Haarer, D. Kakhniashvili, and D.C. Amberg. 2011. Diverse protective roles of the actin cytoskeleton during oxidative stress. *Cytoskeleton (Hoboken)*. 68:340-354.

Flemmig, J., H. Spalteholz, K. Schubert, S. Meier, and J. Arnhold. 2009. Modification of phosphatidylserine by hypochlorous acid. *Chem Phys Lipids*. 161:44-50.

Folch, J., M. Lees, and G.H. Sloane Stanley. 1957. A simple method for the isolation and purification of total lipides from animal tissues. *J Biol Chem*. 226:497-509.

Formigli, L., L. Papucci, A. Tani, N. Schiavone, A. Tempestini, G.E. Orlandini, S. Capaccioli, and S.Z. Orlandini. 2000. Aponecrosis: morphological and biochemical exploration of a syncretic process of cell death sharing apoptosis and necrosis. *J Cell Physiol*. 182:41-49.

France-Lanord, V., B. Brugg, P.P. Michel, Y. Agid, and M. Ruberg. 1997. Mitochondrial free radical signal in ceramide-dependent apoptosis: a putative mechanism for neuronal death in Parkinson's disease. *J Neurochem*. 69:1612-1621.

Fruhwirth, G.O., A. Moumtzi, A. Loidl, E. Ingolic, and A. Hermetter. 2006. The oxidized phospholipids POVPC and PGPC inhibit growth and induce apoptosis in vascular smooth muscle cells. *Biochim Biophys Acta*. 1761:1060-1069.

Fu, X., D.M. Mueller, and J.W. Heinecke. 2002. Generation of intramolecular and intermolecular sulfenamides, sulfinamides, and sulfonamides by hypochlorous acid: a potential pathway for oxidative cross-linking of low-density lipoprotein by myeloperoxidase. *Biochemistry*. 41:1293-1301.

Funato, K., and H. Riezman. 2001. Vesicular and nonvesicular transport of ceramide from ER to the Golgi apparatus in yeast. *J Cell Biol*. 155:949-959.

Furtmuller, P.G., J. Arnhold, W. Jantschko, H. Pichler, and C. Obinger. 2003. Redox properties of the couples compound I/compound II and compound II/native enzyme of human myeloperoxidase. *Biochem Biophys Res Commun*. 301:551-557.

Furtmuller, P.G., U. Burner, W. Jantschko, G. Regelsberger, and C. Obinger. 2000. Two-electron reduction and one-electron oxidation of organic hydroperoxides by human myeloperoxidase. *FEBS Lett*. 484:139-143.

Gable, K., H. Slife, D. Bacikova, E. Monaghan, and T.M. Dunn. 2000. Tsc3p is an 80-amino acid protein associated with serine palmitoyltransferase and required for optimal enzyme activity. *J Biol Chem*. 275:7597-7603.

Galluzzi, L., and G. Kroemer. 2008. Necroptosis: a specialized pathway of programmed necrosis. *Cell*. 135:1161-1163.

Galvan, C., P.G. Camoletto, F. Cristofani, P.P. Van Veldhoven, and M.D. Ledesma. 2008. Anomalous surface distribution of glycosyl phosphatidyl inositol-anchored proteins in neurons lacking acid sphingomyelinase. *Mol Biol Cell*. 19:509-522.

Gatt, S. 1963. Enzymic Hydrolysis and Synthesis of Ceramides. *J Biol Chem*. 238:3131-3133.

Gault, C.R., L.M. Obeid, and Y.A. Hannun. 2010. An overview of sphingolipid metabolism: from synthesis to breakdown. *Adv Exp Med Biol*. 688:1-23.

Gaut, J.P., G.C. Yeh, H.D. Tran, J. Byun, J.P. Henderson, G.M. Richter, M.L. Brennan, A.J. Lusis, A. Belaaouaj, R.S. Hotchkiss, and J.W. Heinecke. 2001. Neutrophils employ the myeloperoxidase system to generate antimicrobial brominating and chlorinating oxidants during sepsis. *Proc Natl Acad Sci U S A*. 98:11961-11966.

Ghafourifar, P., S.D. Klein, O. Schucht, U. Schenk, M. Pruschy, S. Rocha, and C. Richter. 1999. Ceramide induces cytochrome c release from isolated mitochondria. Importance of mitochondrial redox state. *J Biol Chem*. 274:6080-6084.

Goll, D.E., V.F. Thompson, H. Li, W. Wei, and J. Cong. 2003. The calpain system. *Physiol Rev*. 83:731-801.

Goni, F.M., and A. Alonso. 2002. Sphingomyelinases: enzymology and membrane activity. *FEBS Lett*. 531:38-46.

Gorska, M., E. Baranczuk, and A. Dobrzyn. 2003. Secretory Zn2+-dependent sphingomyelinase activity in the serum of patients with type 2 diabetes is elevated. *Horm Metab Res*. 35:506-507.

Goti, D., Z. Balazs, U. Panzenboeck, A. Hrzenjak, H. Reicher, E. Wagner, R. Zechner, E. Malle, and W. Sattler. 2002. Effects of lipoprotein lipase on uptake and transcytosis of low density lipoprotein (LDL) and LDL-associated alpha-tocopherol in a porcine in vitro blood-brain barrier model. *J Biol Chem*. 277:28537-28544.

Graber, D., R. Salvayre, and T. Levade. 1994. Accurate Differentiation of Neuronopathic and Nonneuronopathic Forms of Niemann-Pick Disease by Evaluation of the Effective Residual Lysosomal Sphingomyelinase Activity in Intact-Cells. *Journal of Neurochemistry*. 63:1060-1068.

Gray, E., T.L. Thomas, S. Betmouni, N. Scolding, and S. Love. 2008a. Elevated activity and microglial expression of myeloperoxidase in demyelinated cerebral cortex in multiple sclerosis. *Brain Pathol*. 18:86-95.

Gray, E., T.L. Thomas, S. Betmouni, N. Scolding, and S. Love. 2008b. Elevated myeloperoxidase activity in white matter in multiple sclerosis. *Neurosci Lett*. 444:195-198.

Green, P.S., A.J. Mendez, J.S. Jacob, J.R. Crowley, W. Growdon, B.T. Hyman, and J.W. Heinecke. 2004. Neuronal expression of myeloperoxidase is increased in Alzheimer's disease. *J Neurochem*. 90:724-733.

Gudz, T.I., K.Y. Tserng, and C.L. Hoppel. 1997. Direct inhibition of mitochondrial respiratory chain complex III by cell-permeable ceramide. *J Biol Chem*. 272:24154-24158.

Gulbins, E., B. Brenner, K. Schlottmann, J. Welsch, H. Heinle, U. Koppenhoefer, O. Linderkamp, K.M. Coggeshall, and F. Lang. 1996. Fas-induced programmed cell death is mediated by a Ras-regulated O2- synthesis. *Immunology*. 89:205-212.

Gullberg, U., N. Bengtsson, E. Bulow, D. Garwicz, A. Lindmark, and I. Olsson. 1999. Processing and targeting of granule proteins in human neutrophils. *J Immunol Methods*. 232:201-210.

Halliwell, B. 2006. Oxidative stress and neurodegeneration: where are we now? *J Neurochem*. 97:1634-1658.

Halliwell, B., and M. Whiteman. 2004. Measuring reactive species and oxidative damage in vivo and in cell culture: how should you do it and what do the results mean? *Br J Pharmacol*. 142:231-255.

Hanada, K. 2003. Serine palmitoyltransferase, a key enzyme of sphingolipid metabolism. *Biochim Biophys Acta*. 1632:16-30.

Hanada, K., K. Kumagai, S. Yasuda, Y. Miura, M. Kawano, M. Fukasawa, and M. Nishijima. 2003. Molecular machinery for non-vesicular trafficking of ceramide. *Nature*. 426:803-809.

Hanada, K., M. Nishijima, T. Fujita, and S. Kobayashi. 2000. Specificity of inhibitors of serine palmitoyltransferase (SPT), a key enzyme in sphingolipid biosynthesis, in intact cells. A novel

evaluation system using an SPT-defective mammalian cell mutant. *Biochem Pharmacol*. 59:1211-1216.

Hannun, Y.A., and L.M. Obeid. 2008. Principles of bioactive lipid signalling: lessons from sphingolipids. *Nat Rev Mol Cell Biol*. 9:139-150.

Hansen, S.H., K. Sandvig, and B. van Deurs. 1993. Clathrin and HA2 adaptors: effects of potassium depletion, hypertonic medium, and cytosol acidification. *J Cell Biol*. 121:61-72.

Hansson, M., I. Olsson, and W.M. Nauseef. 2006. Biosynthesis, processing, and sorting of human myeloperoxidase. *Arch Biochem Biophys*. 445:214-224.

Harel, R., and A.H. Futerman. 1993. Inhibition of sphingolipid synthesis affects axonal outgrowth in cultured hippocampal neurons. *J Biol Chem*. 268:14476-14481.

Haughey, N.J., V.V. Bandaru, M. Bae, and M.P. Mattson. 2010. Roles for dysfunctional sphingolipid metabolism in Alzheimer's disease neuropathogenesis. *Biochim Biophys Acta*. 1801:878-886.

Hawkins, C.L., D.I. Pattison, and M.J. Davies. 2003. Hypochlorite-induced oxidation of amino acids, peptides and proteins. *Amino Acids*. 25:259-274.

Hazell, L.J., L. Arnold, D. Flowers, G. Waeg, E. Malle, and R. Stocker. 1996. Presence of hypochlorite-modified proteins in human atherosclerotic lesions. *J Clin Invest*. 97:1535-1544.

Hazen, S.L. 2008. Oxidized phospholipids as endogenous pattern recognition ligands in innate immunity. *J Biol Chem*. 283:15527-15531.

Hazen, S.L., and J.W. Heinecke. 1997. 3-Chlorotyrosine, a specific marker of myeloperoxidase-catalyzed oxidation, is markedly elevated in low density lipoprotein isolated from human atherosclerotic intima. *J Clin Invest*. 99:2075-2081.

Hazen, S.L., F.F. Hsu, K. Duffin, and J.W. Heinecke. 1996. Molecular chlorine generated by the myeloperoxidase-hydrogen peroxide-chloride system of phagocytes converts low density lipoprotein cholesterol into a family of chlorinated sterols. *J Biol Chem*. 271:23080-23088.

He, X., F. Chen, A. Dagan, S. Gatt, and E.H. Schuchman. 2003. A fluorescence-based, high-performance liquid chromatographic assay to determine acid sphingomyelinase activity and diagnose types A and B Niemann-Pick disease. *Anal Biochem*. 314:116-120.

Hedskog, L., S. Zhang, and M. Ankarcrona. 2011. Strategic Role for Mitochondria in Alzheimer's Disease and Cancer. *Antioxid Redox Signal*.

Heinecke, J.W., W. Li, D.M. Mueller, A. Bohrer, and J. Turk. 1994. Cholesterol chlorohydrin synthesis by the myeloperoxidase-hydrogen peroxide-chloride system: potential markers for lipoproteins oxidatively damaged by phagocytes. *Biochemistry*. 33:10127-10136.

Heinrich, M., M. Wickel, W. Schneider-Brachert, C. Sandberg, J. Gahr, R. Schwandner, T. Weber, P. Saftig, C. Peters, J. Brunner, M. Kronke, and S. Schutze. 1999. Cathepsin D targeted by acid sphingomyelinase-derived ceramide. *EMBO J*. 18:5252-5263.

Hill, M.M., C. Adrain, P.J. Duriez, E.M. Creagh, and S.J. Martin. 2004. Analysis of the composition, assembly kinetics and activity of native Apaf-1 apoptosomes. *EMBO J*. 23:2134-2145.

Hitomi, J., T. Katayama, M. Taniguchi, A. Honda, K. Imaizumi, and M. Tohyama. 2004. Apoptosis induced by endoplasmic reticulum stress depends on activation of caspase-3 via caspase-12. *Neurosci Lett*. 357:127-130.

Hofmann, K., S. Tomiuk, G. Wolff, and W. Stoffel. 2000. Cloning and characterization of the mammalian brain-specific, Mg2+-dependent neutral sphingomyelinase. *Proc Natl Acad Sci U S A*. 97:5895-5900.

Holthuis, J.C., T. Pomorski, R.J. Raggers, H. Sprong, and G. Van Meer. 2001. The organizing potential of sphingolipids in intracellular membrane transport. *Physiol Rev*. 81:1689-1723.

Hornemann, T., S. Richard, M.F. Rutti, Y. Wei, and A. von Eckardstein. 2006. Cloning and initial characterization of a new subunit for mammalian serine-palmitoyltransferase. *J Biol Chem*. 281:37275-37281.

Hoyer, A., H.J. Bardenheuer, E. Martin, and K. Plaschke. 2005. Amyloid precursor protein (APP) and its derivatives change after cellular energy depletion. An in vitro-study. *J Neural Transm*. 112:239-253.

Hrzenjak, A., F. Moinfar, M.L. Kremser, B. Strohmeier, P.B. Staber, K. Zatloukal, and H. Denk. 2006. Valproate inhibition of histone deacetylase 2 affects differentiation and decreases proliferation of endometrial stromal sarcoma cells. *Mol Cancer Ther*. 5:2203-2210.

Huang, H., C.A. Joazeiro, E. Bonfoco, S. Kamada, J.D. Leverson, and T. Hunter. 2000. The inhibitor of apoptosis, cIAP2, functions as a ubiquitin-protein ligase and promotes in vitro monoubiquitination of caspases 3 and 7. *J Biol Chem*. 275:26661-26664.

Huitema, K., J. van den Dikkenberg, J.F. Brouwers, and J.C. Holthuis. 2004. Identification of a family of animal sphingomyelin synthases. *EMBO J*. 23:33-44.

Hurwitz, R., K. Ferlinz, G. Vielhaber, H. Moczall, and K. Sandhoff. 1994. Processing of human acid sphingomyelinase in normal and I-cell fibroblasts. *J Biol Chem*. 269:5440-5445.

Hutter, E., H. Unterluggauer, A. Garedew, P. Jansen-Durr, and E. Gnaiger. 2006. High-resolution respirometry--a modern tool in aging research. *Exp Gerontol*. 41:103-109.

Igney, F.H., and P.H. Krammer. 2002. Death and anti-death: tumour resistance to apoptosis. *Nat Rev Cancer*. 2:277-288.

Ikonen, E. 2008. Cellular cholesterol trafficking and compartmentalization. *Nat Rev Mol Cell Biol*. 9:125-138.

Jacob, J.S., D.P. Cistola, F.F. Hsu, S. Muzaffar, D.M. Mueller, S.L. Hazen, and J.W. Heinecke. 1996. Human phagocytes employ the myeloperoxidase-hydrogen peroxide system to synthesize dityrosine, trityrosine, pulcherosine, and isodityrosine by a tyrosyl radical-dependent pathway. *J Biol Chem*. 271:19950-19956.

Jaffrezou, J.P., J.M. Herbert, T. Levade, M.N. Gau, P. Chatelain, and G. Laurent. 1991. Reversal of multidrug resistance by calcium channel blocker SR33557 without photoaffinity labeling of P-glycoprotein. *J Biol Chem*. 266:19858-19864.

Jana, A., and K. Pahan. 2004. Fibrillar amyloid-beta peptides kill human primary neurons via NADPH oxidase-mediated activation of neutral sphingomyelinase. Implications for Alzheimer's disease. *J Biol Chem*. 279:51451-51459.

Jana, A., and K. Pahan. 2010a. Fibrillar amyloid-beta-activated human astroglia kill primary human neurons via neutral sphingomyelinase: implications for Alzheimer's disease. *J Neurosci*. 30:12676-12689.

Jana, A., and K. Pahan. 2010b. Sphingolipids in multiple sclerosis. *Neuromolecular Med*. 12:351-361.

Jana, M., C.A. Palencia, and K. Pahan. 2008. Fibrillar amyloid-beta peptides activate microglia via TLR2: implications for Alzheimer's disease. *J Immunol*. 181:7254-7262.

Jantschko, W., P. Georg Furtmuller, M. Zederbauer, M. Lanz, C. Jakopitsch, and C. Obinger. 2003. Direct conversion of ferrous myeloperoxidase to compound II by hydrogen peroxide: an anaerobic stopped-flow study. *Biochem Biophys Res Commun*. 312:292-298.

Jelks, K.B., and M.G. Miller. 2001. alpha-Chlorohydrin inhibits glyceraldehyde-3-phosphate dehydrogenase in multiple organs as well as in sperm. *Toxicol Sci*. 62:115-123.

Jennemann, R., R. Sandhoff, L. Langbein, S. Kaden, U. Rothermel, H. Gallala, K. Sandhoff, H. Wiegandt, and H.J. Grone. 2007. Integrity and barrier function of the epidermis critically depend on glucosylceramide synthesis. *J Biol Chem*. 282:3083-3094.

Jennemann, R., R. Sandhoff, S. Wang, E. Kiss, N. Gretz, C. Zuliani, A. Martin-Villalba, R. Jager, H. Schorle, M. Kenzelmann, M. Bonrouhi, H. Wiegandt, and H.J. Grone. 2005. Cell-specific deletion of glucosylceramide synthase in brain leads to severe neural defects after birth. *Proc Natl Acad Sci U S A*. 102:12459-12464.

Jiang, X., and X. Wang. 2004. Cytochrome C-mediated apoptosis. *Annu Rev Biochem*. 73:87-106.

Johnson, K.R., W.M. Nauseef, A. Care, M.J. Wheelock, S. Shane, S. Hudson, H.P. Koeffler, M. Selsted, C. Miller, and G. Rovera. 1987. Characterization of cDNA clones for human myeloperoxidase: predicted amino acid sequence and evidence for multiple mRNA species. *Nucleic Acids Res*. 15:2013-2028.

Jourdain, A., and J.C. Martinou. 2009. Mitochondrial outer-membrane permeabilization and remodelling in apoptosis. *Int J Biochem Cell Biol*. 41:1884-1889.

Kagan, V.E., G.G. Borisenko, Y.Y. Tyurina, V.A. Tyurin, J. Jiang, A.I. Potapovich, V. Kini, A.A. Amoscato, and Y. Fujii. 2004. Oxidative lipidomics of apoptosis: redox catalytic interactions of cytochrome c with cardiolipin and phosphatidylserine. *Free Radic Biol Med*. 37:1963-1985.

Kagan, V.E., V.A. Tyurin, J. Jiang, Y.Y. Tyurina, V.B. Ritov, A.A. Amoscato, A.N. Osipov, N.A. Belikova, A.A. Kapralov, V. Kini, Vlasova, II, Q. Zhao, M. Zou, P. Di, D.A. Svistunenko, I.V. Kurnikov, and G.G. Borisenko. 2005. Cytochrome c acts as a cardiolipin oxygenase required for release of proapoptotic factors. *Nat Chem Biol*. 1:223-232.

Kalyankrishna, S., J.H. Parmentier, and K.U. Malik. 2002. Arachidonic acid-derived oxidation products initiate apoptosis in vascular smooth muscle cells. *Prostaglandins Other Lipid Mediat*. 70:13-29.

Kanety, H., R. Hemi, M.Z. Papa, and A. Karasik. 1996. Sphingomyelinase and ceramide suppress insulin-induced tyrosine phosphorylation of the insulin receptor substrate-1. *J Biol Chem*. 271:9895-9897.

Karasawa, K., X. Qiu, and T. Lee. 1999. Purification and characterization from rat kidney membranes of a novel platelet-activating factor (PAF)-dependent transacetylase that catalyzes the hydrolysis of PAF, formation of PAF analogs, and C2-ceramide. *J Biol Chem*. 274:8655-8661.

Kashkar, H., K. Wiegmann, B. Yazdanpanah, D. Haubert, and M. Kronke. 2005. Acid sphingomyelinase is indispensable for UV light-induced Bax conformational change at the mitochondrial membrane. *J Biol Chem*. 280:20804-20813.

Kasischke, K.A., H.D. Vishwasrao, P.J. Fisher, W.R. Zipfel, and W.W. Webb. 2004. Neural activity triggers neuronal oxidative metabolism followed by astrocytic glycolysis. *Science*. 305:99-103.

Kawai, Y., H. Kiyokawa, Y. Kimura, Y. Kato, K. Tsuchiya, and J. Terao. 2006. Hypochlorous acid-derived modification of phospholipids: characterization of aminophospholipids as regulatory molecules for lipid peroxidation. *Biochemistry*. 45:14201-14211.

Kilkus, J., R. Goswami, F.D. Testai, and G. Dawson. 2003. Ceramide in rafts (detergent-insoluble fraction) mediates cell death in neurotumor cell lines. *J Neurosci Res*. 72:65-75.

Kilkus, J.P., R. Goswami, S.A. Dawson, F.D. Testai, E.V. Berdyshev, X. Han, and G. Dawson. 2008. Differential regulation of sphingomyelin synthesis and catabolism in oligodendrocytes and neurons. *J Neurochem*. 106:1745-1757.

Kim, W.J., R.A. Okimoto, L.E. Purton, M. Goodwin, S.M. Haserlat, F. Dayyani, D.A. Sweetser, A.I. McClatchey, O.A. Bernard, A.T. Look, D.W. Bell, D.T. Scadden, and D.A. Haber. 2008. Mutations in the neutral sphingomyelinase gene SMPD3 implicate the ceramide pathway in human leukemias. *Blood*. 111:4716-4722.

Kinkade, J.M., Jr., S.O. Pember, K.C. Barnes, R. Shapira, J.K. Spitznagel, and L.E. Martin. 1983. Differential distribution of distinct forms of myeloperoxidase in different azurophilic granule subpopulations from human neutrophils. *Biochem Biophys Res Commun*. 114:296-303.

Klebanoff, S.J. 1967. Iodination of bacteria: a bactericidal mechanism. *J Exp Med*. 126:1063-1078.

Klebanoff, S.J. 1968. Myeloperoxidase-halide-hydrogen peroxide antibacterial system. *J Bacteriol*. 95:2131-2138.

Klebanoff, S.J. 2005. Myeloperoxidase: friend and foe. *J Leukoc Biol*. 77:598-625.

Klebanoff, S.J., W.H. Clem, and R.G. Luebke. 1966. The peroxidase-thiocyanate-hydrogen peroxide antimicrobial system. *Biochim Biophys Acta*. 117:63-72.

Klebanoff, S.J., and F. Kazazi. 1995. Inactivation of human immunodeficiency virus type 1 by the amine oxidase-peroxidase system. *J Clin Microbiol*. 33:2054-2057.

Knott, A.B., G. Perkins, R. Schwarzenbacher, and E. Bossy-Wetzel. 2008. Mitochondrial fragmentation in neurodegeneration. *Nat Rev Neurosci*. 9:505-518.

Koch, C. 1974. Effect of sodium azide upon normal and pathological granulocyte function. *Acta Pathol Microbiol Scand B Microbiol Immunol*. 82:136-142.

Koivusalo, M., M. Jansen, P. Somerharju, and E. Ikonen. 2007. Endocytic trafficking of sphingomyelin depends on its acyl chain length. *Mol Biol Cell*. 18:5113-5123.

Kok, J.W., T. Babia, K. Klappe, and D. Hoekstra. 1995. Fluorescent, short-chain C6-NBD-sphingomyelin, but not C6-NBD-glucosylceramide, is subject to extensive degradation in the plasma membrane: implications for signal transduction related to cell differentiation. *Biochem J*. 309 (Pt 3):905-912.

Kolter, T., and K. Sandhoff. 2006. Sphingolipid metabolism diseases. *Biochim Biophys Acta*. 1758:2057-2079.

Kondo, T., T. Kitano, K. Iwai, M. Watanabe, Y. Taguchi, T. Yabu, H. Umehara, N. Domae, T. Uchiyama, and T. Okazaki. 2002. Control of ceramide-induced apoptosis by IGF-1: involvement of PI-3 kinase, caspase-3 and catalase. *Cell Death Differ*. 9:682-692.

Kornhuber, J., P. Tripal, M. Reichel, L. Terfloth, S. Bleich, J. Wiltfang, and E. Gulbins. 2008. Identification of new functional inhibitors of acid sphingomyelinase using a structure-property-activity relation model. *J Med Chem*. 51:219-237.

Koval, M., and R.E. Pagano. 1989. Lipid recycling between the plasma membrane and intracellular compartments: transport and metabolism of fluorescent sphingomyelin analogues in cultured fibroblasts. *J Cell Biol*. 108:2169-2181.

Koval, M., and R.E. Pagano. 1991. Intracellular transport and metabolism of sphingomyelin. *Biochim Biophys Acta*. 1082:113-125.

Kratzer, I., K. Wernig, U. Panzenboeck, E. Bernhart, H. Reicher, R. Wronski, M. Windisch, A. Hammer, E. Malle, A. Zimmer, and W. Sattler. 2007. Apolipoprotein A-I coating of protamine-oligonucleotide nanoparticles increases particle uptake and transcytosis in an in vitro model of the blood-brain barrier. *J Control Release*. 117:301-311.

Kroemer, G., and J.C. Reed. 2000. Mitochondrial control of cell death. *Nat Med*. 6:513-519.

Kroesen, B.J., S. Jacobs, B.J. Pettus, H. Sietsma, J.W. Kok, Y.A. Hannun, and L.F. de Leij. 2003. BcR-induced apoptosis involves differential regulation of C16 and C24-ceramide formation and sphingolipid-dependent activation of the proteasome. *J Biol Chem*. 278:14723-14731.

Kubbutat, M.H., and K.H. Vousden. 1997. Proteolytic cleavage of human p53 by calpain: a potential regulator of protein stability. *Mol Cell Biol*. 17:460-468.

Kudo, N., K. Kumagai, N. Tomishige, T. Yamaji, S. Wakatsuki, M. Nishijima, K. Hanada, and R. Kato. 2008. Structural basis for specific lipid recognition by CERT responsible for nonvesicular trafficking of ceramide. *Proc Natl Acad Sci U S A*. 105:488-493.

Kuerschner, L., C.S. Ejsing, K. Ekroos, A. Shevchenko, K.I. Anderson, and C. Thiele. 2005. Polyene-lipids: a new tool to image lipids. *Nat Methods*. 2:39-45.

Kumagai, K., M. Kawano, F. Shinkai-Ouchi, M. Nishijima, and K. Hanada. 2007. Interorganelle trafficking of ceramide is regulated by phosphorylation-dependent cooperativity between the PH and START domains of CERT. *J Biol Chem*. 282:17758-17766.

Kwak, D.H., K. Yu, S.M. Kim, D.H. Lee, J.U. Jung, J.W. Seo, N. Kim, S. Lee, K.Y. Jung, H.K. You, H.A. Kim, and Y.K. Choo. 2006. Dynamic changes of gangliosides expression during the differentiation of embryonic and mesenchymal stem cells into neural cells. *Exp Mol Med*. 38:668-676.

Lahiri, S., and A.H. Futerman. 2005. LASS5 is a bona fide dihydroceramide synthase that selectively utilizes palmitoyl-CoA as acyl donor. *J Biol Chem*. 280:33735-33738.

Lannert, H., C. Bunning, D. Jeckel, and F.T. Wieland. 1994. Lactosylceramide is synthesized in the lumen of the Golgi apparatus. *FEBS Lett*. 342:91-96.

Laviad, E.L., L. Albee, I. Pankova-Kholmyansky, S. Epstein, H. Park, A.H. Merrill, Jr., and A.H. Futerman. 2008. Characterization of ceramide synthase 2: tissue distribution, substrate specificity, and inhibition by sphingosine 1-phosphate. *J Biol Chem*. 283:5677-5684.

Lavrik, I.N., A. Golks, and P.H. Krammer. 2005. Caspases: pharmacological manipulation of cell death. *J Clin Invest*. 115:2665-2672.

Ledesma, M.D., B. Brugger, C. Bunning, F.T. Wieland, and C.G. Dotti. 1999. Maturation of the axonal plasma membrane requires upregulation of sphingomyelin synthesis and formation of protein-lipid complexes. *EMBO J*. 18:1761-1771.

Lehrer, R.I. 1971. Inhibition by sulfonamides of the candidacidal activity of human neutrophils. *J Clin Invest*. 50:2498-2505.

Leininger-Muller, B., A. Hoy, B. Herbeth, M. Pfister, J.M. Serot, M. Stavljenic-Rukavina, L. Massana, P. Passmore, G. Siest, and S. Visvikis. 2003. Myeloperoxidase G-463A polymorphism and Alzheimer's disease in the ApoEurope study. *Neurosci Lett*. 349:95-98.

Levade, T., F. Vidal, S. Vermeersch, N. Andrieu, S. Gatt, and R. Salvayre. 1995. Degradation of fluorescent and radiolabelled sphingomyelins in intact cells by a non-lysosomal pathway. *Biochim Biophys Acta*. 1258:277-287.

Levy, M., S.S. Castillo, and T. Goldkorn. 2006. nSMase2 activation and trafficking are modulated by oxidative stress to induce apoptosis. *Biochem Biophys Res Commun*. 344:900-905.

Li, J., B. Lee, and A.S. Lee. 2006. Endoplasmic reticulum stress-induced apoptosis: multiple pathways and activation of p53-up-regulated modulator of apoptosis (PUMA) and NOXA by p53. *J Biol Chem*. 281:7260-7270.

Lin, M.T., and M.F. Beal. 2006. Mitochondrial dysfunction and oxidative stress in neurodegenerative diseases. *Nature*. 443:787-795.

Lin, S.S., M.C. Bassik, H. Suh, M. Nishino, J.D. Arroyo, W.C. Hahn, S.J. Korsmeyer, and T.M. Roberts. 2006. PP2A regulates BCL-2 phosphorylation and proteasome-mediated degradation at the endoplasmic reticulum. *J Biol Chem*. 281:23003-23012.

Lin, W.C., C.F. Lin, C.L. Chen, C.W. Chen, and Y.S. Lin. 2011. Inhibition of neutrophil apoptosis via sphingolipid signaling in acute lung injury. *J Pharmacol Exp Ther*. 339:45-53.

Linardic, C.M., and Y.A. Hannun. 1994. Identification of a distinct pool of sphingomyelin involved in the sphingomyelin cycle. *J Biol Chem*. 269:23530-23537.

Linke, T., G. Wilkening, S. Lansmann, H. Moczall, O. Bartelsen, J. Weisgerber, and K. Sandhoff. 2001a. Stimulation of acid sphingomyelinase activity by lysosomal lipids and sphingolipid activator proteins. *Biol Chem*. 382:283-290.

Linke, T., G. Wilkening, F. Sadeghlar, H. Mozcall, K. Bernardo, E. Schuchman, and K. Sandhoff. 2001b. Interfacial regulation of acid ceramidase activity. Stimulation of ceramide degradation by lysosomal lipids and sphingolipid activator proteins. *J Biol Chem*. 276:5760-5768.

Liston, P., W.G. Fong, and R.G. Korneluk. 2003. The inhibitors of apoptosis: there is more to life than Bcl2. *Oncogene*. 22:8568-8580.

Locksley, R.M., N. Killeen, and M.J. Lenardo. 2001. The TNF and TNF receptor superfamilies: integrating mammalian biology. *Cell*. 104:487-501.

Loidl, A., R. Claus, H.P. Deigner, and A. Hermetter. 2002. High-precision fluorescence assay for sphingomyelinase activity of isolated enzymes and cell lysates. *J Lipid Res*. 43:815-823.

Loidl, A., E. Sevcsik, G. Riesenhuber, H.P. Deigner, and A. Hermetter. 2003. Oxidized phospholipids in minimally modified low density lipoprotein induce apoptotic signaling via activation of acid sphingomyelinase in arterial smooth muscle cells. *J Biol Chem*. 278:32921-32928.

Luberto, C., D.F. Hassler, P. Signorelli, Y. Okamoto, H. Sawai, E. Boros, D.J. Hazen-Martin, L.M. Obeid, Y.A. Hannun, and G.K. Smith. 2002. Inhibition of tumor necrosis factor-induced cell death in MCF7 by a novel inhibitor of neutral sphingomyelinase. *J Biol Chem*. 277:41128-41139.

Luo, X., I. Budihardjo, H. Zou, C. Slaughter, and X. Wang. 1998. Bid, a Bcl2 interacting protein, mediates cytochrome c release from mitochondria in response to activation of cell surface death receptors. *Cell*. 94:481-490.

Ly, J.D., D.R. Grubb, and A. Lawen. 2003. The mitochondrial membrane potential (deltapsi(m)) in apoptosis; an update. *Apoptosis*. 8:115-128.

Lynch, N.J., C.L. Willis, C.C. Nolan, S. Roscher, M.J. Fowler, E. Weihe, D.E. Ray, and W.J. Schwaeble. 2004. Microglial activation and increased synthesis of complement component C1q precedes blood-brain barrier dysfunction in rats. *Mol Immunol*. 40:709-716.

Maceyka, M., S. Milstien, and S. Spiegel. 2009. Sphingosine-1-phosphate: the Swiss army knife of sphingolipid signaling. *J Lipid Res*. 50 Suppl:S272-276.

Maceyka, M., H. Sankala, N.C. Hait, H. Le Stunff, H. Liu, R. Toman, C. Collier, M. Zhang, L.S. Satin, A.H. Merrill, Jr., S. Milstien, and S. Spiegel. 2005. SphK1 and SphK2, sphingosine kinase isoenzymes with opposing functions in sphingolipid metabolism. *J Biol Chem*. 280:37118-37129.

Majno, G., and I. Joris. 1995. Apoptosis, oncosis, and necrosis. An overview of cell death. *Am J Pathol*. 146:3-15.

Maki, R.A., V.A. Tyurin, R.C. Lyon, R.L. Hamilton, S.T. DeKosky, V.E. Kagan, and W.F. Reynolds. 2009. Aberrant expression of myeloperoxidase in astrocytes promotes phospholipid oxidation and memory deficits in a mouse model of Alzheimer disease. *J Biol Chem*. 284:3158-3169.

Malle, E., P.G. Furtmuller, W. Sattler, and C. Obinger. 2007. Myeloperoxidase: a target for new drug development? *Br J Pharmacol*. 152:838-854.

Malle, E., L. Hazell, R. Stocker, W. Sattler, H. Esterbauer, and G. Waeg. 1995. Immunologic detection and measurement of hypochlorite-modified LDL with specific monoclonal antibodies. *Arterioscler Thromb Vasc Biol*. 15:982-989.

Malle, E., G. Marsche, J. Arnhold, and M.J. Davies. 2006. Modification of low-density lipoprotein by myeloperoxidase-derived oxidants and reagent hypochlorous acid. *Biochim Biophys Acta*. 1761:392-415.

Mandon, E.C., I. Ehses, J. Rother, G. van Echten, and K. Sandhoff. 1992. Subcellular localization and membrane topology of serine palmitoyltransferase, 3-dehydrosphinganine reductase, and sphinganine N-acyltransferase in mouse liver. *J Biol Chem*. 267:11144-11148.

Manes, S., E. Mira, C. Gomez-Mouton, R.A. Lacalle, P. Keller, J.P. Labrador, and A.C. Martinez. 1999. Membrane raft microdomains mediate front-rear polarity in migrating cells. *EMBO J*. 18:6211-6220.

Manes, S., and A. Viola. 2006. Lipid rafts in lymphocyte activation and migration. *Mol Membr Biol*. 23:59-69.

Marchesini, N., and Y.A. Hannun. 2004. Acid and neutral sphingomyelinases: roles and mechanisms of regulation. *Biochem Cell Biol*. 82:27-44.

Marchesini, N., C. Luberto, and Y.A. Hannun. 2003. Biochemical properties of mammalian neutral sphingomyelinase 2 and its role in sphingolipid metabolism. *J Biol Chem*. 278:13775-13783.

Marchesini, N., W. Osta, J. Bielawski, C. Luberto, L.M. Obeid, and Y.A. Hannun. 2004. Role for mammalian neutral sphingomyelinase 2 in confluence-induced growth arrest of MCF7 cells. *J Biol Chem*. 279:25101-25111.

Marik, C., P.A. Felts, J. Bauer, H. Lassmann, and K.J. Smith. 2007. Lesion genesis in a subset of patients with multiple sclerosis: a role for innate immunity? *Brain*. 130:2800-2815.

Marks, D.L., R. Bittman, and R.E. Pagano. 2008. Use of Bodipy-labeled sphingolipid and cholesterol analogs to examine membrane microdomains in cells. *Histochem Cell Biol*. 130:819-832.

Marsche, G., R. Heller, G. Fauler, A. Kovacevic, A. Nuszkowski, W. Graier, W. Sattler, and E. Malle. 2004. 2-chlorohexadecanal derived from hypochlorite-modified high-density lipoprotein-associated plasmalogen is a natural inhibitor of endothelial nitric oxide biosynthesis. *Arterioscler Thromb Vasc Biol*. 24:2302-2306.

Marsche, G., R. Zimmermann, S. Horiuchi, N.N. Tandon, W. Sattler, and E. Malle. 2003. Class B scavenger receptors CD36 and SR-BI are receptors for hypochlorite-modified low density lipoprotein. *J Biol Chem*. 278:47562-47570.

Martinon, F., and J. Tschopp. 2007. Inflammatory caspases and inflammasomes: master switches of inflammation. *Cell Death Differ*. 14:10-22.

Mathias, S., A. Younes, C.C. Kan, I. Orlow, C. Joseph, and R.N. Kolesnick. 1993. Activation of the sphingomyelin signaling pathway in intact EL4 cells and in a cell-free system by IL-1 beta. *Science*. 259:519-522.

McCollister, B.D., J.T. Myers, J. Jones-Carson, D.R. Voelker, and A. Vazquez-Torres. 2007. Constitutive acid sphingomyelinase enhances early and late macrophage killing of Salmonella enterica serovar Typhimurium. *Infect Immun*. 75:5346-5352.

McGovern, M.M., and E.H. Schuchman. 1993. Acid Sphingomyelinase Deficiency.

Merrill, A.H., Jr. 2002. De novo sphingolipid biosynthesis: a necessary, but dangerous, pathway. *J Biol Chem*. 277:25843-25846.

Messner, M.C., C.J. Albert, F.F. Hsu, and D.A. Ford. 2006. Selective plasmenylcholine oxidation by hypochlorous acid: formation of lysophosphatidylcholine chlorohydrins. *Chem Phys Lipids*. 144:34-44.

Michel, C., G. van Echten-Deckert, J. Rother, K. Sandhoff, E. Wang, and A.H. Merrill, Jr. 1997. Characterization of ceramide synthesis. A dihydroceramide desaturase introduces the 4,5-trans-double bond of sphingosine at the level of dihydroceramide. *J Biol Chem*. 272:22432-22437.

Milhas, D., C.J. Clarke, and Y.A. Hannun. 2010. Sphingomyelin metabolism at the plasma membrane: implications for bioactive sphingolipids. *FEBS Lett*. 584:1887-1894.

Miljkovic-Lolic, M., R. Silbergleit, G. Fiskum, and R.E. Rosenthal. 2003. Neuroprotective effects of hyperbaric oxygen treatment in experimental focal cerebral ischemia are associated with reduced brain leukocyte myeloperoxidase activity. *Brain Res*. 971:90-94.

Mimeault, M., R. Hauke, and S.K. Batra. 2008. Recent advances on the molecular mechanisms involved in the drug resistance of cancer cells and novel targeting therapies. *Clin Pharmacol Ther*. 83:673-691.

Miranda, L., S. Carpentier, A. Platek, N. Hussain, M.A. Gueuning, D. Vertommen, Y. Ozkan, B. Sid, L. Hue, P.J. Courtoy, M.H. Rider, and S. Horman. 2010. AMP-activated protein kinase induces actin cytoskeleton reorganization in epithelial cells. *Biochem Biophys Res Commun*. 396:656-661.

Mizutani, Y., A. Kihara, and Y. Igarashi. 2005. Mammalian Lass6 and its related family members regulate synthesis of specific ceramides. *Biochem J*. 390:263-271.

Nagan, N., and R.A. Zoeller. 2001. Plasmalogens: biosynthesis and functions. *Prog Lipid Res*. 40:199-229.

Nagata, S. 1997. Apoptosis by death factor. *Cell*. 88:355-365.

Nagra, R.M., B. Becher, W.W. Tourtellotte, J.P. Antel, D. Gold, T. Paladino, R.A. Smith, J.R. Nelson, and W.F. Reynolds. 1997. Immunohistochemical and genetic evidence of myeloperoxidase involvement in multiple sclerosis. *J Neuroimmunol*. 78:97-107.

Nakagawa, T., H. Zhu, N. Morishima, E. Li, J. Xu, B.A. Yankner, and J. Yuan. 2000. Caspase-12 mediates endoplasmic-reticulum-specific apoptosis and cytotoxicity by amyloid-beta. *Nature*. 403:98-103.

Nakagawa, Y., M. Iinuma, T. Naoe, Y. Nozawa, and Y. Akao. 2007. Characterized mechanism of alpha-mangostin-induced cell death: caspase-independent apoptosis with release of endonuclease-G from mitochondria and increased miR-143 expression in human colorectal cancer DLD-1 cells. *Bioorg Med Chem*. 15:5620-5628.

Nara, F., M. Tanaka, T. Hosoya, K. Suzuki-Konagai, and T. Ogita. 1999. Scyphostatin, a neutral sphingomyelinase inhibitor from a discomycete, Trichopeziza mollissima: taxonomy of the producing organism, fermentation, isolation, and physico-chemical properties. *J Antibiot (Tokyo)*. 52:525-530.

Neumann, S., and G. van Meer. 2008. Sphingolipid management by an orchestra of lipid transfer proteins. *Biol Chem*. 389:1349-1360.

Neumeyer, J., C. Hallas, O. Merkel, S. Winoto-Morbach, M. Jakob, L. Thon, D. Adam, W. Schneider-Brachert, and S. Schutze. 2006. TNF-receptor I defective in internalization allows for cell death through activation of neutral sphingomyelinase. *Exp Cell Res*. 312:2142-2153.

Nichols, B.A., and D.F. Bainton. 1973. Differentiation of human monocytes in bone marrow and blood. Sequential formation of two granule populations. *Lab Invest*. 29:27-40.

Nicholson, D.W. 1999. Caspase structure, proteolytic substrates, and function during apoptotic cell death. *Cell Death Differ*. 6:1028-1042.

Niemela, P.S., M.T. Hyvonen, and I. Vattulainen. 2006. Influence of chain length and unsaturation on sphingomyelin bilayers. *Biophys J*. 90:851-863.

Nikolova-Karakashian, M., A. Karakashian, and K. Rutkute. 2008. Role of neutral sphingomyelinases in aging and inflammation. *Subcell Biochem*. 49:469-486.

Norbury, C.J., and B. Zhivotovsky. 2004. DNA damage-induced apoptosis. *Oncogene*. 23:2797-2808.

Norenberg, M.D., and K.V. Rao. 2007. The mitochondrial permeability transition in neurologic disease. *Neurochem Int*. 50:983-997.

Novgorodov, S.A., Z.M. Szulc, C. Luberto, J.A. Jones, J. Bielawski, A. Bielawska, Y.A. Hannun, and L.M. Obeid. 2005. Positively charged ceramide is a potent inducer of mitochondrial permeabilization. *J Biol Chem*. 280:16096-16105.

Nusshold, C., M. Kollroser, H. Kofeler, G. Rechberger, H. Reicher, A. Ullen, E. Bernhart, S. Waltl, I. Kratzer, A. Hermetter, H. Hackl, Z. Trajanoski, A. Hrzenjak, E. Malle, and W. Sattler. 2010. Hypochlorite modification of sphingomyelin generates chlorinated lipid species that induce apoptosis and proteome alterations in dopaminergic PC12 neurons in vitro. *Free Radic Biol Med*. 48:1588-1600.

O'Brien, J.S., and E.L. Sampson. 1965. Lipid composition of the normal human brain: gray matter, white matter, and myelin. *J Lipid Res*. 6:537-544.

Odell, E.W., and A.W. Segal. 1988. The bactericidal effects of the respiratory burst and the myeloperoxidase system isolated in neutrophil cytoplasts. *Biochim Biophys Acta*. 971:266-274.

Ogretmen, B., and Y.A. Hannun. 2004. Biologically active sphingolipids in cancer pathogenesis and treatment. *Nat Rev Cancer*. 4:604-616.

Okazaki, T., R.M. Bell, and Y.A. Hannun. 1989. Sphingomyelin turnover induced by vitamin D3 in HL-60 cells. Role in cell differentiation. *J Biol Chem*. 264:19076-19080.

Omae, F., M. Miyazaki, A. Enomoto, M. Suzuki, Y. Suzuki, and A. Suzuki. 2004. DES2 protein is responsible for phytoceramide biosynthesis in the mouse small intestine. *Biochem J*. 379:687-695.

Pagano, R.E., R. Watanabe, C. Wheatley, and C.S. Chen. 1999. Use of N-[5-(5,7-dimethyl boron dipyrromethene difluoride-sphingomyelin to study membrane traffic along the endocytic pathway. *Chem Phys Lipids*. 102:55-63.

Palmer, K.J., P. Watson, and D.J. Stephens. 2005. The role of microtubules in transport between the endoplasmic reticulum and Golgi apparatus in mammalian cells. *Biochem Soc Symp*:1-13.

Panasenko, O.M., T. Vakhrusheva, V. Tretyakov, H. Spalteholz, and J. Arnhold. 2007. Influence of chloride on modification of unsaturated phosphatidylcholines by the myeloperoxidase/hydrogen peroxide/bromide system. *Chem Phys Lipids*. 149:40-51.

Paris, F., Z. Fuks, A. Kang, P. Capodieci, G. Juan, D. Ehleiter, A. Haimovitz-Friedman, C. Cordon-Cardo, and R. Kolesnick. 2001. Endothelial apoptosis as the primary lesion initiating intestinal radiation damage in mice. *Science*. 293:293-297.

Park, S.Y., Y.H. Kim, and S.J. Lee. 2010. 1,3-Dichloro-2-propanol induces apoptosis via both calcium and ROS in mouse melanoma cells. *Biotechnol Lett*. 32:45-51.

Pastorino, J.G., M. Tafani, R.J. Rothman, A. Marcinkeviciute, J.B. Hoek, and J.L. Farber. 1999. Functional consequences of the sustained or transient activation by Bax of the mitochondrial permeability transition pore. *J Biol Chem*. 274:31734-31739.

Pattison, D.I., and M.J. Davies. 2001. Absolute rate constants for the reaction of hypochlorous acid with protein side chains and peptide bonds. *Chem Res Toxicol*. 14:1453-1464.

Pattison, D.I., and M.J. Davies. 2005. Kinetic analysis of the role of histidine chloramines in hypochlorous acid mediated protein oxidation. *Biochemistry*. 44:7378-7387.

Pattison, D.I., and M.J. Davies. 2006. Reactions of myeloperoxidase-derived oxidants with biological substrates: gaining chemical insight into human inflammatory diseases. *Curr Med Chem*. 13:3271-3290.

Pattison, D.I., C.L. Hawkins, and M.J. Davies. 2003. Hypochlorous acid-mediated oxidation of lipid components and antioxidants present in low-density lipoproteins: absolute rate constants, product analysis, and computational modeling. *Chem Res Toxicol*. 16:439-449.

Pattison, D.I., C.L. Hawkins, and M.J. Davies. 2009. What are the plasma targets of the oxidant hypochlorous acid? A kinetic modeling approach. *Chem Res Toxicol*. 22:807-817.

Pellerin, L., A.K. Bouzier-Sore, A. Aubert, S. Serres, M. Merle, R. Costalat, and P.J. Magistretti. 2007. Activity-dependent regulation of energy metabolism by astrocytes: an update. *Glia*. 55:1251-1262.

Pennathur, S., C. Bergt, B. Shao, J. Byun, S.Y. Kassim, P. Singh, P.S. Green, T.O. McDonald, J. Brunzell, A. Chait, J.F. Oram, K. O'Brien, R.L. Geary, and J.W. Heinecke. 2004. Human atherosclerotic intima and blood of patients with established coronary artery disease contain high density lipoprotein damaged by reactive nitrogen species. *J Biol Chem*. 279:42977-42983.

Peskin, A.V., and C.C. Winterbourn. 2001. Kinetics of the reactions of hypochlorous acid and amino acid chloramines with thiols, methionine, and ascorbate. *Free Radic Biol Med*. 30:572-579.

Peter, M.E., and P.H. Krammer. 2003. The CD95(APO-1/Fas) DISC and beyond. *Cell Death Differ*. 10:26-35.

Pewzner-Jung, Y., S. Ben-Dor, and A.H. Futerman. 2006. When do Lasses (longevity assurance genes) become CerS (ceramide synthases)?: Insights into the regulation of ceramide synthesis. *J Biol Chem*. 281:25001-25005.

Piccinini, M., F. Scandroglio, S. Prioni, B. Buccinna, N. Loberto, M. Aureli, V. Chigorno, E. Lupino, G. DeMarco, A. Lomartire, M.T. Rinaudo, S. Sonnino, and A. Prinetti. 2010. Deregulated sphingolipid metabolism and membrane organization in neurodegenerative disorders. *Mol Neurobiol*. 41:314-340.

Piccinotti, A., G. Benaglia, R. Bresciani, D. Zizioli, M. Presta, A. Preti, and S. Marchesini. 2000. Nerve growth factor induces sphingomyelin accumulation in pheochromocytoma cells. *FEBS Lett*. 472:143-147.

Pike, L.J. 2009. The challenge of lipid rafts. *J Lipid Res*. 50 Suppl:S323-328.

Pop, C., and G.S. Salvesen. 2009. Human caspases: activation, specificity, and regulation. *J Biol Chem*. 284:21777-21781.

Proskuryakov, S.Y., A.G. Konoplyannikov, and V.L. Gabai. 2003. Necrosis: a specific form of programmed cell death? *Exp Cell Res*. 283:1-16.

Prutz, W.A., R. Kissner, W.H. Koppenol, and H. Ruegger. 2000. On the irreversible destruction of reduced nicotinamide nucleotides by hypohalous acids. *Arch Biochem Biophys*. 380:181-191.

Puri, V., R. Watanabe, R.D. Singh, M. Dominguez, J.C. Brown, C.L. Wheatley, D.L. Marks, and R.E. Pagano. 2001. Clathrin-dependent and -independent internalization of plasma membrane sphingolipids initiates two Golgi targeting pathways. *J Cell Biol*. 154:535-547.

Pyne, S., and N.J. Pyne. 2000. Sphingosine 1-phosphate signalling in mammalian cells. *Biochem J*. 349:385-402.

Quarles, R.H. 2007. Myelin-associated glycoprotein (MAG): past, present and beyond. *J Neurochem*. 100:1431-1448.

Rajasekaran, S.A., L.G. Palmer, S.Y. Moon, A. Peralta Soler, G.L. Apodaca, J.F. Harper, Y. Zheng, and A.K. Rajasekaran. 2001. Na,K-ATPase activity is required for formation of tight junctions, desmosomes, and induction of polarity in epithelial cells. *Mol Biol Cell*. 12:3717-3732.

Ramstedt, B., P. Leppimaki, M. Axberg, and J.P. Slotte. 1999. Analysis of natural and synthetic sphingomyelins using high-performance thin-layer chromatography. *Eur J Biochem*. 266:997-1002.

Rastogi, R.P., Richa, and R.P. Sinha. 2009. Apoptosis: Molecular Mechanisms and Pathogenicity. *Excli J*. 8:155-181.

Reagan, J.W., Jr., M.L. Hubbert, and G.S. Shelness. 2000. Posttranslational regulation of acid sphingomyelinase in niemann-pick type C1 fibroblasts and free cholesterol-enriched chinese hamster ovary cells. *J Biol Chem*. 275:38104-38110.

Reynolds, W.F., J. Rhees, D. Maciejewski, T. Paladino, H. Sieburg, R.A. Maki, and E. Masliah. 1999. Myeloperoxidase polymorphism is associated with gender specific risk for Alzheimer's disease. *Exp Neurol*. 155:31-41.

Riboni, L., R. Bassi, A. Prinetti, P. Viani, and G. Tettamanti. 1999. Predominance of the acylation route in the metabolic processing of exogenous sphingosine in neural and extraneural cells in culture. *Biochem J*. 338 (Pt 1):147-151.

Riboni, L., P. Viani, R. Bassi, P. Giussani, and G. Tettamanti. 2000. Cultured granule cells and astrocytes from cerebellum differ in metabolizing sphingosine. *J Neurochem*. 75:503-510.

Richter, G., C. Schober, R. Suss, B. Fuchs, C. Birkemeyer, and J. Schiller. 2008. Comparison of the positive and negative ion electrospray ionization and matrix-assisted laser desorption ionization-time-of-flight mass spectra of the reaction products of phosphatidylethanolamines and hypochlorous acid. *Anal Biochem*. 376:157-159.

Riebeling, C., J.C. Allegood, E. Wang, A.H. Merrill, Jr., and A.H. Futerman. 2003. Two mammalian longevity assurance gene (LAG1) family members, trh1 and trh4, regulate dihydroceramide synthesis using different fatty acyl-CoA donors. *J Biol Chem*. 278:43452-43459.

Robaszkiewicz, A., F.H. Greig, A.R. Pitt, C.M. Spickett, G. Bartosz, and M. Soszynski. 2010. Effect of phosphatidylcholine chlorohydrins on human erythrocytes. *Chem Phys Lipids*. 163:639-647.

Roberg, K., U. Johansson, and K. Ollinger. 1999. Lysosomal release of cathepsin D precedes relocation of cytochrome c and loss of mitochondrial transmembrane potential during apoptosis induced by oxidative stress. *Free Radic Biol Med*. 27:1228-1237.

Romero, I.A., R.J. Rist, M.W. Chan, and N.J. Abbott. 1997. Acute energy deprivation syndromes: investigation of m-dinitrobenzene and alpha-chlorohydrin toxicity on immortalized rat brain microvessel endothelial cells. *Neurotoxicology*. 18:781-791.

Romiti, E., V. Vasta, E. Meacci, M. Farnararo, T. Linke, K. Ferlinz, K. Sandhoff, and P. Bruni. 2000. Characterization of sphingomyelinase activity released by thrombin-stimulated platelets. *Mol Cell Biochem*. 205:75-81.

Rossi, F., and M. Zatti. 1964. Biochemical aspects of phagocytosis in polymorphonuclear leucocytes. NADH and NADPH oxidation by the granules of resting and phagocytizing cells. *Experientia*. 20:21-23.

Rother, J., G. van Echten, G. Schwarzmann, and K. Sandhoff. 1992. Biosynthesis of sphingolipids: dihydroceramide and not sphinganine is desaturated by cultured cells. *Biochem Biophys Res Commun*. 189:14-20.

Rotolo, J.A., J. Zhang, M. Donepudi, H. Lee, Z. Fuks, and R. Kolesnick. 2005. Caspase-dependent and -independent activation of acid sphingomyelinase signaling. *J Biol Chem*. 280:26425-26434.

Rutkute, K., R.H. Asmis, and M.N. Nikolova-Karakashian. 2007. Regulation of neutral sphingomyelinase-2 by GSH: a new insight to the role of oxidative stress in aging-associated inflammation. *J Lipid Res*. 48:2443-2452.

Ruvolo, P.P., X. Deng, T. Ito, B.K. Carr, and W.S. May. 1999. Ceramide induces Bcl2 dephosphorylation via a mechanism involving mitochondrial PP2A. *J Biol Chem*. 274:20296-20300.

Saba, J.D., and T. Hla. 2004. Point-counterpoint of sphingosine 1-phosphate metabolism. *Circ Res*. 94:724-734.

Sadeghlar, F., K. Sandhoff, and G. van Echten-Deckert. 2000. Cell type specific localization of sphingomyelin biosynthesis. *FEBS Lett*. 478:9-12.

Sakahira, H., M. Enari, and S. Nagata. 1998. Cleavage of CAD inhibitor in CAD activation and DNA degradation during apoptosis. *Nature*. 391:96-99.

Sathishkumar, S., B. Boyanovsky, A.A. Karakashian, K. Rozenova, N.V. Giltiay, M. Kudrimoti, M. Mohiuddin, M.M. Ahmed, and M. Nikolova-Karakashian. 2005. Elevated sphingomyelinase activity and ceramide concentration in serum of patients undergoing high dose spatially fractionated radiation treatment: implications for endothelial apoptosis. *Cancer Biol Ther*. 4:979-986.

Sawada, M., S. Nakashima, Y. Banno, H. Yamakawa, K. Hayashi, K. Takenaka, Y. Nishimura, N. Sakai, and Y. Nozawa. 2000. Ordering of ceramide formation, caspase activation, and Bax/Bcl-2 expression during etoposide-induced apoptosis in C6 glioma cells. *Cell Death Differ*. 7:761-772.

Scandroglio, F., J.K. Venkata, N. Loberto, S. Prioni, E.H. Schuchman, V. Chigorno, A. Prinetti, and S. Sonnino. 2008. Lipid content of brain, brain membrane lipid domains, and neurons from acid sphingomyelinase deficient mice. *J Neurochem*. 107:329-338.

Schiller, J., R. Suss, J. Arnhold, B. Fuchs, J. Lessig, M. Muller, M. Petkovic, H. Spalteholz, O. Zschornig, and K. Arnold. 2004. Matrix-assisted laser desorption and ionization time-of-flight (MALDI-TOF) mass spectrometry in lipid and phospholipid research. *Prog Lipid Res*. 43:449-488.

Schiller, J., O. Zschornig, M. Petkovic, M. Muller, J. Arnhold, and K. Arnold. 2001. Lipid analysis of human HDL and LDL by MALDI-TOF mass spectrometry and (31)P-NMR. *J Lipid Res*. 42:1501-1508.

Schimmer, A.D. 2004. Inhibitor of apoptosis proteins: translating basic knowledge into clinical practice. *Cancer Res*. 64:7183-7190.

Schissel, S.L., X. Jiang, J. Tweedie-Hardman, T. Jeong, E.H. Camejo, J. Najib, J.H. Rapp, K.J. Williams, and I. Tabas. 1998a. Secretory sphingomyelinase, a product of the acid sphingomyelinase gene, can hydrolyze atherogenic lipoproteins at neutral pH. Implications for atherosclerotic lesion development. *J Biol Chem*. 273:2738-2746.

Schissel, S.L., G.A. Keesler, E.H. Schuchman, K.J. Williams, and I. Tabas. 1998b. The cellular trafficking and zinc dependence of secretory and lysosomal sphingomyelinase, two products of the acid sphingomyelinase gene. *J Biol Chem*. 273:18250-18259.

Schissel, S.L., E.H. Schuchman, K.J. Williams, and I. Tabas. 1996. Zn2+-stimulated sphingomyelinase is secreted by many cell types and is a product of the acid sphingomyelinase gene. *J Biol Chem*. 271:18431-18436.

Schober, C., J. Schiller, F. Pinker, J.G. Hengstler, and B. Fuchs. 2009. Lysophosphatidylethanolamine is - in contrast to - choline - generated under in vivo conditions exclusively by phospholipase A2 but not by hypochlorous acid. *Bioorg Chem*. 37:202-210.

Schuchman, E.H. 2010. Acid sphingomyelinase, cell membranes and human disease: lessons from Niemann-Pick disease. *FEBS Lett*. 584:1895-1900.

Schuchman, E.H., O. Levran, L.V. Pereira, and R.J. Desnick. 1992. Structural organization and complete nucleotide sequence of the gene encoding human acid sphingomyelinase (SMPD1). *Genomics*. 12:197-205.

Schultz, J., and K. Kaminker. 1962. Myeloperoxidase of the leucocyte of normal human blood. I. Content and localization. *Arch Biochem Biophys*. 96:465-467.

Schutze, S., K. Potthoff, T. Machleidt, D. Berkovic, K. Wiegmann, and M. Kronke. 1992. TNF activates NF-kappa B by phosphatidylcholine-specific phospholipase C-induced "acidic" sphingomyelin breakdown. *Cell*. 71:765-776.

Schwartz, M.K. 1995. Tissue cathepsins as tumor markers. *Clin Chim Acta*. 237:67-78.

Schwarz, A., and A.H. Futerman. 1997. Distinct roles for ceramide and glucosylceramide at different stages of neuronal growth. *J Neurosci*. 17:2929-2938.

Scorrano, L., S.A. Oakes, J.T. Opferman, E.H. Cheng, M.D. Sorcinelli, T. Pozzan, and S.J. Korsmeyer. 2003. BAX and BAK regulation of endoplasmic reticulum Ca2+: a control point for apoptosis. *Science*. 300:135-139.

Segui, B., N. Andrieu-Abadie, S. Adam-Klages, O. Meilhac, D. Kreder, V. Garcia, A.P. Bruno, J.P. Jaffrezou, R. Salvayre, M. Kronke, and T. Levade. 1999. CD40 signals apoptosis through FAN-regulated activation of the sphingomyelin-ceramide pathway. *J Biol Chem*. 274:37251-37258.

Shao, B., C. Bergt, X. Fu, P. Green, J.C. Voss, M.N. Oda, J.F. Oram, and J.W. Heinecke. 2005. Tyrosine 192 in apolipoprotein A-I is the major site of nitration and chlorination by myeloperoxidase, but only chlorination markedly impairs ABCA1-dependent cholesterol transport. *J Biol Chem*. 280:5983-5993.

Sharma, D.K., J.C. Brown, A. Choudhury, T.E. Peterson, E. Holicky, D.L. Marks, R. Simari, R.G. Parton, and R.E. Pagano. 2004. Selective stimulation of caveolar endocytosis by glycosphingolipids and cholesterol. *Mol Biol Cell*. 15:3114-3122.

Sharma, D.K., A. Choudhury, R.D. Singh, C.L. Wheatley, D.L. Marks, and R.E. Pagano. 2003. Glycosphingolipids internalized via caveolar-related endocytosis rapidly merge with the clathrin pathway in early endosomes and form microdomains for recycling. *J Biol Chem*. 278:7564-7572.

Shayman, J.A., and A. Abe. 2000. 1-O-acylceramide synthase. *Methods Enzymol*. 311:105-117.

Sheline, C.T., and D.W. Choi. 1998. Neuronal death in cultured murine cortical cells is induced by inhibition of GAPDH and triosephosphate isomerase. *Neurobiol Dis*. 5:47-54.

Simons, K., and W.L. Vaz. 2004. Model systems, lipid rafts, and cell membranes. *Annu Rev Biophys Biomol Struct*. 33:269-295.

Singh, I., K. Pahan, M. Khan, and A.K. Singh. 1998. Cytokine-mediated induction of ceramide production is redox-sensitive. Implications to proinflammatory cytokine-mediated apoptosis in demyelinating diseases. *J Biol Chem*. 273:20354-20362.

Singh, R.D., Y. Liu, C.L. Wheatley, E.L. Holicky, A. Makino, D.L. Marks, T. Kobayashi, G. Subramaniam, R. Bittman, and R.E. Pagano. 2006. Caveolar endocytosis and microdomain association of a glycosphingolipid analog is dependent on its sphingosine stereochemistry. *J Biol Chem*. 281:30660-30668.

Singh, R.D., V. Puri, J.T. Valiyaveettil, D.L. Marks, R. Bittman, and R.E. Pagano. 2003. Selective caveolin-1-dependent endocytosis of glycosphingolipids. *Mol Biol Cell*. 14:3254-3265.

Singleton, P.A., T. Mirzapoiazova, Y. Guo, S. Sammani, N. Mambetsariev, F.E. Lennon, L. Moreno-Vinasco, and J.G. Garcia. 2010. High-molecular-weight hyaluronan is a novel inhibitor of pulmonary vascular leakiness. *Am J Physiol Lung Cell Mol Physiol*. 299:L639-651.

Siskind, L.J., R.N. Kolesnick, and M. Colombini. 2002. Ceramide channels increase the permeability of the mitochondrial outer membrane to small proteins. *J Biol Chem*. 277:26796-26803.

Skaff, O., D.I. Pattison, and M.J. Davies. 2008. The vinyl ether linkages of plasmalogens are favored targets for myeloperoxidase-derived oxidants: a kinetic study. *Biochemistry*. 47:8237-8245.

Skamarauskas, J., W. Carter, M. Fowler, A. Madjd, T. Lister, G. Mavroudis, and D.E. Ray. 2007. The selective neurotoxicity produced by 3-chloropropanediol in the rat is not a result of energy deprivation. *Toxicology*. 232:268-276.

Slee, E.A., C. Adrain, and S.J. Martin. 2001. Executioner caspase-3, -6, and -7 perform distinct, non-redundant roles during the demolition phase of apoptosis. *J Biol Chem*. 276:7320-7326.

Slotte, J.P., and B. Ramstedt. 2007. The functional role of sphingomyelin in cell membranes. *Eur J Lipid Sci Tech*. 109:977-981.

Sonnino, S., and V. Chigorno. 2000. Ganglioside molecular species containing C18- and C20-sphingosine in mammalian nervous tissues and neuronal cell cultures. *Biochim Biophys Acta*. 1469:63-77.

Spalteholz, H., K. Wenske, O.M. Panasenko, J. Schiller, and J. Arnhold. 2004. Evaluation of products upon the reaction of hypohalous acid with unsaturated phosphatidylcholines. *Chem Phys Lipids*. 129:85-96.

Spickett, C.M. 2007. Chlorinated lipids and fatty acids: an emerging role in pathology. *Pharmacol Ther*. 115:400-409.

Spiegel, S., and S. Milstien. 2003. Sphingosine-1-phosphate: an enigmatic signalling lipid. *Nat Rev Mol Cell Biol*. 4:397-407.

Stacey, M.M., A.V. Peskin, M.C. Vissers, and C.C. Winterbourn. 2009. Chloramines and hypochlorous acid oxidize erythrocyte peroxiredoxin 2. *Free Radic Biol Med*. 47:1468-1476.

Staellberg-Stenhagen, S., and L. Svennerholm. 1965. Fatty Acid Composition of Human Brain Sphingomyelins: Normal Variation with Age and Changes during Myelin Disorders. *J Lipid Res*. 6:146-155.

Steinman, R.M., I.S. Mellman, W.A. Muller, and Z.A. Cohn. 1983. Endocytosis and the recycling of plasma membrane. *J Cell Biol*. 96:1-27.

Stennicke, H.R., and G.S. Salvesen. 1998. Properties of the caspases. *Biochim Biophys Acta*. 1387:17-31.

Stiban, J., R. Tidhar, and A.H. Futerman. 2010. Ceramide synthases: roles in cell physiology and signaling. *Adv Exp Med Biol*. 688:60-71.

Sturn, A., J. Quackenbush, and Z. Trajanoski. 2002. Genesis: cluster analysis of microarray data. *Bioinformatics*. 18:207-208.

Subathra, M., A. Qureshi, and C. Luberto. 2011. Sphingomyelin synthases regulate protein trafficking and secretion. *PLoS One*. 6:e23644.

Summers, S.A., L.A. Garza, H. Zhou, and M.J. Birnbaum. 1998. Regulation of insulin-stimulated glucose transporter GLUT4 translocation and Akt kinase activity by ceramide. *Mol Cell Biol*. 18:5457-5464.

Tafesse, F.G., K. Huitema, M. Hermansson, S. van der Poel, J. van den Dikkenberg, A. Uphoff, P. Somerharju, and J.C. Holthuis. 2007. Both sphingomyelin synthases SMS1 and SMS2 are required for sphingomyelin homeostasis and growth in human HeLa cells. *J Biol Chem*. 282:17537-17547.

Tafesse, F.G., P. Ternes, and J.C. Holthuis. 2006. The multigenic sphingomyelin synthase family. *J Biol Chem*. 281:29421-29425.

Takahashi, M., M. Murate, M. Fukuda, S.B. Sato, A. Ohta, and T. Kobayashi. 2007. Cholesterol controls lipid endocytosis through Rab11. *Mol Biol Cell*. 18:2667-2677.

Takeshita, J., J. Byun, T.Q. Nhan, D.K. Pritchard, S. Pennathur, S.M. Schwartz, A. Chait, and J.W. Heinecke. 2006. Myeloperoxidase generates 5-chlorouracil in human atherosclerotic tissue: a potential pathway for somatic mutagenesis by macrophages. *J Biol Chem*. 281:3096-3104.

Tam, C., V. Idone, C. Devlin, M.C. Fernandes, A. Flannery, X. He, E. Schuchman, I. Tabas, and N.W. Andrews. 2010. Exocytosis of acid sphingomyelinase by wounded cells promotes endocytosis and plasma membrane repair. *J Cell Biol*. 189:1027-1038.

Tani, M., Y. Igarashi, and M. Ito. 2005. Involvement of neutral ceramidase in ceramide metabolism at the plasma membrane and in extracellular milieu. *J Biol Chem*. 280:36592-36600.

Tani, M., and O. Kuge. 2009. Sphingomyelin synthase 2 is palmitoylated at the COOH-terminal tail, which is involved in its localization in plasma membranes. *Biochem Biophys Res Commun*. 381:328-332.

Targonski, P.V., P.O. Bonetti, G.M. Pumper, S.T. Higano, D.R. Holmes, Jr., and A. Lerman. 2003. Coronary endothelial dysfunction is associated with an increased risk of cerebrovascular events. *Circulation*. 107:2805-2809.

Tepper, A.D., P. Ruurs, T. Wiedmer, P.J. Sims, J. Borst, and W.J. van Blitterswijk. 2000. Sphingomyelin hydrolysis to ceramide during the execution phase of apoptosis results from phospholipid scrambling and alters cell-surface morphology. *J Cell Biol*. 150:155-164.

Tessier, J.P., B. Thurner, E. Jungling, A. Luckhoff, and Y. Fischer. 2003. Impairment of glucose metabolism in hearts from rats treated with endotoxin. *Cardiovasc Res*. 60:119-130.

Testai, F.D., M.A. Landek, R. Goswami, M. Ahmed, and G. Dawson. 2004. Acid sphingomyelinase and inhibition by phosphate ion: role of inhibition by phosphatidyl-myo-inositol 3,4,5-triphosphate in oligodendrocyte cell signaling. *Journal of Neurochemistry*. 89:636-644.

Tettamanti, G., R. Bassi, P. Viani, and L. Riboni. 2003. Salvage pathways in glycosphingolipid metabolism. *Biochimie*. 85:423-437.

Thome, M., P. Schneider, K. Hofmann, H. Fickenscher, E. Meinl, F. Neipel, C. Mattmann, K. Burns, J.L. Bodmer, M. Schroter, C. Scaffidi, P.H. Krammer, M.E. Peter, and J. Tschopp. 1997. Viral FLICE-inhibitory proteins (FLIPs) prevent apoptosis induced by death receptors. *Nature*. 386:517-521.

Thornberry, N.A. 1997. The caspase family of cysteine proteases. *Br Med Bull*. 53:478-490.

Thukkani, A.K., F.F. Hsu, J.R. Crowley, R.B. Wysolmerski, C.J. Albert, and D.A. Ford. 2002. Reactive chlorinating species produced during neutrophil activation target tissue plasmalogens: production of the chemoattractant, 2-chlorohexadecanal. *J Biol Chem*. 277:3842-3849.

Thukkani, A.K., B.D. Martinson, C.J. Albert, G.A. Vogler, and D.A. Ford. 2005. Neutrophil-mediated accumulation of 2-ClHDA during myocardial infarction: 2-ClHDA-mediated myocardial injury. *Am J Physiol Heart Circ Physiol*. 288:H2955-2964.

Thukkani, A.K., J. McHowat, F.F. Hsu, M.L. Brennan, S.L. Hazen, and D.A. Ford. 2003. Identification of alpha-chloro fatty aldehydes and unsaturated lysophosphatidylcholine molecular species in human atherosclerotic lesions. *Circulation*. 108:3128-3133.

Tinel, A., and J. Tschopp. 2004. The PIDDosome, a protein complex implicated in activation of caspase-2 in response to genotoxic stress. *Science*. 304:843-846.

Tiruppathi, C., T. Naqvi, Y. Wu, S.M. Vogel, R.D. Minshall, and A.B. Malik. 2004. Albumin mediates the transcytosis of myeloperoxidase by means of caveolae in endothelial cells. *Proc Natl Acad Sci U S A*. 101:7699-7704.

Tomiuk, S., K. Hofmann, M. Nix, M. Zumbansen, and W. Stoffel. 1998. Cloned mammalian neutral sphingomyelinase: functions in sphingolipid signaling? *Proc Natl Acad Sci U S A*. 95:3638-3643.

Tomono, S., N. Miyoshi, H. Shiokawa, T. Iwabuchi, Y. Aratani, T. Higashi, H. Nukaya, and H. Ohshima. 2011. Formation of cholesterol ozonolysis products in vitro and in vivo through a myeloperoxidase-dependent pathway. *J Lipid Res*. 52:87-97.

Trump, B.F., I.K. Berezesky, S.H. Chang, and P.C. Phelps. 1997. The pathways of cell death: oncosis, apoptosis, and necrosis. *Toxicol Pathol*. 25:82-88.

Tyurin, V.A., Y.Y. Tyurina, W. Feng, A. Mnuskin, J. Jiang, M. Tang, X. Zhang, Q. Zhao, P.M. Kochanek, R.S. Clark, H. Bayir, and V.E. Kagan. 2008. Mass-spectrometric characterization of phospholipids and their primary peroxidation products in rat cortical neurons during staurosporine-induced apoptosis. *J Neurochem*. 107:1614-1633.

U, M., T. Miyashita, Y. Ohtsuka, Y. Okamura-Oho, Y. Shikama, and M. Yamada. 2001. Extended polyglutamine selectively interacts with caspase-8 and -10 in nuclear aggregates. *Cell Death Differ*. 8:377-386.

Ullen, A., G. Fauler, H. Kofeler, S. Waltl, C. Nusshold, E. Bernhart, H. Reicher, H.J. Leis, A. Wintersperger, E. Malle, and W. Sattler. 2010. Mouse brain plasmalogens are targets for hypochlorous acid-mediated modification in vitro and in vivo. *Free Radic Biol Med*. 49:1655-1665.

Vacaru, A.M., F.G. Tafesse, P. Ternes, V. Kondylis, M. Hermansson, J.F. Brouwers, P. Somerharju, C. Rabouille, and J.C. Holthuis. 2009. Sphingomyelin synthase-related protein SMSr controls ceramide homeostasis in the ER. *J Cell Biol*. 185:1013-1027.

Vakifahmetoglu, H., M. Olsson, S. Orrenius, and B. Zhivotovsky. 2006. Functional connection between p53 and caspase-2 is essential for apoptosis induced by DNA damage. *Oncogene*. 25:5683-5692.

Valsecchi, M., L. Mauri, R. Casellato, S. Prioni, N. Loberto, A. Prinetti, V. Chigorno, and S. Sonnino. 2007. Ceramide and sphingomyelin species of fibroblasts and neurons in culture. *J Lipid Res*. 48:417-424.

van Dalen, C.J., M.W. Whitehouse, C.C. Winterbourn, and A.J. Kettle. 1997. Thiocyanate and chloride as competing substrates for myeloperoxidase. *Biochem J*. 327 (Pt 2):487-492.

van der Veen, B.S., M.P. de Winther, and P. Heeringa. 2009. Myeloperoxidase: molecular mechanisms of action and their relevance to human health and disease. *Antioxid Redox Signal*. 11:2899-2937.

van Echten-Deckert, G., and T. Herget. 2006. Sphingolipid metabolism in neural cells. *Biochim Biophys Acta*. 1758:1978-1994.

van Echten, G., and K. Sandhoff. 1989. Modulation of ganglioside biosynthesis in primary cultured neurons. *J Neurochem*. 52:207-214.

van Meer, G., and S. Hoetzl. 2010. Sphingolipid topology and the dynamic organization and function of membrane proteins. *FEBS Lett*. 584:1800-1805.

van Meer, G., and J.C. Holthuis. 2000. Sphingolipid transport in eukaryotic cells. *Biochim Biophys Acta*. 1486:145-170.

van Meer, G., and R.M. Liskamp. 2005. Brilliant lipids. *Nat Methods*. 2:14-15.

van Meer, G., D.R. Voelker, and G.W. Feigenson. 2008. Membrane lipids: where they are and how they behave. *Nat Rev Mol Cell Biol*. 9:112-124.

Van Overloop, H., S. Gijsbers, and P.P. Van Veldhoven. 2006. Further characterization of mammalian ceramide kinase: substrate delivery and (stereo)specificity, tissue distribution, and subcellular localization studies. *J Lipid Res*. 47:268-283.

Vanmeer, G., and W. Vanthof. 1993. Epithelial Sphingolipid Sorting Is Insensitive to Reorganization of the Golgi by Nocodazole, but Is Abolished by Monensin in Mdck Cells and by Brefeldin-a in Caco-2 Cells. *Journal of Cell Science*. 104:833-842.

Veatch, S.L., and S.L. Keller. 2005. Miscibility phase diagrams of giant vesicles containing sphingomyelin. *Phys Rev Lett*. 94:148101.

Venkataraman, K., C. Riebeling, J. Bodennec, H. Riezman, J.C. Allegood, M.C. Sullards, A.H. Merrill, Jr., and A.H. Futerman. 2002. Upstream of growth and differentiation factor 1 (uog1), a mammalian homolog of the yeast longevity assurance gene 1 (LAG1), regulates N-stearoyl-sphinganine (C18-(dihydro)ceramide) synthesis in a fumonisin B1-independent manner in mammalian cells. *J Biol Chem*. 277:35642-35649.

Verhagen, A.M., E.J. Coulson, and D.L. Vaux. 2001. Inhibitor of apoptosis proteins and their relatives: IAPs and other BIRPs. *Genome Biol*. 2:REVIEWS3009.

Vicca, S., C. Hennequin, T. Nguyen-Khoa, Z.A. Massy, B. Descamps-Latscha, T.B. Drueke, and B. Lacour. 2000. Caspase-dependent apoptosis in THP-1 cells exposed to oxidized low-density lipoproteins. *Biochem Biophys Res Commun*. 273:948-954.

Vicca, S., Z.A. Massy, C. Hennequin, D. Rihane, T.B. Drueke, and B. Lacour. 2003. Apoptotic pathways involved in U937 cells exposed to LDL oxidized by hypochlorous acid. *Free Radic Biol Med*. 35:603-615.

Villa, P.G., W.J. Henzel, M. Sensenbrenner, C.E. Henderson, and B. Pettmann. 1998. Calpain inhibitors, but not caspase inhibitors, prevent actin proteolysis and DNA fragmentation during apoptosis. *J Cell Sci*. 111 (Pt 6):713-722.

Viola, A., and N. Gupta. 2007. Tether and trap: regulation of membrane-raft dynamics by actin-binding proteins. *Nat Rev Immunol*. 7:889-896.

Vissers, M.C., A.C. Carr, and A.L. Chapman. 1998. Comparison of human red cell lysis by hypochlorous and hypobromous acids: insights into the mechanism of lysis. *Biochem J*. 330 (Pt 1):131-138.

Vissers, M.C., A.C. Carr, and C.C. Winterbour. 2001. Fatty acid chlorohydrins and bromohydrins are cytotoxic to human endothelial cells. *Redox Rep*. 6:49-55.

Wajant, H. 2002. The Fas signaling pathway: more than a paradigm. *Science*. 296:1635-1636.

Wang, K.K. 2000. Calpain and caspase: can you tell the difference? *Trends Neurosci*. 23:20-26.

Wang, L.H., K.G. Rothberg, and R.G. Anderson. 1993. Mis-assembly of clathrin lattices on endosomes reveals a regulatory switch for coated pit formation. *J Cell Biol*. 123:1107-1117.

Wang, Z., S.J. Nicholls, E.R. Rodriguez, O. Kummu, S. Horkko, J. Barnard, W.F. Reynolds, E.J. Topol, J.A. DiDonato, and S.L. Hazen. 2007. Protein carbamylation links inflammation, smoking, uremia and atherogenesis. *Nat Med*. 13:1176-1184.

Wanner, R., M. Peiser, and B. Wittig. 2004. Keratinocytes rapidly readjust ceramide-sphingomyelin homeostasis and contain a phosphatidylcholine-sphingomyelin transacylase. *J Invest Dermatol*. 122:773-782.

Waschołowski, V., and A. Giannis. 2006. Sphingolactones: selective and irreversible inhibitors of neutral sphingomyelinase. *Angew Chem Int Ed Engl*. 45:827-830.

Watson, P., and D.J. Stephens. 2005. ER-to-Golgi transport: form and formation of vesicular and tubular carriers. *Biochim Biophys Acta*. 1744:304-315.

Whatmore, J.L., and D. Allan. 1994. Phospholipid asymmetry in plasma membrane vesicles derived from BHK cells. *Biochim Biophys Acta*. 1192:88-94.

Whiteman, M., P. Rose, J.L. Siau, N.S. Cheung, G.S. Tan, B. Halliwell, and J.S. Armstrong. 2005. Hypochlorous acid-mediated mitochondrial dysfunction and apoptosis in human hepatoma HepG2 and human fetal liver cells: role of mitochondrial permeability transition. *Free Radic Biol Med*. 38:1571-1584.

Wildsmith, K.R., C.J. Albert, F.F. Hsu, J.L. Kao, and D.A. Ford. 2006. Myeloperoxidase-derived 2-chlorohexadecanal forms Schiff bases with primary amines of ethanolamine glycerophospholipids and lysine. *Chem Phys Lipids*. 139:157-170.

Willard, B.B., C.I. Ruse, J.A. Keightley, M. Bond, and M. Kinter. 2003. Site-specific quantitation of protein nitration using liquid chromatography/tandem mass spectrometry. *Anal Chem*. 75:2370-2376.

Williams, R.D., E. Wang, and A.H. Merrill, Jr. 1984. Enzymology of long-chain base synthesis by liver: characterization of serine palmitoyltransferase in rat liver microsomes. *Arch Biochem Biophys*. 228:282-291.

Willis, C.L., G.L. Taylor, and D.E. Ray. 2007. Microvascular P-glycoprotein expression at the blood-brain barrier following focal astrocyte loss and at the fenestrated vasculature of the area postrema. *Brain Res*. 1173:126-136.

Winterbourn, C.C. 1985. Comparative reactivities of various biological compounds with myeloperoxidase-hydrogen peroxide-chloride, and similarity of the oxidant to hypochlorite. *Biochim Biophys Acta*. 840:204-210.

Winterbourn, C.C., and S.O. Brennan. 1997. Characterization of the oxidation products of the reaction between reduced glutathione and hypochlorous acid. *Biochem J*. 326 (Pt 1):87-92.

Winterbourn, C.C., H. Pichorner, and A.J. Kettle. 1997. Myeloperoxidase-dependent generation of a tyrosine peroxide by neutrophils. *Arch Biochem Biophys*. 338:15-21.

Winterbourn, C.C., J.J. van den Berg, E. Roitman, and F.A. Kuypers. 1992. Chlorohydrin formation from unsaturated fatty acids reacted with hypochlorous acid. *Arch Biochem Biophys*. 296:547-555.

Wong, M.L., B. Xie, N. Beatini, P. Phu, S. Marathe, A. Johns, P.W. Gold, E. Hirsch, K.J. Williams, J. Licinio, and I. Tabas. 2000. Acute systemic inflammation up-regulates secretory sphingomyelinase in vivo: a possible link between inflammatory cytokines and atherogenesis. *Proc Natl Acad Sci U S A*. 97:8681-8686.

Wood, D.E., A. Thomas, L.A. Devi, Y. Berman, R.C. Beavis, J.C. Reed, and E.W. Newcomb. 1998. Bax cleavage is mediated by calpain during drug-induced apoptosis. *Oncogene*. 17:1069-1078.

Xin, M., and X. Deng. 2006. Protein phosphatase 2A enhances the proapoptotic function of Bax through dephosphorylation. *J Biol Chem*. 281:18859-18867.

Yamada, M., and K. Kurahashi. 1984. Regulation of myeloperoxidase gene expression during differentiation of human myeloid leukemia HL-60 cells. *J Biol Chem*. 259:3021-3025.

Yamashita, T., R. Wada, T. Sasaki, C. Deng, U. Bierfreund, K. Sandhoff, and R.L. Proia. 1999. A vital role for glycosphingolipid synthesis during development and differentiation. *Proc Natl Acad Sci U S A*. 96:9142-9147.

Yan, N., and Y. Shi. 2005. Mechanisms of apoptosis through structural biology. *Annu Rev Cell Dev Biol*. 21:35-56.

Yap, Y.W., M. Whiteman, B.H. Bay, Y. Li, F.S. Sheu, R.Z. Qi, C.H. Tan, and N.S. Cheung. 2006. Hypochlorous acid induces apoptosis of cultured cortical neurons through activation of calpains and rupture of lysosomes. *J Neurochem*. 98:1597-1609.

Yap, Y.W., M. Whiteman, and N.S. Cheung. 2007. Chlorinative stress: an under appreciated mediator of neurodegeneration? *Cell Signal*. 19:219-228.

Yokomatsu, T., T. Murano, T. Akiyama, J. Koizumi, S. Shibuya, Y. Tsuji, S. Soeda, and H. Shimeno. 2003. Synthesis of non-competitive inhibitors of sphingomyelinases with significant activity. *Bioorg Med Chem Lett*. 13:229-236.

Yoshimura, S., Y. Banno, S. Nakashima, K. Hayashi, H. Yamakawa, M. Sawada, N. Sakai, and Y. Nozawa. 1999. Inhibition of neutral sphingomyelinase activation and ceramide formation by glutathione in hypoxic PC12 cell death. *J Neurochem*. 73:675-683.

Zappia, M., I. Manna, P. Serra, R. Cittadella, V. Andreoli, A. La Russa, F. Annesi, P. Spadafora, N. Romeo, G. Nicoletti, D. Messina, A. Gambardella, and A. Quattrone. 2004. Increased risk for Alzheimer disease with the interaction of MPO and A2M polymorphisms. *Arch Neurol*. 61:341-344.

Zeidan, Y.H., and Y.A. Hannun. 2007. Activation of acid sphingomyelinase by protein kinase Cdelta-mediated phosphorylation. *J Biol Chem*. 282:11549-11561.

Zeidan, Y.H., R.W. Jenkins, and Y.A. Hannun. 2008. Remodeling of cellular cytoskeleton by the acid sphingomyelinase/ceramide pathway. *J Cell Biol*. 181:335-350.

Zeiss, C.J. 2003. The apoptosis-necrosis continuum: insights from genetically altered mice. *Vet Pathol*. 40:481-495.

Zheng, L., B. Nukuna, M.L. Brennan, M. Sun, M. Goormastic, M. Settle, D. Schmitt, X. Fu, L. Thomson, P.L. Fox, H. Ischiropoulos, J.D. Smith, M. Kinter, and S.L. Hazen. 2004. Apolipoprotein A-I is a selective target for myeloperoxidase-catalyzed oxidation and functional impairment in subjects with cardiovascular disease. *J Clin Invest*. 114:529-541.

Zitomer, N.C., T. Mitchell, K.A. Voss, G.S. Bondy, S.T. Pruett, E.C. Garnier-Amblard, L.S. Liebeskind, H. Park, E. Wang, M.C. Sullards, A.H. Merrill, Jr., and R.T. Riley. 2009. Ceramide synthase inhibition by fumonisin B1 causes accumulation of 1-deoxysphinganine: a novel category of bioactive 1-deoxysphingoid bases and 1-deoxydihydroceramides biosynthesized by mammalian cell lines and animals. *J Biol Chem*. 284:4786-4795.

Zmijewski, J.W., D.R. Moellering, C. Le Goffe, A. Landar, A. Ramachandran, and V.M. Darley-Usmar. 2005. Oxidized LDL induces mitochondrially associated reactive oxygen/nitrogen species formation in endothelial cells. *Am J Physiol Heart Circ Physiol*. 289:H852-861.

Zou, H., Y. Li, X. Liu, and X. Wang. 1999. An APAF-1.cytochrome c multimeric complex is a functional apoptosome that activates procaspase-9. *J Biol Chem*. 274:11549-11556.